ÄSPÖLABORATORIET

INTERNATIONAL COOPERATION REPORT 94-12

Modelling the LPT2 Pumping and Tracer Test at Äspö

Pumping test

Veikko Taivassalo, Lasse Koskinen,
Mikko Laitinen, Jari Löfman, Ferenc Mészáros

VTT Energy

November 1994

Supported by TVO, Finland

SVENSK KÄRNBRÄNSLEHANTERING AB
SWEDISH NUCLEAR FUEL AND WASTE MANAGEMENT CO
BOX 5864 S-102 40 STOCKHOLM
TEL. +46-8-665 28 00 TELEX 13108 SKB TELEFAX +46-8-661 57 19

Rec'd via letter dtd 4/24/95

ISSN 1104-3210
ISRN SKB-ICR--94/12--SE

MODELLING THE LPT2 PUMPING AND TRACER TEST AT ÄSPÖ

PUMPING TEST

Veikko Taivassalo
Lasse Koskinen
Mikko Laitinen
Jari Löfman
Ferenc Mészáros

VTT Energy

November 1994

Supported by TVO, Finland

1028

MODELLING THE LPT2 PUMPING AND TRACER TEST AT ÄSPÖ

Pumping test

Veikko Taivassalo
Lasse Koskinen
Mikko Laitinen
Jari Löfman
Ferenc Mészáros

VTT Energy

Supported by TVO, Finland

November 1994
Espoo

ABSTRACT

The LPT2 experiment was a long-term pumping and tracer test performed at the Äspö site. Groundwater flow conditions during the test are analyzed in this report. The primary motivation of the study was to improve our understanding on the site by developing a site-scale groundwater flow model. The flow model was based on the structural model of the site. The structural model evolved during the modelling, and both the base and updated models are examined. We concentrate on the updated model.

The heterogeneity of the bedrock was considered throughout the study. The bedrock was divided into fracture zones and the remaining rock matrix. The modelling of the pressure field was based on the concept of an equivalent continuum. The geometry of the fracture zones was followed carefully in the finite element meshes. In calculating the groundwater flux, the influence of the spatial variation of the local transmissivities was studied.

The models were calibrated to improve the agreement with the field data. Regarding the base model, LPT2 and another long-term pumping test, LPT1, were applied. When calibrating the updated model, another four pumping tests and the undisturbed flow conditions were studied. The pressure drawdowns measured in the withdrawal holes were given as boundary conditions. The computed drawdowns along the cored holes and the total inflow to the withdrawal hole as well as its distribution were compared with the field data. The cross-zone transmissivities of several zones were modified and the transmissivities of the near-field parts of the zones intersecting the withdrawal holes were conditioned.

Four sets of simulation results for the LPT2 test are presented: for the base and updated models before and after the calibration. The steady-state pressure drawdown in the observation sections of the cored and percussion boreholes is compared with the measured values. The base and updated models simulate the drawdown for LPT2 successfully even before the calibration. The drawdown from the transient simulations is plotted with the field data for several observation sections. The amount of groundwater flowing through the injection sections was computed and scrutinized in the light of the field data. Pathlines representing the routes of tracers from a few injection points to the withdrawal hole were simulated as well.

The study showed that the equivalent-continuum approximation is satisfactory in simulating the pressure drawdown on a site scale. The concept also supports fast computation of the drawdown, which is required when several pumping tests are studied. Efficient methods to create detail test-specific finite element meshes are also necessary. Distributions for the flow rate through borehole sections can be calculated stochastically but the results are determined by parameters whose values are unknown.

TABLE OF CONTENTS

EXECUTIVE SUMMARY

Background and objectives

The Äspö Hard Rock Laboratory (HRL) is currently constructed below the island of Äspö. Extensive field investigations have been carried out to study the properties of the bedrock. The LPT2 test is a long-term pumping and tracer test, which was performed to identify and characterize the major water-bearing structures of the bedrock.

Groundwater flow conditions during the LPT2 test were analyzed in this study by means of numerical simulations. Five other pumping tests and undisturbed flow conditions were also examined and modelled when calibrating the models. The main motivation of this study was our effort of developing a site-scale model characterizing the groundwater flow at Äspö.

During the modelling study, the structural model for the Äspö site evolved. Both the base and updated structural models were considered but this study concentrated on the updated model.

Modelling approach

The heterogeneity of the bedrock was taken into account throughout the study. The bedrock was divided into identified fracture zones and the remaining rock matrix. The zones intersected by a withdrawal hole were conceptually treated in two parts: the near-field area of a zone and the rest of it. The spatial variation of the hydraulic properties was also considered.

The numerical simulation method varied depending on the quantity and scale studied. On a site scale, the fracture zones as well as the rock matrix were each represented by a homogeneous feature, and the calculation of the pressure (drawdown) was based on the concept of an equivalent continuum in each subdomain. To estimate the flow rate through the tracer injection sections, stochastic simulations were also applied. The FEFLOW code developed at VTT was used in the numerical simulations.

The geometry of the fracture zones was followed in finite element meshes. When simulating the pumping tests, only the influence of pumping on the pressure drawdown field was calculated. The drawdown measured in the withdrawal holes was used as a boundary condition, and the inflow to the withdrawal holes was calculated. No-flow boundary conditions were assigned for the island area. The pressure at the other boundary nodes was assumed to remain. The type of the boundary conditions on the bottom and side faces is not critical because of the large size of the simulation model.

The initially employed values of the transmissivities and hydraulic conductivity were based on the values reported. The final values were found through the calibration process.

Calibration

The base model was calibrated only tentatively utilizing the two long-term pumping tests, LPT1 and LPT2. The transmissivities of a few zones were adjusted to improve the agreement of the simulation results with the field data. A satisfactory agreement was obtained with modest modifications.

In calibrating the updated model, besides the LPT1 and LPT2 tests, the pumping tests performed in KAS12, KAS13, KAS14 and KAS16 as well as undisturbed flow conditions were examined. The transmissivities of the zones intersecting the withdrawal holes were conditioned to obtain the measured distribution of the inflow. Several other zones were also considered in fitting the drawdown field. The average cross-zone transmissivities and near-field transmissivities of the zones were handled separately. Since the undisturbed pressure field is mainly determined by the salt concentration, the undisturbed flow conditions are not very useful in the calibration.

Several modifications were incorporated in the updated model. The extent of the most conductive parts of two zones (EW-5 and NE-1) was reduced. The average transmissivity was modified significantly only for zone EW-3. The near-field transmissivities were modified up to two orders of magnitude compared to the calibrated values. Several other possible explanations for the discrepancies between the field data and the simulation results were studied: the influence of additional zones, various orientations of the present zones, the highly-conductive surface layer and the low-conductive sea bottom were examined as well. The calibrated models reproduce the main features of the field experiments.

Simulation results for the LPT2 test

The performance of the models was evaluated by comparing the calculated drawdown, the inflow distribution and the flow rate through the injection sections with the field data. The computed steady-state drawdown for LPT2 along the cored boreholes is presented with the experimental data in the figure (pp. x and xi). The agreement in the drawdown is satisfactory even before the calibration. The differences between experimental and computational results can mainly be explained by the simplifications inherent to the model. The time-dependence of the simulated drawdown was examined in comparison with the field data.

The calculated total inflow to the withdrawal hole was close to the pumping rate applied even with the initial parameters. The distribution of the inflow differed from the experimental data, however.

The agreement between the simulation results and the field data was the poorest for the amount of water flowing through the tracer injection sections. The groundwater flow rate is mainly defined by a local value of the transmissivity, and it is obvious that the average groundwater fluxes calculated from the cross-zone transmissivities do not coincide with the field data. By employing stochastic simulations, flow rate distributions that cover the field values could be obtained in most cases.

Conclusions

The selected modelling approach proved to be successful. When applied separately on each subdomain, the concept of an equivalent continuum is satisfactory for modelling the drawdown, which was the primary parameter in the calibration and in evaluating the performance of the models. In addition, the continuum approximation supports the fast computation of the drawdown field, which was essential because several pumping tests were applied in the calibration.

The fast and largely automatized software system applied for creating element meshes made it possible to model six pumping tests and to use several structural models including a number of fracture zones. The approach also facilitated the phase of exploring investigations in which the influences of additional features in the simulation model were examined.

The simulations for the LPT2 test and especially the calibration phase as well as the sensitivity and uncertainty studies helped us to understand better the flow system at the Äspö site. A surprising observation was that the initial models were simulating relatively well the drawdowns only for LPT1 and LPT2. The initial simulation results especially for the pumping tests in KAS12, KAS13 and KAS16 differ significantly from the field data. After the calibration, the model simulated most pumping tests successfully but the results of the pumping tests in KAS14 and especially in KAS16 were much more difficult to explain. The equivalent transmissivities of the zones that are far from any of the withdrawal holes can, however, be significantly larger or smaller.

Considering groundwater flow, both the base as well as the updated structural models for the Äspö site are largely plausible. Most of the differences in the structural models did not influence the simulation results of LPT1 and LPT2. Yet this study indicates the following modifications in the structural model: a connection between KAS12 and NNW-2, an additional zone intersecting KAS13, and the extent of NNW-1 and NNW-2 smaller in vertical direction. Regarding the properties, the simulations indicate that the transmissivity of EW-5 is high for at least a restricted part around KAS06, NNW-1 is anisotropic having a highly-conductive part around the intersection point with KAS07, the northern part of NNW-1 possesses a large conductive and the transmissivity of the southern part of NNW-2 high. The simulations also strengthen the earlier conclusion that large uncertainties are associated with EW-3.

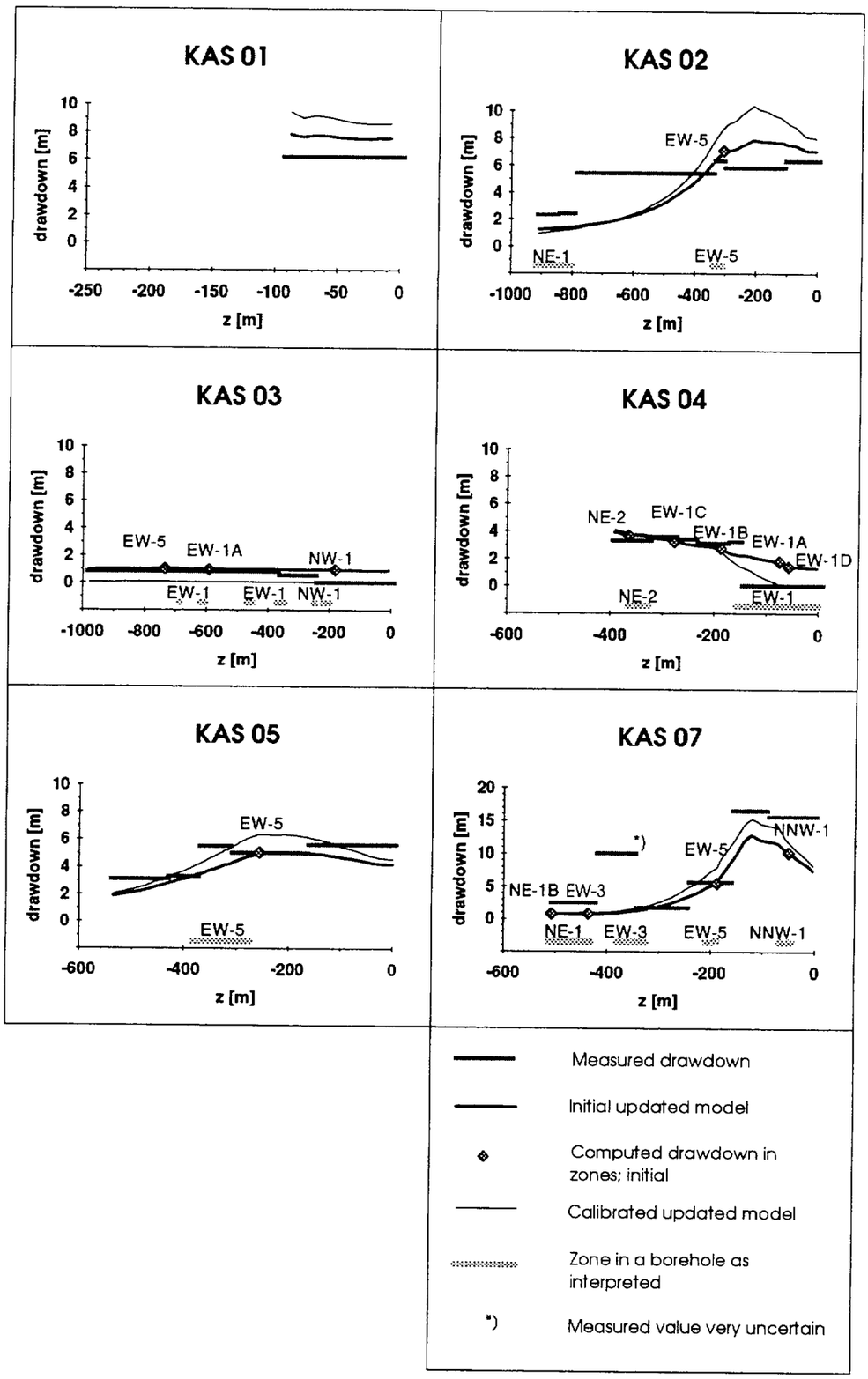

Measured and simulated pressure drawdowns in the cored boreholes for the LPT2 test. The computed results are for steady-state simulations and for the updated structural model of the Äspö site. The experimental values are the drawdowns measured at the end of the pumping period.

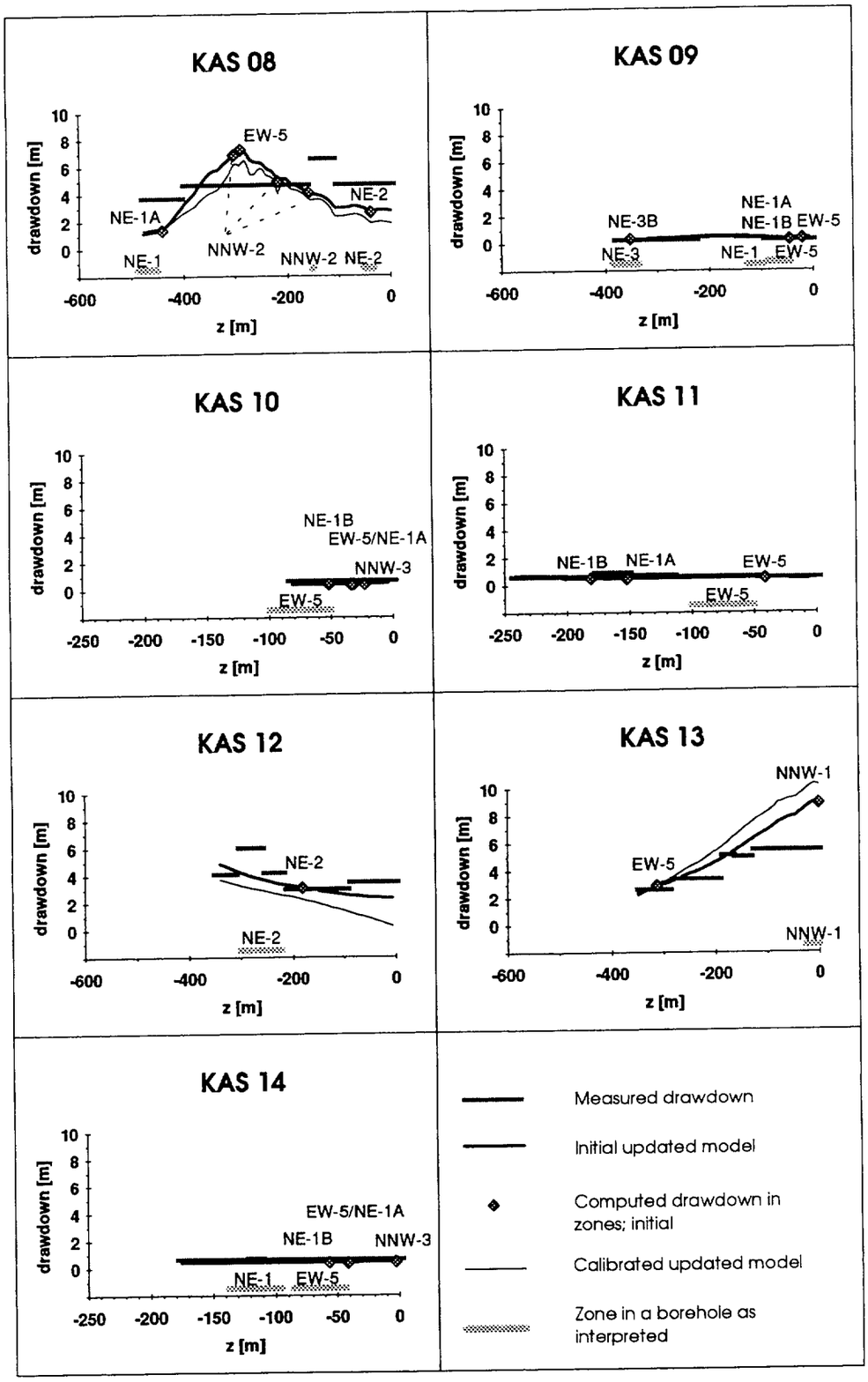
KAS 08
drawdown [m]
z [m]
EW-5
NE-2
NE-1A
NE-1
NNW-2
NNW-2
NE-2
KAS 09
drawdown [m]
z [m]
NE-1A
NE-3B
NE-1B
EW-5
NE-3
NE-1
EW-5
KAS 10
drawdown [m]
z [m]
NE-1B
EW-5/NE-1A
NNW-3
EW-5
KAS 11
drawdown [m]
z [m]
NE-1B
NE-1A
EW-5
EW-5
KAS 12
drawdown [m]
z [m]
NE-2
NE-2
KAS 13
drawdown [m]
z [m]
NNW-1
EW-5
NNW-1
KAS 14
drawdown [m]
z [m]
EW-5/NE-1A
NE-1B
NNW-3
NE-1
EW-5
Measured drawdown
Initial updated model
Computed drawdown in zones; initial
Calibrated updated model
Zone in a borehole as interpreted

1 INTRODUCTION

1.1 BACKGROUND

The Swedish Nuclear Fuel and Management Company (SKB) is currently excavating an access tunnel to an underground research laboratory called the Äspö Hard Rock Laboratory (HRL). The laboratory will be constructed below the island of Äspö, which is located in southeast Sweden, about 20 km north of the town of Oskarshamn. The HRL project is a part of SKB's program aimed to support the design and construction of a deep repository for nuclear waste and to identify and investigate a suitable site for the repository. The main goal of the HRL project is to study various methods of investigating and modelling a fractured crystalline bedrock and the phenomena involved. In addition, some optional construction techniques for deep excavations are tested in practice. The goals, objectives and execution of the HRL project are discussed in detail in a background report to SKB's RD&D-Programme 92 /SKB, 1992/.

The HRL project is divided into three main phases. In the pre-investigation phase, the Äspö island was selected to be the location of the underground laboratory. Field investigations were conducted on the island, both at the surface and in a number of boreholes. The pre-investigation phase also included a study of making preliminary predictions for the conditions in the excavation area. The laboratory is excavated in the construction phase scheduled for years 1992 - 1994. During the excavation, the predictions as well as the pre-investigation methods are evaluated. The updated characterization of the bedrock is taken into account in the final layout of the laboratory and when locating various experimental areas. The third phase is the operating phase, and its program is currently under planning.

1.2 OVERVIEW OF THE LPT2 TEST

The pre-investigation phase involved geological, geophysical, geo-hydrological and hydrogeochemical field studies. The hydraulic experiments included pumping tests in which open boreholes were pumped to identify major water-bearing structures. A long-term pumping and tracer test was performed in borehole KAS06 (Figure 1-1). This experiment is called LPT2.

Borehole KAS06 is 600 m long. During the experiment, it was open and was pumped for about three months /Rhén et al., 1992/. The pumping rate was 2.25 l/s for the most part of the pumping period. The drawdown of the pressure in the withdrawal hole as well as in most of the other boreholes in the area was monitored during the pumping. The drawdown of the water level in KAS06 was about 52 m at the end of the pumping period. The

measured final pressure drawdowns in the observation sections of the other boreholes are presented in Appendix B. The drawdown was still increasing in many of the observation sections when the pumping was stopped. The recovery period lasted another month.

Several tracers were injected during the pumping in six packed-off sections in five boreholes (KAS02, KAS05, KAS07, KAS08 and KAS12, cf. Figure 1-1). Tracers from three injection sections were detected in the withdrawal borehole. The distribution of the tracer inflows along KAS06 was measured. The quantity of groundwater flowing through the tracer injection sections was also measured with the dilution technique /Rhén et al., 1992/.

The distribution of the groundwater inflow to borehole KAS06 was measured with a spinner /Nilsson, 1990/. The spinner survey did not, however, cover the first 100 m of KAS06, and the inflow to the top part of the borehole was estimated from the tracer data /Rhén et al., 1992/.

The execution and results of the LPT2 pumping and tracer test are reported in detail by Rhén et al. /1992/. Nilsson /1990/ evaluates the other hydraulic experiments conducted in KAS06.

1.3 OBJECTIVES AND SCOPE OF THE STUDY

The LPT2 test was selected as the first exercise to be studied by the Äspö project's Task Force on the modelling of groundwater flow and transport of solutes. The modelling of the LPT2 test was divided into two tasks, 1A and 1B, concerning the pumping test and the tracer experiment, respectively.

The Task Force defined the following performance measures for Task 1A /Ström, 1992/:

1) The calculated and measured drawdown of the pressure as a function of the distance for the observation boreholes. The difference between the calculated and measured drawdowns as a function of the distance.

2) A list of calculated drawdowns with absolute and relative deviations.

3) The computed and measured drawdown as a function of time for observation sections considered interesting.

4) The calculated quantity of groundwater flowing through the tracer injection sections.

5) Distribution of the calculated water inflow in the withdrawal hole.

The experimental results needed in evaluating the performance of a model were reported by Rhén et al. /1992/.

This study covers the numerical simulations of the groundwater flow conditions during the LPT2 test. Results for the performance measures given above are presented. The tracer experiment part of the LPT2 test is studied in the second part of this report /Hautojärvi, 1994/.

The primary motivation of this study was an opportunity to improve our understanding on the Äspö site. The analysis of the LPT2 tests helps to characterize groundwater flow in the bedrock by facilitating the creation of a realistic flow model for the site. The modelling of the LPT2 test is one step in the process of developing, testing and adjusting the flow model. The other pumping tests, especially the other long-term pumping test, LPT1, can and must be utilized as well. The superiority of LPT2 over the other pumping tests is the long duration of the pumping period and the most comprehensive data set. The flow model developed may be used in designing future field experiments and in predicting their results. It can also be utilized when simulating the flow conditions after the completion of the laboratory excavations.

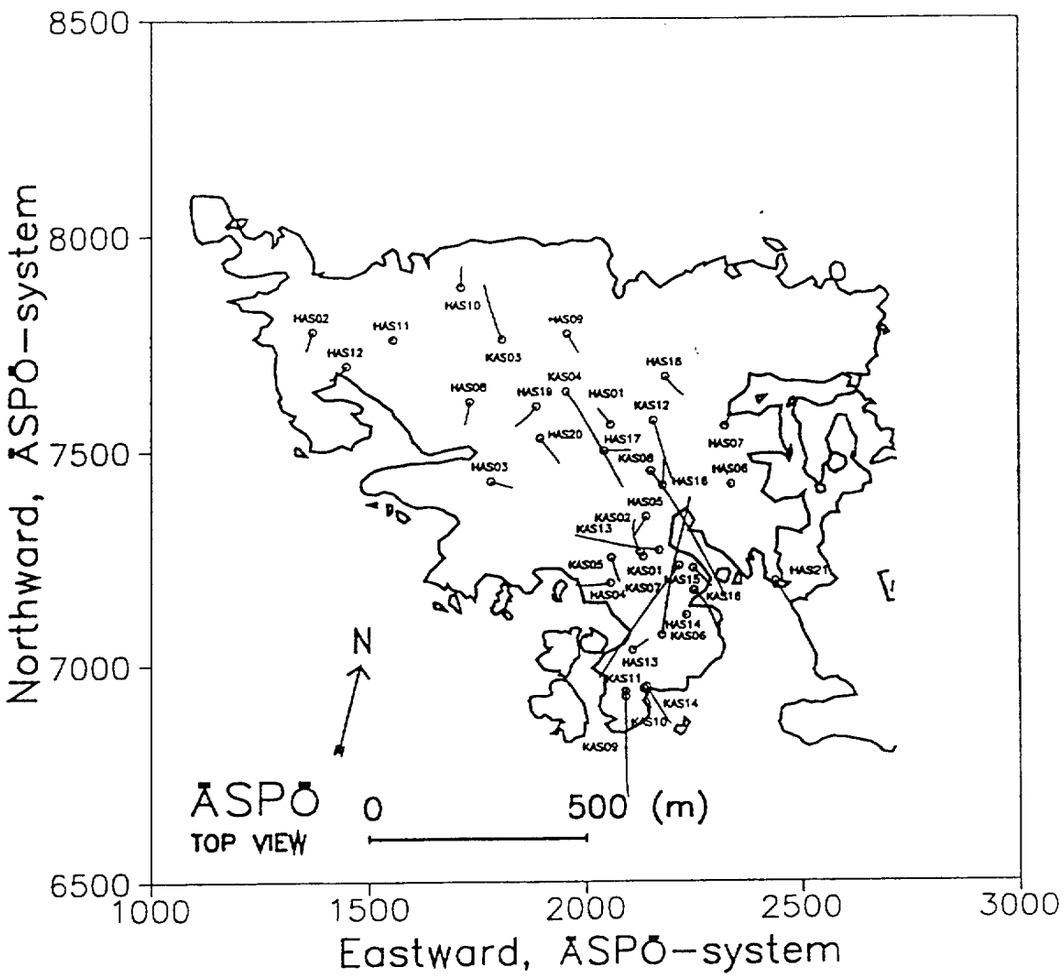

Figure 1-1. *Äspö island and the location of the boreholes /Forsmark, 1992a/.*

The objectives of the study affected how the modelling was carried out. As we were mainly interested in the groundwater flow on a site scale, small-scale models or LPT2-specific models were not applicable. The support of the LPT2 simulations in the development of a site-scale flow model is optimized by applying the same approach as is applied on a site scale.

1.4 THIS REPORT

This report summarizes the modelling study of VTT for both the base structural model and its update. During the modelling new information on the site, on the LPT2 test and on the other field investigations was received. The structural model of the bedrock, i.e., the geometry of the fracture zones evolved. The modelling was nevertheless always based on the latest structural model available. A consequence of this was that it was not considered rational to complete fully the modelling efforts concerning the early structural models. We were, however, encouraged to report the modelling results computed for the base structural model given by Wikberg et al. /1991/ although the corresponding flow model was calibrated only tentatively. We concentrated on the updated structural model which is reported by Ström /1993/.

The modelling study was performed in the framework of the Task Force and this report is written according to the directives given by the Task Force. The reporting of the computed values for the performance measures is emphasized. We discuss only briefly the calibration phases, which actually were the most time-consuming stages of the study.

Simulation results and performance measures are presented for both the initial and calibrated flow models. As the modelling performed for two structural models and for their initial and calibrated versions are presented, four sets of results for the performance measures are reported. The sets of the results are not complete for all of the cases, however.

This report is organized in the following manner. The evolution of the structural model of the Äspö site is introduced in Chapter 2. Chapter 3 discusses the main concepts and assumptions applied as well as the modelling approaches and computer codes employed in this study. The modelling, calibration and simulation results for the base structural model are presented in Chapter 4. The simulations based on the updated structural model are discussed in Chapter 5. Chapter 6 summarizes the results and conclusions.

2 STRUCTURAL MODELS OF THE SITE

The structural model for the Äspö area evolves continuously along with the improved understanding and updated interpretation of the results of field investigations. The flow models dealt with in this report are based on two structural models, which represent different stages of the model evolution. These structural models are called the "base model" and "updated model", and have been reported by Wikberg et al. /1991/ and Ström /1993/, respectively. The layouts at the ground level of these structural models are shown in Figures 2–1 and 2–2. The fracture zones with identifying markings are more than about 5 m wide and they extend over several hundred meters. In addition to the surface layout shown in Figure 2–2, Ström /1993/ defined each fracture zone in the updated model with three points on the plane of the zone.

According to Figures 2–1 and 2–2, the largest difference between the base and updated structural models is that the subzones of NE-1 were modified to intersect at the ground surface. The EW-5 zone was also moved northward about 50 m. It should, however, be noted that this zone was drawn in the former location in Figure 2–2 /Ström, 1993a/.

The extent of the fracture zones is in many cases uncertain. Even though several fractures zones are classified as "certain" at the Äspö site, their regional extensions are not generally known as indicated in Figures 2–1 and 2–2. The depth extent of the zones is not explicitly reported.

The two structural models formed the basis of the flow simulations. Sections 4 and 5 describe the characteristics of the models in detail as well as discuss the differences between them.

To avoid confusion, this report uses a slightly different naming convention of the zones than those of Wikberg et al. /1991/ and Ström /1993/. Besides a structural model, Wikberg et al. /1991/ provided a simplified geohydraulical flow model, and they attached extension "w" to the name of a fracture zone when referring to the zone in their flow model (see Figure 2–1). This naming convention was introduced to distinguish the flow-model zones from those in the structural model but not included in the flow model. On the other hand, Ström /1993/ used the "w" extension to stand for a "water-bearing structure".

In this report we omit the extension "w" unless it is needed for the sake of clarity when citing these two references. For the updated geometry, we also separate subzones by capital letters (A, B, C etc.) in the numerical modelling. For example, EW-1 comprises four subzones, which we call EW-1A, EW-1B, EW-1C and EW-1D (see Section 5.1.1).

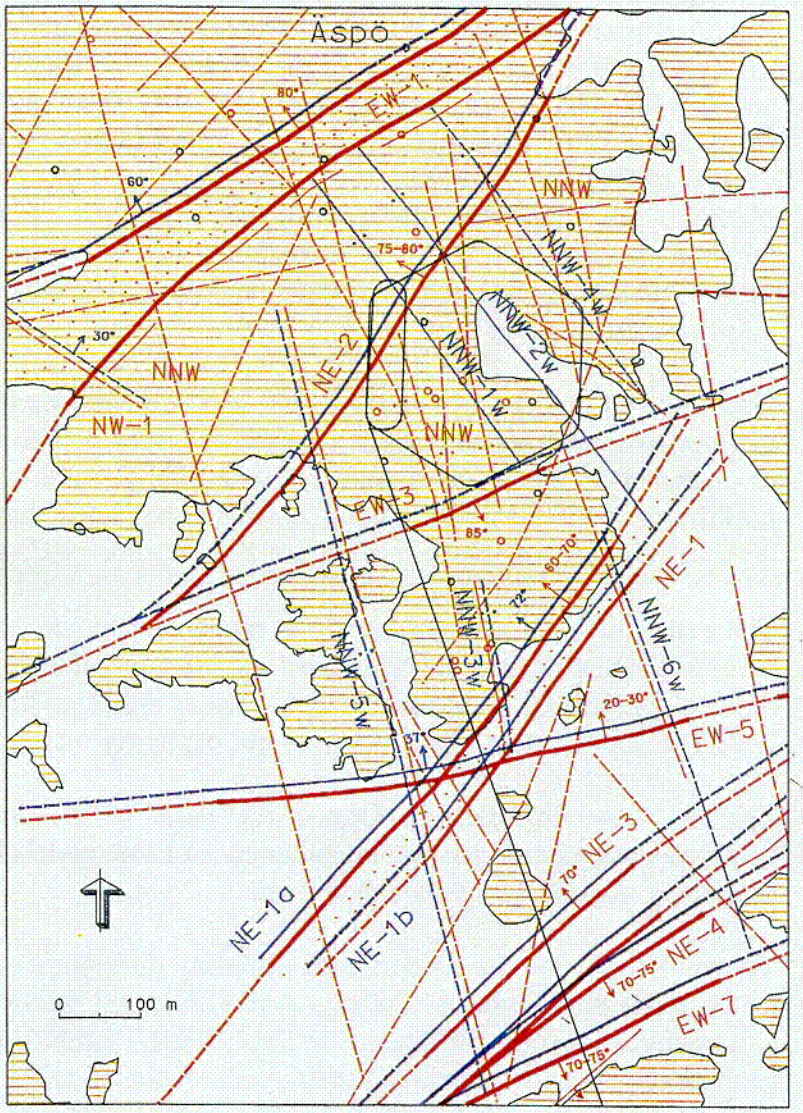

Figure 2–1. *Base structural model for the Äspö area at the ground level /Wikberg et al., 1991/. A solid line means that a fracture zone is confirmed by borehole or surface investigations. A blue line indicates a certain hydraulic conductor and a dashed blue line means a possible hydraulic conductor.*

C-01

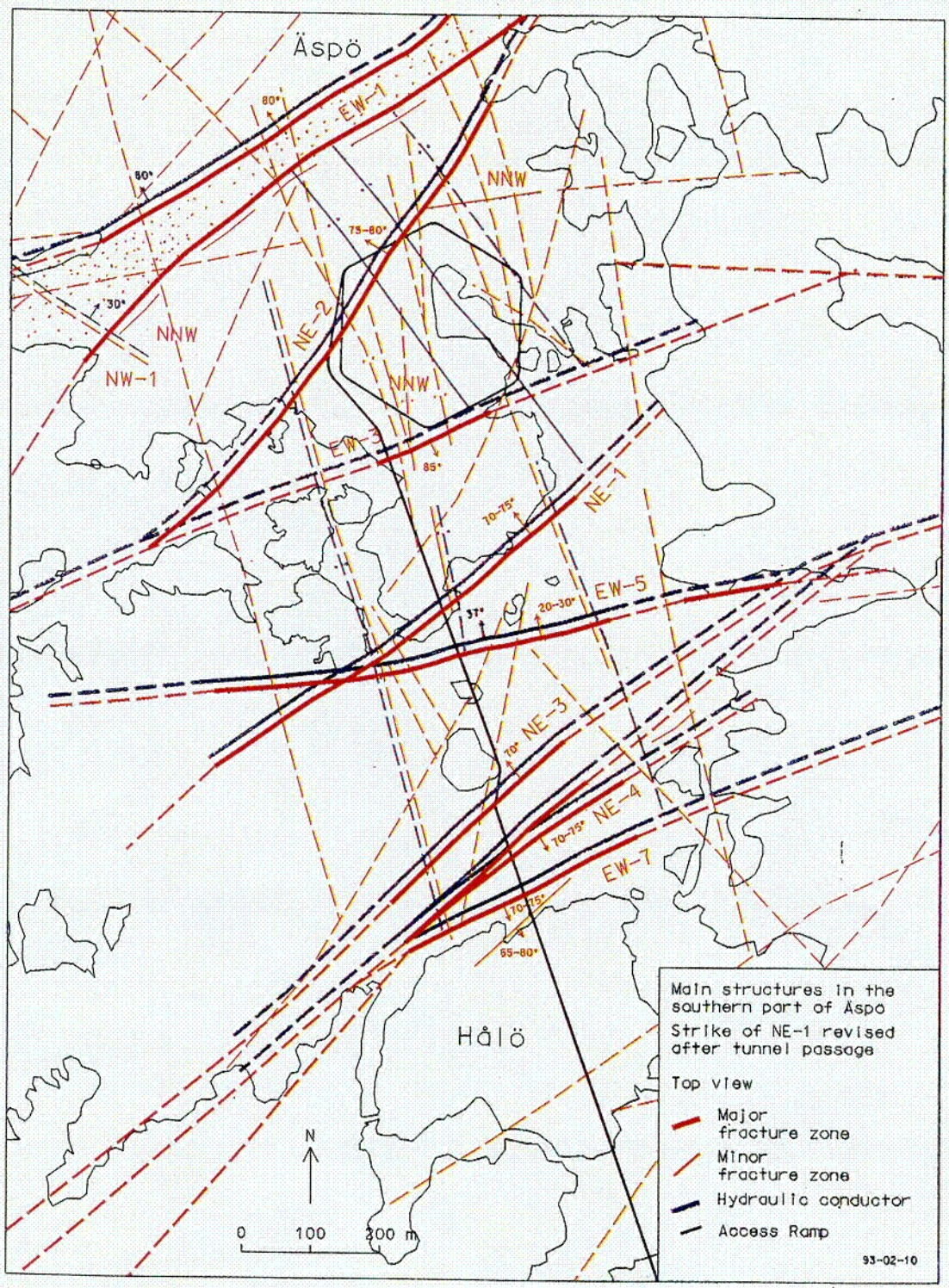

Figure 2–2. *Updated structural model for the Äspö area at the ground level /Ström, 1993/. A solid line means that a fracture zone is confirmed by borehole or surface investigations. A blue line indicates a certain hydraulic conductor and a dashed blue line means a possible hydraulic conductor. Fracture zone EW-5 is drawn 50 m to the south from its estimated location /Ström, 1993a/.*

C-02

3 MODELLING APPROACH

3.1 THE BASIC ASSUMPTIONS

The proportion of groundwater in the bedrock is typically very small even in the saturated zone. The flow of water is driven by pressure differences, which in natural, hydraulically undisturbed conditions are attributed to the undulating water table. Precipitation sustains the undulation of the water table. The portion of the rainfall infiltrating into the bedrock depends on the water table and on the hydraulic properties of the soil and bedrock. For instance, the calculations concerning the regional area surrounding Äspö (i.e., the Simpevarp area) and based on various methods gave 10 mm /Grundfeld et al., 1989/ and up to 60–125 mm /Liedholm et al., 1987/ for the average annual infiltration rate into the bedrock.

Besides the pressure differences, the variation in the density of the groundwater may significantly affect the groundwater flow since the heavier water seeks lower. The largest differences in the density are commonly caused by the varying salt concentration. The salt content of groundwater usually increases with the depth. High salt concentrations can also be found relatively close to the surface, especially in coastal areas. Another factor resulting in density differences is the temperature. The temperature also affects the flow characteristics of water through the viscosity. Although the temperature of the bedrock increases with depth, its influence is insignificant compared to that of the salinity. The uncertainties associated with the geometry of fracture zones, the hydraulic properties of the bedrock and the boundary conditions of a simulation model are also far more important than the natural temperature differences.

In a crystalline rock, water flows unevenly through an intricate network of preferred paths formed by fracture intersections and the flow channels on fracture planes. Field investigations indicate that groundwater flow may be very discretely distributed over the rock, i.e., water flows along paths with little contact to other paths /e.g., Neretnieks et al. 1990/. Accordingly, there are scales on which the hydraulic properties of the crystalline bedrock are evidently different from those of a homogenous medium.

Fracturing in the bedrock varies. In the "intact" rock, called the rock matrix in this report, the fracture density is low resulting in a heterogenous and discontinuous character with low hydraulic conductivity. Zones with high fracture density possess in turn a greater ability to conduct water even though the correlation between the fracture density and the hydraulic conductivity is often unclear. The fracture zones are also commonly heterogenous. The same applies to an individual fracture, the hydraulic properties of which may vary on very small scale. The variations in the

hydraulic properties of the fractures and in the fracture density actually cause the heterogeneity of the bedrock.

When modelling groundwater flow in the bedrock, the characteristics of the bedrock need to be considered. From a conceptual point of view, the study of water flow in a fractured rock may be carried out by adopting various models. The selection of the modelling approach is affected by the results wanted, the data available and some practical limitations like computational resources. The results required also determine the scale of interest, which may influence the feasibility of various methods.

The hydraulic properties of the bedrock often vary significantly even on a local scale but the small-scale local heterogeneities may be omitted if water flow on a large scale is analyzed. It is then assumed that a subvolume of the bedrock can be treated as a continuum. In this equivalent-continuum approximation, the hydraulic properties of the subvolume are chosen such that the real volume concerned and its representing equivalent continuum as whole behave identically considering the water flow. The smallest volume having that feature is often called the representative elementary volume (REV). The equivalent properties depend on several fracture parameters (permeability, density, size and orientation distribution). Yet the existence of the REV is not certain in practical applications.

There are modelling approaches that deal with the bedrock more realistically than the equivalent-continuum approximation. For instance, in the fracture network modelling, the fracture system of the bedrock is considered. Each significant fracture is in principle simulated. Due to practical limitations, fractures are treated with statistical methods and the values characterizing the appropriate distributions are based on the interpretations of field investigations. Commonly, the dominating conceptual model that considers the impact of each fracture is the parallel-plate concept, i.e., there is no channelling inside an individual fracture. In this type of fracture network modelling, the continuum approximation is thus also employed but on a fracture scale.

The influence of the heterogeneity of a medium is studied by means of numerical simulations in Appendix C. The ratio of the scale of heterogeneity to the scale of interest is the decisive factor. If that ratio is small, i.e., the scale of interest is much larger than the scale of heterogeneity, the equivalent-continuum approximation is justified. Furthermore, whichever modelling approach is applied, the scale of the heterogeneity should be known.

The justification of the continuum approximation is often questionable in practical applications. One reason for this is the scarcity of field data (see, e.g., Carlsson, 1987). The selection of equivalent hydraulic properties is difficult and constitutes a major source of uncertainty in flow analyses. On the other hand, a study by Herbert & Gale /1989/ dealing with a densely fractured hard rock concludes that it is possible to define a relatively small scale of fractured rock on which the continuum approximation is valid.

Modelling results have to be interpreted taking into account the assumptions of the approach applied. From the standpoint of the groundwater flow itself, the equivalent continuum approach is not very restrictive. The pressure fields and average fluxes can reliably be computed. To study groundwater flow locally, we must know or assume more on the variation of the properties of the bedrock. The results from the modelling on a larger scale can nevertheless be used to determine boundary conditions for local models. The continuum approximation becomes more restricting when transport phenomena are studied.

This study employs the assumption that the bedrock can be divided into zones having higher hydraulic conductivity than the rock matrix comprising the rest of the bedrock. The hydraulic properties of zones and the rock matrix vary in space. The scale of heterogeneity in both of them was assumed to be small compared with the distances between the withdrawal hole and the observation boreholes. The equivalent-continuum approximation can thus be used when computing the pressure response. Values for the groundwater flux calculated from the equivalent properties and from large-scale pressure gradients are average fluxes for areas/volumes significantly greater than the scale of the heterogeneity. The scale of the dominating heterogeneity is assumed to be large compared to the diameter of the boreholes and therefore the equivalent-continuum fluxes are not expected to be close to the measured values. The assumption on the scale of the heterogeneity can, however, be used to study stochastically the amount of water flowing through the tracer injection sections.

3.2 GROUNDWATER FLOW MODEL

The concept of a flow model was utilized in this study. A flow model is a representation of the real system. It includes geometrical parameters (the geometry of fracture zones) and hydraulic properties. In practical applications, flow models are simplifications of the real systems concerned. In fact, a flow model should be as simple as possible and still hydraulically equivalent with the real system. Uncomplicated models are easy to handle, understand and modify.

The concept of the flow model also provides a measure for data management and documentations. The objectives of the flow analysis, the prior information on the system, the modelling approach, the general knowledge of groundwater flow, the numerical method and the computer codes affect how a flow model is constructed from a structural bedrock model.

The groundwater flow model of the Äspö area is summarized in Table 3–1. The domain to be modelled was divided into hydraulic units: the rock matrix with low hydraulic conductivity and fracture zones with high hydraulic conductivities. For each zone and the rock matrix, equivalent-continuum values of the transmissivity and hydraulic conductivity, respectively, were assigned on the basis of the prior data. The corresponding

average values of transmissivities needed in the small-scale stochastic simulations were determined (the method introduced in Appendix C). The standard deviation of the logarithm of the transmissivity was assumed to be equal to unity.

Each hydrogeologic unit in the flow model is assumed to be homogeneous and isotropic. It is likely, however, that anisotropy is present due to lithostatic mechanical stresses and an anisotropic fracture network in the bedrock. These phenomena, on the other hand, include considerable uncertainties preventing any quantitative evaluation of their influences.

The flow model constructed using the prior data from field measurements and their interpretations is called initial model to distinguish it from the calibrated flow model. In calibration, the parameters of the flow model are adjusted, not those of an individual spatial discretization, like an element mesh.

Table 3–1. Characteristics of the groundwater flow model of the Äspö site.

GROUNDWATER FLOW MODEL OF THE ÄSPÖ SITE	
Process description Continuity equation Equation of motion (Darcy's law including effects of variable density of water)	
CONCEPTS	DATA
Geometric framework and parameters	
3-D volume divided into: (i) 2-D fracture zones (location, orientation, extent) (ii) Rock matrix	Zone geometry from the structural model
Bedrock properties	
Transmissivity (zones), hydraulic conductivity (rock matrix), specific storage, dispersion lengths, molecular diffusion coefficient, porosity	The initial equivalent-continuum values of T and K from the prior data, and the final values are searched in calibration; Heterogeneity: the average of K and T to result in the equivalent-continuum values, st.dev(log(T)) = 1; The others based on general knowledge
Spatial assignment model	
Deterministic or stochastic approach applied depending on the quantity in question (pressure field, salinity, flux etc.) and the modelling scale	
Salinity model	Salinity field from the prior data when prescribed salinity used

Following the evaluation of the structural model, several flow models have also been created for the Äspö area. This work concentrates on those two flow models that were created for the base structural model and for the updated structural model. The corresponding flow models are also called the base and updated flow models. Detailed description of these flow models for the Äspö site is given in Sections 4.1 and 5.1.

3.3 MATHEMATICAL MODEL

The mathematical model for the flow of groundwater is based on the assumption that a sub-volume of the bedrock can be treated as an equivalent continuum, in which the water flow is caused by the pressure field. We ignore the effects of other physical phenomena (e.g., turbulence) and chemical reactions, and assume that Darcy's law is valid. Darcy's law expressed in terms of the residual pressure p (i.e., the actual pressure without the hydrostatic component caused by fresh water) at point (x,y,z) can be written as follows (see, e.g., Bear /1979/)

$$\boldsymbol{q} = -\frac{\boldsymbol{k}}{\mu}\nabla(p+(\rho-\rho_0)gz) \ . \qquad 3\text{-}1$$

Here $\boldsymbol{q}$ is the Darcy velocity (m/s), $\boldsymbol{k}$ is the permeability (tensor) of the medium (m^2), ρ is the density of water (kg/m^3), ρ_0 is the density of water with zero concentration (fresh water), μ is the viscosity of water (kg/m^3) and g is the gravitational acceleration (9.81 m^2/s). When substituted to the law of conservation of the mass

$$\nabla\cdot(\rho\boldsymbol{q}) = 0 \ , \qquad 3\text{-}2$$

Equation 3-1 yields a flow equation

$$\nabla\cdot\left(\frac{\rho\boldsymbol{k}}{\mu}\nabla(p+(\rho-\rho_0)gz)\right) = 0 \ . \qquad 3\text{-}3$$

Equation 3-3 is valid for steady groundwater flow with no sources or sinks. The general time dependent form of the flow equation is

$$\nabla\cdot\left(\frac{\rho\boldsymbol{k}}{\mu}\nabla(p+(\rho-\rho_0)gz)\right)-\rho Q = \frac{\partial(\rho\phi)}{\partial t} \ , \qquad 3\text{-}4$$

where Q is the flow rate per unit volume (1/s) representing sinks (−) or sources (+) and ϕ is the total porosity. The right-hand side takes into account the compressibility of the water (change in the density) and the medium (change in the porosity of the rock).

The solute transport equation can be expressed as follows

$$\nabla\cdot(\rho \boldsymbol{D}\nabla C)-\nabla\cdot(\rho \boldsymbol{q}C)+\rho Q_{in}C_{in}-\rho Q_{out}C = \frac{\partial(\rho\phi_k C)}{\partial t} , \qquad 3\text{-}5$$

where C is the concentration of a solute (kg/m^3). The first term in the left-hand side represents mass transport by dispersion, which is characterized by the dispersion coefficient (tensor) $\boldsymbol{D}$ (m^2/s). The second term corresponds to the advection of the solute with the flow. The third and fourth term represent sources and sinks, respectively. The right-hand term, besides including the influence of the compressibility of water and the change in the kinematic porosity ϕ_k, takes into account the temporal change in the concentration.

The components of the dispersion tensor are

$$D_{ij} = \varepsilon_T|\boldsymbol{q}|\delta_{ij}+(\varepsilon_L-\varepsilon_T)\frac{q_i q_j}{|\boldsymbol{q}|}+\phi_d D^* ; \quad i,j = 1,2,3 , \qquad 3\text{-}6$$

where ε_L and ε_T are the longitudinal and transversal dispersion lengths (m), respectively, ϕ_d is the diffusion porosity, D^* is the molecular diffusion coefficient (m^2/s) in water and δ_{ij} is the Kronecker delta function.

The relation between the density and the salt concentration is formulated as

$$\rho = \rho_0+a_C C , \qquad 3\text{-}7$$

where a_C is the coefficient giving the dependence of the density on the salt concentration (a_C = 0.71 /CRC, 1971/).

Equations 3-1, 3-4, 3-5 and 3-7 form a general closed set of equations describing time dependent groundwater flow taking the effects of the salinity into account. In this work, however, we restrict to assess only special cases that are described in sections 4 and 5.

3.4 COMPUTER CODES

The numerical simulations of the groundwater flow were based on the finite element method. The programs employed can be divided into two groups. The HERO package comprises programs used in creating finite element meshes (Figure 3-1). With these codes, a base mesh consisting of three-dimensional elements (in three-dimensional case) is modified to correspond to the geometry and properties of the flow model as precisely as possible. The base mesh is created with PATRAN /1989/, which is a commercial pre- and post-processor for finite element codes, by exploiting its extensive support for the three-dimensional visualization hardware of graphical workstations. PATRAN is also used to visualize the results of flow simulations.

Fracture zones can be represented in element meshes with two-dimensional elements. They can be added in an optimal way on the faces or diagonals of three-dimensional elements by means of the PAAWI program. Each fracture zone is defined for PAAWI with the corner coordinates of one or more triangles or quadrangles. New two-dimensional elements are defined using the pre-existing nodes of three-dimensional elements.

Due to the finite resolution of the original three-dimensional mesh, the new elements cannot naturally be located along the plane of an arbitrary-orientated fracture zone. The ELMO program can be employed to optimize the planarity of the set of two-dimensional elements representing a planar part of the fracture zone. This is done by moving the nodes of each two-dimensional element onto the plane with which the element is associated. When adding two-dimensional elements, no new nodes are thus created and the nodal connectivity of the original elements is maintained. With this approach, it is possible to model complex geometries with ease. Finite elements for additional zones can also be included in the existing finite element mesh without any difficulty.

The POMO program is used to change the properties of the three-dimensional elements to model hydrogeologic features having three-dimensional characteristics on the modelling scale (like major zones or repositories). One-dimensional objects (such as boreholes and tunnels) can be described with one-dimensional bar elements added by the ONNI code. ONNI was not utilized in this study.

Flow simulations were performed with the FEFLOW code package developed at VTT for the analyses of groundwater flow. FEFLOW is based on the finite element method and it is capable of simulating fluid flow, heat transfer and solute transport in non-coupled and coupled situations (a brief summary on the code in Appendix A). Problems to be modelled can be steady state or transient. The code employs linear one-, two- and three-dimensional elements. The resulting matrix equations are solved using a direct frontal solver or an iterative solver, which is based on the Gauss-Seidel method. In coupled cases, a set of non-linear equations is solved applying the Picard iterative approach with under-relaxation. FEFLOW has been partly verified and validated through the participation in the international HYDROCOIN project /HYDROCOIN 1988, 1990, 1991 and 1992/. The core of FEFLOW consists of programs FPH1, FPH2 and FPH3 (Figure 3–1), which solve the desired quantities.

The derived quantities include flow paths computed with the FPATH program, the Darcy velocity calculated with the DVELO program and flow rates obtained with the FRATE code. In addition, the comparison of measured and calculated quantities is carried out with program GOODNESS, which can calculate the value of a pre-defined goodness-of-fit function.

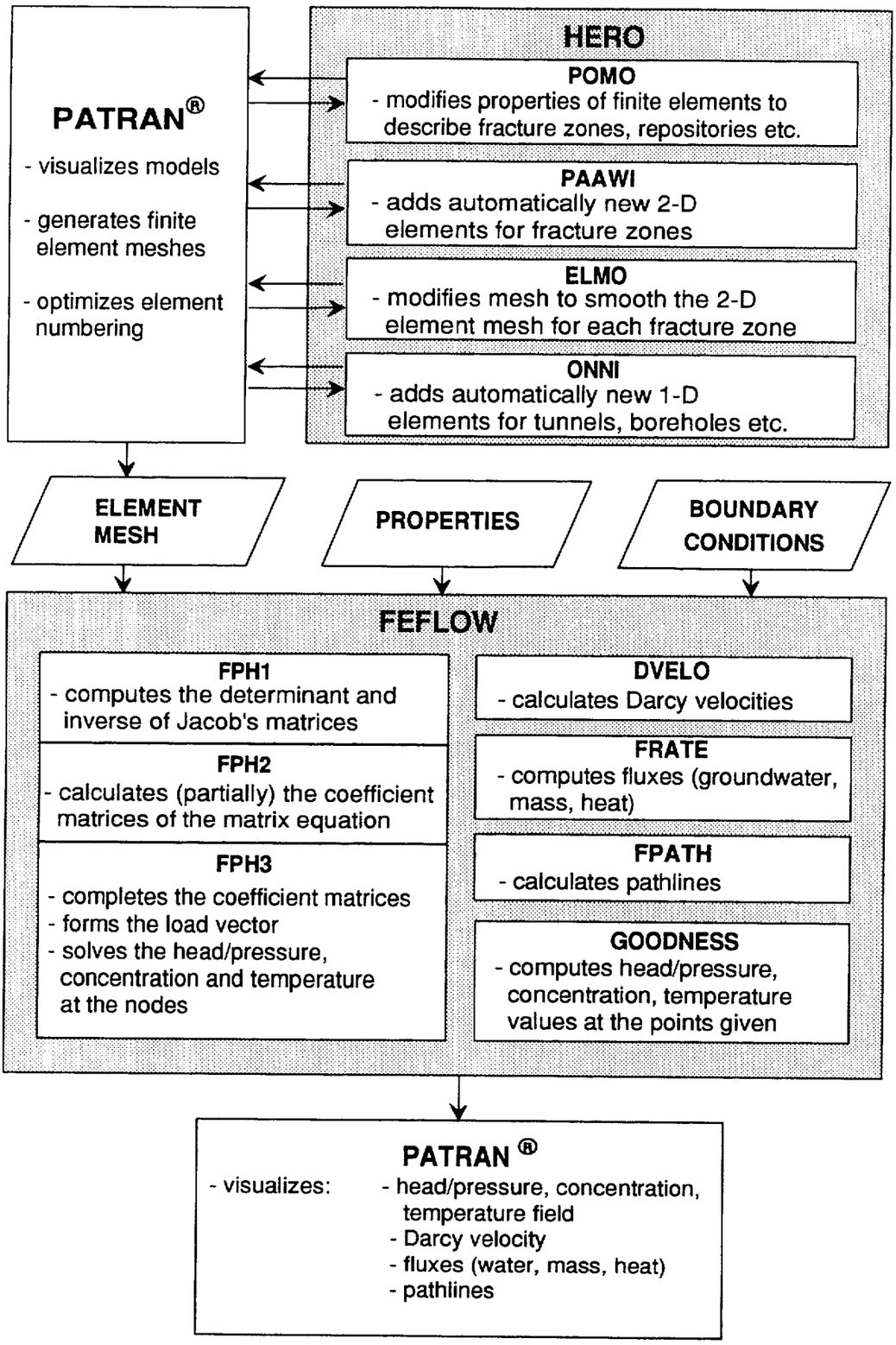

Figure 3–1. *The main components in the groundwater flow simulation system applied at VTT. PATRAN /1989/ is a commercial pre- and post-processing software for finite element codes.*

The INTER program can be employed when assigning boundary conditions for the top nodes of a mesh. It interpolates values for surface nodes using digitized equivalue contours of the water table.

A commonly applied technique in the field of numerical hydrogeological modelling is the use of a system of nested element meshes so that the boundary conditions for bordering faces of a smaller model are extracted from the solution computed with a larger model. The HBOUND program facilitates the labourless application of this technique.

3.5 SIMULATING HYDRAULICALLY UNDISTURBED CONDITIONS

Since the salt concentration of the groundwater at Äspö varies, the realistic simulation of the flow conditions calls for the coupled modelling of groundwater flow and salt transport. In this study the modelling of the undisturbed conditions is limited to the simulation of steady groundwater flow and salt transport described with the time-independent forms of Equations 3-4 and 3-5. Equations 3-4 and 3-5 are coupled through Equations 3-1 and 3-7.

Boundary conditions

For the upper boundary of the model domain, the boundary condition associated with the pressure is obtained from the equicontour map of the water table given by Wikberg et al. /1991/. This map is based on the average water levels measured in the boreholes between years 1987–1989 (Figure 3-2). For areas not covered by the borehole measurements, the water table was estimated from a regression curve representing the relationship between the water table and the topography. During 1987–1989, the level of the Baltic sea ranged from -0.5 to +0.8 m with reference to its mean value. The normal fluctuations are ± 0.3 m. The importance of the sea-level variations is small compared to the effects of the uncertainties associated with the other modelling assumptions, and they were not considered in the numerical simulations.

The vertical faces of the model domain were defined to follow the sea around the Äspö island. The pressure at the vertical boundaries was assumed to be hydrostatic. The drawback of this assumption is that it requires knowledge of the flow conditions on the boundaries. Furthermore, this assumption requires the information on the salinity distribution. The boundary conditions associated with the salinity are poorly known. Therefore, the effects of the salinity were studied by applying three different salinity models as explained at the end of this section.

The depth of the model domain for the simulation of the undisturbed conditions was 1500 m, where the no-flow boundary condition is presumed

to be valid. This is based on the assumption that the amount of the infiltrated water flowing deeper than 1500 m is insignificant.

Finite element mesh

The model domain was discretized into a finite element mesh according to the process described in the preceding section. The base mesh containing only three-dimensional elements representing the rock matrix was modified by adding two-dimensional elements for fracture zones. The mesh for the simulations of the undisturbed conditions is called the "*site model*". It contains about 32000 elements (Figure 3-3), the average element volume being slightly less than 50^3 m^3.

The physical properties were assigned to the elements by property identification numbers. Each property identification number is assigned to a set of parameters describing the properties of the hydrogeological unit that is represented by a set of the elements in the mesh. These properties include the transmissivities and storativities of the fracture zones, the hydraulic conductivity and specific storage of the rock matrix. The equivalent-continuum values were used (the values are given in Section 5.3.4). The dispersion lengths were selected as 100 m in the longitudinal direction and 10 m in the transverse direction. The porosity of zones and the rock matrix was chosen to be 10^{-4}.

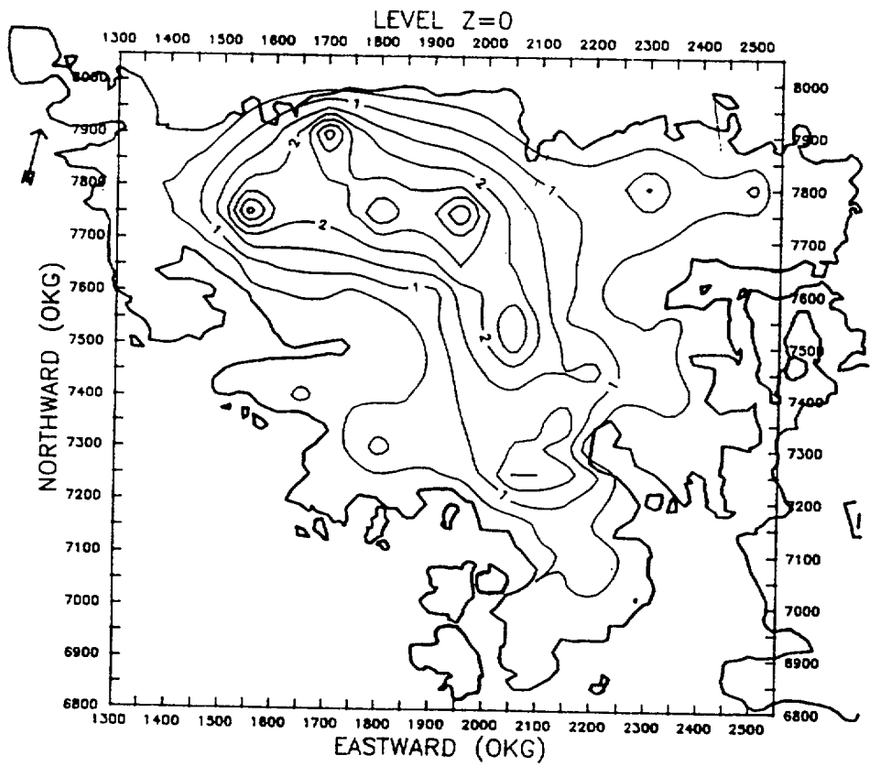

Figure 3-2. *Water table on the Äspö island under hydraulically undisturbed conditions /Wikberg et al., 1991/.*

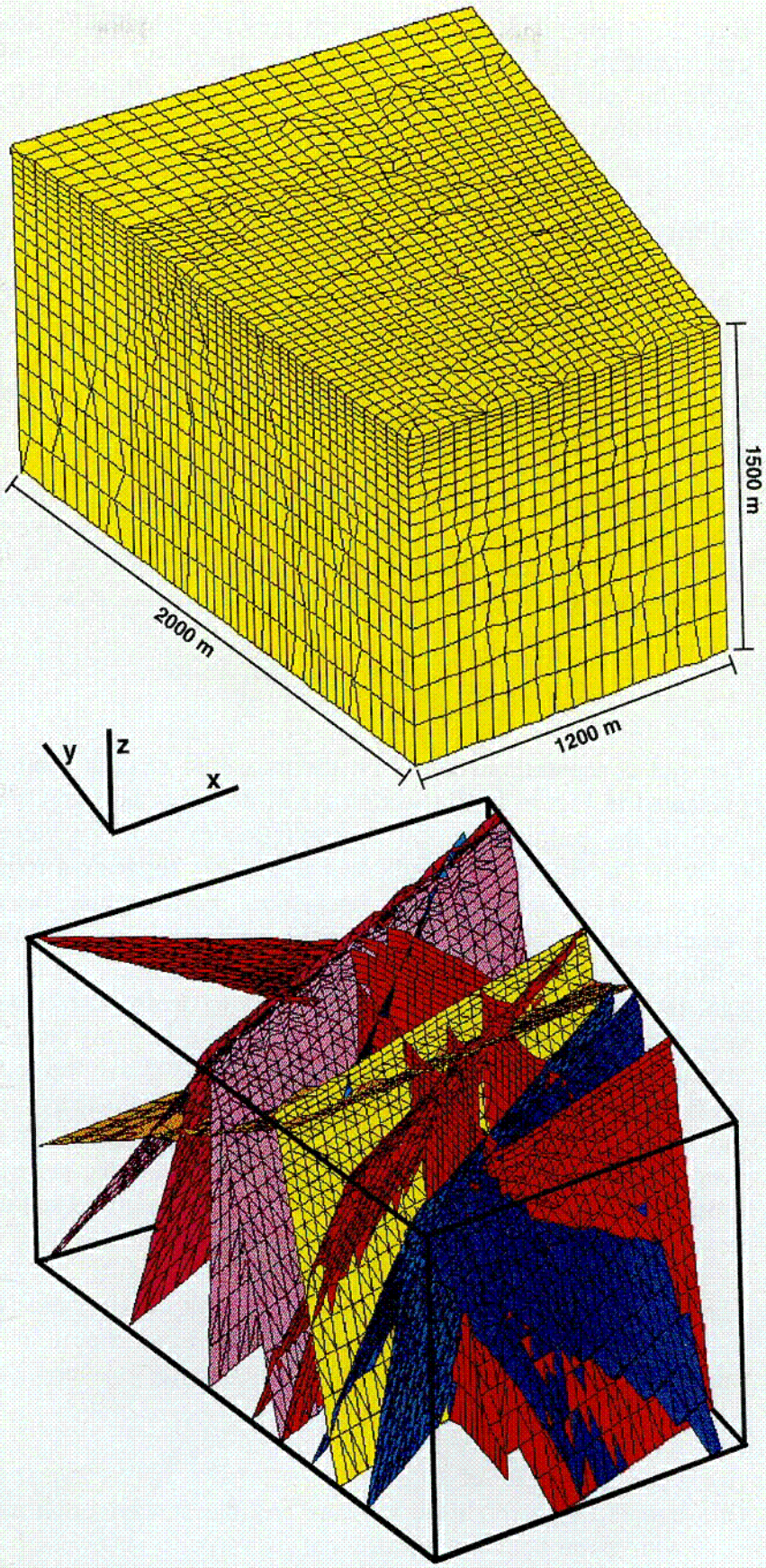

Figure 3-3. Site model (finite element mesh) for the numerical simulations of hydraulically undisturbed conditions. The three-dimensional elements are shown in the top and the two-dimensional elements in the bottom part.

C-03

Boundary conditions representing the prescribed hydraulic head, pressure, concentration (salinity) were assigned to appropriate nodes. The prescribed hydraulic head or pressure values for the top nodes were interpolated from the equivalue contours of the water table.

Salinity models

The differences in the density of the groundwater affect the flow conditions. The most important source of the differences in the density is the varying salt concentration of the groundwater. According to Wikberg et al. /1991/, the measured salinity at Äspö increases, roughly speaking, by 1 g/l per 100 m increase in depth.

Rhén & Forsmark /1993/ reported the measured electric conductivity as a function of the depth for the cored boreholes. They also gave a formula that relates the measured electric conductivities S (in units mS/m) and the salt concentration C:

$$C = \frac{4.67 \cdot 10^{-3}}{0.741} \cdot S \ . \qquad 3\text{-}8$$

The salt concentrations based on the measured electric conductivities are presented in Figure 5–10 (Section 5.3.2). It is worth noting that especially deep in the bedrock the salt concentration exceeds the value prevailing today in the Baltic sea (7 g/l), which strongly suggests a relict sea-water source and groundwater-rock interaction. Furthermore, there are large variations in the salinity and, obviously, the depth is not the only factor that influences the concentration. Since the last glaciation about 12000 years ago, the island of Äspö has been covered by freshwater lakes and saline seas. The most saline water existed during the Litorina stage that started about 7000 years ago and lasted until Äspö rose above the sea level some 3000 years ago. Sharp variations in the salinity may thus have resulted from the transient flow field caused by the land uplift. The high salt concentrations can also be a consequence of the periodic permafrost. Every time, when the permafrost penetrates deeper, it also drives salt deeper in the bedrock.

The dependence of the water density on the salt concentration is expressed in Equation 3-7. Three different salinity models were used as the basis of the calculations to study the effects of the salinity:

(i) fresh water
(ii) constant salinity of 10 g/l
(iii) coupled case (both the pressure and the concentration are computed with given boundary conditions).

The fresh-water model shows how well the observed pressure field can be understood by ignoring the effects of the salinity. The constant-salinity model shows, in turn, the effects of a salinity distribution, which is very

simple but still justifiable. The constant salinity value of 10 g/l is in a good agreement with the observed salinity for some boreholes (e.g., KAS09, KAS11 and KAS14) although it clearly contradicts the high salt concentrations observed deep in some boreholes (e.g., KAS02 and KAS03). On the other hand, because the measured salinity values highly exceeding the constant value occur only at great depths, the simple salinity model can be used to represent salt concentrations at the depths of interest, say, for a depth interval from 50 to 500 m.

In the coupled case, the boundary conditions for the salt concentration were defined such that on the upper boundary of the model, a value of 0 g/l was used for the area that represents the Äspö island and a value of 7 g/l for the area representing the area below the Baltic sea. On the upper part of the vertical boundaries ($-1000 \leq z \leq 0$ m), the concentration was assumed to increase linearly with the depth from a value at the surface level 7 g/l to 19 g/l. Below the depth of 1000 m, the concentration was assumed to be constant (19 g/l).

The calculated results concerning the flow under hydraulically undisturbed conditions comprise the pressure and salinity fields. They can be compared to the experimental values measured in a number of boreholes.

3.6 SIMULATING A PUMPING TEST

The modelling of the LPT2 test and the other pumping tests utilized in the calibration procedure was based on the principle of superposition. Only the influence of pumping on flow conditions was simulated. The dependent variable solved was the drawdown of the pressure. The infiltration to the bedrock was assumed to remain equal to the annual average and not having changed because of the pumping.

The model applied to simulate the pressure drawdown for the LPT2 test is summarized in Table 3–2. The computed drawdown field was used to determine the inflow of groundwater to the withdrawal hole. The change of the mean groundwater flux in the bedrock as a result of the pumping can also be estimated with the model. Yet, as stated above, the heterogeneity of the bedrock controls the local flux measured in field experiments and it has to be considered explicitly.

When modelling pumping tests, the effects of the salinity were not considered for two reasons. First, the actual distribution of the salinity over the bedrock of Äspö is not known, although some salinity values can be deduced from the electric conductivity measurements at several boreholes /Rhén & Forsmark, 1993/. Secondly, a pumping test simulation assuming a constant salinity (see Section 3.5) resulted in only about 5% maximum change in the pressure drawdown compared to the result of a fresh-water simulation. Omitting the salinity greatly simplifies the numerical calculations since only the pressure (drawdown) field governed by Equation 3-4 needs to be solved.

Table 3–2. Simulation model of the LPT2 test for the pressure drawdown.

SIMULATION MODEL FOR LPT2 - DRAWDOWNS Equivalent continuum	
Process description Implicit continuity equation (mass rate) Equation of motion (Darcy's law)	
CONCEPTS	DATA
Mesh characteristics	
Mesh covers large area 3-D elements for the rock matrix 2-D elements for zones 1-D elements for the withdrawal hole	Size: 12 km^2×1.5 km Irregular finite element mesh 17000/18000 elements
Element properties	
Zones: transmissivity, storativity Rock matrix: hydraulic conductivity, specific storage	According to the flow model (Table 3-1)
Boundary conditions	
No-flow or no-drawdown for the faces Pumping: measured drawdown or pumping rate	The area of the island: no-flow Other boundaries: no-drawdown Relevance and need to modify studied in calibration
Numerical tool	
FEFLOW	
Output parameters	
Drawdown of the pressure (Derived parameters: inflows, average Darcy velocity)	

In order to simulate numerically the LPT2 test and the other pumping tests, specially crafted test-specific finite element meshes were created. In this report term "pumping model" refers always and only to a finite element mesh that is used for a numerical simulation of a pumping test.

The element meshes for the numerical simulations of the pumping tests are based on a base mesh, which is modified to follow to the orientation of a withdrawal hole and to the geometry of the flow model. The base model contains only three-dimensional elements representing the rock matrix and one-dimensional elements at the very centre of the mesh representing the pumping borehole (Figure 3-4). The radius of this cylindrical mesh is about 2 km. In modelling a pumping test (LPT2, for example), this mesh is moved to the location of the withdrawal hole (KAS06) and modified so that the array of the one-dimensional elements lay along the withdrawal hole. Next,

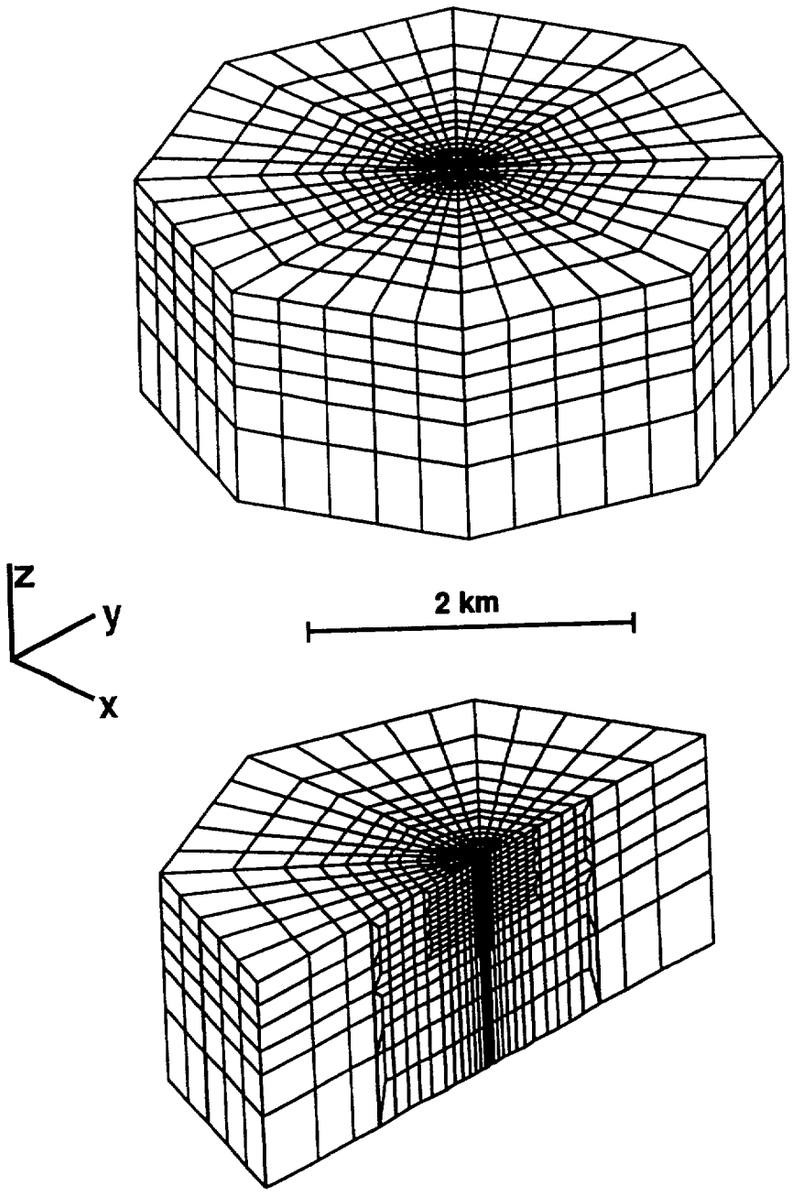

Figure 3-4. *Base finite element mesh for the numerical simulations of pumping tests. On the top the whole mesh and on the bottom a half of the mesh are shown. The base mesh contains only three-dimensional elements representing the rock matrix and one-dimensional elements representing the pumped borehole. The one-dimensional elements follow the vertical centre line of the mesh. The radius of the mesh is 2 km and the depth is 1.5 km. The one-dimensional elements extend to a depth of 500 m. For the numerical simulation of a pumping test, this centre is moved to the actual location of a withdrawal hole and the mesh is modified to correspond to the orientation of the hole. Two-dimensional elements are added to follow the geometry of zones. See the text for more detailed discussion.*

two-dimensional elements representing the fracture zones are added by means of the PAAWI and ELMO programs as described in Section 3.4. The influence of the observation sections was assumed to be insignificant and they were not incorporated in the simulation models. The total number of finite elements in the LPT2 pumping model created on the basis of the base structural model is about 17000 (18000 in the mesh for the updated model).

A difficult problem encountered in the finite element modelling of pumping tests is that a finite element mesh should comprise a large block of the bedrock to ensure that the effect of pumping does not reach beyond the boundaries of the mesh. The spatial discretization should also be very dense in areas where there is a significant gradient in the pressure due to pumping. On the other hand, the number of elements is limited by the available computational resources. These contrary requirements make the sizes of elements vary to a large extent. The horizontal extent of the elements varies from about 3 m next to the pumping borehole to about 150 m at the boundaries of the pumping model.

As only the change in the pressure was simulated and the infiltration rate was assumed to remain, no-flow boundary conditions were applied over the area of the island. For the rest of the model surface, i.e., for the areas under the sea, no-drawdown boundary conditions were used. Fixed-pressure boundary conditions were applied all over the side and bottom faces of the model, too. The significance of the boundary conditions of the side and bottom faces were studied by numerical simulations (cf. Section 4.2).

When calibrating the flow models, only steady state simulations of the pumping tests were performed. More resource-demanding transient simulations were performed only for the calibrated models. The evaluation of the steady-state simulations is not easy because steady state was not achieved in the field experiments. We, however, assumed that a pseudo-steady states were reached in the field experiments before pumping was stopped.

The simulations of the pumping tests were carried out applying two different implementations of the effect of pumping: the prescribed drawdown and the flow rate at a node connected to the withdrawal hole. The prescribed drawdown was derived from the drawdown measured in a withdrawal hole (taking into account the linearity of the shape functions used in the Galerkin approximation). The calculated total inflow to the pumped hole and its distribution were compared with measured values. On the other hand, the prescribed flow rate boundary condition, i.e., the applied pumping rate, was expected to result in the magnitudes of the drawdown corresponding to the values measured in the withdrawal hole. Both methods were applied in transient simulations carried out for the calibrated models.

In steady-state simulations, the drawdown measured in a pumped hole was assigned as boundary conditions to the nodes representing the withdrawal hole. The inflow to the pumped hole was then calculated and compared with the measured one. This approach simplifies the evaluation of the computed

drawdowns because the computed values can directly be compared. The difference between the measured and calculated total inflows is a consequence of the deviation of the hydraulic conductivities of a model from those of the bedrock. Accordingly, this approach is especially fruitful in adjusting model parameters.

The evaluation of the results of simulations in which the effect of pumping was introduced into the model by assigning the pumping rate applied in the field test would have been far more complicated. In this case, the total inflow to the pumped borehole would naturally agree with the pumping rate. However, as at least the initial values of the hydraulic conductivities in the model differ from the actual values around the pumping hole, the calculated drawdown in the pumping hole does not agree with the measured one. Consequently, the same ratio between the simulated and measured drawdowns would appear in the other boreholes, too. Even minor differences in the local hydraulic conductivities around the withdrawal hole would cause a significant contribution to the differences in the measured and computed drawdowns in the observation boreholes. The comparison of the spatial distributions of the modelled and measured drawdowns would require an adjustment of the drawdowns for the pumped hole. This is actually achieved directly by assigning the measured drawdown directly to the nodes representing the pumping hole.

When the inflow is used as a boundary condition, the drawdown for a node representing the pumped hole is not obtained directly from the numerical solution provided by the finite element method because of spatial discretization. The linear elements around the borehole approximate a radial drawdown field. On the other hand, the pumping hole has a finite radius whereas in a model it is represented by a node (or line). The actual drawdown can nevertheless usually be estimated accurately enough from the values computed for the nodes farther away from the pumped node. A two-dimensional approach can be used, since in practice at least one fracture zone intersects a pumping interval. Assuming a radial flow field, the drawdown in the pumped borehole section, $\Delta h(r_0)$, is obtained from the equation

$$\Delta h(r_0) = \Delta h(r_i) + \frac{Q_T}{2\pi T} \ln(r_0/r_i) \ , \qquad 3\text{-}9$$

where r_0 is the radius of the withdrawal hole, $\Delta h(r_i)$ is the drawdown computed for a node i at the distance r_i, Q_T is the inflow from the fracture zone of the transmissivity T. Several nodes around the pumped node were used and the actual drawdown was obtained as an arithmetic mean of the values calculated with Equation 3-9. The high hydraulic conductivity of the one-dimensional elements for the pumped section assumes that the drawdown is constant in the borehole elements.

When the drawdown was given as a boundary condition, the same drawdown was assigned for the whole withdrawal holes. In many of the pumping tests, the uppermost parts of the withdrawal holes were above the

level of water. The magnitude of the correct drawdown in those parts of the boreholes varies as a function of the depth. On the other hand, other phenomena, which are not considered can be significant, too. For instance, the fractures intersecting the withdrawal holes above the water level are not saturated and the two-phase flow of groundwater is involved.

3.7 CALIBRATING FLOW MODELS

The objective of the calibration process was to improve the agreement of a flow model with the real bedrock at the Äspö site. The initial flow models were based on the estimations made from field investigations. The fracture zones were identified at one point or at few points on the ground surface and/or in the boreholes, and their extent as well as transmissivity were predicted /Wikberg et al., 1991/. The hydraulic conductivity of the rock matrix was derived from point measurements. The predicted geometry of the zones naturally includes uncertainties and the initial values of the hydraulic parameters may not correspond to the values needed when applying the concept of an equivalent continuum.

The calibration studies involved analysing and selecting field experiments to be utilized in the calibration, computing parameters for which there exist experimental values, identifying the discrepancies between the calculated and measured results and deducing their sources, adjusting the model parameters, and re-computing. This iterative process was continued until a satisfactory agreement between the model and the field data was reached.

The agreement of a model with the real bedrock can be assessed quantitatively (by employing a goodness-of-fit function) or qualitatively (by visually comparing the computed responses against the field data). Both approaches have their advantages and disadvantages. The advantages of the quantitative assessment are the objectivity and easy ranking of the trial cases, and the drawbacks include the difficulty of defining a proper goodness-of-fit function. A reliable goodness-of-fit function was not attempted to be elaborated because of several reasons. First, the measurement errors are not quantified. Secondly, the weights of the various terms in a goodness-of-fit function arising from the drawdown, total inflow rate and distribution of the inflows were not identified. Thirdly, it would be a major task to develop weights for the information which various boreholes represent with their location relative to the withdrawal hole and the zones as well as the varying number and length of the observation sections. Fourthly, the varying density of observation boreholes over the site also introduces an unknown weight factor to the various differences. On the other hand, a visual check of the agreement often provides a better insight into the model's functioning, while a visualization system that is capable of efficiently showing the agreement is usually tedious to develop.

In this study, the evaluation of the goodness of the agreement between a flow model and the field data was mainly based on a qualitative assessment. In comparing the performance of the model in trial cases against the

measured data, the errors inherent in the simulation results and in the measured values were considered as well. Calculation and evaluation of a goodness-of-fit function during the calibration did not play a significant role. Although the sum of the squared differences between the computed and measured values was calculated, this measure had only a limited significance and did not prove informative enough in the calibration. For example, a specific zone in the flow model may occur in a borehole at a depth that corresponds to a different packed-off section than in reality. In this case the directly calculated difference between the computed drawdown and the measured value can be highly misleading.

The performance of a flow model was evaluated by comparing the parameters and responses of the model with the experimental data. In spite of the difficulties involved in the phase of interpreting the results of point measurements, the field data considered reliable were respected throughout the model calibration. Accordingly, since the initial values of the model parameters were derived from the experimental data, the maximum improvement was searched with the minimum changes in the model.

As mainly the fracture zones control the hydraulic responses of a system, their properties must and can be adjusted in more detail. The parameters of the zones in the model are their location and extent as well as the magnitude of the transmissivity assigned to them. In transient cases, the storativity of the zones is needed as well. When adjusting the flow models for the Äspö site, the transmissivity of the zones and the reduction of their extent were considered. Modification of the orientation of the zones would have involved a re-generation of the finite element mesh for each change, which would have resulted in an excessive increase in the modelling work. Occasional changes in the model geometry did not impose major difficulties with the tools available (cf. Section 3.4). A systematic or random search for the most probable fracture zone geometry and for the magnitudes of their hydraulic conductivity from all possible options suggested by the hydrological data would, however, have led to a disproportionately and (with the present hardware and software instruments) most likely uncontrollably complex calibration process. The influence of the reduction of the extent was nevertheless studied for few important zones. The extent of the zones could in principle easily be varied if, in the generation of a finite element mesh, two-dimensional elements were created for the maximum plausible extent of the zones. Very low hydraulic conductivities could be assigned to their uncertain parts, thus restricting their effective extent. During the search for the optimal model geometry, the restricted areas inside the zones could have been varied (in effect: removed) by re-assigning hydraulic conductivities to certain sets of finite elements. More comprehensive calibration of the model geometry was not considered justified with the Äspö site, because the field studies continue and thus the structural model still evolves.

This study involved the calibration of the flow models based on both the base and the updated structural models, with more efforts spent on the latter. In calibrating the flow model corresponding the base structural model,

the LPT2 test and the other long-term pumping test, LPT1 /Rhén, 1991/ were applied. It was assumed that in the withdrawal holes (KAS06 and KAS07) the initial transmissivity of a zone defines its cross-zone transmissivity. (With the cross-zone transmissivity we mean the equivalent-continuum transmissivity of the zone on a large scale.) This is hardly ever true due to the inhomogeneity of the zones in nature. The transmissivities of the zones intersecting with the withdrawal holes were first adjusted to obtain the water inflow equal to the pumping rate applied in the field test and the inflow distribution similar to experimental one by using the experimental drawdown in the withdrawal holes. Next, the transmissivities of the other zones were adjusted to obtain the pressure drawdown field that favourably compares with the experimental values.

The calibration of the flow model based on the updated structural model was more complicated. Six pumping tests and hydraulically undisturbed flow conditions were considered. The fracture zones were conceptually divided into two parts: the near-field parts around the withdrawal holes and the far-field parts characterized by the equivalent-continuum transmissivity. The transmissivity of the near-field part can differ significantly from the equivalent-continuum transmissivity. The calibration of the updated model is discussed more in section 5.3.

4 BASE MODEL

4.1 INITIAL FLOW MODEL

4.1.1 Geometry of the zones

In addition to the base structural model, Wikberg et al. /1991/ presented a conceptual flow model that simplifies the bedrock geometry. The flow model consists of 15 fracture zones, whose strikes as well as dip angles and directions are given in Figure 4–1. The fracture zone geometry of the base flow model in this study is also based on that figure. In the vertical direction, all the fracture zones extend to the bottom of the model /Rhén, 1992/. The depth of the flow model was selected to be 1500 m. Figure 4–2 depicts the fracture zones in a three-dimensional view.

The correspondence between the flow model and the field investigations in the cored boreholes is summarized in Figure 4–3. In the figure, the most significant differences are following (references to the field data in this list are based on the compilation by Wikberg et al. /1991/):

- KAS02 does not intersect NE–1 in the flow model.
- According to the field data, neither KAS08 nor KAS03 intersects EW–5 as they do in the flow model.
- KAS08 does not quite intersect NNW–2 in the flow model but goes very close to it.
- KAS13 does not quite intersect NNW–1 in the flow model although the distance between them is very small at the ground surface.
- According to the field data, KAS14 does not intersect NNW–3.

These differences are mainly due to the simplifications made while constructing the flow model, e.g., the fracture zones in the flow model are smooth planes while their true shape is more or less rugged. These differences must and have been considered when interpreting and comparing the results.

4.1.2 Hydraulic conductivities

The initial values of the transmissivities of the fracture zones and the hydraulic conductivity of the rock matrix are based on the values compiled by Wikberg et al. /1991/. The transmissivities of four fracture zones

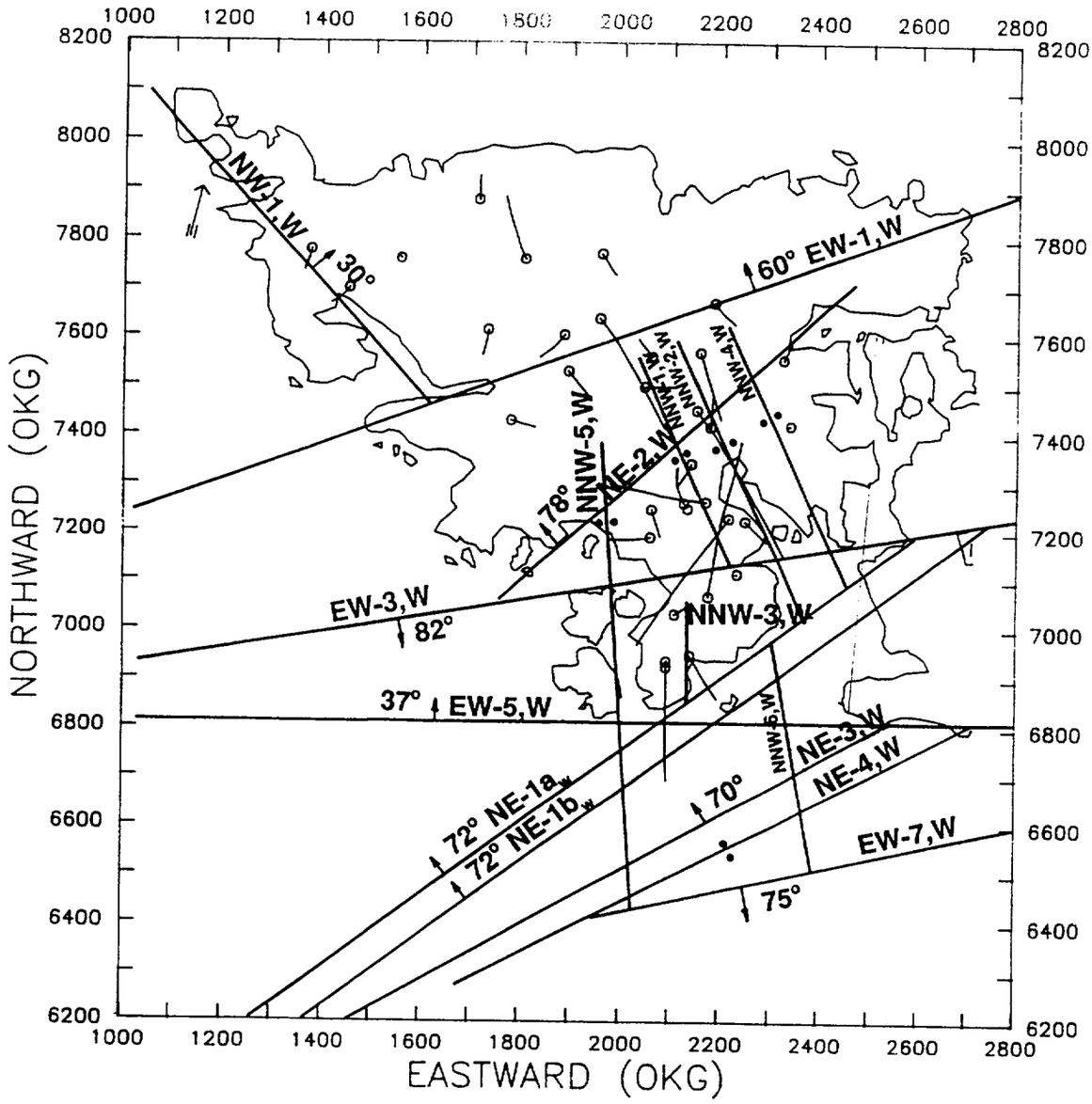

Figure 4–1. *Locations as well as the dip angels and directions of the zones in the base structural model /Wikberg et al., 1991/.*

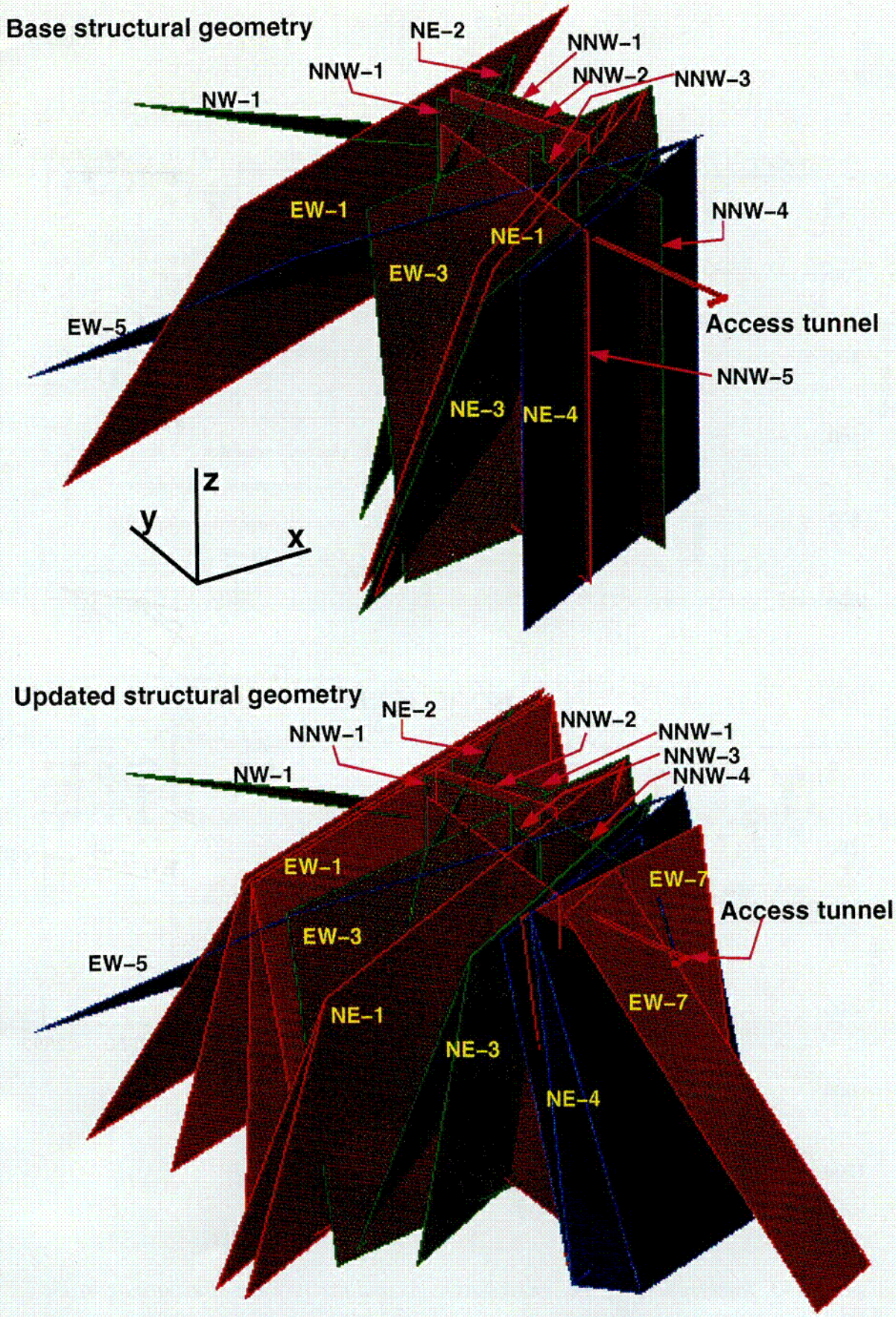

Figure 4–2. Zone geometries in the base (top) and updated (bottom) flow models.

C-04

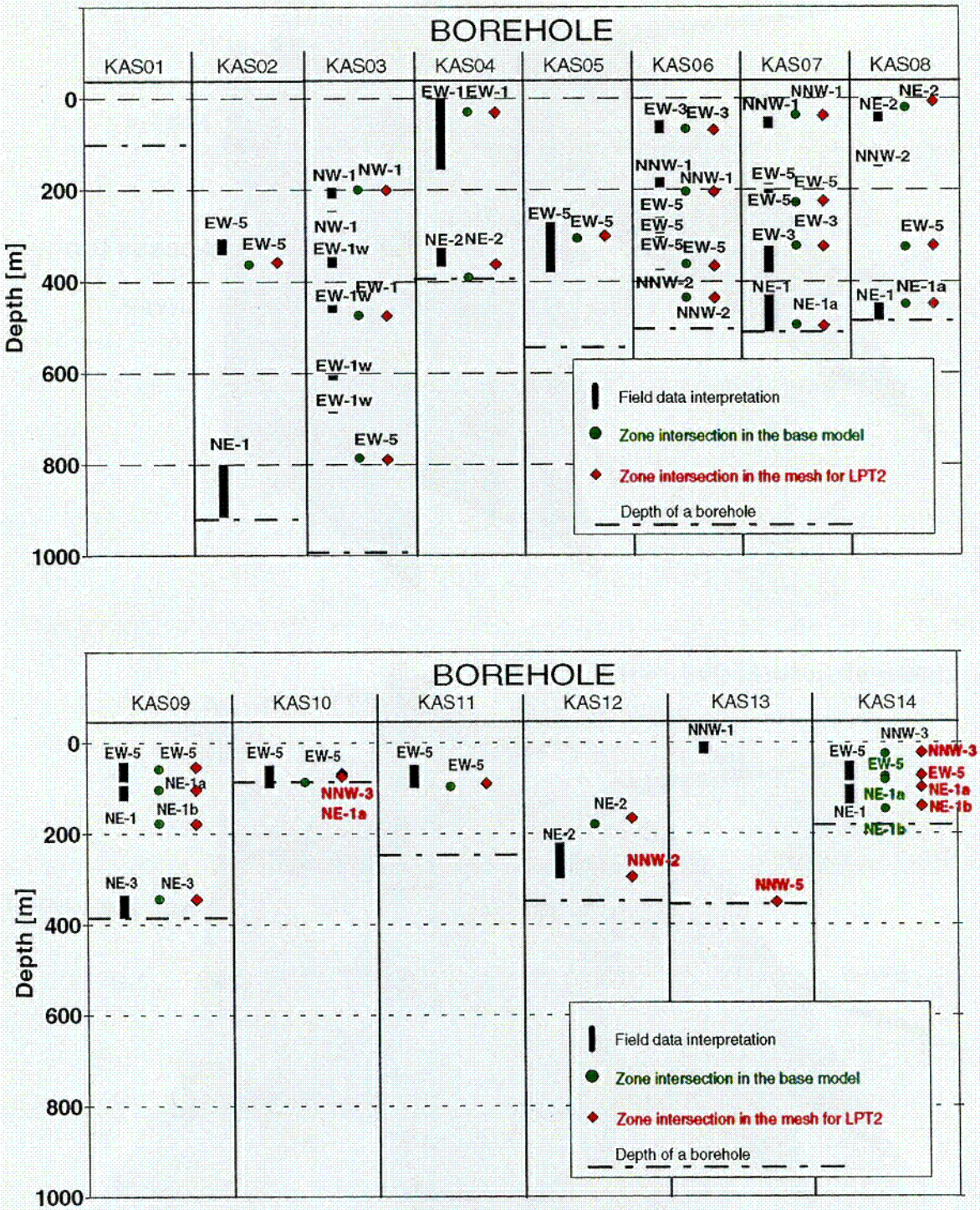

Figure 4–3. *Intersections of the cored boreholes and fracture zones according to the field data interpretations /Wikberg et al., 1991/, the base flow model geometry and the corresponding finite element mesh for LPT2.*

C-05

changed during the calibration process, which is described in Section 4.3. The initial as well as calibrated values are shown in Table 4–1. The change in the transmissivity is shown only for those zones the calibrated value of which differs from the initial value.

On the site scale, Wikberg et al. /1991/ define the rock matrix at Äspö to consist of four different "rock mass units" whose estimated geometric means for the hydraulic conductivity vary from $1.0 \cdot 10^{-10}$ m/s to $7.9 \cdot 10^{-10}$ m/s. We used in this study the value of $1.0 \cdot 10^{-9}$ m/s for the rock matrix throughout the site.

Table 4–1. Transmissivities of the fracture zones of the base model and the hydraulic conductivity of the rock matrix. The initial values are based on the compilation by Wikberg et al. /1991/. A relative change in the transmissivity is shown only if the transmissivity was modified in the model calibration (see Section 4.3).

Fracture zone	Initial transmissivity (10^{-5} m^2/s)	Calibrated transmissivity given as a relative change to the initial value
NW–1	0.7	
EW–1	2	
EW–3	0.05	20×
EW–5	2	
NE–1a	20	0.1×
NE–1b	20	
NE–2	0.4	10×
NNW–1	1.5	
NNW–2	4	0.5×
NNW–3	2	
NNW–4	4	
NNW–5	5	
NNW–6	5	
NE–3	3	
NE–4	35	
EW–7	0.7	
Hydraulic conductivity of the rock matrix is $1.0 \cdot 10^{-9}$ m/s		

4.2 SIMULATION OF LPT2 WITH THE INITIAL BASE MODEL

Simulation model

A simulation model to compute the drawdowns for the LPT2 test was created as described in Section 3.6. A condensed description of the model is given in Table 3-2. An element mesh of 17000 elements was created for numerical computations. The element mesh follows in detail the structure of the flow model as demonstrated in Figure 4-3. In most of the holes and especially in the withdrawal hole, KAS06, the pumping model agrees with the flow model as well as the field data. The fracture zones in the model along borehole KAS06 are: NNW-1, EW-5, EW-3 and NE-1a at depths of about 40, 220, 330 and 500 m, respectively. The boundary conditions and the execution of the numerical simulations are described in Section 3.6.

Steady-state simulations

In the steady state simulations, the drawdown measured in KAS06 at the end of the pumping period was assigned to the nodes representing the hole in the simulation model.

The computed drawdown of the pressure along the cored boreholes is plotted in Figure 4-4. The diamonds mark the drawdowns at the intersections of the holes and the fracture-zone elements. The figure also shows the drawdowns measured at the end of the pumping period. The measured values were assumed to correspond to a pseudo steady state. The intervals in which the fracture zones were in reality interpreted to occur in the boreholes are also indicated (cf. Figure 4-3).

The simulation results as a whole compare successfully with the field data. However, some differences exist. In KAS04 the computed drawdown is twice as large as the measured values for most of the hole. The depth dependence of the drawdown is nevertheless the same. In the upper part of KAS13, the computed drawdown is significantly larger than the measured one. The computed drawdown is, on the contrary, smaller in the two uppermost packed-off sections of KAS07.

In the second lowest section of KAS07, the measured drawdown is evaluated to be about 10 m whereas the simulated value is only about 2 m. However, due to the problems with the field measurements in KAS07, the measured value is considered very uncertain /Ström, 1993a/. During the pumping period of the field experiment, the measured drawdown in this section first increases up to 15 m and then decreases to the final value, which is about 2 m and is considered incorrect. In the following, the evaluation of the computed values for this section is thus omitted.

When comparing the computed and measured drawdowns, the simplifications in the simulation model should be considered. Because of

these simplifications, the boreholes do not intersect the zones exactly at the same depths as (is interpreted to happen) in reality. For instance, in KAS08 the depth dependence of the calculated drawdown along the borehole differs from the field results. That is predominantly because KAS08 and NNW-2 are almost parallel and in the model borehole KAS08 does not quite intersect NNW-2 (Figure 4-5). The largest simulated drawdown is transferred to the hole through EW-5, which intersects KAS08 at a depth of 420 m (EW-5 is not interpreted to occur in KAS08, see Figure 4-3). Zone NNW-2 is interpreted to intersect KAS08 at a depth of 150 m, where the largest measured drawdown in KAS08 appears. Therefore, we should compare the largest value of the simulated drawdown in KAS08 with the drawdown measured in the second highest section.

In the lowermost section of KAS08, the computed drawdown is about a half of the measured value. This indicates an actual difference between the model and the real bedrock because the bottom of KAS08 intersects the major fracture zone NE-1.

The influence of the boundary conditions of the pumping model on the computed drawdowns was investigated. In the results presented in Figure 4-4, the (sub)vertical sides and bottom of the model were assumed to be fixed-pressure boundaries. Figure 4-6 shows the drawdown for a simulation case in which no-flow boundary conditions were assumed for the sides and bottom. Changing the boundary conditions affects drawdown only in the deepest holes. It is actually the change of the boundary conditions of the model bottom (1500 m), which causes the differences. The sides of the pumping model are so far (2000 m) from the pumped hole that their boundary conditions do not affect drawdowns in the cored holes. Based on the comparison with the field data, neither of the boundary condition sets can thus be assessed to be better because there are several other potential reasons for the differences between the measured and computed values.

4.2.1 Performance measures

Drawdown

The simulated drawdown for each observation section of the cored and percussion boreholes is presented in Appendix B. The calculated drawdown is in most cases for the midpoint of a section. However, when a packer interval intersects a zone, the drawdown of the section is taken according to the drawdown in the zone. If an interval intersects more than one zone, the drawdown for the zone having the highest transmissivity is assumed for the whole interval.

Appendix B shows the measured drawdowns as well as the absolute and relative deviations of the simulated values. The values in the "distance" column of Appendix B are those reported by Rhén et al. /1992/ for the packer intervals. (The "distance" represents the distance of a packer interval

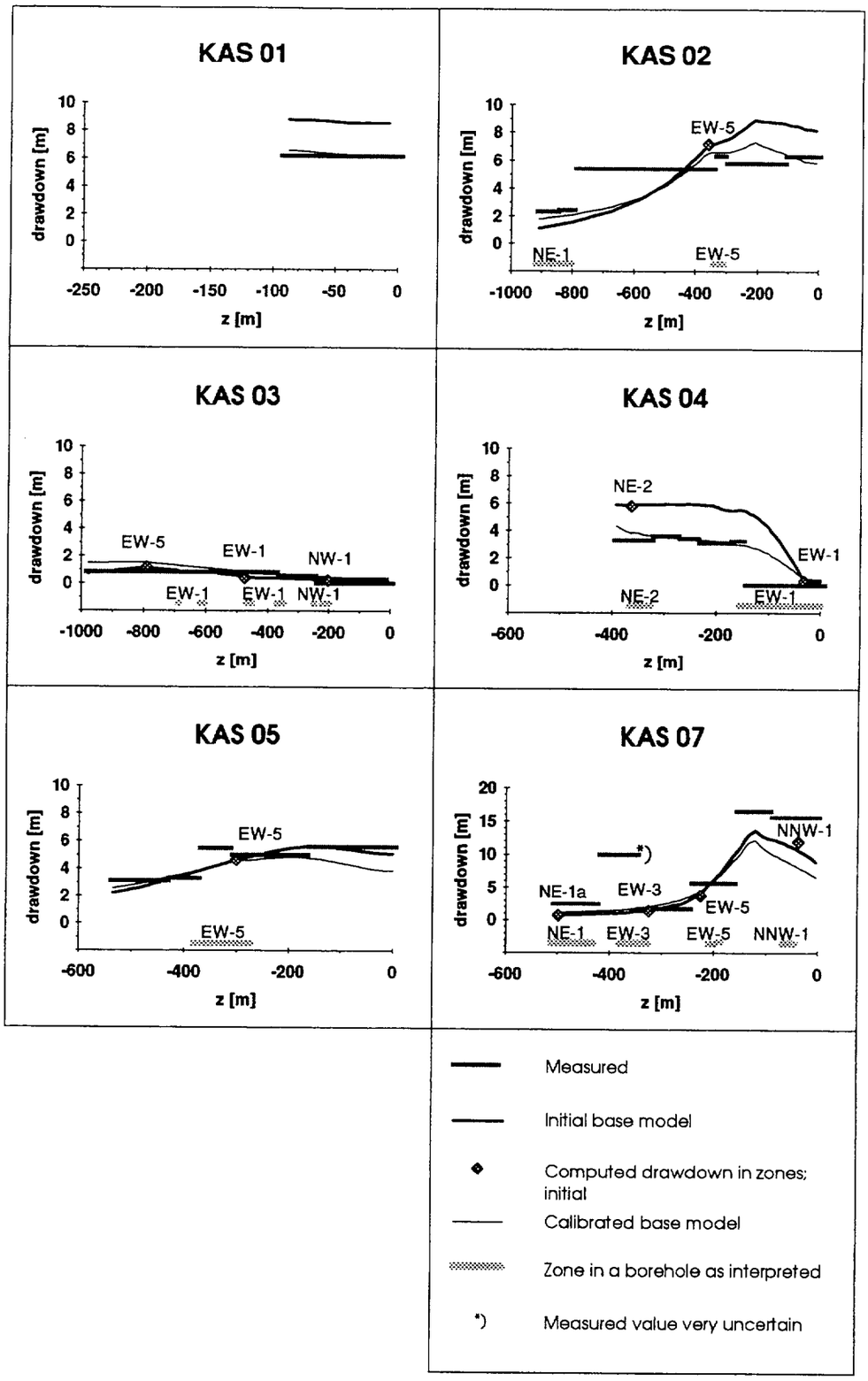

Figure 4-4. *Measured /Rhén et al., 1992 and Ström, 1993a/ and simulated steady-state pressure drawdowns in the cored boreholes for the LPT2 test. The computed results are for the base structural model reported by Wikberg et al. /1991/ before and after the model calibration.*

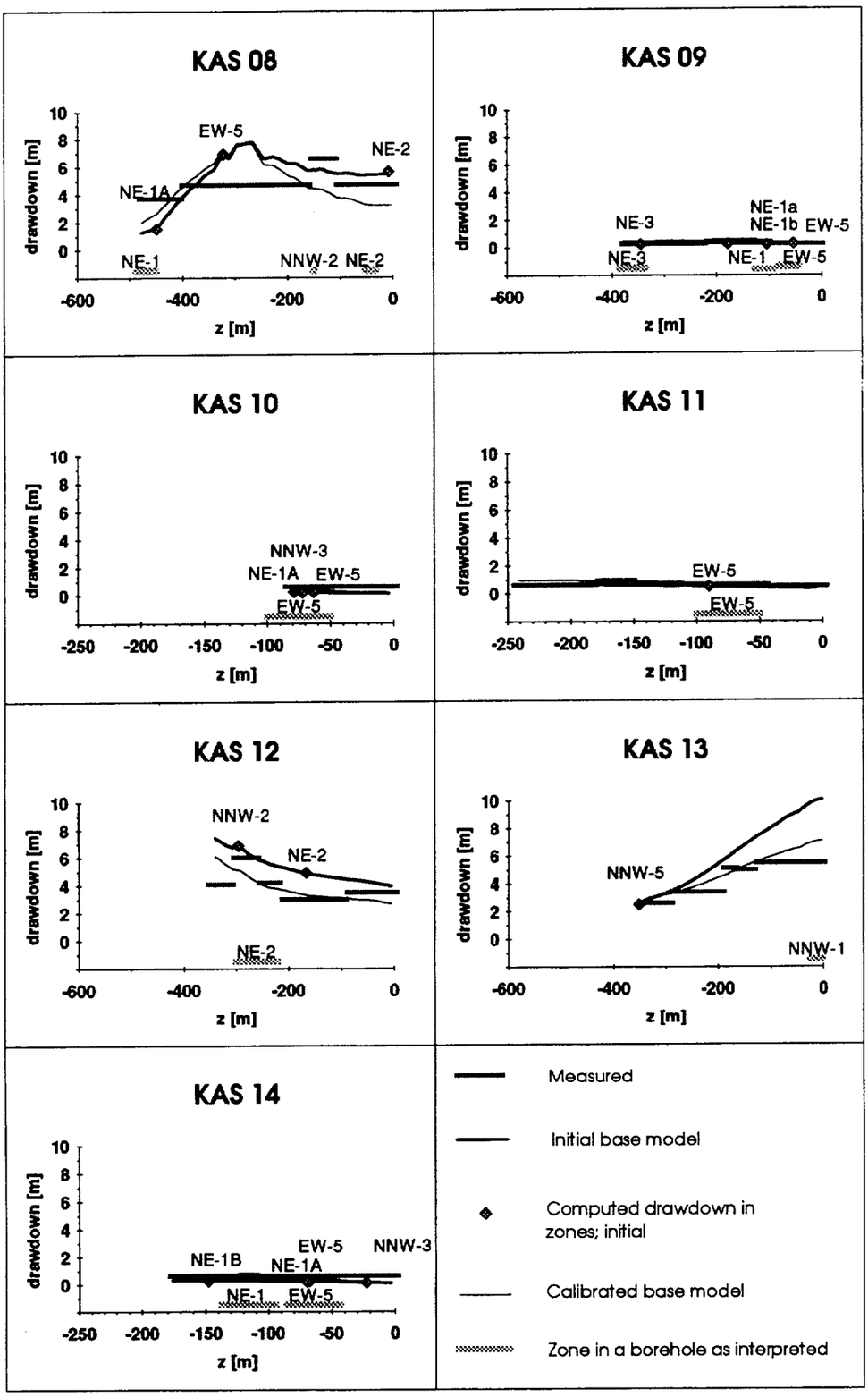

Figure 4-4. (Continued.)

from KAS06.) In comparing the measured and computed drawdowns section-by-section, one must, as stated above, also consider what are the differences in the occurrence of the zones in the boreholes in reality and, on the other hand, in the model (cf. Figure 4-3). Some drawdown differences arise from small geometrical simplifications, which are unimportant on the site scale.

The largest deviation of the computational drawdown from the experimental results is in the upper section of borehole HAS14. The measured drawdown is less than 5 m and the simulated value is more than 12 m due to the close location of HAS14 to KAS06.

In Figure 4-7, the measured and computed drawdowns given in Appendix B are plotted as a function of the "distance" (the values for the second lowest packed-off section of KAS07 are not included). The differences between the measured and calculated drawdowns are presented in Figure 4-8.

The distribution of the differences of the measured and computed drawdowns is presented in Figure 4-9. The computed drawdowns are in average 0.8 m larger than the measured ones. The standard deviation of the drawdown differences is about 2 m.

Water inflow to KAS06

For the initial model, the calculated total inflow of groundwater to the pumped hole, KAS06, is 2.8 l/min as the pumping rate applied in the field experiment was 2.25 l/min. The measured and calculated distributions of the total water inflow among the rock matrix and various fracture zones intersecting KAS06 are presented in Table 4-2.

Table 4-2. Measured /Rhén et al., 1992/ and simulated distributions of the water inflow to KAS06. The calculated values are for the base model before and after the model calibration.

Hydrological unit	Measured (%)	Initial model (%)	Calibrated model (%)
EW-3	15	0.7	15
NNW-1	21	17	21
EW-5	33	32	34
NNW-2	26	51	29
NNW-x	5	-	-
Matrix	-	0.7	0.9

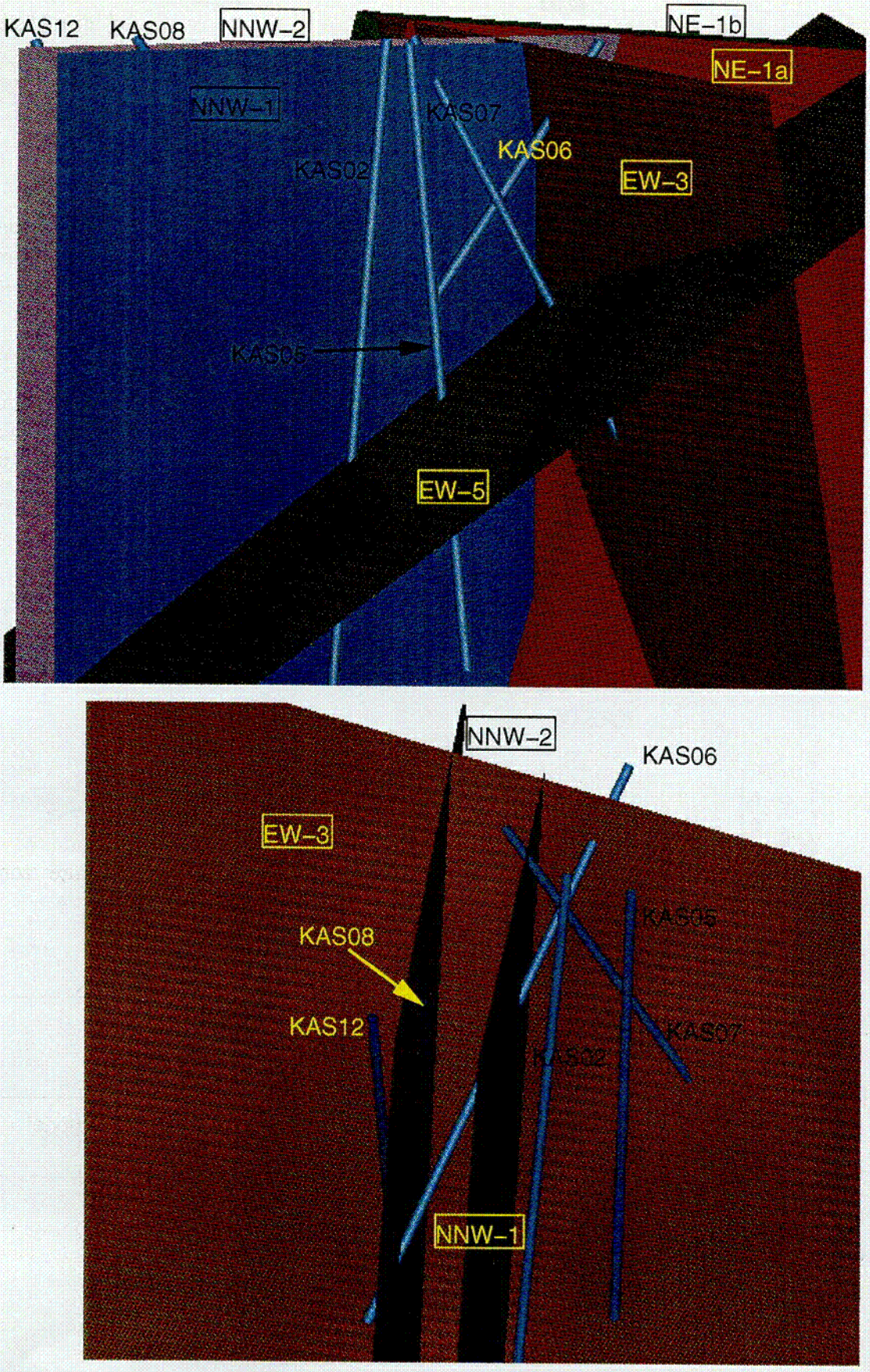

Figure 4-5. *Certain boreholes and zones in the base model as seen from the north-west in the upper part and from the north in the lower part.*

C-06

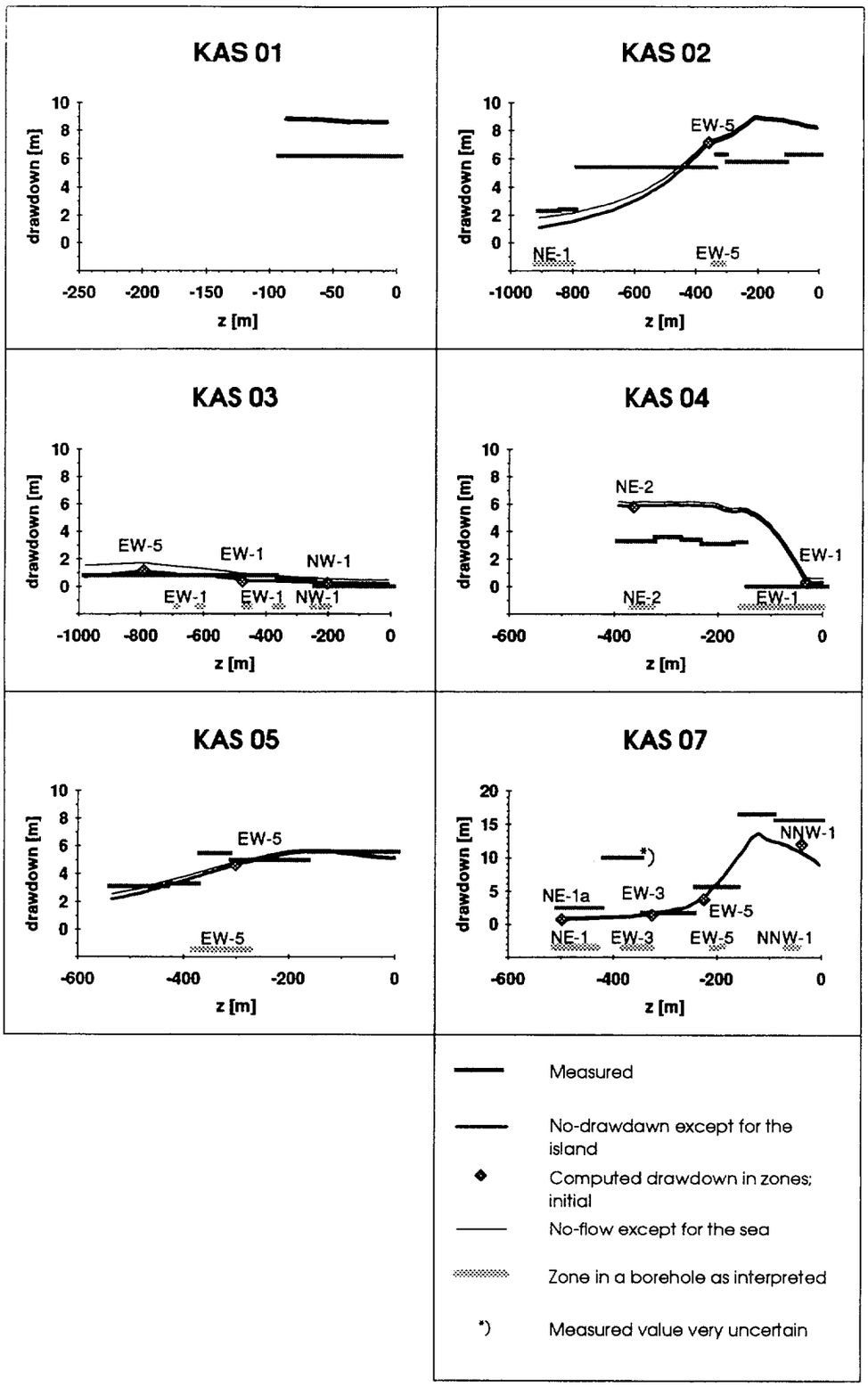

Figure 4-6. *Effect of the boundary conditions of the LPT2 simulation model on the drawdown. The computed drawdowns are for the initial base model with two different boundary conditions (see the text for details). The measured values are from Rhén et al., 1992 and Ström, 1993a.*

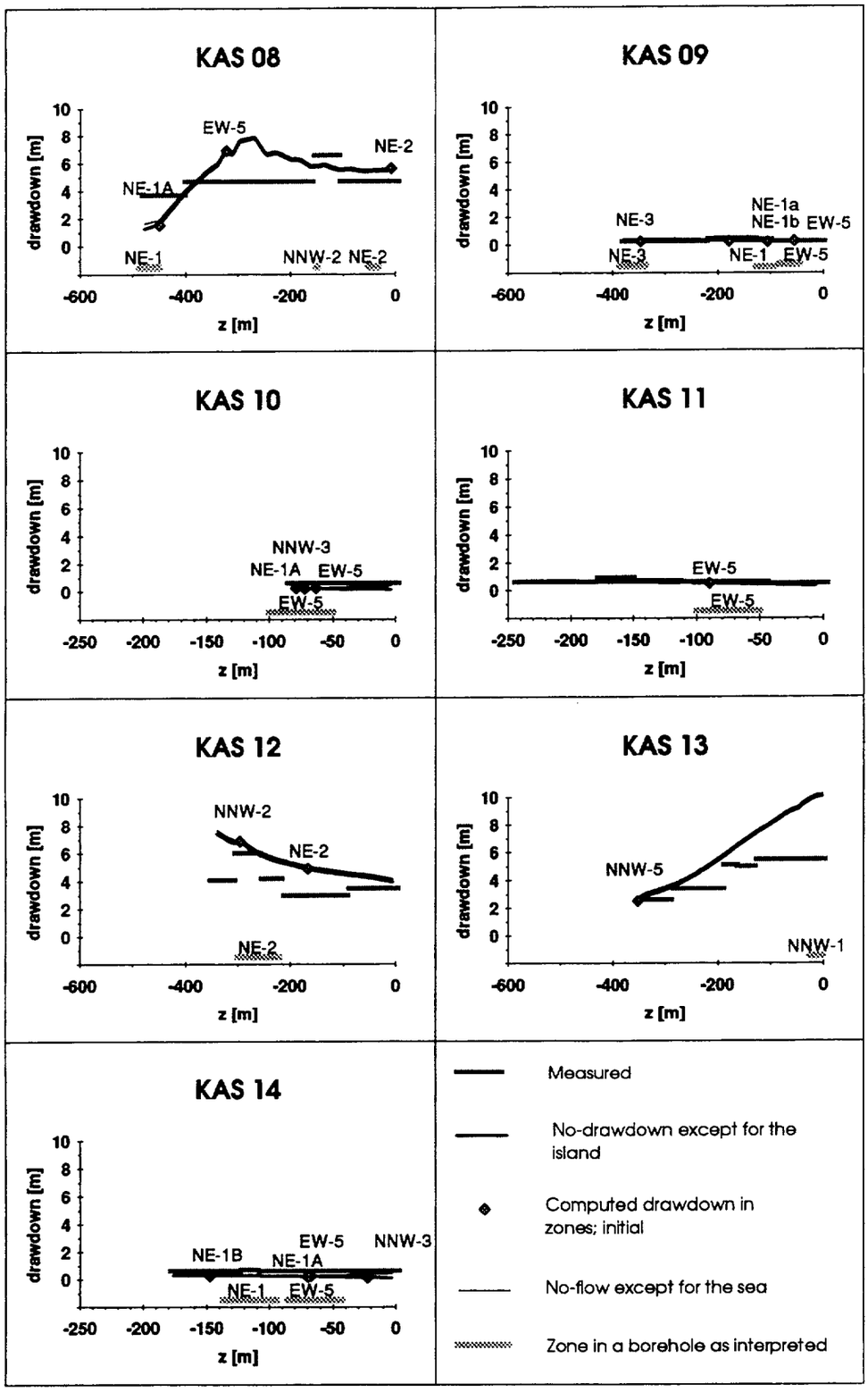

Figure 4-6. (Continued.)

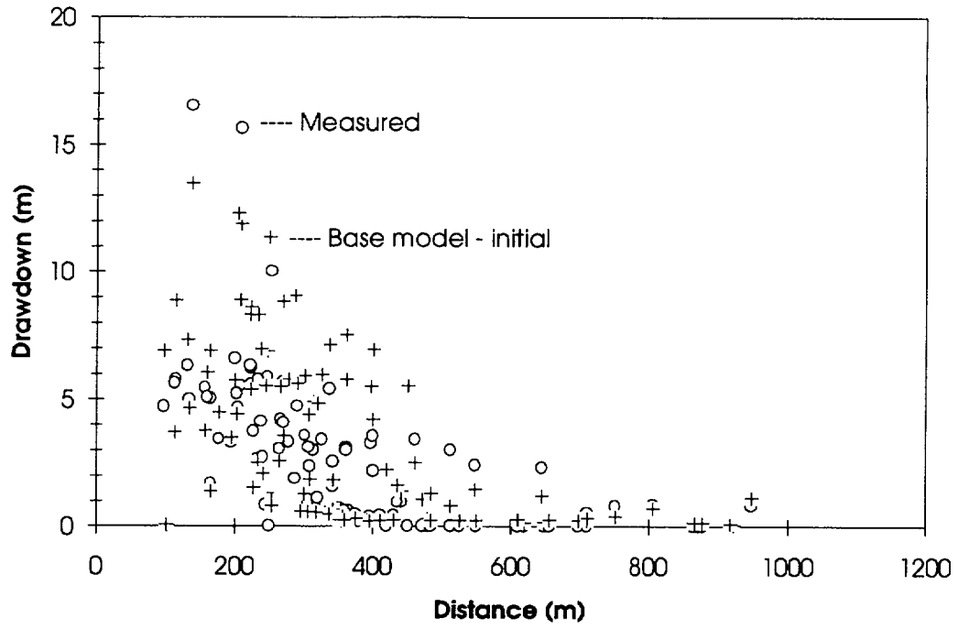

Figure 4-7. *Measured and simulated pressure drawdown in the observation sections of the cored and percussion boreholes as a function of the "distance" for LPT2. The computed values are for the initial base model. The "distance" and measured drawdowns from Rhén et al. /1992/ and Ström /1993a/.*

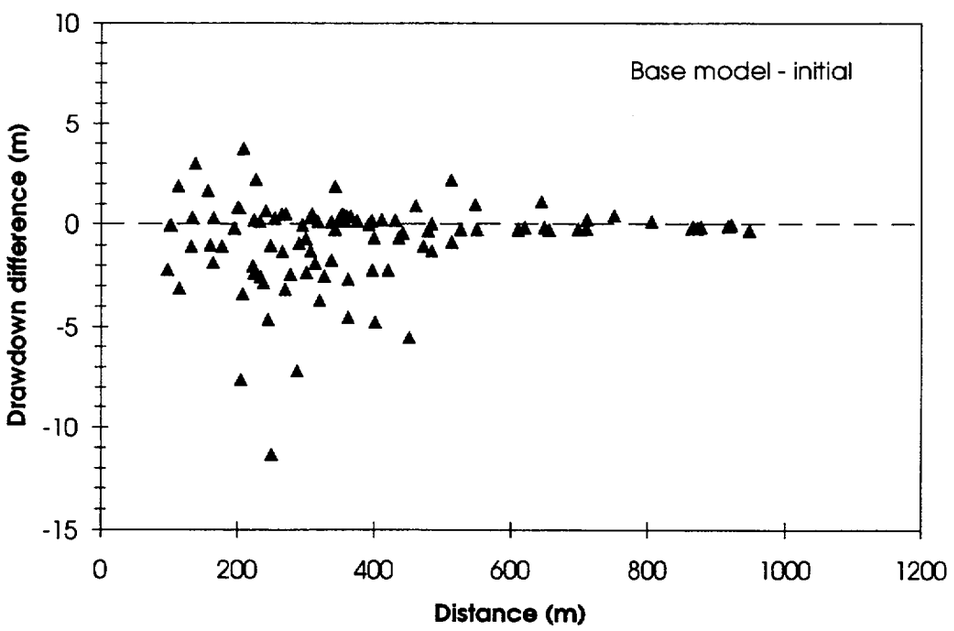

Figure 4-8. *Difference between the measured and simulated pressure drawdowns shown in Figure 4-7. The "distance" for each observation section from Rhén et al., 1992.*

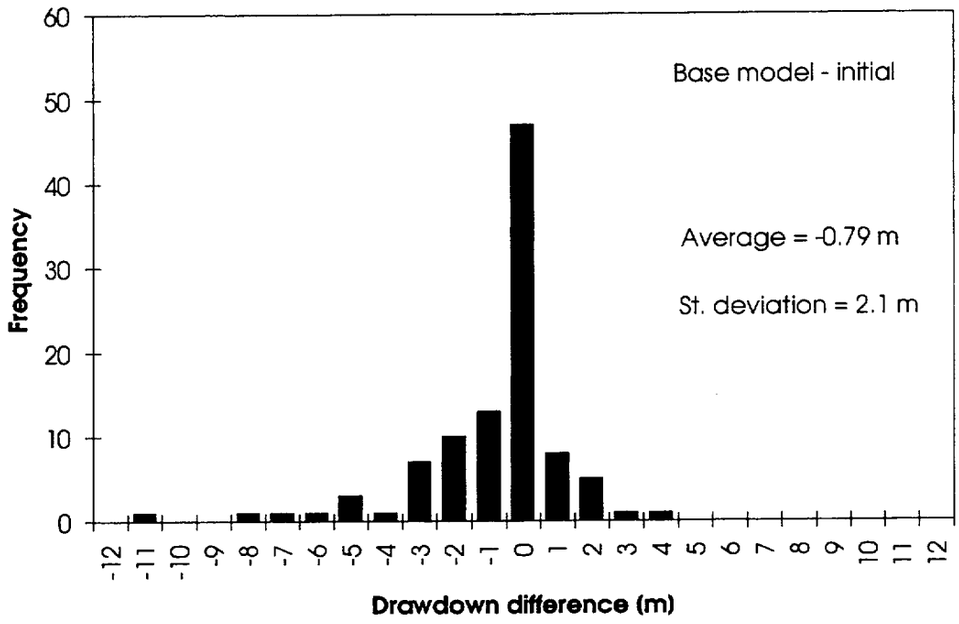

Figure 4-9. *Distribution of the differences between the measured and simulated drawdowns shown in Figure 4-8.*

Flow rate through the tracer injection sections

So far we have discussed the pressure response and the groundwater inflow to the withdrawal hole due to the pumping. When considering only these parameters, the groundwater salinity and the change in the water table need not to be taken into account. However, if we are interested in how water flows in the bedrock during the pumping test, the actual flow field needs to be analyzed. This is the case when the groundwater flux through the tracer injection sections is studied. Therefore, in order to calculate the quantity of groundwater flowing through the injection sections, the hydraulically undisturbed conditions were also simulated. The total flow field prevailing during the pumping test was obtained by summing the Darcy velocities under undisturbed conditions and in the pressure drawdown field computed for LPT2.

The simulation of undisturbed flow conditions is described in Section 3.5. It was assumed that the pumping does not change the infiltration rate. In the boreholes far from KAS06, the calculated Darcy velocity for undisturbed flow conditions is the same order of magnitude as the change of the Darcy velocity due to the pumping. In few sections, the pumping actually changes the direction of flow and, consequently, the final Darcy velocity can be smaller than without pumping.

Since the hydraulic conductivities used were equivalent-continuum values, the Darcy velocity obtained for a zone at a point represents average groundwater flux in that zone. Local fluxes depend on the heterogeneity of the zone.

Two approaches were applied to calculate the amount of groundwater flowing through the injection sections. First we omitted the heterogeneity of the bedrock, and the flow rate through the injection sections was calculated deterministically by multiplying the total Darcy velocity with the assumed thickness of a zone and with a width of two times the borehole diameter (a borehole draws the pathlines towards itself). The value of the thickness is irrelevant because the same value was applied in calculating the Darcy velocity. The measured flow rates through the tracer injection sections and those calculated with the initial model are presented in Table 4-3. As the pressure gradient does not vary much among the borehole sections under undisturbed flow conditions or even during the pumping, the most important factor resulting in dispersion in the flux is the transmissivity. As these results are based on the equivalent transmissivities and hence represent the average flux in a zone, the measured values are expected to be both higher and lower than those calculated. In most of the sections, the calculated fluxes are smaller than the measured values. The difference is the largest in

Table 4-3. Measured /Rhén et al., 1992/ and computed amount of water flowing through the tracer injection sections during the LPT2 pumping test. The computed values are based on the equivalent-continuum approximation and calculated for the initial base model.

Injection section	Zone interpreted	Measured (ml/min)	Computed (ml/min)
KAS02-4	EW-5	2	5.1
KAS02-2	NE-1	4	[1]
KAS05-3	EW-5	9	3.5
KAS05-1	(no zones)	11	[2]
KAS07-4	EW-5	18	4.1
KAS08-3	NNW-2	21	6.1
KAS08-1	NE-1	48	9.2
KAS12-2	NE-2	107	0.5
KAS13-3	(no zones)	3.3	[2]
KAS14-2	NE-1	11	3.5

[1] In the simulation model borehole KAS02 does not intersect zone NE-1, see Figure 4-3. The calculated flow rate is very small in the matrix.
[2] No zone is interpreted for this section, see Figure 4-3, and the calculated flow rate is very small in the rock matrix.

section KAS12-2 in which the measured flux is the largest. Yet the smallest calculated flux is obtained for the same section. The calculated value reflects the small transmissivity of NE-2 (Table 4-1). Many of the measured values include significant measuring errors /Rhén et al. 1992/. On the other hand, water can flow along the relatively long injection section, which can enlarge the measured flow rate but is not considered in the simulation.

On a borehole scale, the heterogeneity of the bedrock is important, however. Therefore, the flow rate through the tracer injection sections was also studied by means of stochastic simulations. Two-dimensional simulations were used to study the subareas of the zones around the injection sections. Boundary conditions were assigned to obtain the same average Darcy velocity, i.e., the average flux as determined by the large-scale modelling discussed above. The area studied was divided into finite elements having a lognormally distributed hydraulic conductivity. The size of the elements was small compared with the modelling area and the parameters of the hydraulic conductivity distribution were selected to result in a value of the equivalent hydraulic conductivity that is consistent to that used in the three-dimensional simulations. The standard deviation of the logarithm of the hydraulic conductivities of the elements was selected to be unity. The distribution of the groundwater flow rates based on the stochastic simulations through the injection section in KAS02 that intersects EW-5 is shown in Figure 4-10. As expected, in most of the realizations, the flow rate is close to the value corresponding to the equivalent hydraulic conductivity (Table 4-3). The simulations for the other injection sections with the same approach naturally resulted in flow rate distributions with the same shape. As the standard deviation of the hydraulic conductivities was maintained, the changes in the boundary conditions according to the average Darcy velocity or in the average of the hydraulic conductivities do not affect the shape of the flux distribution. The average of the flow rates of stochastical

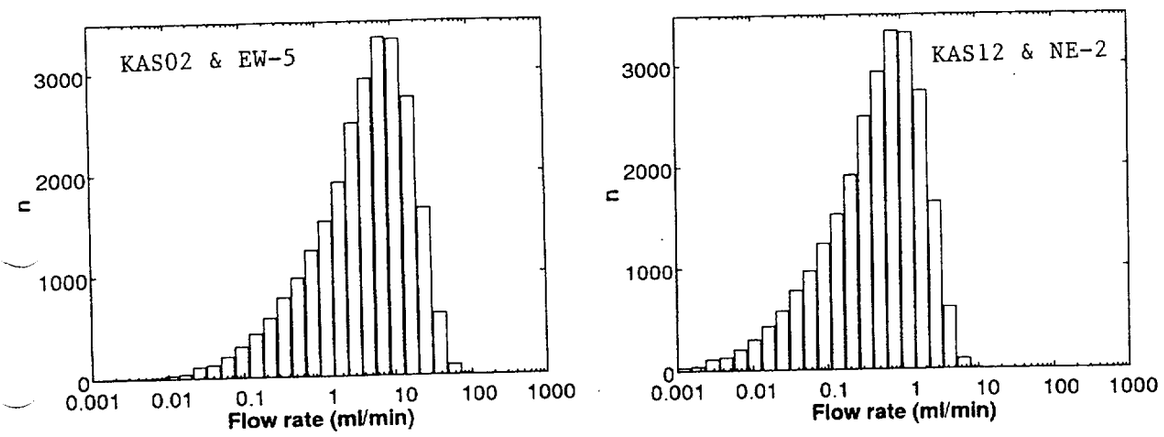

Figure 4-10. *Stochastically simulated distributions of the flow rate through those tracer injection sections in KAS02 and KAS12 that were interpreted to intersect zones EW-5 and NE-2, respectively.*

simulations varies with the flow rate of the deterministic modelling. Figure 4-10 shows also results for the section in KAS12 intersecting NE-2. The stochastic simulations do not predict as high flux as measured (Table 4-3).

The results of the stochastic simulations include many realizations that are not consistent with the field data. If the hydraulic conductivity measured for the injection section we are interested in is high, realizations having very small conductivity for the element representing the zone around an injection section should be excluded. In a more advanced study, the hydraulic conductivity measurement performed should be simulated with each realization and only those realizations being consistent with the field data should be included in the analysis. This would obviously reduce the dispersion of the flux.

4.2.2 Discussion

Some simulation results of the initial model are close to the field data. Especially the measured and the computed pressure drawdown distributions agree well with each other (Figure 4-7). In most of the cored boreholes, the variation of the calculated drawdown along a borehole is qualitatively the same as that of the measured values. Yet in several observation sections (like in the upper section of HAS14), the simulated drawdowns are considerably larger than those measured. These differences can, however, be a consequence of the steady-state assumption, which is not valid for the field experiment as the drawdown was still increasing when the pumping was stopped.

With the initial model, the computed total inflow to the pumped borehole, KAS06, is somewhat larger than the measured one. The distribution of the total inflow among the zones intersecting KAS06 also differs from the field results. Therefore, at least around KAS06, the model transmissivities of zones EW-3 and NNW-2 do not agree with the properties of the bedrock.

The high flow rates in some tracer injection sections suggest channelled groundwater flow. The values calculated from the average groundwater flux were not expected to coincide with the measured flow rates. The measured flow rates are mainly controlled by the local transmissivities around the injection sections. The stochastic simulations indicate that flow rate distributions that cover the field results can be obtained. The parameters needed in the stochastic simulations are, however, unknown.

4.3 CALIBRATION

The calibration procedure is described in Section 3.7. Only tentative calibration was carried out for the flow model based on the base structural model before the structural model was updated. After receiving the updated geometry of the zones, it was not considered rational to continue the calibration study with the base model.

4.3.1 Calibration cases

The calibration of the base flow model was based on the two long-term pumping tests, LPT2 and LPT1, performed at the Äspö site. These two calibration cases were handled with the same weight throughout the calibration. However, the LPT2 case was more informative, because more field data for it were available.

LPT2

When the model was calibrated against the results of LPT2, the drawdowns, the total groundwater inflow to the withdrawal hole and the distribution of the inflow among the zones intersecting KAS06 were used. The inflow to the first 100 m of KAS06 was assumed to have been contributed by EW-3.

LPT1

The LPT1 was a pumping test, in which borehole KAS07 was the withdrawal hole /Rhén, 1991/. KAS07 is 604 m long and dips to the southwest (Figure 1-1). Pumping was carried out for about 52 days and the average pumping rate was 1.25 l/s. At the end of the pumping period, the water level in KAS07 had decreased about 58 m. Rhén /1991/ reports the pressure drawdown in several boreholes during the drawdown period as a function of time.

As in LPT2, despite of the long duration of the pumping period, the pressure field did not reach a steady state. The level of water was lowering even in the withdrawal hole KAS07 when the pumping was stopped /Rhén, 1991/. In some observation sections (e.g., in KAS04) the drawdown was still increasing notably. The flow system is anyhow assumed to have been in a pseudo-steady state at the end of pumping period.

After starting the pumping in KAS07, the first responses were observed in KAS05 and KAS06. The section in KAS06 intersecting NNW-1 responded fast as can be expected because the withdrawal hole also intersects NNW-1. The next response in the second uppermost section of KAS05 is unexpected since this observation section is not connected directly to KAS07 in the structural model. The next responses were measured in those sections of KAS02 and KAS05 that are interpreted to intersect EW-5. On the other hand, the uppermost section of KAS04 responded late implying possibly that NNW-1 does not intersect with the top part of KAS04.

The drawdowns measured at the end of the pumping period are presented in Figure 4-11 for those cored boreholes which were used as observation holes. The highest drawdown, about 19 m, was measured in the same section of KAS06 in which the first response was observed. The drawdown in the other sections of KAS06 was only from 2 to 3 m. In KAS01 and KAS05 as well as in the uppermost sections of KAS05, the drawdown was about 5 m.

No drawdown was observed in KAS03 and in the uppermost section of KAS04.

A spinner survey was conducted to measure the distribution of the groundwater inflow to KAS07 /Nilsson, 1990/. The spinner measurement did not cover the first 100 m of the borehole, however. On the other hand, because the correlation between the spinner value reported and the flow rate in the hole is not given, the total amount of the inflow to the rest of the borehole is not known. Therefore, the inflow from various zones to KAS07 is not known quantitatively. Only the relative significance of each zone compared to the others was determined. As the uncertainties of the inflow distribution were unknown, it was not used in the calibration of the base model.

Zones NNW-1, EW-5, EW-3 and NE-1 have been interpreted to occur in KAS07 /Wikberg et al., 1991/. KAS07 intersects the same structures also in the flow model with the exception that only subzone NE-1a is intersected by KAS07 (Figure 4-3). In the element mesh for LPT1, the two-dimensional elements representing the zones follow in detail the geometry of the zones and KAS07 intersects the same structures as in the flow model.

4.3.2 Adjusting hydraulic conductivities

The LPT1 and LPT2 tests were modelled in the same way during the calibration. A similar test-specific element mesh was created for LPT1 as for LPT2 (see Section 3.6). Fixed-pressure boundary conditions were applied for the sea area as well as for the side and bottom faces of the model. No-flow boundary conditions were applied over the island. The pressure field at the end of the pumping period was assumed to have reached a steady state.

In the LPT2 calibration case, even the agreement of the initial model with the measured values in terms of drawdowns in the cored boreholes, the inflow to the withdrawal hole and its distribution are satisfactory (Figure 4–4 and Table 4–2).

In the LPT1 calibration case, the computed drawdowns for the initial model exhibit a modest agreement with the field data (Figure 4-11). The simulated inflow to KAS07 (7 l/s) is about six times the measured value.

In adjusting the hydraulic conductivities in the model, the inflows were first emphasized and, consequently, we started with those zones that intersect boreholes KAS06 and KAS07. This approach targeted the tuning of the total inflows to the withdrawal holes and, in the case of LPT2, the inflow distribution among the zones. The inflow to borehole KAS06 was adjusted (2.4 l/s calculated versus 2.25 l/s measured) by reducing the transmissivity of NNW-2 by a factor of two and increasing the transmissivity of EW-3 by a factor of twenty. In LPT1, the amount of the calculated total inflow (2 l/s) to borehole KAS07, which corresponds better to the applied pumping rate

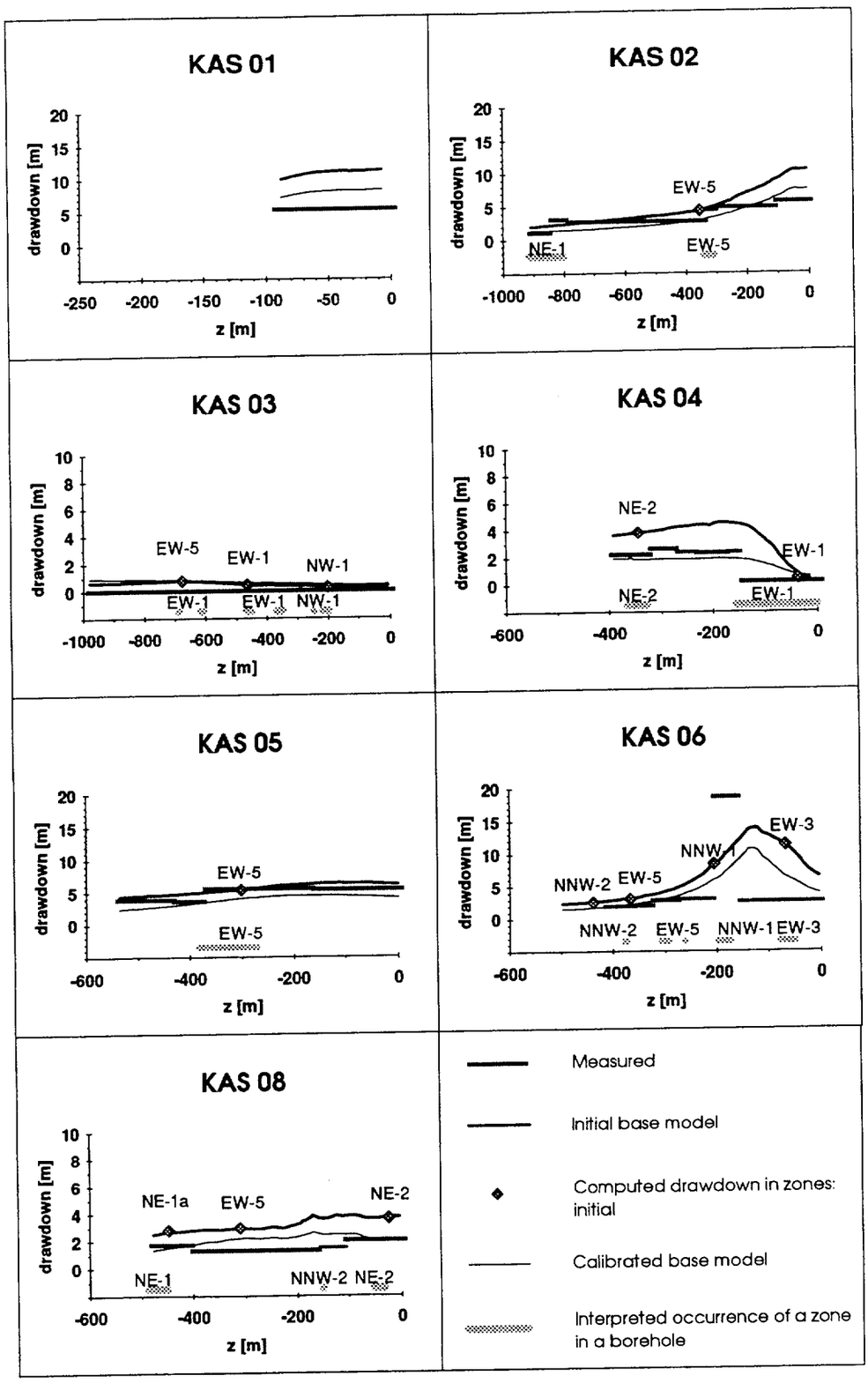

Figure 4-11. *The measured /Rhén, 1991/ and simulated steady-state pressure drawdowns in the cored observation boreholes for the LPT1 test. The computed results are for the base structural model reported by Wikberg et al. /1991/.*

(1.25 l/s) was achieved by reducing the transmissivity of NE-1a by one order of magnitude. The drawdown of the pressure along the other cored boreholes was fitted only by increasing the transmissivity of structure NE-2 to ten-fold (Table 4-1).

The drawdown of the pressure simulated with the calibrated model agrees well with the field data for both the LPT2 and LPT1 calibration cases (Figures 4-4 and 4-11, respectively). The distribution of the inflow among the zones in LPT2 also corresponds to the measured data (Table 4-2).

4.3.3 Discussion

The inflow to the withdrawal hole is more sensitive to transmissivities than the pressure drawdown in the observation holes (the drawdown measured in the withdrawal hole used as a boundary condition). Because the equivalent-continuum approximation for the zones was also assumed to be valid near the withdrawal hole, the inflows determined also the average transmissivities of the zones that intersect the withdrawal holes. The applied reduction in the transmissivity of NE-1 is not, however, consistent with the other field experiments. In measuring the hydraulic conductivity of NE-1a, a value of $2 \cdot 10^{-4}$ m^2/s was obtained in the KAS07 hole /Ström, 1992a/. The pumping experiment was, however, considered more reliable. One can speculate that in a thick zone, like NE-1, the injected water may partially return to the hole outside the packed-off section. This would naturally result in a misleadingly high transmissivity for the zone.

A reasonable agreement was reached by adjusting the hydraulic conductivities of only four bedrock structures. This does not, however, mean that the transmissivities of the other zones and the hydraulic conductivity of the matrix in the model are consistent with the real bedrock. The cases studied in the calibration may also be insensitive to the hydraulic properties of other bedrock structures. Regarding the LPT2 calibration case, this problem is studied in the sensitivity and uncertainty analysis in Section 4.4.2.

The calibrated model still shows some discrepancies with the measured data. We believe, however, that all these discrepancies cannot be eliminated in the presence of the simplifications the model currently includes. Further improvements would have required a more detail understanding of the relevant bedrock features, modifications in the boundary conditions and/or the introduction of inhomogeneity of the zones (most probably as a depth-dependent or anisotropic hydraulic conductivity). Moreover, the flow conditions during the field experiments should be studied in more detail.

The most significant discrepancies in the calibrated model in calibration case LPT1 were the following:

- The drawdown in borehole KAS01 is still about 30% higher than the measured data. However, since borehole KAS01 is a shallow one (101 m), this difference has a smaller importance than differences in the deep holes.

- Although no drawdown was observed in borehole KAS03, the computed magnitudes were up to 1 m. This may be attributed to the boundary conditions or to the steady-state assumption.

- The high (18 m) drawdown measured in borehole KAS06 at its intersection with structure NNW-1 is not achieved by simulations. This is most likely because NNW-1 in the model, as a homogenous structure, is unable to transmit large enough pressure response to that level.

The important discrepancies of the calibrated model in calibration case LPT2 are the following:

- The computed pressure drawdown in the uppermost part of borehole KAS07 falls short of the measured values. Since any approach with isotropic features results in a relatively even distribution of the pressure drawdown, this discrepancy could likely be corrected only with the introduction of a possibly local heterogeneity/anisotropy in structure NNW-1.

- The parallel run of borehole KAS08 and structure NNW-2 causes different variations of the measured and computed values of the drawdown along borehole KAS08. The drawdowns measured in KAS08 have to be compared with those calculated for NNW-2.

- In the lowermost section of KAS08 intersecting NE-1, the calculated drawdown is significantly smaller than the measured one.

- The calculated drawdown in the uppermost section of borehole KAS13 is about 30% higher than the measured data.

4.4 SIMULATION OF LPT2 WITH THE CALIBRATED BASE MODEL

In the calibration phase, the transmissivities of the fracture zones were adjusted as indicated in Table 4-1. The geometry of the zones was similar to the initial model. The extents of the zones were not changed and they remained homogenous and isotropic.

The LPT2 test was simulated with the calibrated flow model in the same way as with the initial model. As the geometrical parameters of the zones were not modified, the same element mesh could be employed. Boundary conditions were the same as originally chosen for the LPT2 model: for the nodes in the area of the Äspö island, no-flow boundary conditions were

applied, and no-drawdown boundary conditions were used elsewhere. Besides steady-state simulations, transient simulations were carried out.

The steady-state simulations were performed as described above in connection with the calibration. The pumping in KAS06 was taken into account assigning the drawdown measured in KAS06 at the end of the pumping period to nodes representing the withdrawal hole. The drawdowns along the cored boreholes calculated with the calibrated model were presented in Figure 4-4 with measured values and the results for the initial model.

The transient simulations of the LPT2 test were computed for two different sets of parameters. Two magnitudes (10^{-7} and 10^{-6} m^{-1}) for the specific storage of the rock matrix were tested. The storativity of all the zones was correspondingly 10^{-7} and 10^{-6}.

In the transient simulations, the effect of the pumping was implemented by assigning both the pumping rate applied in the field experiment and the drawdown measured in the withdrawal hole /Ström, 1992/ as a boundary condition to the nodes representing the withdrawal hole. The pumping rate and consequently the drawdown varied as a function of time as in the field experiment.

4.4.1 Performance measures

Steady state simulations

The computed steady-state drawdowns are listed in Appendix B for the observation sections of the cored and percussion boreholes. Figure 4-12 shows the measured and computed drawdowns as a function of the "distance". The earlier comments regarding the effects of the simplifications of the zone geometries as well as the use of Figures 4-4 and 4-7 and Appendix B apply also to the results for the calibrated model and Figure 4-12.

The differences between the measured and calculated drawdowns are shown in Figure 4-13 as a function of the "distance". The distribution of the differences is presented in Figure 4-14. The mean of the differences is close to zero. The standard deviation is also now smaller (1.6 m) than for the initial model (Figure 4-9).

Despite of the calibration and an improved agreement with the field data, the differences in the pressure drawdown are large in some observation sections. Still the largest difference of almost 9 m is in the upper section of HAS14.

The computed total water inflow to the withdrawal hole, KAS06, is 2.4 l/min. The distribution of the total inflow among the rock matrix and the zones is presented in Table 4-2.

The calculated flow rates through the tracer injection sections are compared with the measured values in Table 4-4. The same approaches were applied in calculating the flow rates as for the initial model (Section 4.2). The undisturbed flow conditions were simulated with the same boundary conditions but with calibrated hydraulic conductivities. The total values for average Darcy velocities were obtained by summing the vectors calculated for undisturbed conditions and the LPT2 test.

The influence of the heterogeneity on the flow rate through the injection sections could also have been investigated as with the initial model. The outcome would, however, have been a similar dispersion of the flow rate relative to the average flux (Table 4-4) as for the initial model (Figure 4-10).

The calculated drawdown field for certain zones is presented in Figure 4-15. The drawdown field as such does not show the direction of water flow. The flow field caused by infiltration may be significant far from the withdrawal hole.

Table 4-4. Measured /Rhén et al., 1992/ and computed amount of water flowing through the tracer injection sections during the LPT2 pumping test. The computed values are based on the equivalent-continuum approximation and calculated for the calibrated base model.

Injection section	Zone interpreted	Measured (ml/min)	Computed (ml/min)
KAS02-4	EW-5	2	4.7
KAS02-2	NE-1	4	[1]
KAS05-3	EW-5	9	3.1
KAS05-1	(no zones)	11	[2]
KAS07-4	EW-5	18	3.3
KAS08-3	NNW-2	21	2.9
KAS08-1	NE-1	48	1.8
KAS12-2	NE-2	107	1.3
KAS13-3	(no zones)	3.3	[2]
KAS14-2	NE-1	11	1.8

[1] In the simulation model borehole KAS02 does not intersect zone NE-1, see Figure 4-3. The calculated flow rate is very small in the matrix.
[2] No zone is interpreted to this section, see Figure 4-3, and the calculated flow rate is very small in the rock matrix.

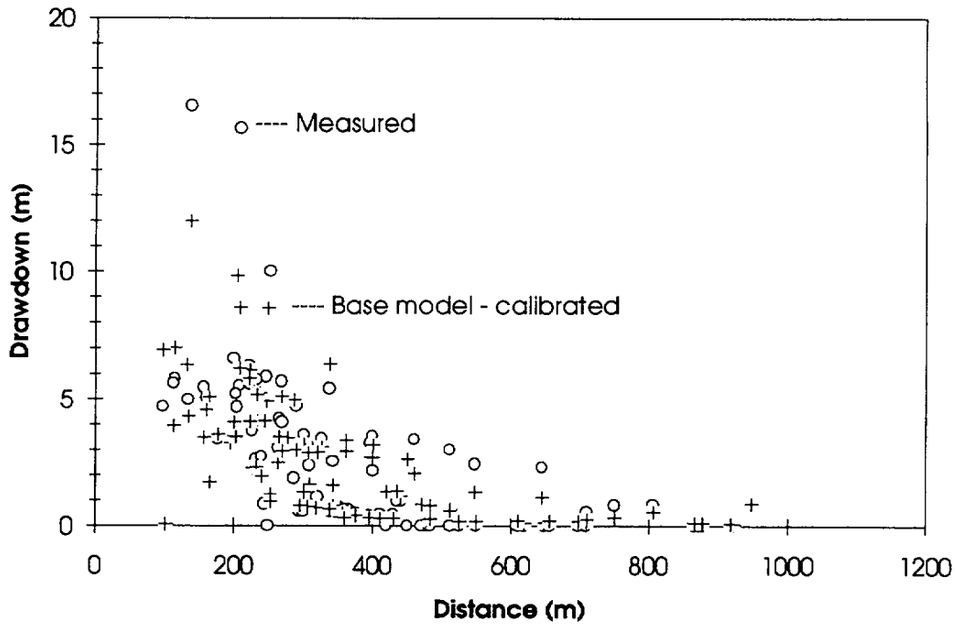

Figure 4-12. *Measured and simulated pressure drawdown in the observation sections of the cored and percussion boreholes as a function of the "distance" for LPT2. The computed values are for the calibrated base model. The "distance" and measured drawdowns from Rhén et al., 1992 and Ström, 1993a.*

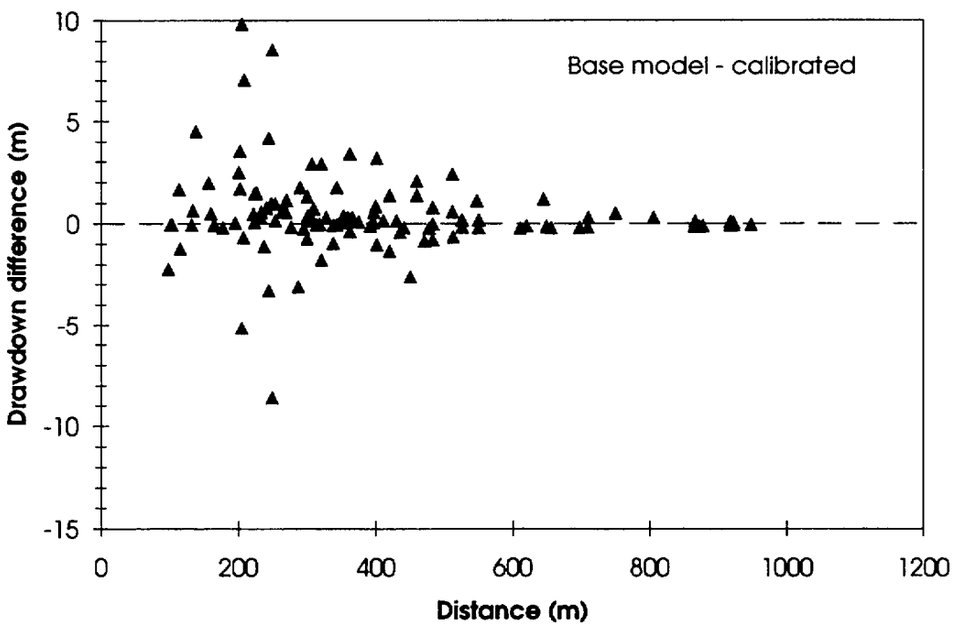

Figure 4-13. *Difference between the measured and simulated drawdowns shown in Figure 4-12. The "distance" for each observation section from Rhén et al., 1992.*

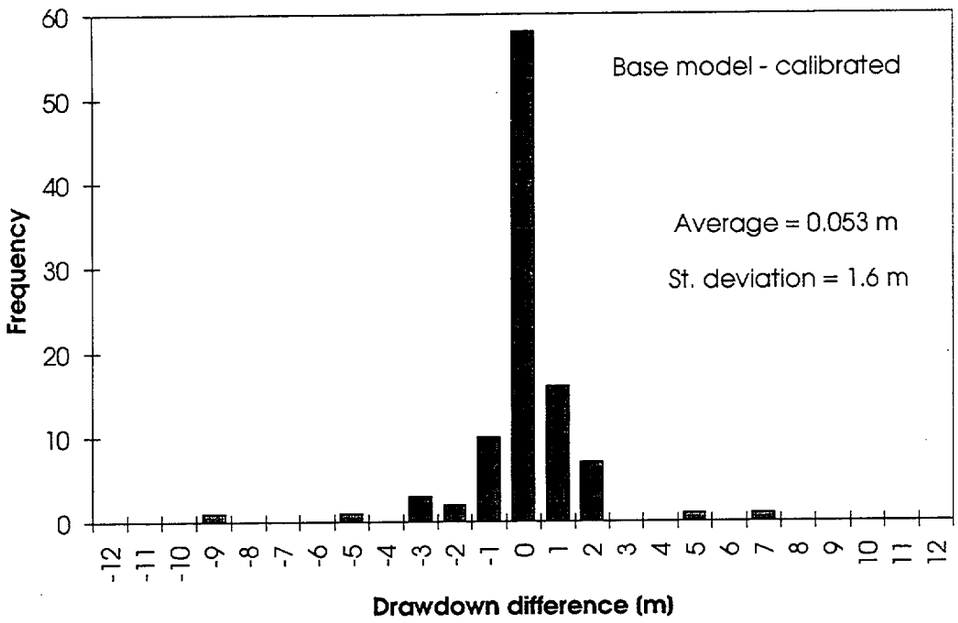

Figure 4-14. Distribution of the differences of the measured and simulated drawdowns shown in Figure 4-13.

Transient simulations

Twelve observation sections were selected to study the transient hydraulic response of the model in comparison with the measured data. Out of the twelve sections, seven intersect a zone and five have been interpreted to be in the rock matrix (Figure 4-16).

The field data is presented for all of the sections in Figure 4-16. In most of the sections, the measured drawdown still increased at the end of the pumping period. In some sections, the rate of the increase was significant. The drawdown did not stabilize in any of the sections that are in the rock matrix. It should be noted that the drawdowns reported by Rhén et al. /1992/ for the end of the pumping period do not for all observation sections coincide with the transient data by Rhén & Forsmark /1993/.

The observation sections in Figure 4-16 can be divided to five groups according to the comparison of the measured data with the computation results. The measured results for section KAS07-J2 are considered very uncertain /Ström, 1993a/ and thus the simulation results of this section cannot be scrutinized. In section KAS07-J6 the measured drawdown is much larger than the computed values, which impairs any comparison. The

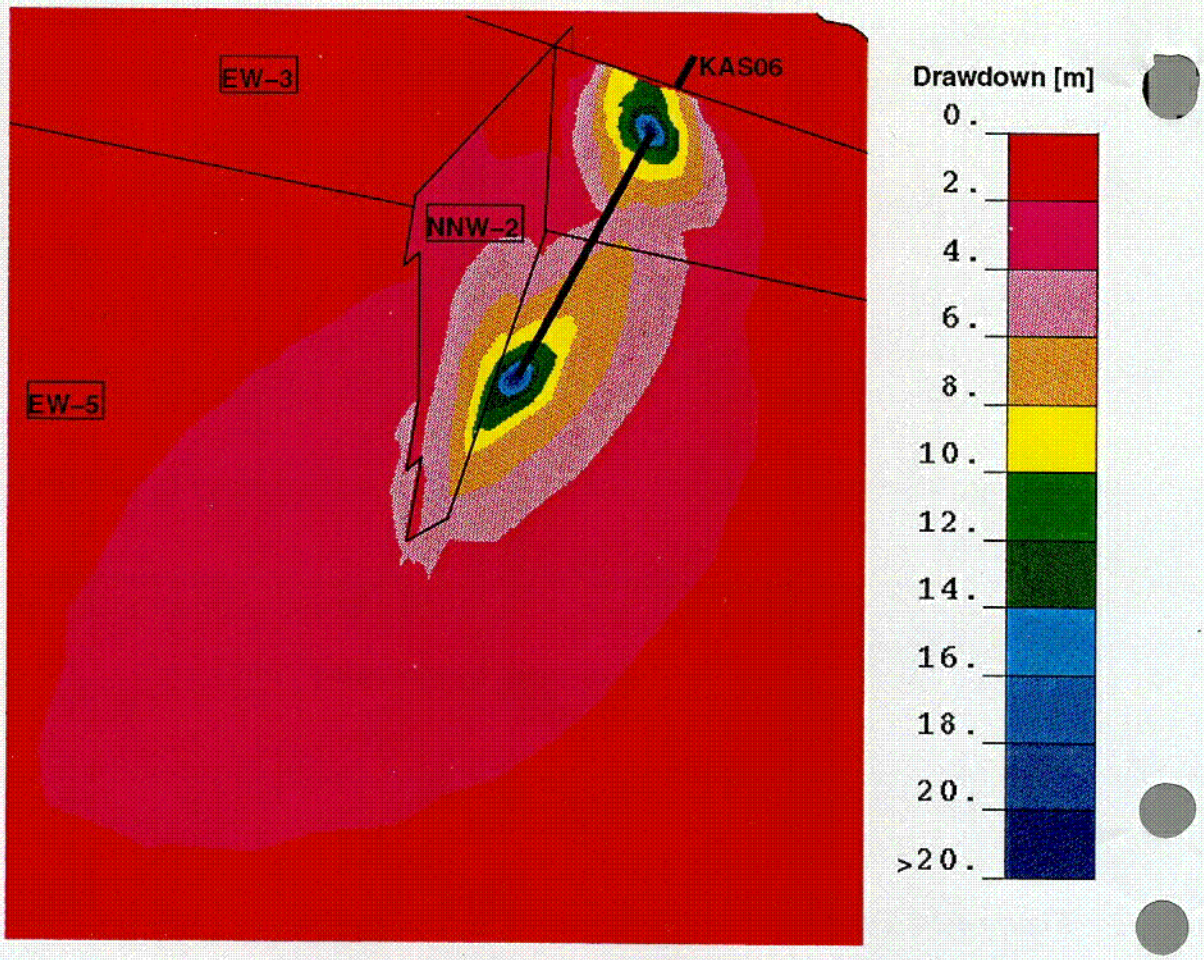

Figure 4-15. *Simulated drawdown of the pressure for LPT2 in zones EW-3, EW-5 and NNW-2.*

time dependence of the measured data is, however, close to the results computed for the specific storage of 10^{-6} m^{-1} and the storativity of 10^{-6}. The third group comprises the sections in which the measured drawdown increases faster than in any of the simulation cases suggesting a smaller specific storage or a direct connection to the pumped hole (KAS05-E1, KAS05-E5, KAS08-M4). All these sections have been interpreted to be in the rock matrix. The rest of the field results in Figure 4-16 can be divided into two groups: to those which behave as the results for the specific storage of 10^{-6} m^{-1} and the storativity of 10^{-6}, and to those following the simulation results for the specific storage of 10^{-7} m^{-1} and the storativity of 10^{-7}. Constant values for the specific storage and storativity are not applicable for the bedrock throughout the site.

C-07

4.4.2 Sensitivity and uncertainty analysis

In the sensitivity and uncertainty analysis, we studied how a significant change in the calibrated hydraulic conductivities affects the simulation results, the inflow and especially the drawdowns in the cored boreholes. The hydraulic conductivity of a fracture zone or the rock matrix was increased and decreased in each case two orders of magnitudes from those in the calibrated model. The LPT2 test was simulated as above. The drawdowns in the cored boreholes and the inflow to the withdrawal hole KAS06 were compared with results computed for the calibrated model as well as with field data. The sensitivity and uncertainty analysis comprises thus another 34 simulation runs.

Increasing or decreasing the hydraulic conductivity of any of those zones that intersect the withdrawal hole (i.e., NNW-1, NNW-2, EW-3 or EW-5) affects significantly the total inflow and its distributions among the zones. Therefore, these cases were not considered likely although in some of these cases, the pressure drawdowns are comparable with the results for the calibrated model. It is anyhow possible that the equivalent (cross-zone) transmissivities of these zones are larger farther away from the pumped hole. Near the withdrawal hole, these zones possess low conductivity parts resulting in a smaller inflow to the pumped hole than determined by the equivalent cross-zone transmissivity. Similarly, these zones can as well be less conductive on a larger scale than in the vicinity of KAS06, and the water could flow to the well conductive part of a zone mainly from other zones. These complicated cases will be studied further in connection with the modelling for the updated structural model in Chapter 5.

The hundred-fold increase of the hydraulic conductivity of the rock matrix causes too large inflow into the pumped hole from the matrix. It is also possible that the equivalent hydraulic conductivity of the matrix is larger on a site scale and only the matrix around KAS06 is relatively tight limiting the inflow. Increasing or decreasing the hydraulic conductivity of the matrix does not affect the drawdowns significantly. The drawdowns for the case with the hydraulic conductivity increased hundred-fold show sharper peaks along the boreholes at locations that are close to KAS06 (in KAS05 and KAS07). In addition, the agreement with the field data is somewhat poorer than for the calibrated case.

A change in the transmissivity of EW-1 influences drawdowns only in boreholes KAS03 and KAS04. Actually, the case in which the transmissivity of EW-1 was assumed to be hundred-fold compared with the calibrated model gives drawdowns with a better agreement with the field data in KAS03 and in the upper part of KAS04. These boreholes are far from the well-characterized area and borehole KAS06. The improvement is not significant because the drawdowns are small. Moreover, the boundary conditions or missing bedrock features are also likely sources of the poorer agreement of the calibrated model. Because of that, the increase in the transmissivity of EW-1 was not considered as an improvement when calibrating the model.

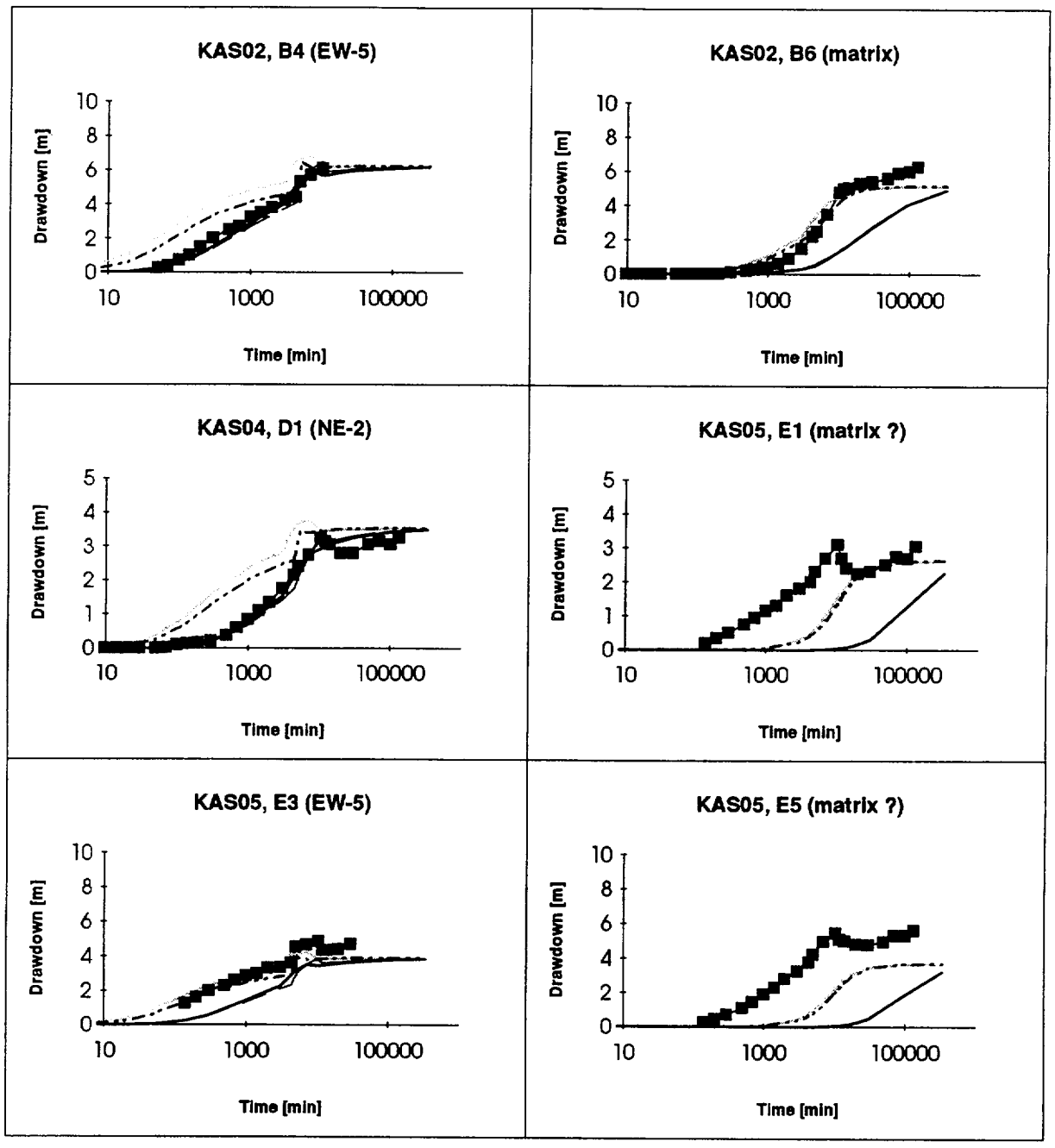

Figure 4-16. *Measured and simulated pressure drawdowns as a function of time in twelve observation sections for LPT2. The computational results are for the calibrated base model. The measured values from Ström, 1992. *) The last value from Rhén et al., 1992.*

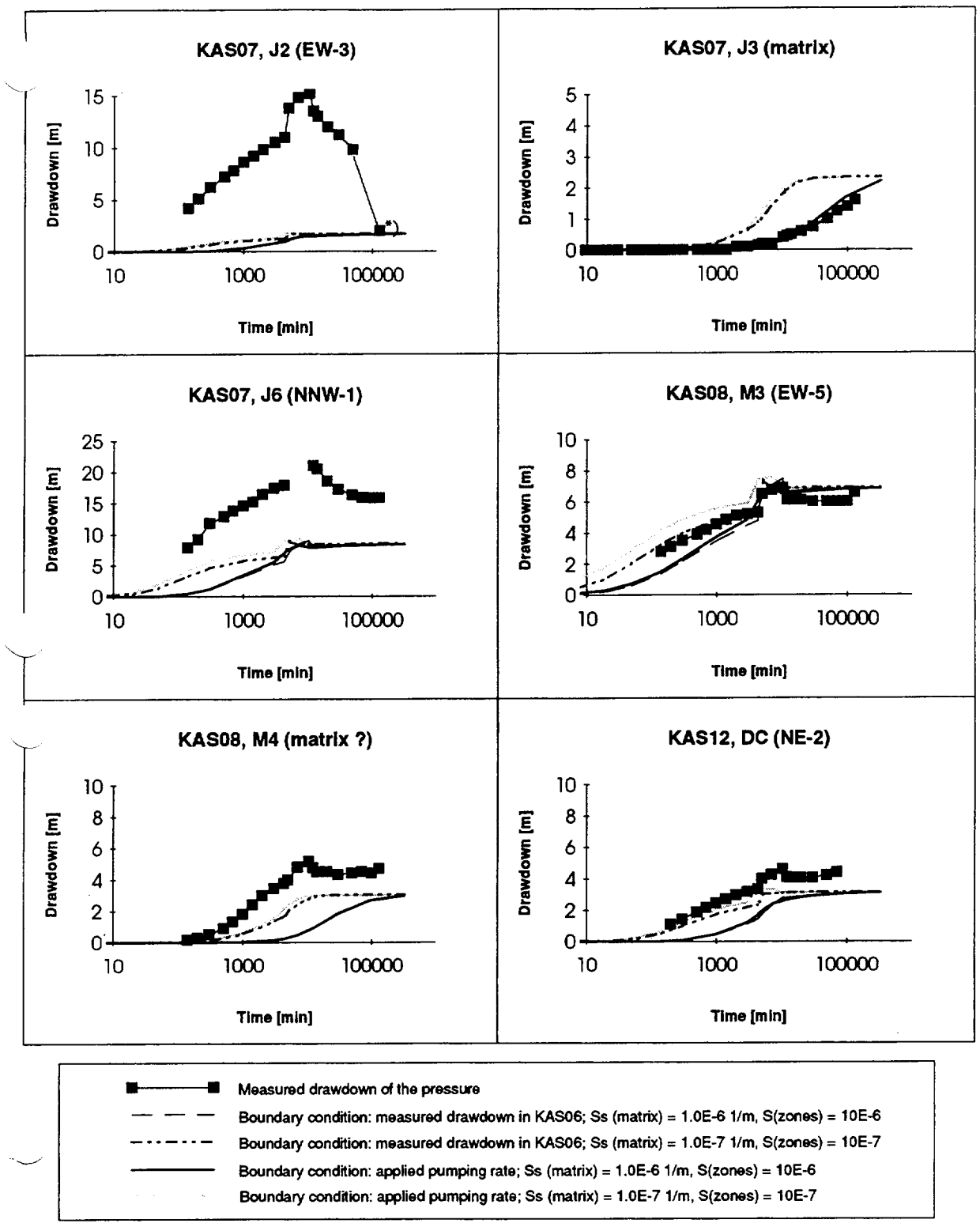

Figure 4-16. *(Continued.)*

Modifying the transmissivity of NE-1a does not result in very significant changes in the drawdown. It would, however, influence the inflow in LPT1. Similarly, modifying the transmissivity of NE-1b does not affect notably the drawdown field. The small influences of the modifications in the transmissivities of either NE-1a or NE-1b are expectable because the zones run parallel and they are highly permeable. Their transmissivities are so large compared to the hydraulic conductivities of other features that an increase in their transmissivity does not influence the pressure responses. On the other hand, decreasing the hydraulic conductivity of one of these zones does not affect the pressure field as the other zone remains conductive enough.

The computed drawdowns are sensitive to the transmissivity of NE-2. Already in the calibration phase, it was increased in order to decrease drawdowns in KAS04. A decrease or increase of two orders of magnitudes in the transmissivity of NE-2 makes the agreement with the field data significantly worse than in the case of the calibrated model.

The pressure responses in the cored boreholes are sensitive to the transmissivities of some NNW zones. Modifying the transmissivities of NNW-1 or NNW-2 changes the drawdowns. As discussed above, the influences on the inflows to the withdrawal hole are even more dramatic and thus these cases are not considered likely. On the other hand, the drawdowns are not affected at all by the transmissivities of NNW-3 and NNW-6. The pressure field is also quite insensitive to the transmissivities of NNW-4 and NNW-5. Only a hundred-fold increase of the transmissivity of NNW-5 makes the agreement of computed drawdowns with the measured ones significantly worse by leading to too small drawdowns in some boreholes.

The conclusions from the sensitivity and uncertainty analysis are following. The pressure responses are insensitive to the transmissivities of most of the zones. Besides the zones intersected by KAS06 (NNW-1, NNW-2, EW-3 and EW-5), only a change in the transmissivity of NE-2 causes a significant deviation from the results of the calibrated model. The uncertainties of the transmissivities of those zones cannot then be bounded on the basis of these simulations. The uncertainty of the hydraulic conductivity of the rock matrix is about two orders of magnitudes from the initial values on the basis of the simulations.

4.4.3 Discussion

Since the flow model is a simplification of the real bedrock, it does not coincide perfectly with the field data interpretations. The discrepancies arise, for instance, from the assumption of the planarity of the zones. In some cases, geometrical simplifications cause differences between the measured and computed drawdowns.

The numerical simulations, especially the calibration phase as well as the sensitivity and uncertainty studies, improved our understanding on the site. Indications on several modifications on the model were also obtained. First, there seems to be a very highly transmissive connection between KAS06 and KAS07. In the bedrock model, that bedrock feature is interpreted to be NNW-1. The simulated drawdowns are not as high as measured (Figure 4–4). A likely explanation is the anisotropy of NNW-1. Secondly, in the north-south direction, the extent of the NNW-1 zone might also be smaller than in the model, which would direct the pressure field more to the up-down direction. This would also explain the small drawdowns to the north from KAS06 (in KAS04), which in the calibrated model were obtained by increasing the transmissivity of NE-2. Thirdly, the boundary conditions may account for the low drawdowns in the middle and northern parts of the island. Finally, the simulations indicate that the vertical extent of NNW-1 or its most permeable part could also be smaller.

According to the field data, there is a highly permeable connection from KAS06 to the second lowest packer interval of KAS07. The hydraulic connection fits well to the EW-3 zone. This connection, on the other hand, should be considered with care because in LPT1 (pumping in KAS07) it does not transfer a large pressure response to the upper part of KAS06. This could be, however, also a result of the anisotropy, the boundary conditions or the extent of the EW-3 zone. In addition, as stated above the ten-meter drawdown in the second lowest packer section in KAS07 during LPT2 is very uncertain /Ström, 1993a/. Therefore, it was not used in evaluating the performance of the model.

The sources of the differences between the computed and the measured drawdowns in the cored boreholes were discussed above in connection with the calibration in Section 4.3. In the uppermost sections of KAS03 and KAS04, no pressure drawdown was observed. The computed values are between one and two meters. The reason for that type of field observation could be that the soil in the northern part of the island acts as water reservoir, and the situation at the end of the pumping period is still transient. This is also supported by the field data /Ström, 1992/. The incompleteness of the steady state in the field experiment is a likely source of the too large simulated drawdowns in a few observation sections.

The sensitivity and uncertainty analysis showed that the hydraulic conductivity of several zones could be modified without affecting the drawdown field. The simulation results are sensitive only to the transmissivities of NE-2 and the zones intersected by the withdrawal hole.

5 UPDATED MODEL

5.1 INITIAL FLOW MODEL

5.1.1 Geometry of the zones

The geometry of the updated flow model is based on the updated structural model reported by Ström /1993/. The updated structural model is depicted at the ground level in Figure 2–2 and at a depth of 300 m in Figure 5–1. The corresponding horizontal cut planes for the updated flow model are presented in Figure 5–2. Figure 5-3 shows the occurrence of the zones in the cored boreholes according to the core-log interpretations and the intersections of the boreholes and the zones in the flow model. The dip angles and directions of the zones are given in Table 5-1.

The most significant changes in the zone geometry between the base and updated flow models are following (see Figures 4-2, 5–2 and 5–3, and compare with Figures 4–1 and 4–3):

- Fracture zone EW-1 is split into four different sub-zones in the updated flow model. This modification was the largest individual change concerning the geometry of the model.
- NW-1 was extended to the east-south well beyond EW-1.
- NE-2 was extended to the north-east to connect EW-1 and EW-3.
- EW-5 was moved about 50 m north of its previous position.
- The vertical fracture zones NNW-1, -2, -3, -4, -5 and -6 are defined by two endpoints by Ström /1993/. This may have led the positions of these fracture zones in the updated flow model to change slightly.
- NE-1 consists of two subzones that intersect each other at the ground level.
- NE-3 comprise two subzones with different locations and dips.
- NE-4 consists of two subzones. In the base structural geometry, the dip of NE-4 was vertical. In the updated model, both of the two sub-zones are sub-vertical.
- EW-7 was not included in the base model.

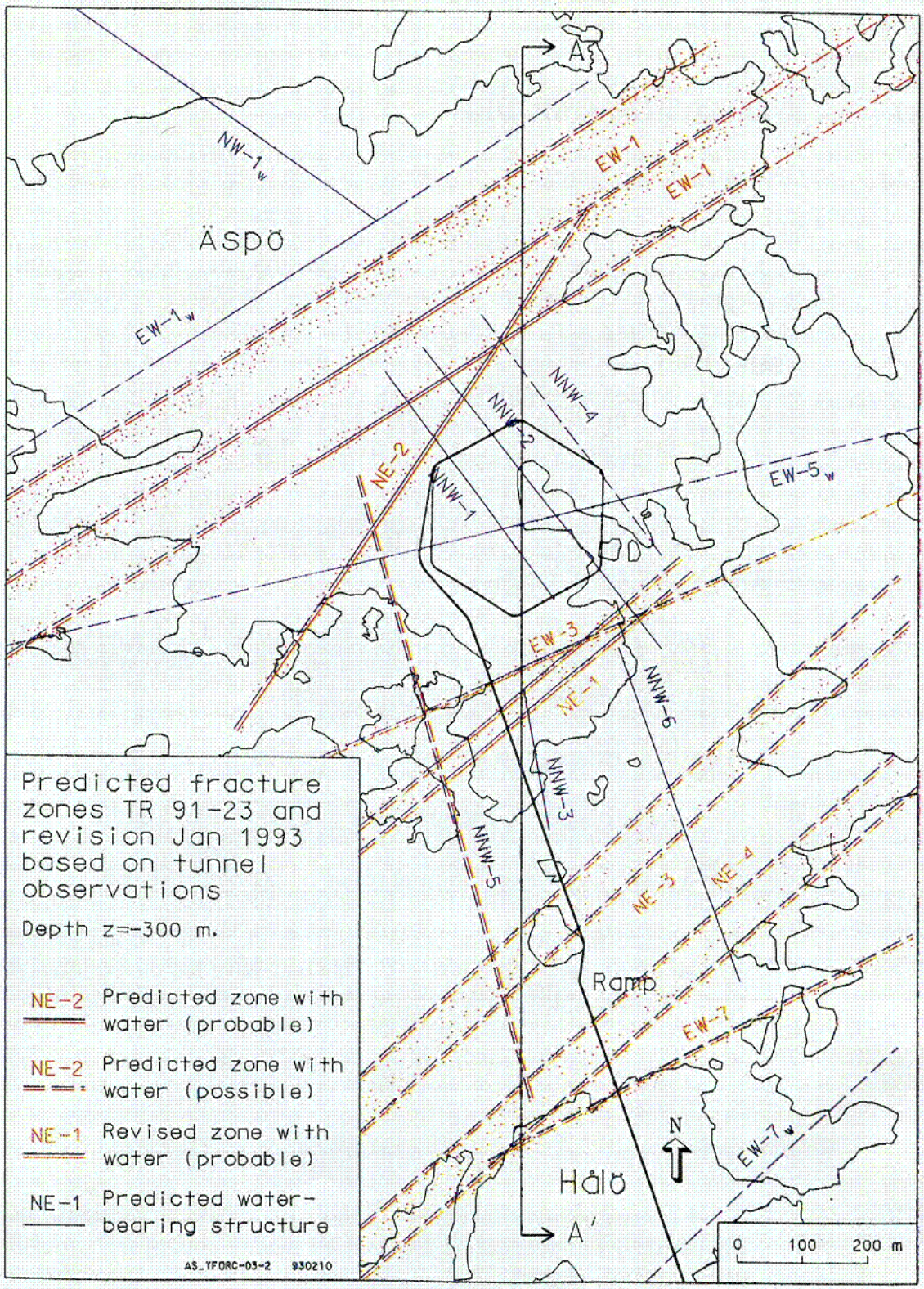

Figure 5–1. *Updated geometry of the structural model by Ström /1993/ at a depth of 300 m. Compare with Figure 2–2.*

C-08

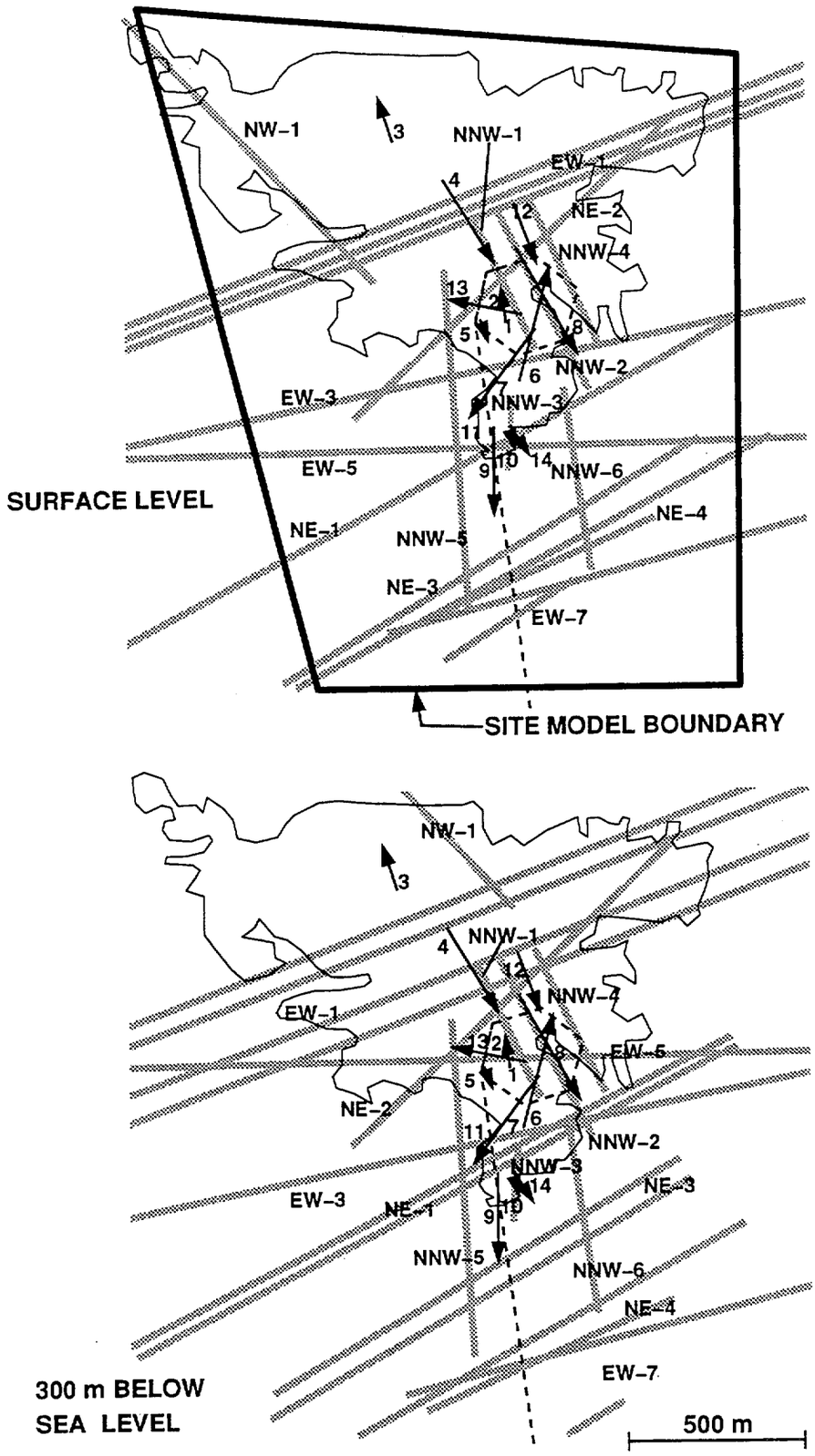

Figure 5–2. *Outlines of the site model and the updated zone geometry in the flow model at the ground surface (top) and at a depth of 300 m (bottom). Compare with Figures 2–2 and 5–1.*

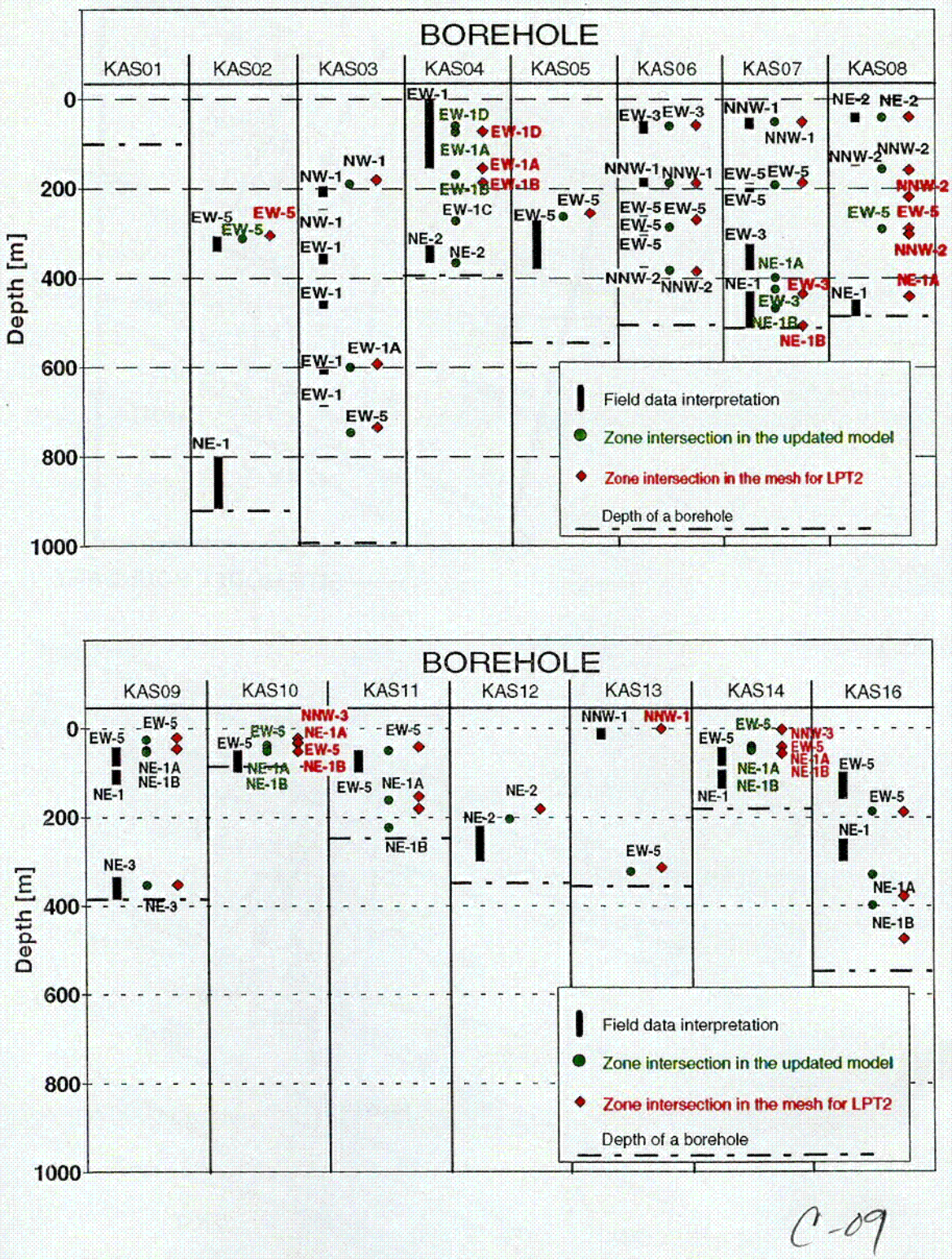

C-09

Figure 5–3. *Intersections of the cored boreholes and the fracture zones according to the field data interpretations, the updated flow model geometry and the corresponding element mesh for LPT2. Compare with Figure 4–3.*

Table 5–1. Dip angles and directions of the fractures zones in the updated flow model. Multiple dip angles mean that the fracture zone consists of two or more subzones (cf. Figures 4–2 and 5–2).

Fracture zone	Dip angle (°) and direction
NW-1	30 NE
EW-1A, B, C, D	60 NW, 88 NW, 78 SE, 75 NW
EW-3	79 S
EW-5	37 N
NE-1A, B	70 NW, 75 NW
NE-2	78 NW
NE-3A, B	80 NW, 70 NW
NE-4A, B	78 SE, 71 SE
NNW-1	vertical
NNW-2	vertical
NNW-3	vertical
NNW-4	vertical
NNW-5	vertical
NNW-6	vertical
EW-7A, B	81 S, 52 SE

5.1.2 Hydraulic conductivities

The initial and calibrated equivalent-continuum values of the transmissivities of the fracture zones and the hydraulic conductivity of the rock matrix are shown in Table 5–2. The initial values are based on the report of Wikberg et al. /1991/. The selection of the value for the hydraulic conductivity of the rock matrix is discussed in Section 4.1.2.

For the fracture zones consisting of several subzones, the initial transmissivities of the subzones (e.g., EW-1A, -1B, -1C and -1D) in the updated model are chosen equal to the values given in Wikberg et al. /1991/ for the corresponding base-model zone (e.g., EW-1).

5.2 SIMULATION OF LPT2 WITH THE INITIAL UPDATED MODEL

With the updated flow model, the pumping during the LPT2 test was simulated with the initial values of the property parameters in the same way as when using the base model. A new finite element mesh was created according to the new geometry of the zones as described in Section 3.6. The

total number of elements in the updated pumping model is about 18000. Borehole KAS06 intersects the same zones in the pumping model as interpreted to occur in reality (Fig. 5-3).

Table 5–2. Initial and calibrated transmissivities of the fracture zones in the updated model and the hydraulic conductivity of the rock matrix. The initial values are based on the compilation by Wikberg et al. /1991/. The relative change in the transmissivity is shown only if the transmissivity was modified in the model calibration (see Section 5.3).

Fracture zone	Initial transmissivity (10^{-5} m^2/s)	Calibrated transmissivity given as a relative change to the initial value
NW–1	0.7	
EW–1A	2	
EW–1B	2	0.1×
EW–1C	2	0.1×
EW–1D	2	
EW–3	0.05	20×
EW–5	2	0.5×[1)]
NE–1A	20	0.5×[1)]
NE–1B	20	0.5×[1)]
NE–2	0.4	
NNW–1	1.5	0.5×
NNW–2	4	
NNW–3	2	
NNW–4	4	
NNW–5	5	
NNW–6	5	
NE–3A	3	
NE–3B	3	
NE–4A	35	
NE–4B	35	
EW–7A	0.7	
EW–7B	0.7	
Hydraulic conductivity of the rock matrix is $1 \cdot 10^{-9}$ m/s		

[1)] Outside the most conductive part of the zone (see Figure 5-21), the transmissivity is an order of magnitude smaller.

The same boundary conditions as originally chosen for the LPT2 modelling with the initial model were applied, i.e., for the nodes on the area of the Äspö island, no-flow boundary condition was applied and the fixed-pressure boundary condition was assumed elsewhere. For the initial model, only steady-state simulations were carried out. The influence of the pumping was implemented in the simulations by assigning the drawdown measured in the withdrawal hole at the end of the pumping to the nodes representing the pumped hole.

The drawdowns in the cored boreholes calculated with the initial model are presented in Figure 5-4 with the measured values. The agreement of the simulated drawdowns with the field data is good. The largest differences between the measured and computed drawdowns are smaller than in the case of the initial base model (cf. Figure 4-4). In KAS01, in the upper part of KAS02 and KAS13, and especially in the lower part of KAS04, the computed results are now closer to the measured ones than those for the base model. On the other hand, the agreement is somewhat poorer in some packed-off sections. The deviation is even larger than for the base model in the lowest section of KAS02. In the uppermost sections of KAS03 and KAS04, the computed drawdown is now between one and two meters as the simulation results of the base model were closer to the measured no-drawdown result. Moreover, in the uppermost section of KAS08, the agreement of the drawdown of the updated model with the measured value is better than with the base model. The results of the initial updated model are in many cored boreholes closer to those of the calibrated base model than the drawdowns of the initial base model. This is the case, for instance, in KAS02, KAS04, KAS05, KAS08 and KAS12.

5.2.1 Performance measures

The computed steady-state drawdowns are listed in Appendix D for the observation sections of the cored and percussion boreholes. Appendix D includes the absolute and relative deviation between the simulated and measured drawdowns.

The comments given above (Section 4.2.1) on the influences of the simplifications of the zone geometries should be considered here as well. The results for observation section KAS07-J2 are not compared due to the uncertainty of the field data /Ström, 1993a/.

Figure 5-5 shows the measured and computed drawdowns as a function of the "distance". (The values of the "distance" from Rhén et al.,1992). The differences between the measured and calculated drawdowns are plotted in Figure 5-6 as a function of the "distance". Figure 5-7 shows the distribution of the differences. The average of the differences is equal to almost zero and thereby smaller than that of the initial base model. For almost half of the sections, the difference is less than 0.5 m. The standard deviation of the differences is also now smaller (1.8 m) than for the initial base model in

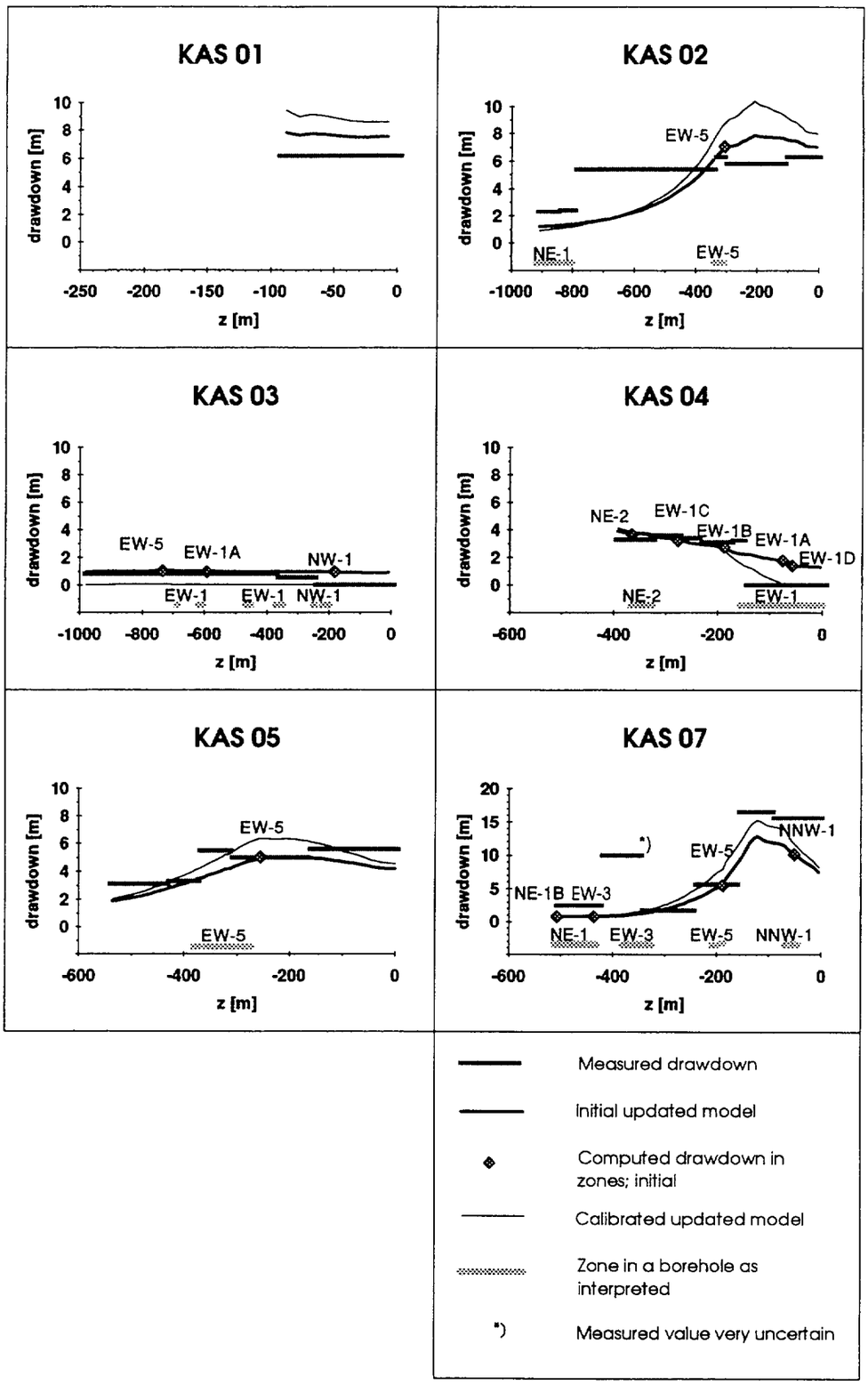

Figure 5-4. *Measured /Rhén et al., 1992 and Ström, 1993a/ and simulated steady-state pressure drawdowns in the cored boreholes for the LPT2 test. The computed values are for the updated structural model reported by Ström /1993/.*

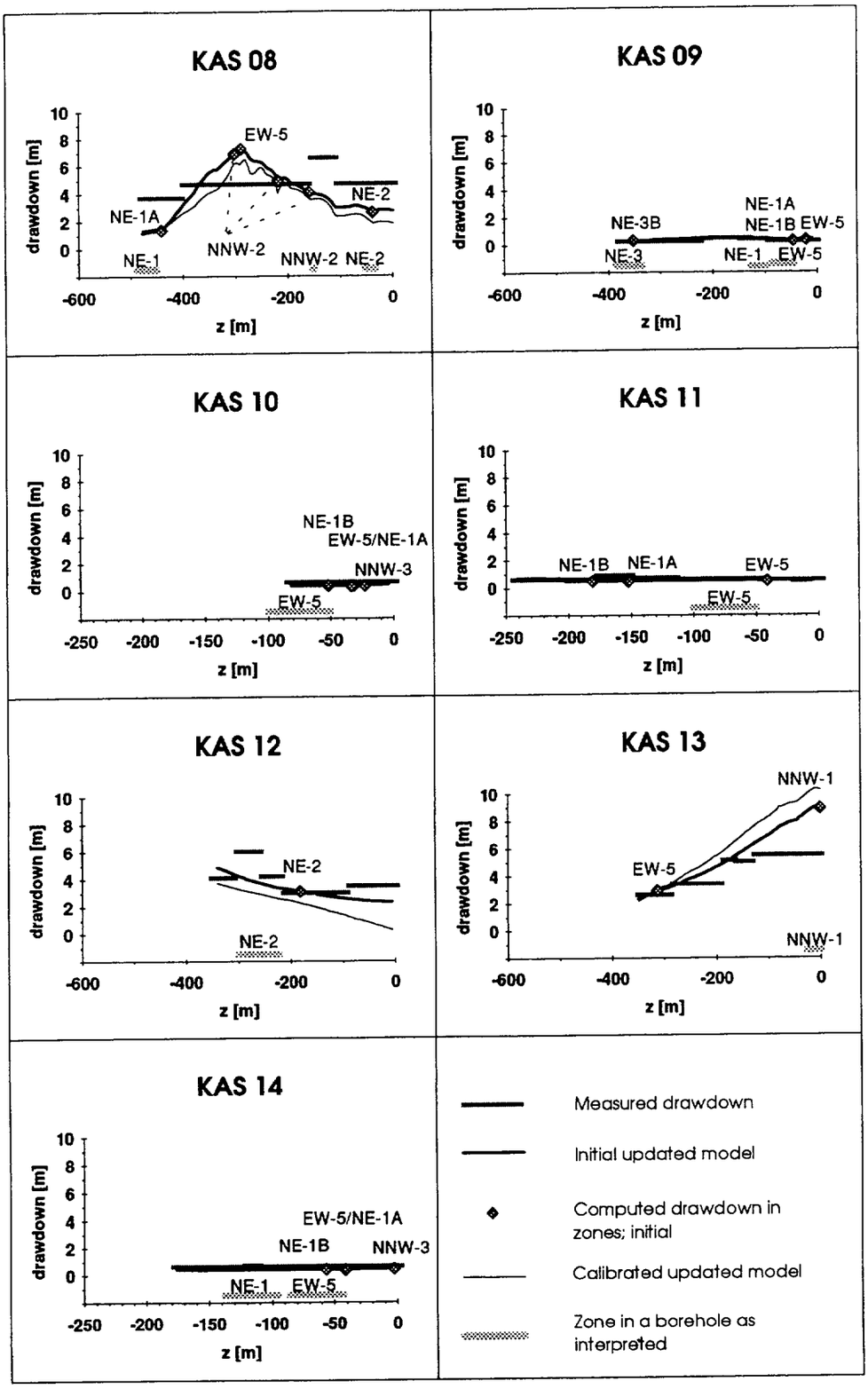

Figure 5-4. (Continued.)

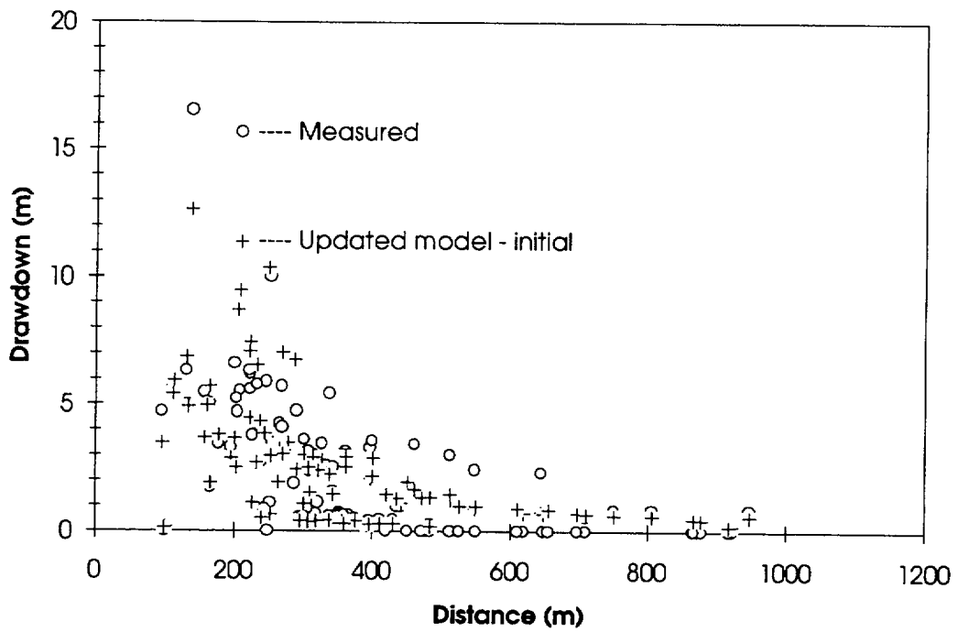

Figure 5-5. *Measured and simulated drawdown in the observation sections of the cored and percussion boreholes as a function of the "distance" for LPT2. The computed values are for the initial updated model. The "distance" and measured drawdowns from Rhén et al., 1992 and Ström, 1993a.*

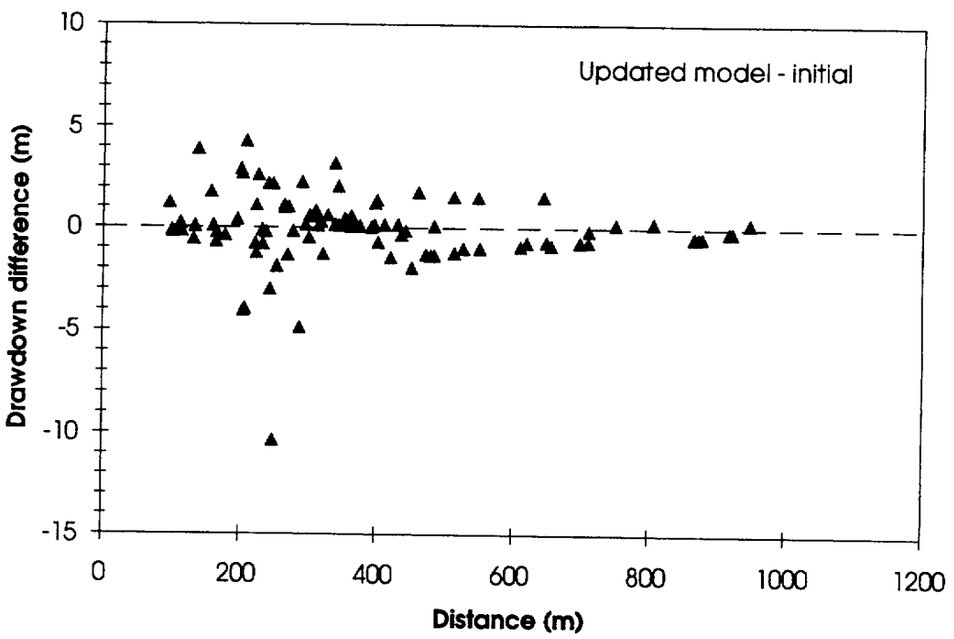

Figure 5-6. *Difference between the measured and simulated pressure drawdowns shown in Figure 5-5. The "distance" for each observation section from Rhén et al., 1992.*

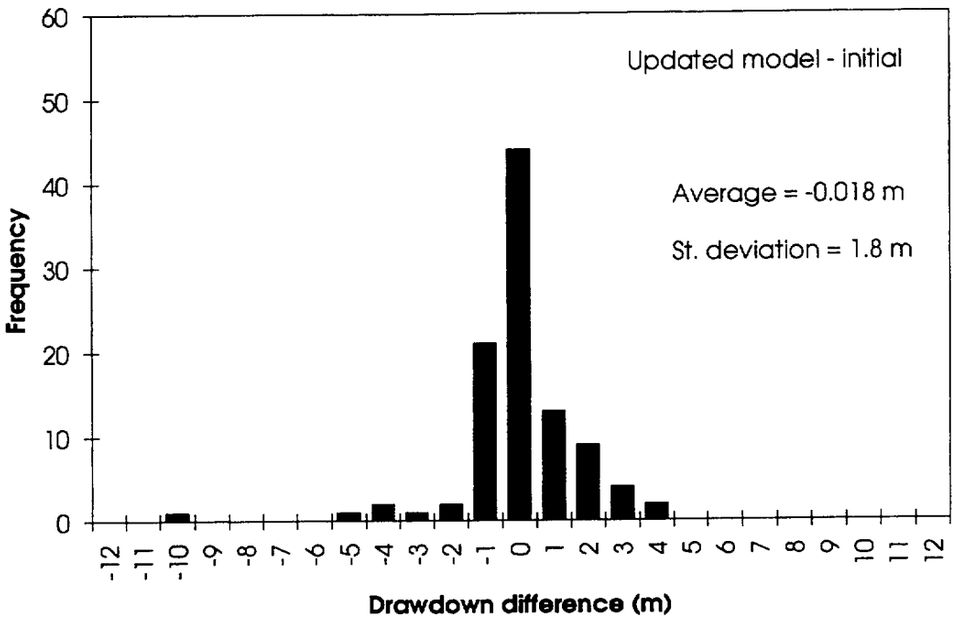

Figure 5-7. *Distribution of the differences between the measured and simulated pressure drawdowns shown in Figure 5-6.*

Figure 4-9. Compared to the results of the calibrated base model (Figure 4-13), the average and the standard deviation of the differences are quite similar.

Since the initial values of the hydraulic conductivities are the same as in the base model, the inflow to the withdrawal hole does not change much. The simulated total water inflow to the pumped borehole, KAS06, is 2.7 l/s. The distribution of the total inflow among the rock matrix and the zones is presented in Table 5-3.

The same approaches as with the initial base model (Section 4.2.1) were employed to calculate the amount of water flowing through the tracer injection sections. Undisturbed flow conditions were simulated as described in Section 3.5 (see Section 5.3.4, too). The computed flow rates are compared with the measured values in Table 5-4. Modelling the heterogeneity of the bedrock would disperse the values around the average fluxes in Table 5-4 as showed for the initial base model in Figure 4-10.

5.2.2 Discussion

Because the geometry of the updated model around the withdrawal borehole, KAS06, is equal to that of the base model and the initial values of the hydraulic conductivities were the same, the simulation results concerning LPT2 are almost equal to those for the initial base model. The

Table 5-3. Measured /Rhén et al., 1992/ and simulated distributions of the water inflow to KAS06. The calculated values are for the updated model.

Hydrological unit	Measured (%)	Initial model (%)	Calibrated model (%)
EW-3	15	0.7	18
NNW-1	21	17	24
EW-5	33	26	35
NNW-2	26	56	24
NNW-x	5	-	-
Matrix	-	0.7	0.9

Table 5-4. Measured /Rhén et al., 1992/ and computed amount of water flowing through the tracer injection sections during the LPT2 test. The computed values are based on the equivalent-continuum approximation and calculated for the initial updated model.

Injection section	Zone interpreted	Measured (ml/min)	Computed (ml/min)
KAS02-4	EW-5	2	5.2
KAS02-2	NE-1	4	[1]
KAS05-3	EW-5	9	4.2
KAS05-1	(no zones)	11	[2]
KAS07-4	EW-5	18	5.0
KAS08-3	NNW-2	21	9.7
KAS08-1	NE-1	48	5.7
KAS12-2	NE-2	107	0.25
KAS13-3	(no zones)	3.3	[2]
KAS14-2	NE-1	11	8.2

[1] In the simulation model borehole KAS02 does not intersect zone NE-1, see Figure 5-3. The calculated flow rate is very small in the matrix.
[2] No zone is interpreted to this section, see Figure 5-3, and the calculated flow rate is very small in the rock matrix.

modified geometry of the zones makes the pressure responses in the observation sections to agree somewhat better with the field data than in the case of the base model. On the other hand, the agreement of the calculated drawdown in the observation section intersecting NE-1 is even poorer than for the initial base model. The largest deviations and their sources are nevertheless the same. The discussion concerning the initial base model (Section 4.2.2) applies thus the initial updated model as well and is not repeated here.

5.3 CALIBRATION

5.3.1 Calibration cases

Only the two long-term pumping tests, LPT1 and LPT2, were used to calibrate the base flow model (Section 4.3). When calibrating the flow model based on the updated structural model, the pumping tests performed in boreholes KAS12, KAS13, KAS14 and KAS16 were studied as well. The location of the boreholes is presented in Figures 1-1 and 5-2. From all the pumping tests conducted in the cored boreholes, the pumping tests in KAS12, KAS13 and KAS14 were selected according to the recommendation by Rhén /1991/. The pumping test carried out in KAS16 was also used because KAS16 is close to borehole KAS06 and therefore the results of the pumping test in KAS16 were expected to be sensitive to the area near KAS06. The duration of the pumping period in the pumping tests in KAS12, KAS13, KAS14 and KAS16 was about three days, considerably shorter than in LPT1 and LPT2 (50 and 92 days, respectively). The results of some other field experiments /Nilsson, 1990; Rhén, 1991; Rhén et al., 1991/ were also studied during the calibration process but no simulations were carried out for them.

The experimental arrangement in all of the pumping tests was the same: An open borehole was pumped and the pumping rate was measured. The drawdown of the water level in the withdrawal hole as well as the drawdown of the pressure in the packed-off sections of observation boreholes was monitored. The number of observation boreholes varied among the pumping tests. The distribution of the water inflow along a withdrawal hole was measured for those parts of the holes that were under the level of water. The inflow distribution to KAS12, KAS13, KAS14 and KAS16 includes thus similar uncertainties as the inflow distribution for LPT1 discussed above in Section 4.3.1. The raw field data of the pumping tests performed in boreholes KAS12, KAS13, KAS14 and KAS16 are introduced in the following section. The field results for LPT1 and LPT2 were discussed above in the introduction and in Section 4.3. The results of the inflow distribution measurements are interpreted in Section 5.3.3 to obtain data that is usable in the model calibration.

In the long-term pumping tests, LPT1 and LPT2, the responses in the pressure appeared very late in some observation sections (Figure 4-16 for LPT2). Steady flow conditions were thus not achieved even in these long-

term pumping tests. However, we presumed that a pseudo-steady state prevailed when pumping was stopped. As the duration of the pumping period of the pumping tests in KAS12, KAS13, KAS14 and KAS16 was short, the pressure responses in many observation sections and, in some cases, the drawdown even in the withdrawal hole were still increasing when pumping was stopped. Obviously the field results call for transient simulations but, because of practical (computing resource) limitations, steady state simulations need to be used in the calibration stage. Therefore, in order to simplify the comparison of simulation results and field data, we estimated drawdowns that would have been achieved if pumping had continued significantly longer. The estimation of these steady-state drawdowns is discussed in Section 5.3.3.

The hydraulically undisturbed conditions, which prevailed at Äspö before field investigations, were also simulated to test the updated model's performance. The boreholes with packers are not assumed to influence the flow conditions, which can therefore be assumed to have been undisturbed until the tunnel reached the Äspö island (and when no hydrological field experiments were conducted). The undisturbed conditions at Äspö reported by Rhén and Forsmark /1993/ are discussed more in the following section.

When calibrating the updated flow model, all the calibration cases were first simulated using the initial model. The simulation results for the initial model are presented in Section 5.3.4. By comparing the simulation results with the experimental data, the potential sources of discrepancies were deduced. The ideas were tested by simulations and the most likely were included in the model. This laborious stage is described briefly in Section 5.3.5. The simulation results for the calibration cases computed with the calibrated model are presented in Section 5.3.6.

5.3.2 Raw field data

The experimental results of the long-term pumping tests, LPT1 and LPT2, were introduced in Sections 1.2, 4.2 and 4.3. The raw field data for the pumping tests performed in KAS12, KAS13, KAS14 and KAS16 are described briefly in the following. The raw field data are presented comprehensively by Rhén /1991/ and Forsmark /1992a/.

Pumping test in KAS12

Borehole KAS12 is located to the north from KAS06 (see Figures 1-1 and 5-2). The depth of KAS12 is 380 m. It is interpreted to intersect zone NE-2 (Figure 5-3). At the ground surface, KAS12 is close to the southern branch of EW-1 (Figure 5-2). The borehole is between NNW-2 and NNW-4 but is interpreted to intersect neither of them.

During the pumping test in KAS12, the average pumping rate was low, 0.7 l/s /Rhén, 1991/. When the pumping was stopped, the drawdown in the

withdrawal hole was about 62 m. The large drawdown with the small inflow suggests that the total transmissivity of KAS12 is lower than that of most of the other deep holes. Comparing to LPT1 and LPT2, in which the drawdowns in the withdrawal holes were roughly the same, the inflow to KAS12 is one half and one third of those in LPT1 and LPT2, respectively. The small inflow to KAS12 is unexpected because during LPT2 the flow rate through a 50-meter long tracer injection section was more than 100 ml/min (1.6 ml/s) which is higher than for any other injection section (Table 5-4).

The fastest pressure responses were observed in the nearest boreholes KAS06 and KAS08 /Rhén, 1991/. The latest responses in the pressure appear in the observation sections not intersected by any of the zones in KAS01, KAS02, KAS05, KAS06 and KAS07 and the drawdown was still increasing notably in them when the pumping was stopped. Figure 5-8 shows the drawdown as a function of time in the observation sections of KAS02. Although the responses appeared late in many uppermost sections, the drawdown in them increased quite linearly and the slope was larger at the end than in any other section.

The drawdown at the end of the pumping period was small in most of the observation boreholes. The largest responses were measured in KAS08. Smaller drawdowns were observed in KAS02, KAS04, KAS05, KAS06 and KAS07. No hydraulic response was detected in the boreholes in the southern part of the island.

A spinner was employed to measure the distribution of the water inflow to KAS12. The contribution of the first 100 meters was not measured. For the rest of the borehole, the inflowing water comes from the depth interval between 240 and 330 m /Rhén et al., 1991/.

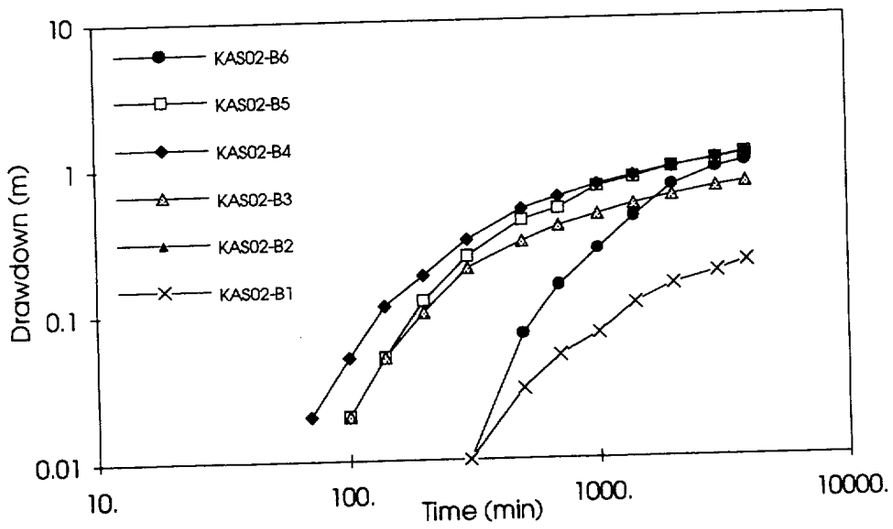

Figure 5-8. *Experimental drawdown in the observation sections of borehole KAS02 as a function of time during the pumping test in KAS12. The data from Rhén, 1991.*

Pumping test in KAS13

The 410 m deep borehole KAS13 is located to the west from KAS06 (Figures 1-1 and 5-2). According to the interpretations of field data, KAS13 intersects only the NNW-1 zone close to the ground surface (Figure 5-3). The bottom of the borehole is close to zones NE-2 and EW-5 (Figure 5-2).

During the pumping test in KAS13, the average pumping rate was 2.4 l/s /Rhén, 1991/. The drawdown in the withdrawal hole was 70 m at the end of the pumping period. The total transmissivity of the borehole is thus close to that of KAS06 pumped in LPT2.

The fastest responses in the pressure were observed in KAS02 and KAS05, which are located close to KAS13. The response appears late especially in the sections that are in the rock matrix. For instance, in the uppermost section of KAS08, the pressure started to decrease late, but reached at the end a higher value than in any other section of the borehole and was still increasing when pumping was stopped. The same characteristics can be recognized in the results of KAS06 and KAS07, too.

The drawdown was significant in several observation boreholes. At the end of the pumping period, the drawdown was higher than could be measured (30 m) in KAS01 and in the uppermost packer sections of KAS02 and KAS05. In KAS04, KAS06 and KAS07 as well as in certain percussion holes, the largest measured drawdowns were about 10 meters. An about five-meter drawdown was measured in the uppermost packer section of KAS08. No drawdown was observed in KAS03 and in the boreholes in the southern part of the island (KAS09, KAS10, KAS11 and KAS14).

The distribution of the inflow to KAS13 was measured with the spinner. The contribution of the first 100 m of the borehole is not known. For the rest, the inflowing water to KAS13 comes from the depth interval between 160 and 220 m.

Pumping test in KAS14

Borehole KAS14 is located further to the south of the area around KAS06 (Figures 1-1 and 5-2). KAS14 is 210 m deep and it is interpreted to intersect EW-5 and NE-1 (Figure 5-3). Zone NNW-3 is also close to the top of the hole (Figure 5-2).

The total transmissivity of KAS14 is high. With the average pumping rate of about 8 l/s, a maximum drawdown of only 16 meters was achieved in the pumped hole /Rhén, 1991/. Naturally the drawdowns in the observation boreholes are also smaller than in many other pumping tests.

After starting pumping in KAS14, the first responses could be identified in KAS09, KAS10 and KAS11. Although the level of water in the withdrawal hole did not change at the end of the pumping, the drawdown was still increasing significantly in many observation sections.

At the end of the pumping period, the drawdowns were largest (about 5 m), in KAS09, KAS10 and KAS11. Significant drawdowns (from 1 to 3 m) were measured also in boreholes KAS02, KAS05, KAS06, KAS07, KAS08 and even in KAS12, which are far from KAS14 (Figure 5-2).

According to the spinner survey /Rhén, 1991/, below the first 100 m all the inflowing water comes from a 50-m long borehole section from 110 to 160 m measured from the top of the borehole.

Pumping test in KAS16

Borehole KAS16 is located close to KAS06 (Figures 1-1 and 5-2). KAS16 is 550 m deep. The main objective of drilling borehole KAS16 was to find out the position of zone NE-1 deep in the bedrock /Forsmark, 1992a/. The borehole intersects NE-1 at a depth of about 400 - 500 meters and zone EW-5 at a depth of about 100 - 200 meters.

Borehole KAS16 was also drilled to investigate the hydraulic properties of NE-1 /Forsmark, 1992a/. In addition to other experimental studies, a pumping test was performed in KAS16. The average pumping rate was about 5 l/s. Before the stop of the pumping, the level of water in KAS16 had dropped about 30 meters. After the three-day pumping period, the drawdown was still increasing in the withdrawal borehole as well as in the observation boreholes.

The first responses for pumping in KAS16 were observed in KAS06, KAS07 and KAS08 /Forsmark, 1992a/. The uppermost sections of KAS02, KAS06 and KAS08 responded as the last ones and the drawdown was increasing in them when the pumping was stopped. Unfortunately in the copy of the report by Forsmark /1992a/ used in this study, the drawdown curves for KAS12 and KAS13 are missing.

Although the final drawdown in the withdrawal borehole was only 30 m, the magnitude of the pressure responses was large in many of the observation boreholes. At the end of the pumping period, the largest drawdowns are about 10 meters in KAS02, KAS05, KAS06, KAS07 and KAS08. Clear drawdowns were measured in all cored boreholes except in KAS03.

The distribution of the inflowing water along KAS16 was measured with an acoustic flow meter /Forsmark, 1992a/. The contribution of the first 100 m of the borehole was not measured, however. About 75% of the inflow to borehole KAS16 was interpreted to have flown from NE-1 and about 20% from EW-5.

Forsmark /1992a/ evaluated the pumping test as well as the other hydraulic tests performed in KAS16. He determined the hydraulic properties of NE-1 and EW-5 applying Jacob's semilog approximation and a log-log type curve method. The transmissivities obtained for NE-1 and EW-5 are in a good agreement with the results based on the data from the other boreholes. In case of EW-5, the data from KAS16 results in a transmissivity of about $3 \cdot 10^{-5}$ m^2/s close to the initial value of $2 \cdot 10^{-5}$ m^2/s. The hydraulic tests in KAS16 indicate a transmissivity value of $1.5 \cdot 10^{-4}$ m^2/s for NE-1. This is also close to the initial value.

Undisturbed flow conditions

Rhén and Forsmark /1993/ provided a summary on the hydraulic pressure under the natural, hydraulically undisturbed flow conditions. The summary is based on the measurements performed in boreholes KAS01–KAS08 in 1990 and KAS09–KAS14 in 1991. The pressure was monitored in five or six packed-off sections in each of the observation boreholes except in four sections in KAS08 and in one section in both KAS01 and KAS10. Rhén and Forsmark /1993/ report the minimum, maximum and average values over the measurement period for each packed-off section. The average values are denoted in Figure 5-9. The values are not time-integrated means but the averages of the lowest and highest values. Differences between the minimum and maximum values are typically 6000–8000 Pa, while the two highest differences, 22000 and 28000 Pa, are associated with KAS03.

Rhén and Forsmark /1993/ state that the measured values of the pressure for KAS09–KAS14 are somewhat uncertain, mainly because at southern Äspö the flow conditions were disturbed during the last six months in 1991. They estimate "the total error in groundwater level under hydraulically undisturbed conditions" in terms of the pressure to be ±1500–12000 Pa for the packed-off sections.

The field data on the salt concentration of the groundwater are based on the measured electric conductivity of water samples taken in 1988 from the packed-off sections of the boreholes mentioned above except boreholes KAS01 and KAS10 /Rhén & Forsmark, 1993/. A number of samples with the electric conductivity ranging from 60 to 3400 mS/m was analyzed and a linear dependence of the concentration on the electric conductivity was sought by means of the least square fit. The salt concentration calculated from the measured electric conductivity is presented in Figure 5-10.

Rhén & Forsmark /1993/ do not directly address the uncertainty of the correlation between the measured electric conductivity and the salt concentration. However, they introduce linear fits for the dependence of the density on the temperature and electric conductivity as well. According to them, a single measurement differs from that straight correlation line at most 1.5 kg/m^3, but normally less than 0.5 kg/m^3. They proceed that, taking into account the possibility of a water sample not being representative for the water in a packed-off section, the maximum error in the density is

±10 kg/m^3. If the total uncertainty in the density is converted to the uncertainty in the salt concentration, the error can be remarkable for an individual concentration value.

5.3.3 Interpretation of the raw field data

The reported data on the undisturbed flow conditions can be utilized as such in evaluating the performance of a model. Most of the field data for the pumping tests could also be used without any further processing. Some field data had to be interpreted, however. The inflow distributions along the withdrawal holes were measured, but the measurements did not cover the first 100 m from the top of the holes. The contribution of the first 100 m needs to be evaluated. Moreover, as stated above, practical limitations force us to restrict to steady-state simulations when calibrating the flow model. A consequence is that the drawdown data have to be interpreted to obtain values that can be compared with the results of steady-state simulations.

Estimating drawdowns for steady states

Steady flow conditions were thus not achieved even during the long-term pumping tests, LPT1 and LPT2. The duration of the pumping periods in these experiments was, however, so long that a pseudo-steady state could be assumed to prevail when pumping was stopped. The drawdowns of steady-state simulations could thus be compared with the drawdowns measured when the pumping was stopped in LPT1 and LPT2. The final drawdowns in the cored observation boreholes are presented in Figure 5-4 for LPT2 and in Figure 5-11 for LPT1. Even with LPT1 and LPT2 this might not have been a proper approach for those packed-off sections in which the pressure response appears late (see Figure 4-16).

It is thus obvious that hydraulically steady conditions were not reached during the three-day pumping tests in KAS12, KAS13, KAS14 and KAS16. Figure 5-8 shows the drawdown in the observation sections of KAS02 during the pumping test in KAS12. The drawdown is notably increasing in many observation sections, especially in the matrix and close to the surface. The time dependence of the drawdowns in various sections also varies which makes the evaluation of the steady-state drawdowns more difficult.

For the pumping tests in KAS12, KAS13 and KAS14, Rhén /1991/ estimated pseudo-steady-state drawdowns that should be equivalent to the drawdowns measured at the end of the pumping period of LPT1. The ratios of the drawdowns after three days and at the end of LPT1 were used to calculate section-specific correction factors. Applying these correction factors, Rhén estimated pseudo-steady-state drawdowns for the other pumping tests. There are several drawbacks of this approach. The time-dependence of the pressure response in an observation section might vary from experiment to experiment because of, for instance, differences in the distances and connections to the withdrawal boreholes. In some cases the

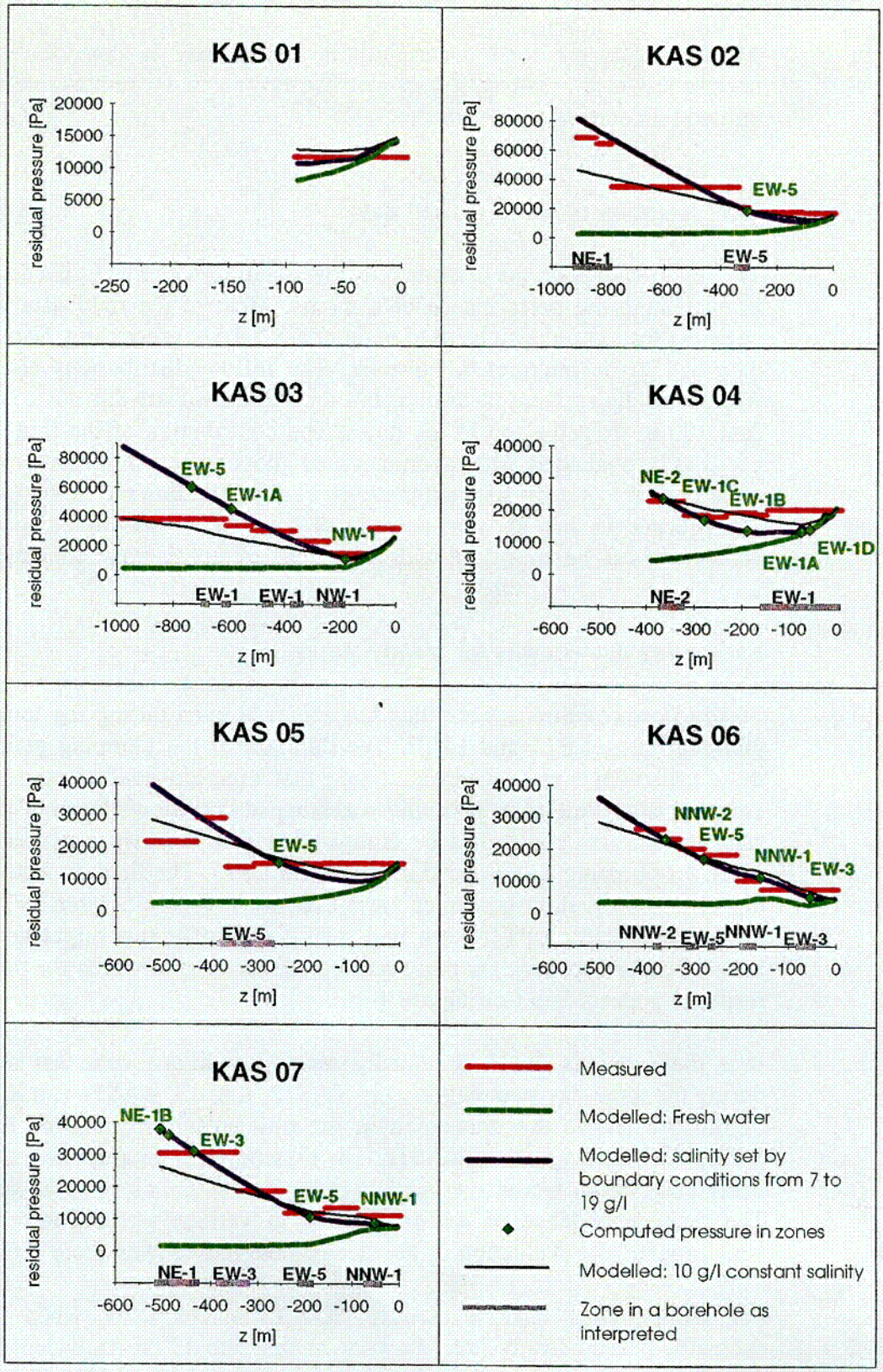

C-10

Figure 5-9. Simulated pressure for the three salinity models (Section 3.5). The green and thin black curves are the computed pressures for the fresh water and salt water (1%), respectively. The continuous blue curve shows pressure computed when solving the coupled equations for water flow and salt transport (cf. Figure 5-10). The red lines show the measured pressure /Rhén & Forsmark, 1993/.

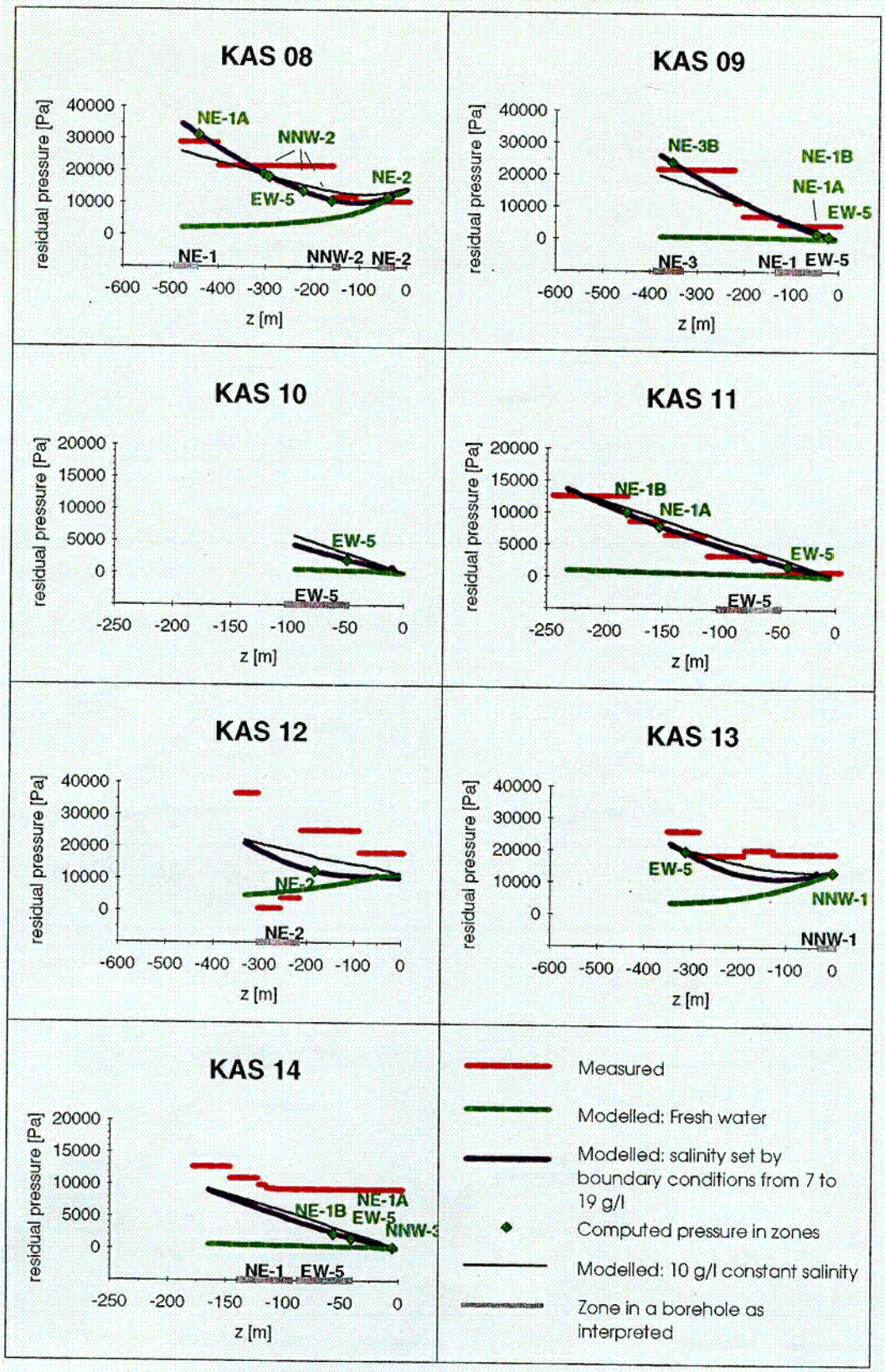

C-11

Figure 5-9. (Continued.)

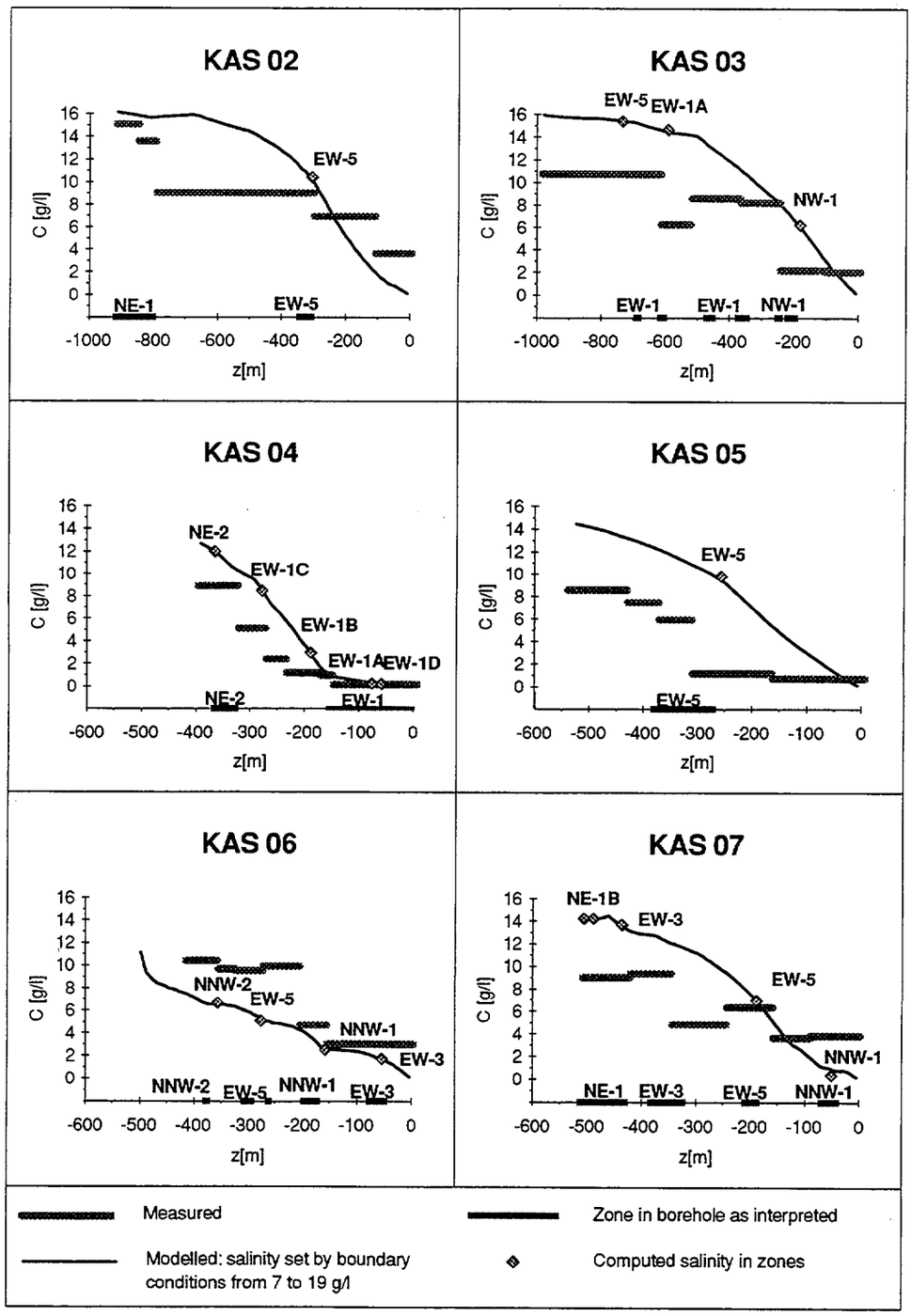

Figure 5-10. Simulated and measured salt concentration in the cored boreholes as a function of depth. The salt concentration computed by solving the coupled equations for water flow and salt transport (cf. Figure 5-9). The measured salt concentration from Rhén & Forsmark, 1993.

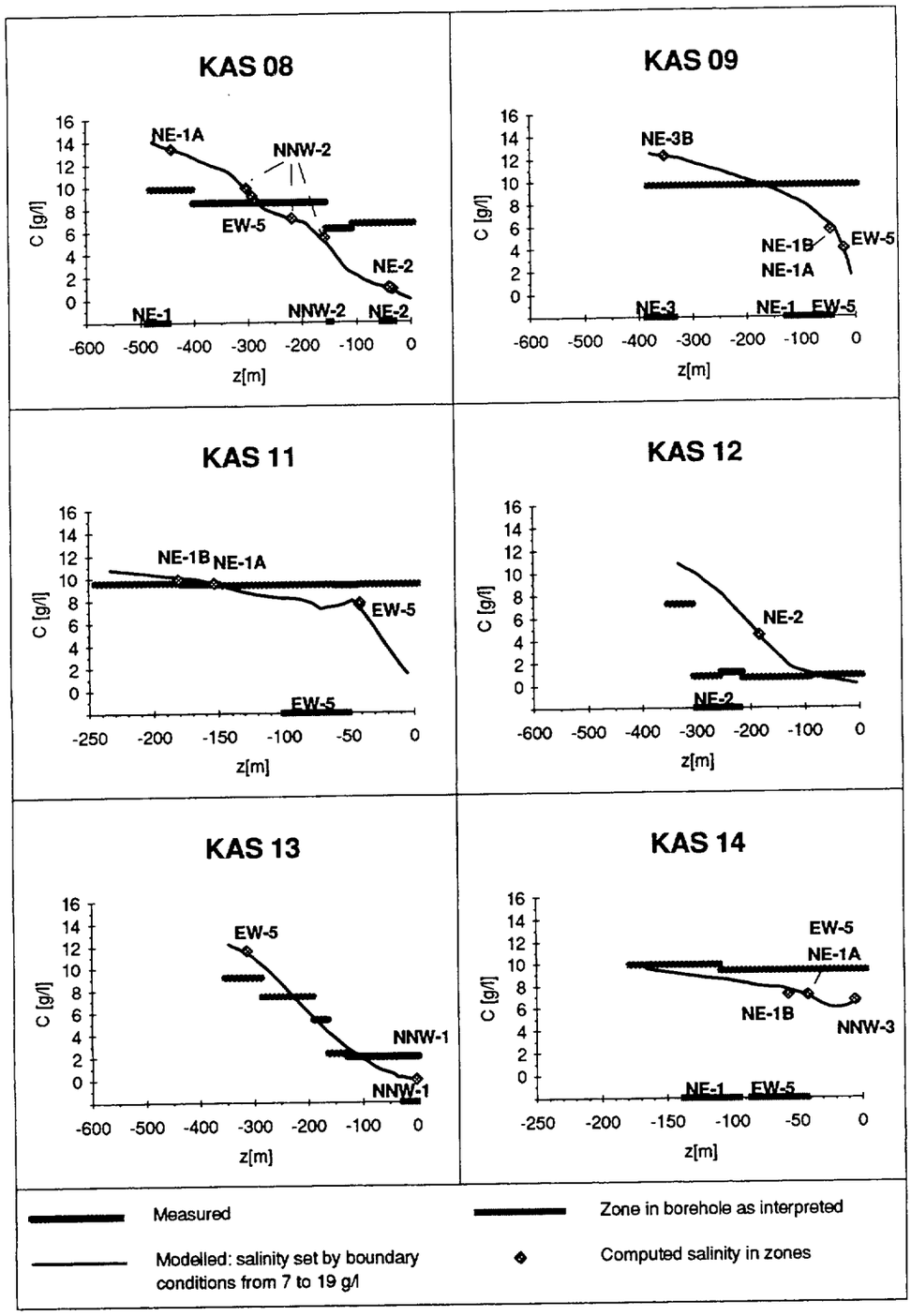

Figure 5-10. (Continued.)

approach results in very different drawdowns for various sections of a borehole although the measured data of the sections for the first three days are identical (for instance, in KAS04 during the pumping test in KAS12). In addition, the drawdown was not measured during LPT1 in all boreholes and for them no correction factor could have been calculated.

We estimated the steady-state drawdowns employing an other kind of approach. (The existence and results of Rhén's study were recognized later.) The drawdown as a function of time for each packed-off section of the cored boreholes was plotted in log-log scale (as in Figure 5-8) for the pumping tests in KAS12, KAS13 and KAS14. The drawdown curves were continued visually. Based on the drawdown versus time curves, we estimated how large the drawdown would have been if pumping had continued forever.

For the pumping test in KAS16, the drawdown versus time curves reported by Forsmark /1992a/ were used to evaluate the steady-state drawdowns. As the drawdown curves for KAS12 and KAS13 were not available, only the drawdowns at the end of the pumping period reported by Forsmark /1992a/ were used in evaluating the steady-state drawdowns.

Obviously the results based on our approach also include uncertainties. In some cases the drawdown was still clearly increasing when pumping was stopped. There are even sections that do not indicate any response during these short pumping periods but the results for LPT1 and LPT2 show that the responses would probably have appeared later. Especially in these cases the evaluation of the time dependence of the drawdown is difficult, and consequently the evaluated steady-state drawdowns involve uncertainties. Because in these sections the estimated drawdowns are in general small, the relative uncertainties are large. On the other hand, the relative uncertainties of the largest drawdowns are usually the smallest. These drawdowns generally occur in sections intersected by fracture zones and having a well-conductive connection to the withdrawal borehole. The drawdown does not typically increase significantly in these sections at the end of pumping.

The results of the two approaches are nevertheless quite similar. The largest differences are in the cases for which there are no field results for LPT1 and a correction factor of 100 % was applied by Rhén /1991/. Furthermore, in some cases when the correction factor is large (40 - 70 %) and the distance from the observation section to a withdrawal hole is smaller than in LPT1, the value obtained by Rhén can be unrealistically high (for instance, in KAS04 during the pumping test in KAS13).

In the following, the drawdown values we estimated to correspond to a steady state are called field data ignoring the word "interpreted".

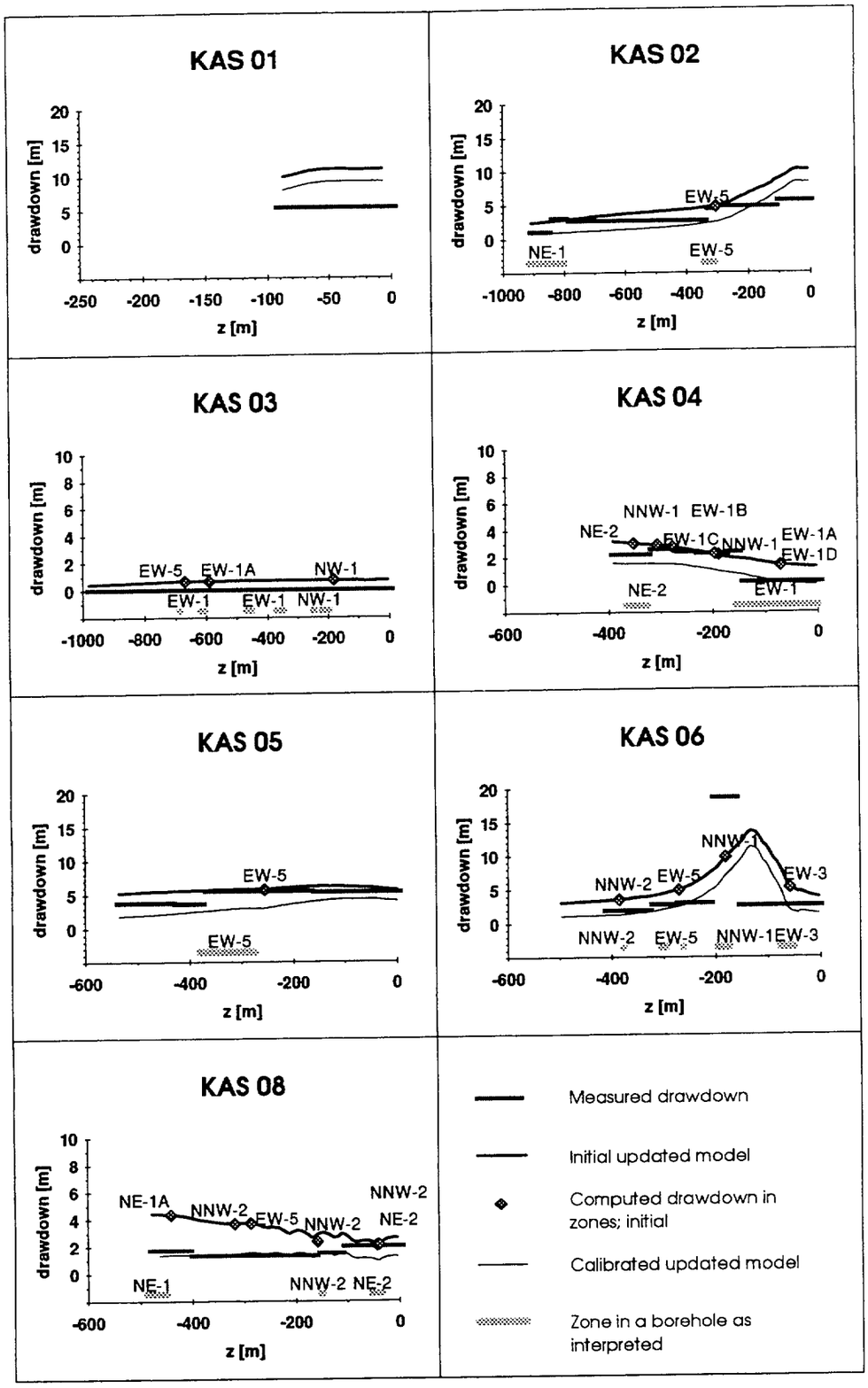

Figure 5-11. *Drawdown for the LPT1 pumping test. The measured values are the drawdowns at the end of the pumping period and reported by Rhén /1991/. The computed results are simulated with the updated structural model.*

The steady-state drawdowns in the cored boreholes estimated for the pumping test in KAS12 are presented in Figure 5-12. Because of the small pumping rate, the flow conditions were closer to a steady state than for the other short-term pumping tests studied. The uncertainties of the estimated drawdowns are thus the smallest.

Figure 5-13 shows the estimated steady-state drawdowns for the pumping test in KAS13. In some of the sections the drawdown increases rapidly outside the measurement range and the evaluation of the steady-state drawdowns includes uncertainties.

The estimated steady-state drawdowns in the cored boreholes are presented in Figure 5-14 for the pumping test performed in KAS14. In most of the cored boreholes, the drawdown is small but notably increasing when the pumping was stopped. The relative uncertainties of the small drawdowns are thus large. In the boreholes close to KAS14, a steady state is almost achieved and the values estimated are reliable.

Figure 5-15 shows the estimated steady-state drawdowns in the cored boreholes for the pumping test in KAS16. It is characteristic to the results of the pumping test in KAS16 that the drawdown varies strongly along some observation boreholes (KAS04, KAS06 and KAS07). An explanation for this may be that the low values are associated with late responses and they are therefore underestimated. On the other hand, the neighboring values could also be overestimated. In a steady state, there should not be large spatial variations in the drawdown.

Estimating the distribution of the water inflow to the withdrawal holes

Concerning LPT1 and the pumping tests in KAS12, KAS13, KAS14 and KAS16, the total inflow to the withdrawal boreholes was assumed to be equal to the average pumping rate applied in the experiment. The inflow to a withdrawal hole equals the pumping rate when the water level in the pumped hole does not change. The water level in the withdrawal holes for all the pumping tests considered was lowering so slowly at the end of the pumping periods that this source of error is insignificant. It is more important that the pumping rate could have changed during the pumping periods. The data available do not indicate any fluctuation in the pumping rate /Rhén, 1991/. For LPT2, the total inflow was assumed to be equal to the pumping rate applied after the first seven days as stated above.

The distribution of the inflowing water along the withdrawal boreholes was thus measured with a spinner or an acoustic flow meter /Rhén, 1991 and Forsmark, 1992a/. The measurements, however, did not cover the first 100 m from the top of the holes. The inflow to the upper parts of the boreholes was then not measured directly. The tracer data were used to evaluate the proportion of the total inflow to the upper part of KAS06 in LPT2 /Rhén et al., 1992/. In the pumping test in KAS16, the flow rate along

the withdrawal hole was measured with a flow meter and then the difference between the average pumping rate and the flow rate measured at a depth of 100 m gives indications on the inflow to the upper part.

Concerning LPT1 and the pumping tests in KAS12, KAS13 and KAS14, the contributions of the uppermost parts of the withdrawal holes are unknown. The data available include the spinner value along the withdrawal holes below the first 100 m and the average pumping rate /Nilsson, 1990 and Rhén et al., 1991/. (Rhén /1991/ reports also the borehole sections with significant inflows and their contribution of the inflow. It seems, however, that the contributions are relative to the highest spinner value at a depth of 100 m. The percentages cannot be converted to flow rates since the contribution of the first 100 m is unknown.) However, the correlation between the spinner value and the flow rate along a borehole is unknown (to us). Therefore, as long as we do not know the contribution of the first 100 meters, we can use the spinner results even for the rest of a borehole only qualitatively.

The contribution of the upper parts of the withdrawal holes could be estimated indirectly if the correlation between the spinner value and the flow rate were known. We assumed that the correlation is the same in all boreholes having the same radius and that the correlation is linear for a wide range. The correlation was estimated by plotting the flow rate as a function of the spinner value. From the boreholes covered by the spinner surveys, there are independent quantitative estimations of the flow rates only for KAS06. Based on the tracer data, the contribution of the first 100 m of KAS06 was thus determined to be 15%. The maximum spinner value in KAS06 should therefore correspond to a flow rate of 85% of 1.2 l/s. The straight line in Figure 5-16 is drawn from origin through the point for this result. Figure 5-16 shows also results for some features in KAS06 for which the increase in the spinner value was measured /Rhén et al., 1991/ and for which the inflow rate was determined independently based on the analyses of the tracer experiment of LPT2 /Hautojärvi, 1994/.

For most of the pumping tests performed at Äspö, the spinner value along the withdrawal holes was reported. The pumping rates versus the maximum spinner values for the pumping tests in KAS06, KAS07, KAS08, KAS09, KAS11, KAS12, KAS13 and KAS14 are also incorporated in Figure 5-16. If our assumptions concerning the spinner are valid, the points should be on the line or above it (of course, the possible error in the inflow contribution of the upper part of KAS06 has to be recognized). If a point is above the line, the difference is the inflow contribution of the upper section of a borehole not covered with the spinner survey. In KAS09, KAS11 and KAS14, the contribution of the upper part of the borehole is significant, about 1, 1.5 and 4 l/s, respectively. These values naturally include uncertainties. On the other hand, Figure 5-16 suggests that probably the inflow from the upper parts of the boreholes is insignificant for the other holes. For LPT1 and the pumping tests in KAS12 and KAS13, the pumping rate can be divided among the zones intersecting a withdrawal hole below the first 100 m.

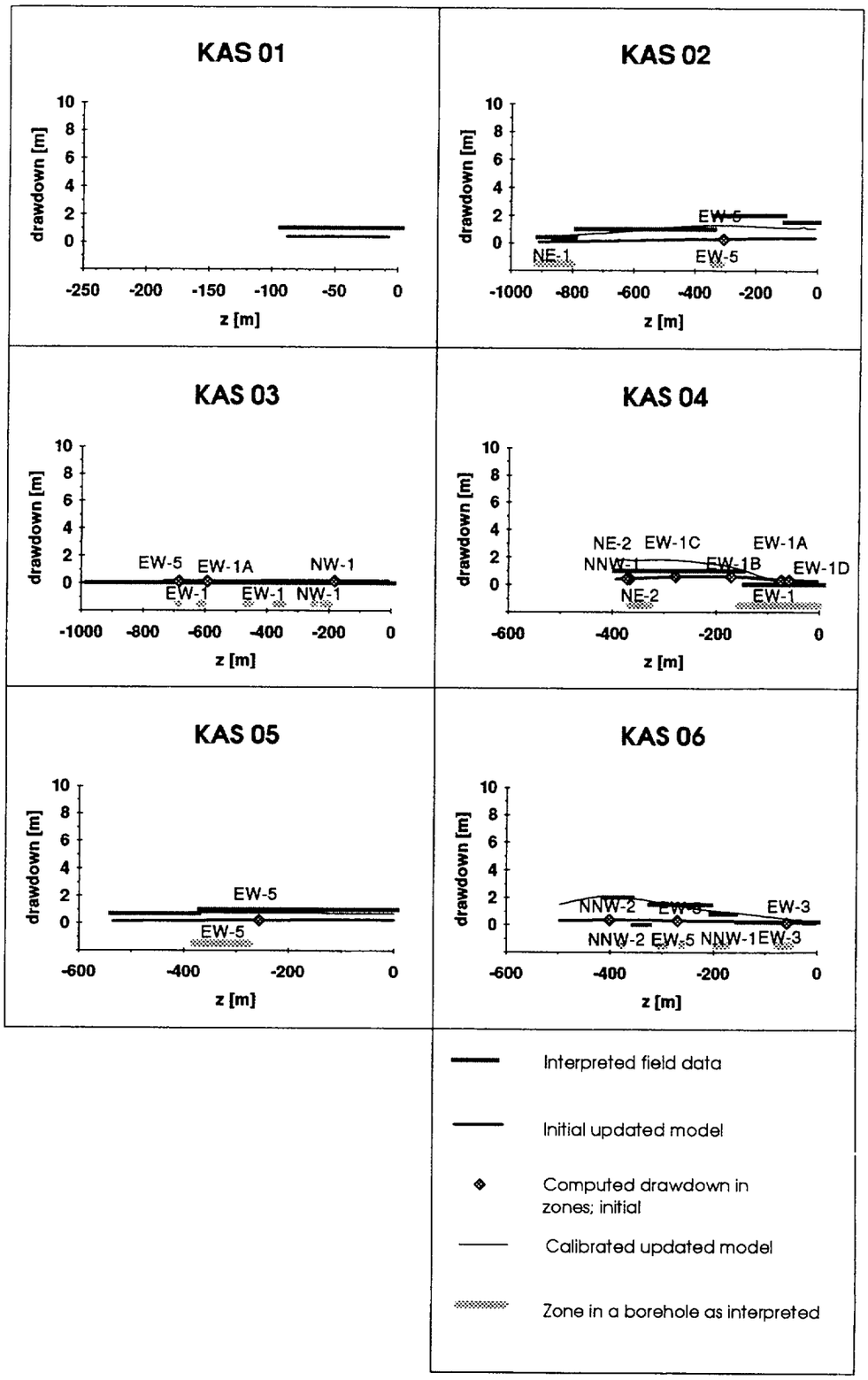

Figure 5-12. *Drawdown for the pumping test in KAS12. The interpreted field data are the values of the drawdown estimated to have been achieved if the pumping had continued. The computed results are simulated for the updated structural model.*

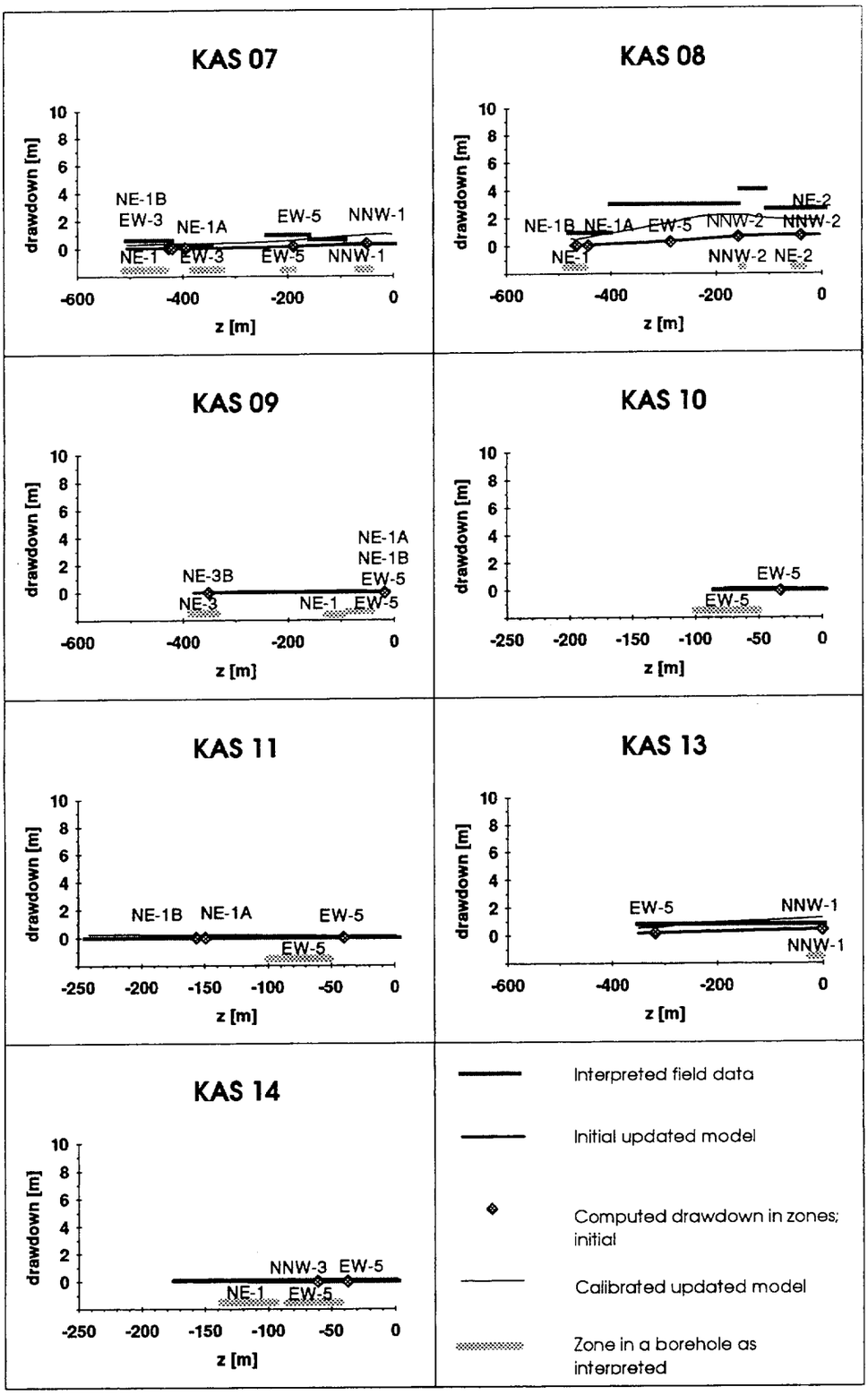

Figure 5-12. (Continued.)

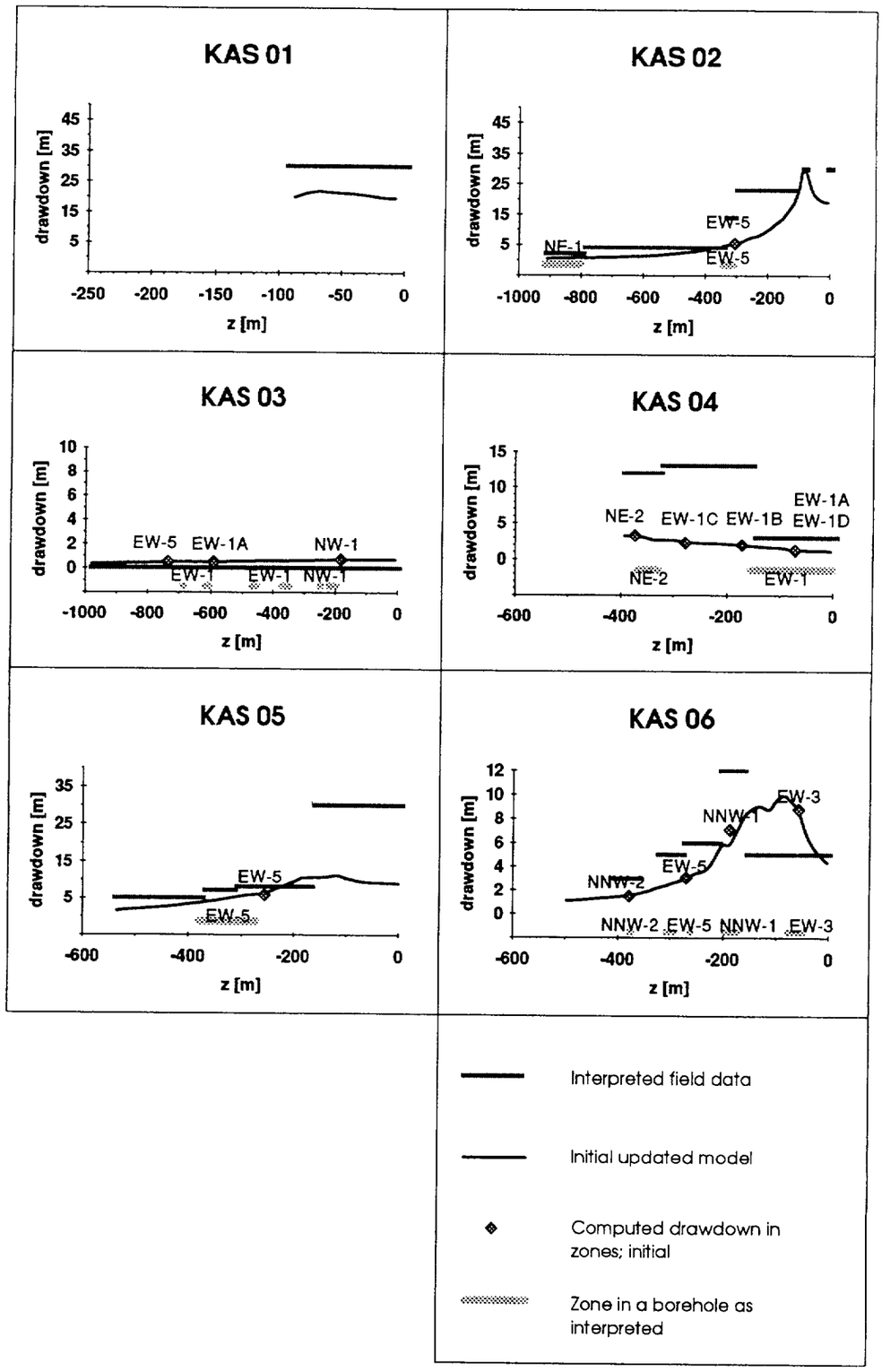

Figure 5-13. *Drawdown for the pumping test in KAS13. The interpreted field data are the values of the drawdown estimated to have been achieved if the pumping had continued. The computed results are simulated for the updated structural model.*

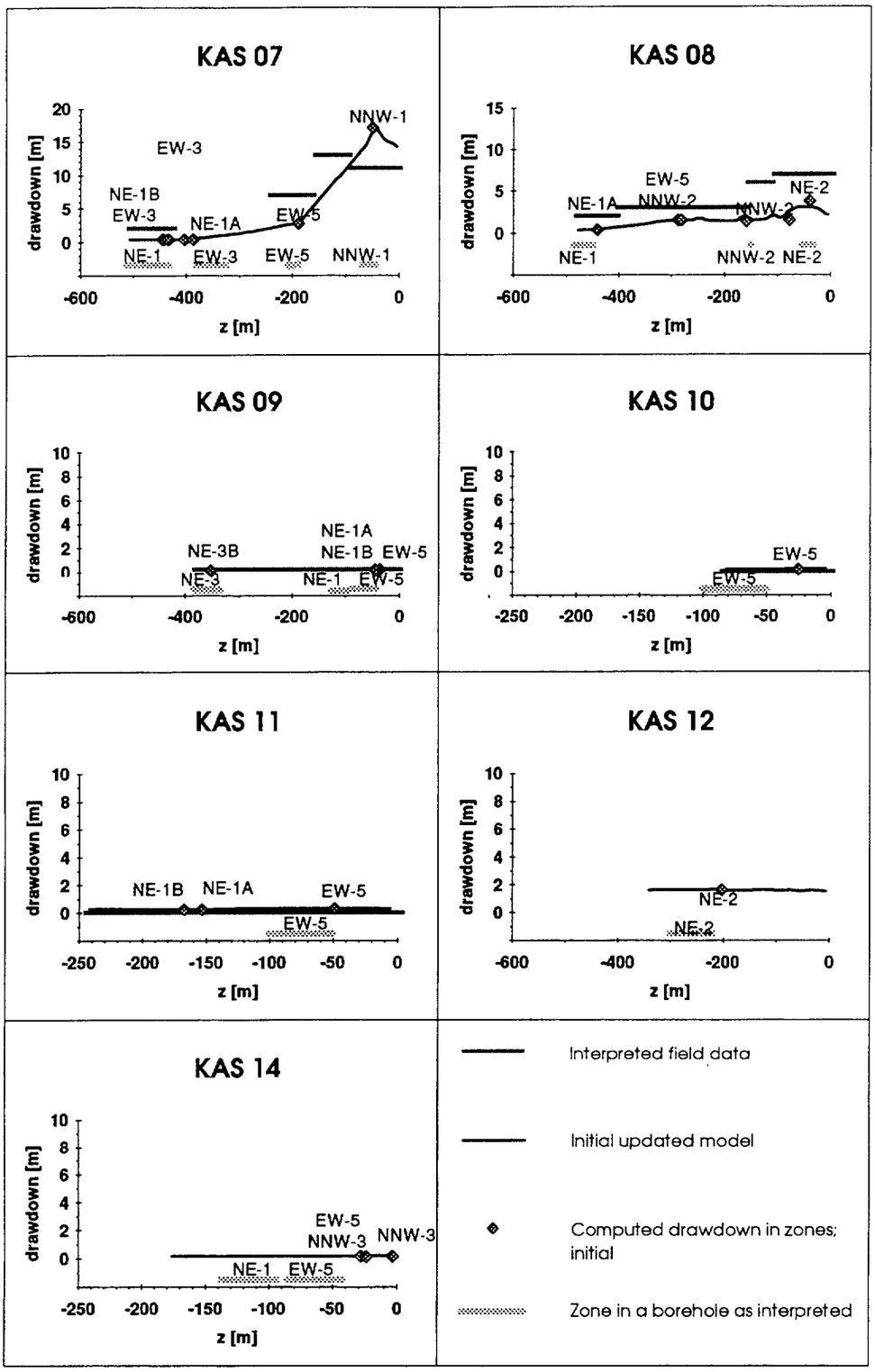

Figure 5-13. *(Continued.)*

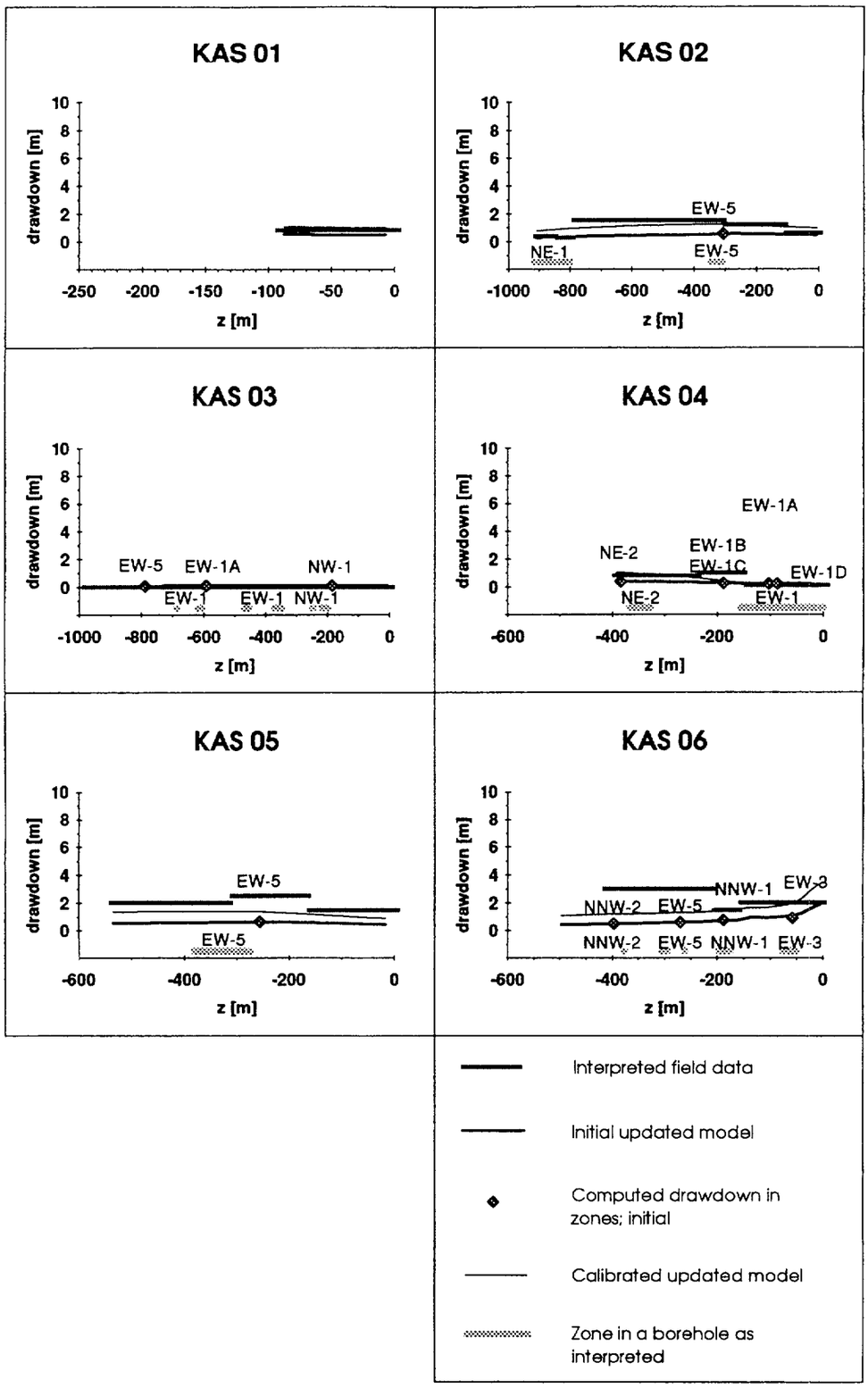

Figure 5-14. *Drawdown for the pumping test in KAS14. The interpreted field data are the values of the drawdown estimated to have been achieved if the pumping had continued. The computed results are simulated for the updated structural model.*

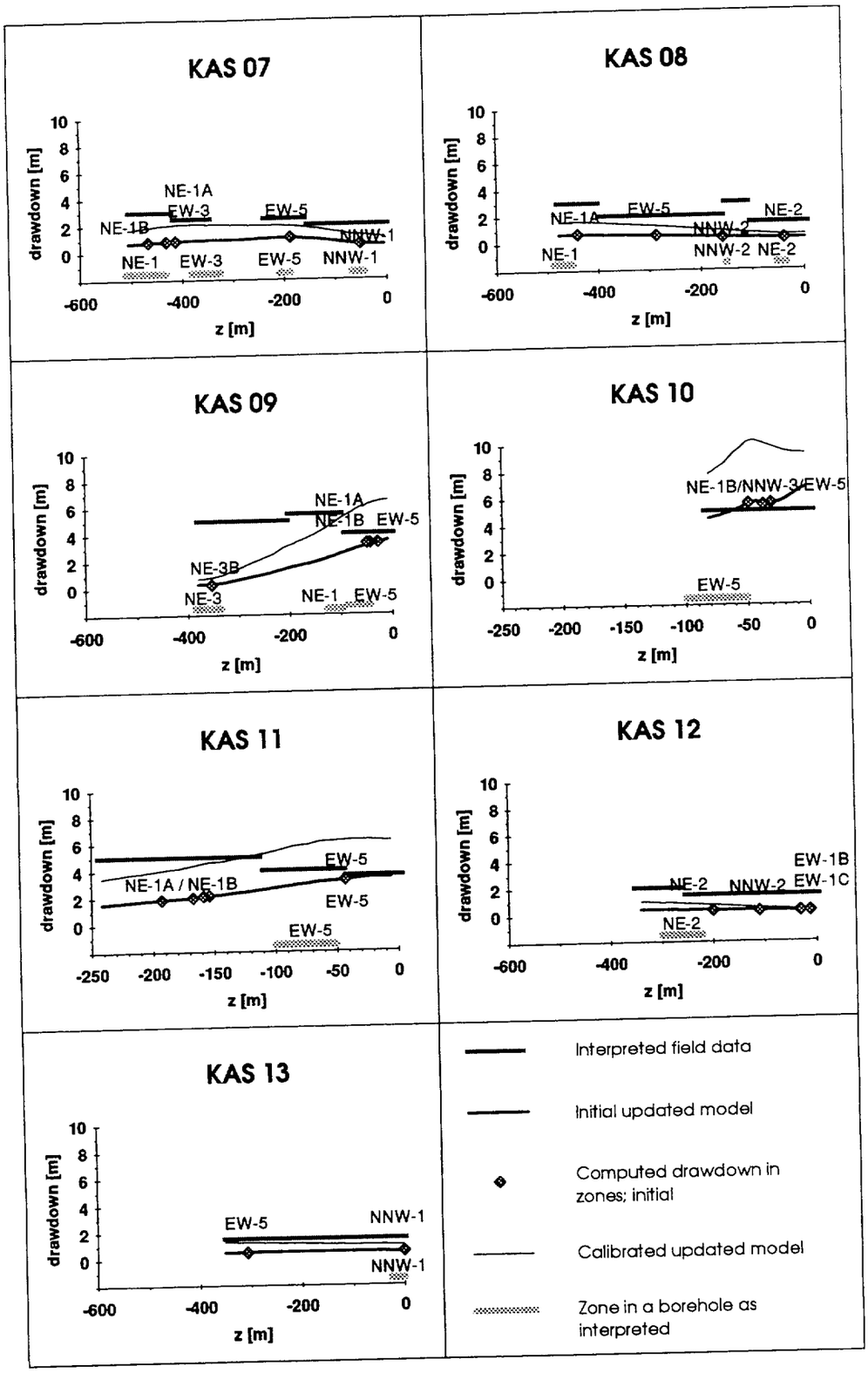

Figure 5-14. (Continued.)

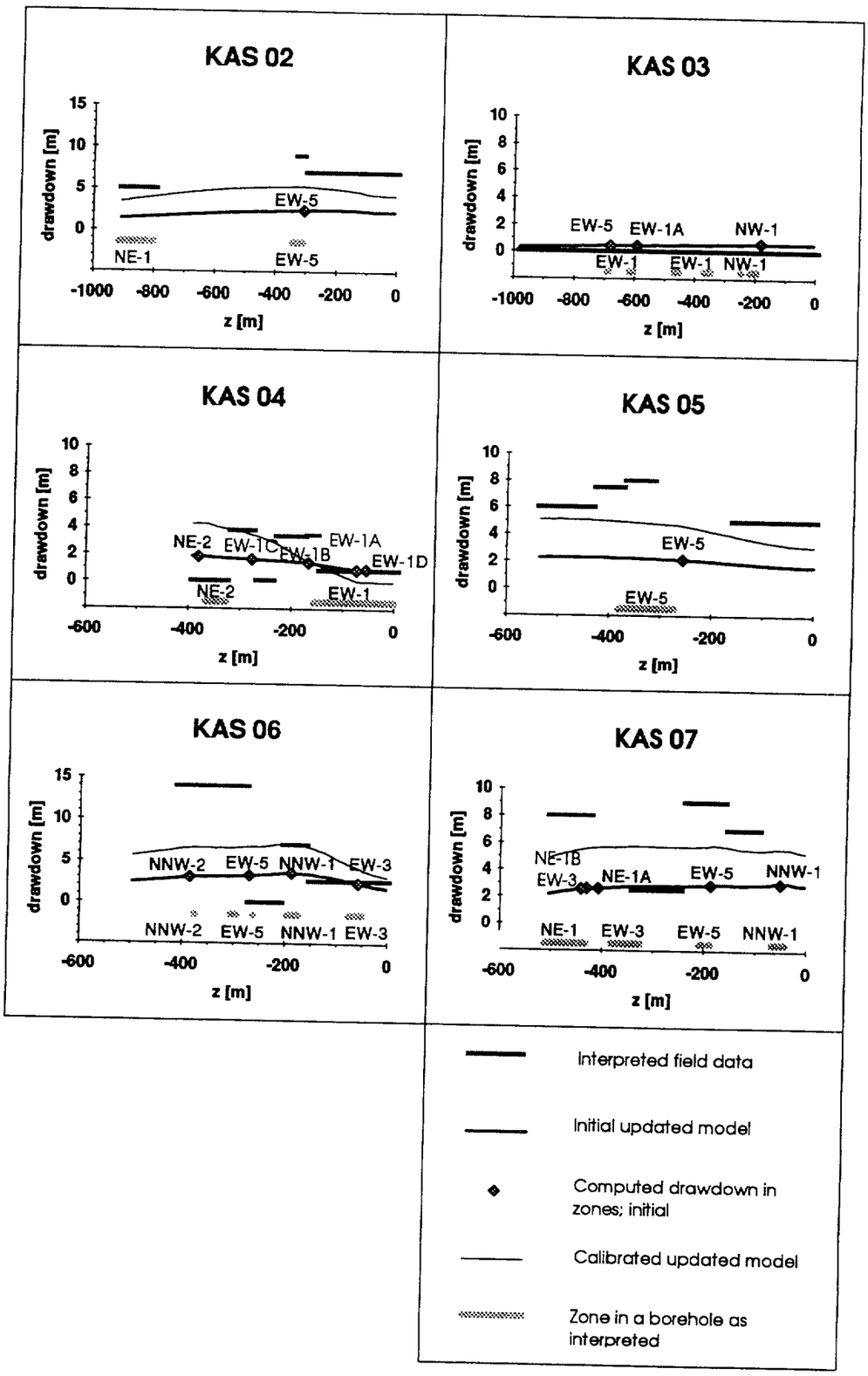

Figure 5-15. *Drawdown for the pumping test in KAS16. The interpreted field data are the values of the drawdown estimated to have been achieved if the pumping had continued. The computed results are simulated for the updated structural model.*

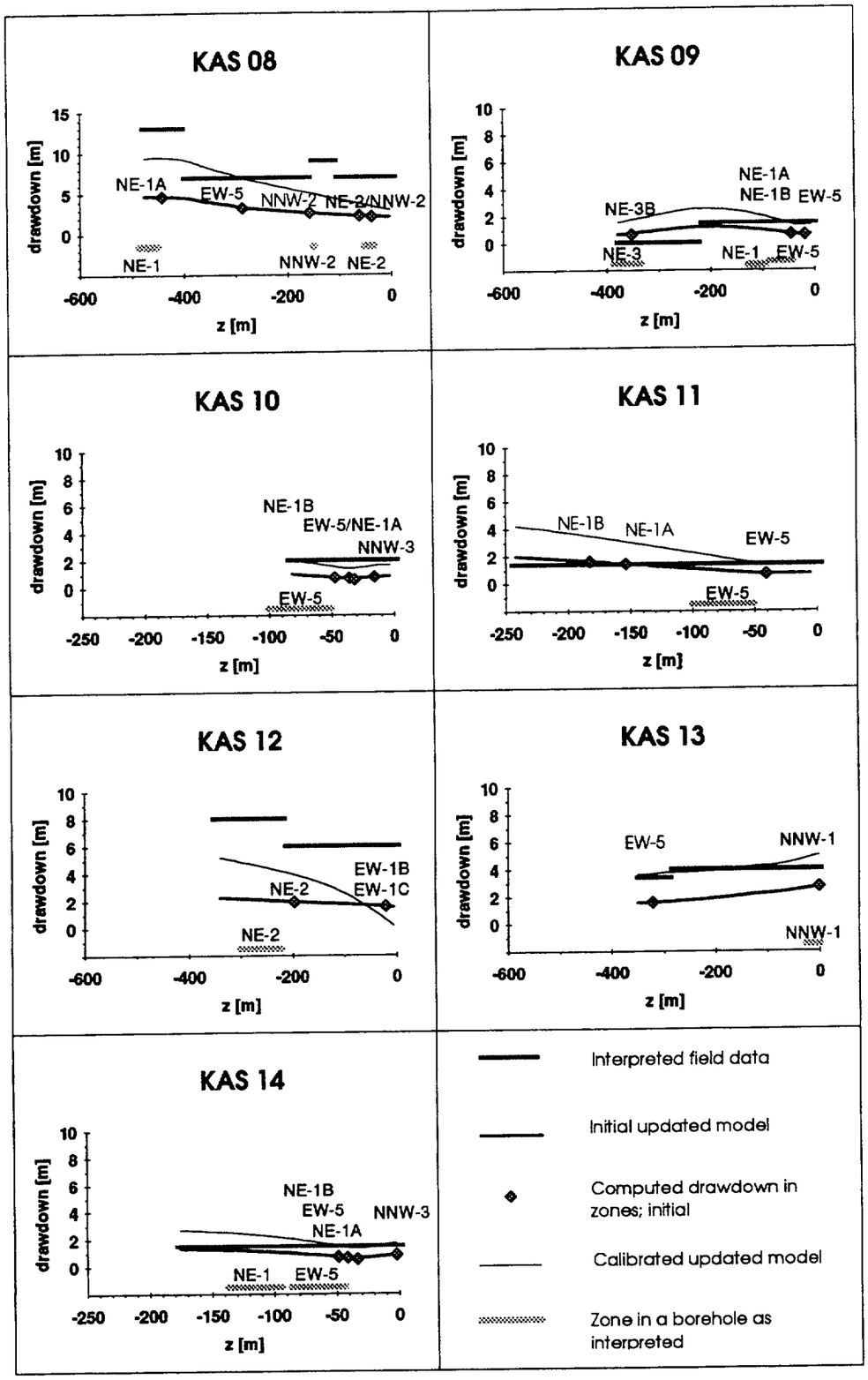

Figure 5-15. (Continued.)

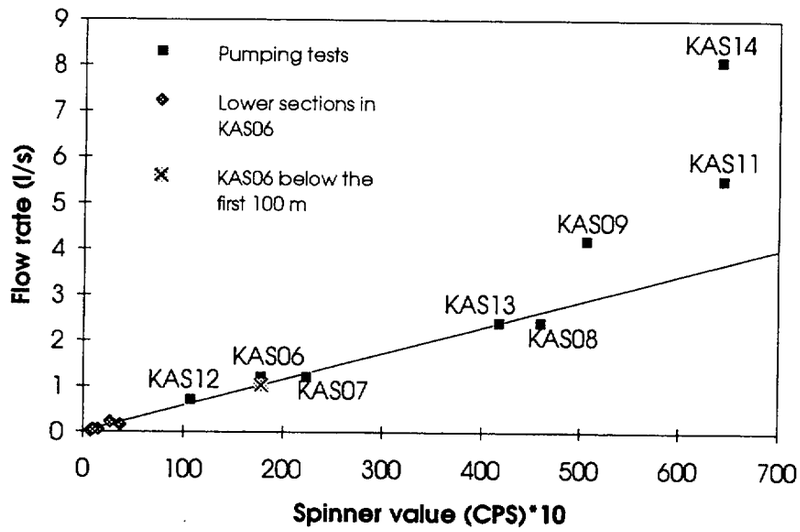

Figure 5-16. *Correlation between the flow rate in a borehole and the spinner value. The spinner values from Nilsson, 1990 and Rhén et al., 1991. The inflows for the lower sections of borehole KAS06 are based on the analyses of the tracer data by Hautojärvi /1994/.*

Tables 5-5 – 5-9 show for the pumping tests utilized in the calibration the zones that are most probably associated with the significant inflows and the estimated distributions of the inflow. The zones were found out on the basis of the results of the spinner surveys /Nilsson, 1990; Rhén et al., 1991/ and the core-log interpretations /Wikberg et al., 1991/ presented in Figure 5-3.

In LPT1 the inflow to the first 100 m of KAS07 was small and (at least almost) all of the inflow came to the rest of the borehole. From the total inflow about 13% came to a borehole interval 122 – 128 m. This inflow was assumed to be associated with NNW-1. About 17% of the inflow came to the interval 222 – 246 m and was interpreted to have been contributed by EW-5. The rest of the inflow came to the bottom part of the borehole. The spinner survey covered the borehole only to a depth of 418 m and therefore we cannot divide the rest of the inflow between NE-1 and EW-3. The contribution of EW-3 is probably very small and most of the water flowed from NE-1.

Concerning KAS12, the inflow to the upper part of the borehole was also small. Almost all of the inflow came to a borehole section which was interpreted to intersect NE-2. KAS12 is close to NNW-2 and it is possible that NNW-2 also contributes to the inflow.

During the pumping test in KAS13, all of the water came to a borehole interval (160 - 220 m) which is not interpreted to intersect any of the identified zones (Figure 5-3). KAS13 is interpreted to intersect NNW-1 close to the surface but the inflow to the top part of the borehole is likely

not be significant (Figure 5-16). The inflow from NNW-1 to the top part of KAS13 that is above the water level could also be reduced because of a low-conductive skin or two-phase flow. KAS13 is not interpreted to intersect EW-5, but if it does so in reality as in the flow model, the inflow from EW-5 was small.

On the basis of Figure 5-16, we can estimate for the pumping test in KAS14 that about a half of the inflow could have come to the upper part of the borehole, which was not covered by the spinner survey. That part of the borehole is interpreted to intersect EW-5 and therefore a half of the pumping rate could be the contribution of EW-5. It is, however, possible that the inflow to the upper part of KAS14 flowed mainly from NE-1 or an unidentified feature (such as local subhorizontal zone or the surface layer of the bedrock). At least half of the inflow is contributed by NE-1.

For the pumping test in KAS16, Forsmark /1992a/ reported the field results of an acoustic flow meter and the zones with which the inflows are associated. The pumping rate was 5.2 l/s but the largest flow rate measured at 100 meters from the top of the hole was about 3.8 l/s. As the accuracy of the flow meter is not known, we cannot decide whether the difference of 1.4 l/s is the error of the flow meter measurements or the contribution of the upper part of the borehole. If the uncertainties of the flow rates measured with the flow meter are significant as can be expected, we do not know the contribution of the upper part of the borehole and the inflow distribution for the rest of the hole is determined only qualitatively.

Table 5-5. Interpreted and simulated distribution of the water inflow to KAS07 during the long-term pumping test LPT1. Experimental data from Nilsson, 1990. The calculated values for the updated flow model.

Hydrological unit	Measured (l/s)	Initial model (l/s)	Calibrated model (l/s)
NNW-1	0.15	0.4	0.2
EW-5	0.2	0.8	0.3
NE-1	0.9-Q_{EW-3}	20	1.2
EW-3	Q_{EW-3}	0.03	0.6
Others	-	0.02	0.02
Section below 100 m	≤1.25	21	2.3
Section above 100 m	small	0.005	0.005
Total	1.25	21	2.3

Table 5-6. Interpreted and simulated distribution of the water inflow to KAS12 during the pumping test performed in KAS12. Experimental data from Rhen et al., 1991. The calculated values for the updated flow model.

Hydrological unit	Measured (l/s)	Initial model (l/s)	Calibrated model (l/s)
NE-2	0.7-Q_{NNW-2}	0.2	0.2
NNW-2	Q_{NNW-2} (?)	-	0.4
Others	0.05	0.02	0.02
Section below 100 m	≤0.7	0.2	0.6
Section above 100 m	small	0.01	0.01
Total	0.7	0.2	0.6

Table 5-7. Interpreted and simulated distribution of the water inflow to KAS13 during the pumping test performed in KAS13. Experimental data from Rhen et al., 1991. The calculated values for the updated flow model.

Hydrological unit	Measured (l/s)	Initial model (l/s)	Calibrated model[2)] (l/s)
NNW-1[1)]	small	0.6	
XX?	2.4		
EW-5	0.06 (?)	1.1	
Others	0	0.02	
Section below 100 m	≤2.4	1.2	
Section above 100 m	small	0.6	
Total	2.4	1.8	

[1)] The first 100 meter of the borehole not covered with the spinner survey is interpreted to intersect NNW-1 (Figure 5-3).
[2)] Simulation of the pumping test in KAS13 with the calibrated model was not considered sensible due to a missing decisive feature (see the text for details).

Table 5-8. Interpreted and simulated distribution of the water inflow to KAS14 during the pumping test performed in KAS14. Experimental data from Rhen et al., 1991. The calculated values for the updated flow model.

Hydrological unit	Measured (l/s)	Initial model (l/s)	Calibrated model (l/s)
NE-1	4(-8)	5	6
EW-5[1)]	Q_{EW-5}(0-4)	0.2	0.2
Others	4-Q_{EW-5}	0.005	0.005
Section below 100 m	~4	5	6
Section above 100 m	~4	0.2	0.2
Total	8.1	5	6

[1)] The first 100 meter of the borehole not covered with the spinner survey is interpreted to intersect EW-5.

Table 5-9. Interpreted and simulated distribution of the water inflow to KAS16 during the pumping test performed in KAS16. Experimental data from Forsmark, 1992aThe calculated values for the updated flow model.

Hydrological unit	Measured (l/s)	Initial model (l/s)	Calibrated model (l/s)
NE-1	3.9 (2.9[1)])	10	8
EW-5	1.0 (0.8[1)])	0.5	0.9
Others	0.3 (0.2[1)])	0.02	0.02
Section below 100 m	5.2 (3.8 [1)])	11	9
Section above 100 m	0 (1.4[1)])	0.005	0.005
Total	5.2	11	9

[1)] Contribution, if the flowmeter value at a depth of 100 m is considered reliable, see Forsmark, 1992a.

5.3.4 Simulation of the calibration cases with the initial model

Steady-state simulations for the pumping tests used as calibration cases were carried out as for the base model (the approach described in Section 3.6): Test-specific finite element meshes were created for all the pumping tests following the updated geometry of the zones. The drawdown measured in a withdrawal hole was assigned to the nodes representing the withdrawal hole in each mesh. The drawdown field was computed by solving equation 3-3. No-flow boundary conditions were given to the nodes at the model surface in the area of the Äspö island. Fixed-pressure boundary conditions were assumed for the rest of the boundaries.

The drawdowns from the steady-state simulations were compared with the drawdowns estimated from the field results as described in the previous section. The total inflow of groundwater to the withdrawal holes as well as its distribution among the fracture zones were compared with the interpreted field data presented in Tables 5-5 – 5-9.

The undisturbed flow conditions were simulated as described in Section 3.5. The simulated pressure and salinity fields were evaluated in the light of the field data.

The LPT1 test

The computed steady-state drawdowns in the observation sections of the cored boreholes are presented and compared with the values based on the field data in Figure 5-11. The simulation results are similar to those for the initial base model (Figure 4-11). The agreement with the field data is, however, somewhat poorer than the results of the base model. The largest difference between the two sets of simulation results is in KAS08. Because of the slightly different location of NNW-2 and because of the southern branches of EW-1, the drawdown in the bottom part of KAS08 for the updated model is almost 5 m compared to 3 m for the base model (Figure 4-11). The modification of EW-1 shows up also in KAS04: the depth dependence of the results for the initial model (Figure 4-11) agrees with the field data better than that of the updated model in Figure 5-11.

The discrepancy between the simulation results of the updated model and the field data is significant in KAS01 and in the bottom part of KAS08. The simulated drawdown is also too large in the uppermost section of KAS04.

The calculated total inflow to the withdrawal hole is more than 20 l/s (experimental 1.25 l/s). For the initial base model, the total inflow to KAS07 in LPT1 was 7 l/s. The increase is mainly because in the updated model, KAS07 intersects both subzones NE-1A and NE-1B whereas in the base model it intersects only NE-1a (Figures 4-3 and 5-3).

The distribution of the inflow is compared with the field data in Table 5-5. The calculated inflow is contributed almost exclusively by NE-1 and the

large contribution of NE-1 is the main reason for the too high total inflow. The calculated inflows from NNW-1 and EW-5 are also somewhat too high.

The LPT2 pumping experiment

The simulation results for LPT2 were presented and discussed above in Section 5.2. The computed drawdowns in the cored boreholes were presented and compared with field data in Figure 5-4 and the distribution of the inflow is shown in Table 5-3.

Pumping test in KAS12

The drawdowns along the cored boreholes computed using the initial updated model are compared with the field data in Figure 5-12. The simulated drawdowns, undoubtedly, do not agree with the measured data. The computed drawdowns are too small in all of the observation sections except in those in which there was not any drawdown during the field experiment (KAS03, KAS10, KAS11 and KAS14). The discrepancies are significant in KAS02, KAS06, KAS07 and KAS08.

The computed inflow of groundwater to the withdrawal hole and its distribution are presented in Table 5-6 with the field data. Almost all the water flows to KAS12 from NE-2. The total amount of the inflowing water is, however, only 30% of the pumping rate.

Distribution of the inflow among the zones in the field experiment is uncertain. Only NE-2 is interpreted to intersect KAS12. The same applies the flow model (Figure 5-3) and the element mesh for the pumping test in KAS12. Borehole KAS12 is, however, close to NNW-2 and it is possible that NNW-2, its branch or even an individual fracture connects the borehole to NNW-2.

Pumping test in KAS13

In the element mesh for the pumping test in KAS13, borehole KAS13 intersects NNW-1 close to the ground surface. In the mesh the KAS13 borehole also intersects EW-5 which is not interpreted to happen in reality.

The simulated drawdowns in the cored boreholes for the pumping test in KAS13 are presented in Figure 5-13. The agreement with the field data is poor in many observation sections in KAS01, KAS04, KAS05 and KAS08. The simulated drawdowns are notably smaller than what the field data suggest especially in the lower part of KAS04 and in the uppermost section of KAS05. From those boreholes in which a significant drawdown was measured, only in KAS02, KAS06 and KAS07, the simulation results are close to the measured values. The computed drawdown is smaller than the

measured one almost in all the cored boreholes except in the uppermost section of KAS07, which intersects with NNW-1.

The calculated total inflow to KAS13 is 30% less than the pumping rate applied (Table 5-7). The distribution of the inflow along the withdrawal hole is, however, completely different. The spinner survey showed that the inflow is mainly from the borehole interval 160 – 220 m. In the simulation, most of the water comes to the bottom part of KAS13 from EW-5. KAS13 is not, however, interpreted to intersect EW-5 (Figure 5-3). The rest of the simulated inflow is contributed by NNW-1, which is intersected by KAS13 close to the ground surface.

Pumping test in KAS14

KAS14 intersects zones EW-5 and NE-1 in the updated flow model consistently with the interpretations of field data (Figure 5-3). The same zones are also intersected by the one-dimensional elements for KAS14 in the pumping model.

The computed drawdowns for the pumping test in KAS14 are compared with the drawdown values based on field data in Figure 5-14. With a few exceptions, the simulation values are too small. Larger drawdowns should be obtained for KAS05, KAS06, KAS07, KAS08, KAS09, KAS12 and KAS13. The simulated drawdowns are high and the agreement is good in KAS10 and in the uppermost section of KAS09.

The computed total inflow to KAS14 (about 5 l/s) compares favorably with the applied pumping rate (8 l/s). According to the simulation, almost all of the water comes from the NE-1 zone (Table 5-8). In the simulation, only 0.2 l/s flows to the first 100 meters of the withdrawal hole as it in reality could have been even 4 l/s.

Pumping test in KAS16

As shown in Figure 5-3, KAS16 is interpreted to intersect the same zones, NE-1 and EW-5, as KAS14. KAS16 intersects the same zones in the flow model as well as in the element mesh for the pumping test in KAS16.

The steady-state drawdowns in the cored boreholes for the pumping test in KAS16 computed applying the initial model are compared with the field data in Figure 5-15. About in a half of the cored boreholes, the agreement with the field data is satisfactory. A common feature can be identified in the other holes. In them at the depth at which a hole intersects EW-5 (KAS02, KAS05, KAS06, KAS07, KAS13), the estimated experimental drawdown is significantly larger than the computed values. An exception is KAS13, in which the agreement is good. The same applies the observation sections intersecting NE-1 (KAS02, KAS07, KAS08, KAS14). The agreement in borehole KAS14 is good, however.

The calculated total inflow to the withdrawal hole is about twice the pumping rate. The distribution of the inflow to the withdrawal hole is compared with the field data in Table 5-9. The calculated inflow from NE-1 is 2 – 3 times the measured one. On the other hand, from EW-5, the calculated inflow is almost a half of the field result. A significant portion of the inflow (1 – 2 l/s) could in the field experiment have come from the upper part of the borehole but there is no inflow contribution to the upper part in the simulation.

The undisturbed flow conditions

The pressure field was simulated applying the three different kinds of models for the salinity as discussed in Section 3.5: The fresh-water and constant-salinity models. In the third approach, the coupled equations for the salt concentration and pressure were solved. The pressure boundary conditions for the top of the model were the same in all cases (the water table), whereas on the vertical model faces the pressure was hydrostatic as explained in Section 3.5. For the bottom of the model, no-flow boundary conditions were always applied.

The computations were performed with the FEFLOW program. The coupled case was computed employing the Picard iterative scheme with under-relaxation (see Sections 3.3 and 3.4).

The simulated pressure for the three cases together with the values measured in the cored boreholes are shown in Figure 5-9. The significance of the salt concentration on the pressure is clearly demonstrated by the differences between the case of fresh water and the two other cases. The pressure calculated with the fresh-water model does not agree with the field data. This fact together with a reasonable agreement of the calculated and measured pressures in the other cases undoubtedly indicates that the salt concentration at Äspö is the most significant individual factor affecting the pressure. It is also worth noting that the simple salinity model of a constant concentration leads to as an equally good overall agreement of the calculated result with the measured pressure as the case of coupled groundwater flow and salt transport. In the simulated results, some details of the measured values are missing, for instance, the small pressure peak in KAS05 at a depth of 400 m, a sudden pressure drop in KAS12 at the depth of about 250 m and the high values of the pressure in the top part of borehole KAS14. Although the differences are mainly due to the imperfect modelling of a complex system, the uncertainties of the field results discussed in Section 5.3.2 must also be considered.

Figure 5-10 shows the salt concentration along the cored boreholes calculated in the coupled case. The computed results agree well with the measured concentrations. For the bottom parts of many boreholes, the computed concentration is higher than measured one. This is mainly due to the very simple boundary conditions applied for the salinity in the

computation (see Section 3.5). The boundary conditions for the salt concentration deep in the bedrock were selected to produce the maximum concentration measured at Äspö, namely 16 g/l at the bottom of KAS02. The uncertainties of the field values discussed in Section 5.3.2 should be considered here as well.

5.3.5 Adjusting model parameters

Conceptual zonation of the fracture zones

When calibrating the updated flow model, the zones were conceptually divided into two parts (Figure 5-17): The far-field part of a zone is characterized by the cross-zone (equivalent-continuum) transmissivity. The near-field part of the zone around a withdrawal hole was considered separately The transmissivity of the near-field part can be higher or lower than the cross-zone transmissivity. The zone's transmissivity and its probability distribution for a borehole intersecting the zone could be estimated by applying a model for the spatial distribution of the transmissivity but the results would be determined by the assumptions.

Considering a pumping test, the near field as well as the far field affect the drawdown field and the inflow to the withdrawal hole. For instance, if in a radial field the near field (radius 5 m) has a ten-fold transmissivity compared to the rest of the zone, the inflow and the drawdown outside the near-field zone (but not close to the boundary) are almost twice the value for a homogenous medium. The factor of two is caused by the fact that in a homogenous medium the drawdown at a distance of 5 m is half of the drawdown in the withdrawal hole. On the other hand, the near field with an order of magnitude smaller transmissivity would result in an inflow rate and drawdowns that are one fifth of the homogenous-medium value.

When adjusting the transmissivities of the zones, an attempt was made to keep the far-field values equal to the initial values. The idea behind this is that the values selected for the zones are the averages of the values measured at several locations and thus represent the cross-zone transmissivities.

In principle, the results of the hydraulic injection tests should give the transmissivity of the zone as it is seen by a borehole. For several reason, these data were not used. First, the interpretations of the hydraulic injection tests were originally available only for KAS06 and KAS07 of the studied boreholes. Secondly, it is unclear how the interpreted transmissivities reflect the average and near-field transmissivities. From the transient results, indications on the transmissivities of various parts could possibly be interpreted. Finally, the results of the hydraulic injection tests for KAS07 and the results of LPT1 are inconsistent: the transmissivity of a number of 3-m packer sections is about $3 \cdot 10^{-4}$ m^2/s, as the total transmissivity of KAS07 in LPT1 was interpreted to be about $5 \cdot 10^{-5}$ m^2/s /Nilsson, 1990/. The result of the pumping test is close to the transmissivity determined from

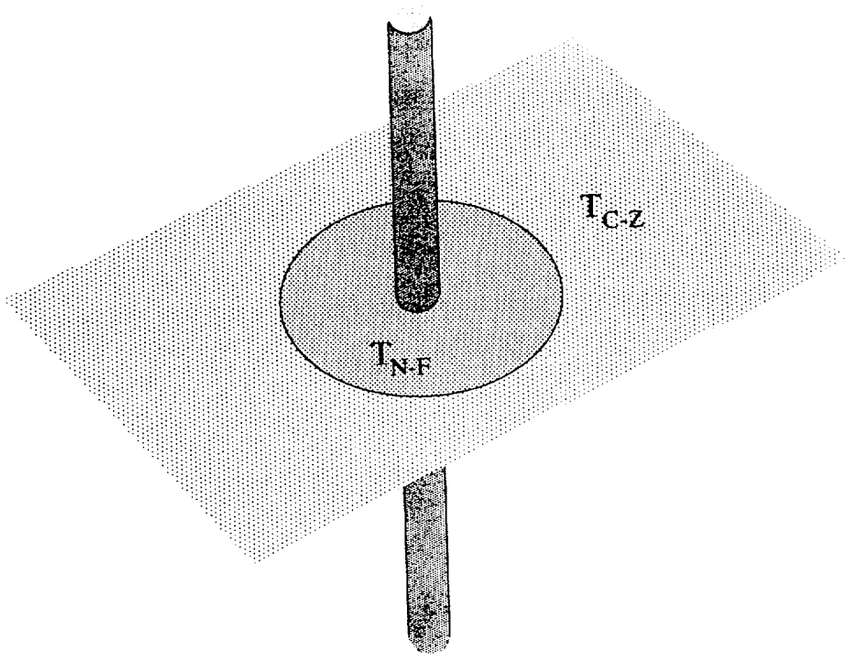

Figure 5-17. *Conceptual zonation of a planar feature to a near-field part around a withdrawal hole and to the rest of it.*

the airlift test ($8 \cdot 10^{-4}$ m^2/s) /Nilsson, 1990/. The discrepancy might be associated with the different duration of the experiments, the hydraulic injection tests might be sensitive especially to the transmissivity of the near field or during the hydraulic injection tests, part of the water injected might have returned into KAS07 above the packed-off section.

Weighting the differences between field data and simulation results

It is obvious that the simple flow model cannot simulate all details of the characteristics of the heterogenous bedrock and reproduce all results of all the field experiments carried out. Therefore, it is necessary to weight the differences between the field data and simulation results. A perfect weighting of all the differences is in practice impossible because of, for instance, unknown uncertainties of the field results. On the other hand, it would also have been too laborious regarding to the expected outcome.

The weighing of the differences in the field and simulation results were thus done qualitatively. The weights of differences were tried to select to be proportional to the reliability of the data used to evaluate the simulation results, i.e., the field data or their interpretations. The field data, especially the drawdowns for the long-term pumping tests LPT1 and LPT2 were considered reliable. The steady-state drawdowns estimated above on the bases of the field results for the other pumping tests include in many cases significant uncertainties arising from the short duration of the experiments.

The large drawdowns can be considered most reliable because in general the sections having the largest drawdowns also responded first and are closest to a steady state at the end of pumping periods. The small drawdowns could have increased in many cases significantly if pumping had continued.

The uncertainties of the total inflows are insignificant from the calibration point of view. The distribution of the inflow is known most reliably for LPT2. For LPT1 and for the pumping test in KAS12 and KAS13, the uncertainties in the inflow distributions are not significant. In the case of KAS07, we do not know the distribution of the inflow between NE-1 and EW-3. For the pumping test in KAS14 and KAS16, the inflow distributions are uncertain.

Concerning the hydraulically undisturbed conditions, the uncertainties of the field data were discussed in Section 5.3.2. Besides the significant uncertainties of the experimental results which can be applied in evaluating the model's performance, the modelling of the undisturbed conditions itself includes uncertainties, such as the poorly known boundary conditions and the possible influences of the modelling simplifications (the matrix diffusion is ignored, for instance).

Indications from comparing the simulation and field results

Water inflow to the withdrawal holes

On the basis of the inflow in LPT1 (Table 5-5), the transmissivity of NE-1 should be smaller at least around KAS07. This is, however, inconsistent with the results of the hydraulic injection test that suggest a high transmissivity for NE-1 in KAS07 /Nilsson, 1990/. The transmissivities of NNW-1 and EW-5 should also be smaller.

LPT2 shows that as the inflow from NNW-2 should be less than a half of that for the initial model, the transmissivity of NNW-2 should be smaller at least around KAS06 (Table 5-3). The inflow to the top part of KAS06 is interpreted to flow from EW-3 and therefore the field data suggest a much larger transmissivity for the zone. It is, however, possible that the inflow to the top part of KAS06 came from an unidentified local (subhorizontal) feature or from the well-conductive surface layer of the bedrock.

The calculated total inflow to KAS12 is too small (Table 5-6). Larger inflow would be obtained if the transmissivity of NE-2 were larger or KAS12 were connected to another zone (NNW-2).

The total inflow to KAS13 in the simulation is close to the pumping rate (Table 5-7). The distribution of the inflow cannot be explained with the current structural model. In reality borehole KAS13 intersects at a depth of 200 m a highly conductive feature, which is an unidentified zone or a single fracture connected to NNW-1 or NNW-5.

The field data for KAS14 suggest that more water should come from EW-5 (Table 5-8). The uncertainties associated with the inflow to the upper part of the borehole are so large that any conclusions based on the inflow distribution in KAS14 are unwarranted.

The total inflow to KAS16 from NE-1 computed using the initial model is too high, which indicates that in the model the transmissivity of NE-1 is too large (Table 5-9). Because more water should flow from EW-5, its transmissivity should be higher.

Drawdowns

In LPT1 the drawdown in KAS08 would be smaller if the transmissivity of zone NE-1 around KAS07 were smaller. The too high simulated drawdowns in KAS03 could be associated with the boundary conditions.

In the case of LPT2, too, the excessively large simulated drawdown in the topmost sections of KAS03 can be an impact of the boundary conditions. There are several potential explanations for the exceptionally low measured drawdown in the top part of KAS13, but most of them require complementing the structural model. To obtain larger drawdowns in the bottom sections of KAS07 and KAS08, the transmissivity of NE-1 should be smaller.

Concerning the pumping test in KAS12, the most important reason for the differences is that according to the interpretations of the field data and to the flow model, too, KAS12 does not intersect NNW-2 (Figure 5-3). However, there is quite probably a highly transmissive connection from KAS12 to NNW-2. Therefore, the pumping model for the KAS12 pumping test was modified to include a connection having a high transmissivity from the bar elements representing borehole KAS12 to NNW-2. With this modification the calculated inflow to the pumping hole (about 3 l/s) is significantly higher than the pumping rate (0.7 l/s). The drawdown calculated after this modification is presented in Figure 5-18. Because of the connection, the simulated drawdowns are too large in all of the boreholes. The spatial distribution of the drawdown, however, agrees with the field data. A less conductive connection between KAS12 and NNW-2 resulted in a satisfactory agreement with the experimental results.

As stated above, a feature contributing at least the major portion of the inflow during the pumping in KAS13 is missing from the structural model. Analyzing the measured drawdowns and comparing them with those simulated using the initial model, orientation of the missing feature could be deduced. The smallest distance between KAS02 and KAS13 is very short (Figure 5-2) and therefore the large drawdown measured in the uppermost section of KAS02 is expectable. The drawdown is, however, also large in KAS01 and in the uppermost observation section of KAS05. Moreover, the magnitudes of the drawdowns are about equal. Actually, in most of the pumping tests studied, the drawdowns in KAS01 and the uppermost sections

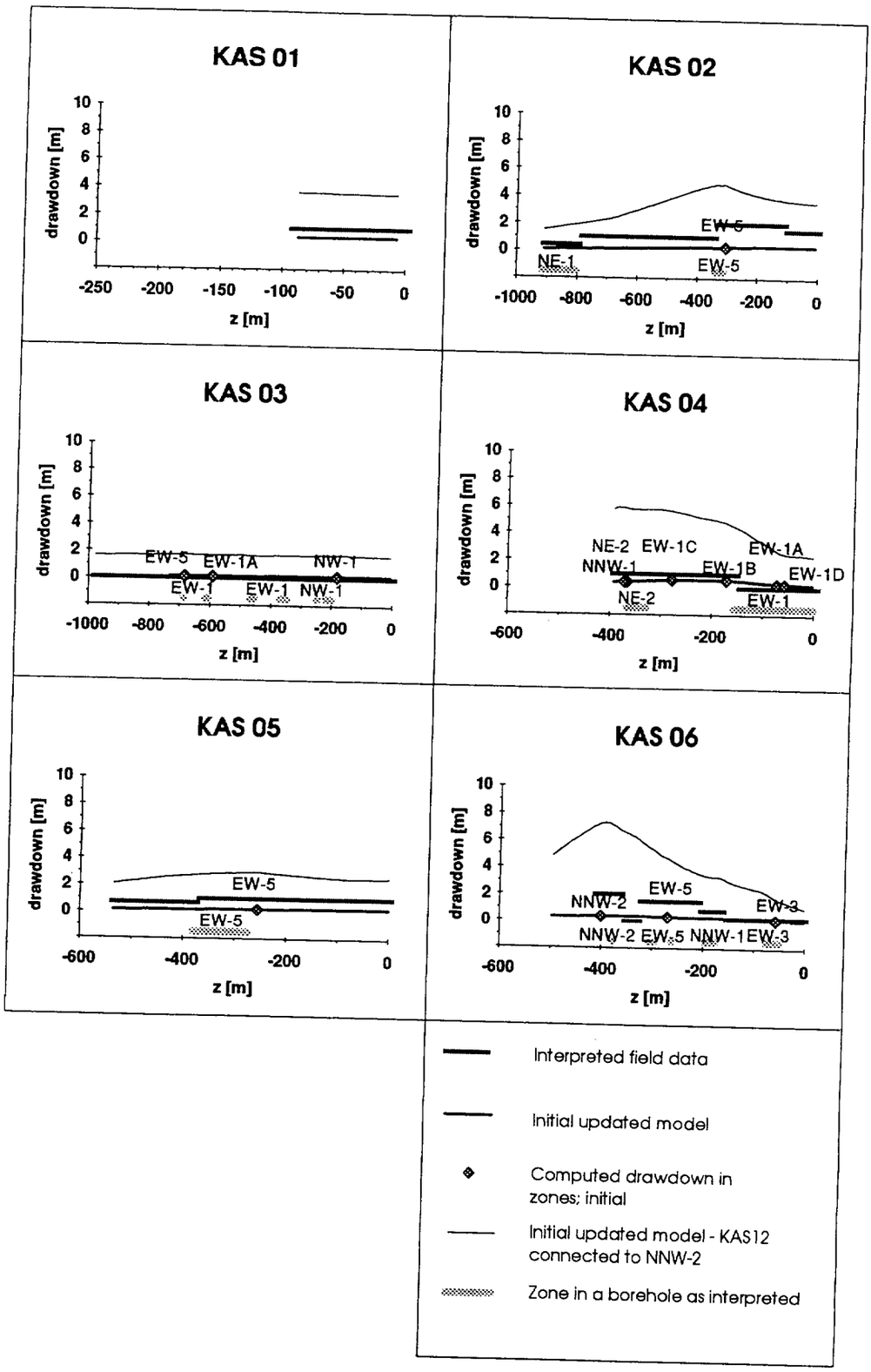

Figure 5-18. *Drawdown for the pumping test in KAS12. The interpreted field data are the values of the drawdown estimated to have been achieved if the pumping had continued. The computed results are simulated for the updated structural model with the initial input parameters but having a highly transmissive connection between KAS12 and NNW-2.*

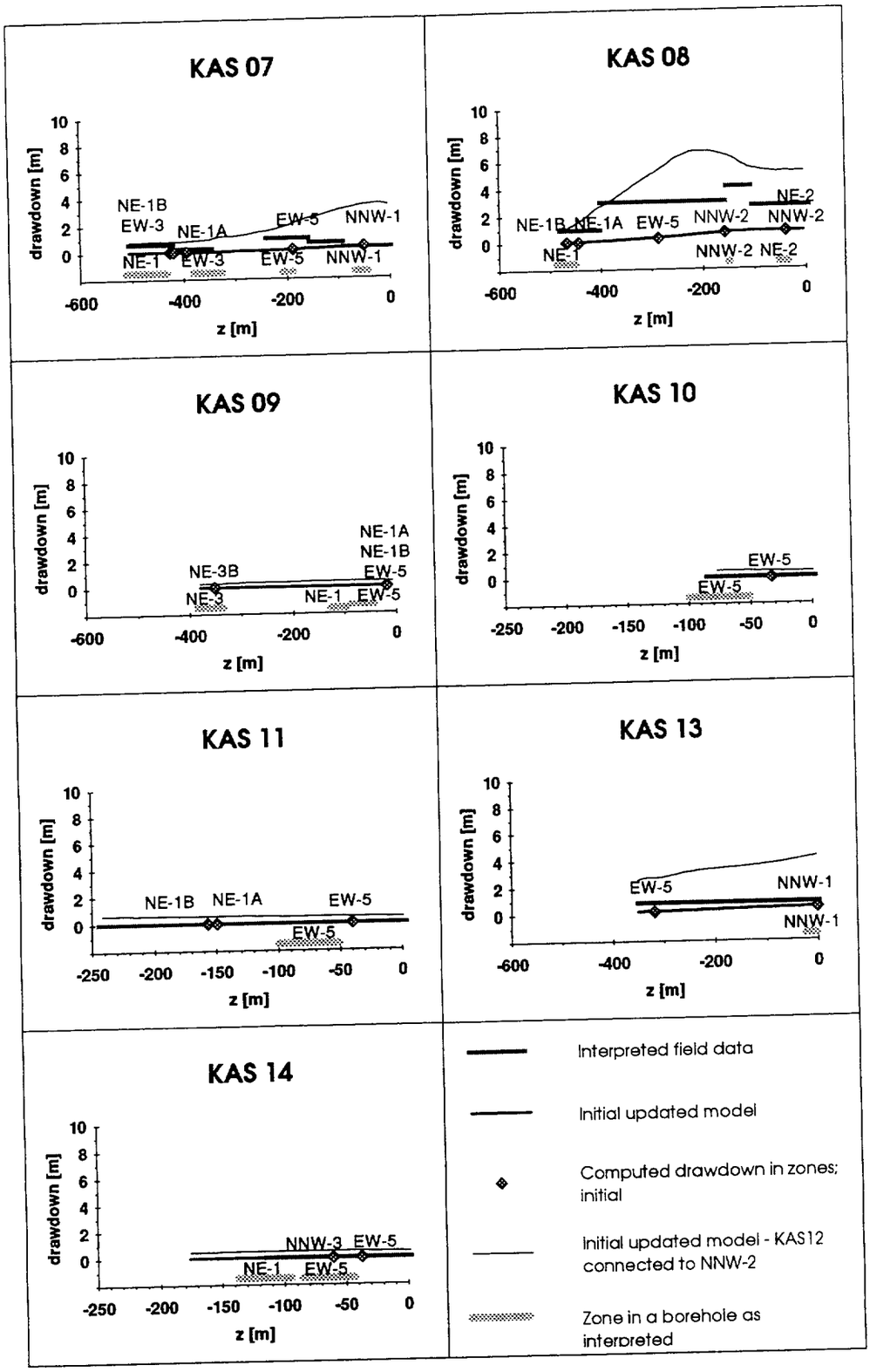

Figure 5-18. (Continued.)

of KAS02, KAS05 and KAS13 are about the same (Figures 5-4, 5-11, 5-14 and 5-16). This suggests that there should be a bedrock feature with an east-west orientation. That feature could contribute the inflow to KAS13 during the pumping test. In addition, if the feature were dipping to the north, it would at least partly explain the large drawdowns measured in the bottom sections of KAS04 (Figure 5-13).

To study whether such a east-west feature could explain the results of the pumping test in KAS13, the finite element mesh for the KAS13 pumping test was modified to include elements for such a zone. The assumed extent on the surface is shown in Figure 5-19. The new zone is dipping to the north (10 degrees). The depth extent was chosen to be 400 m. KAS13 intersects the added zone at a depth of 200 meters.

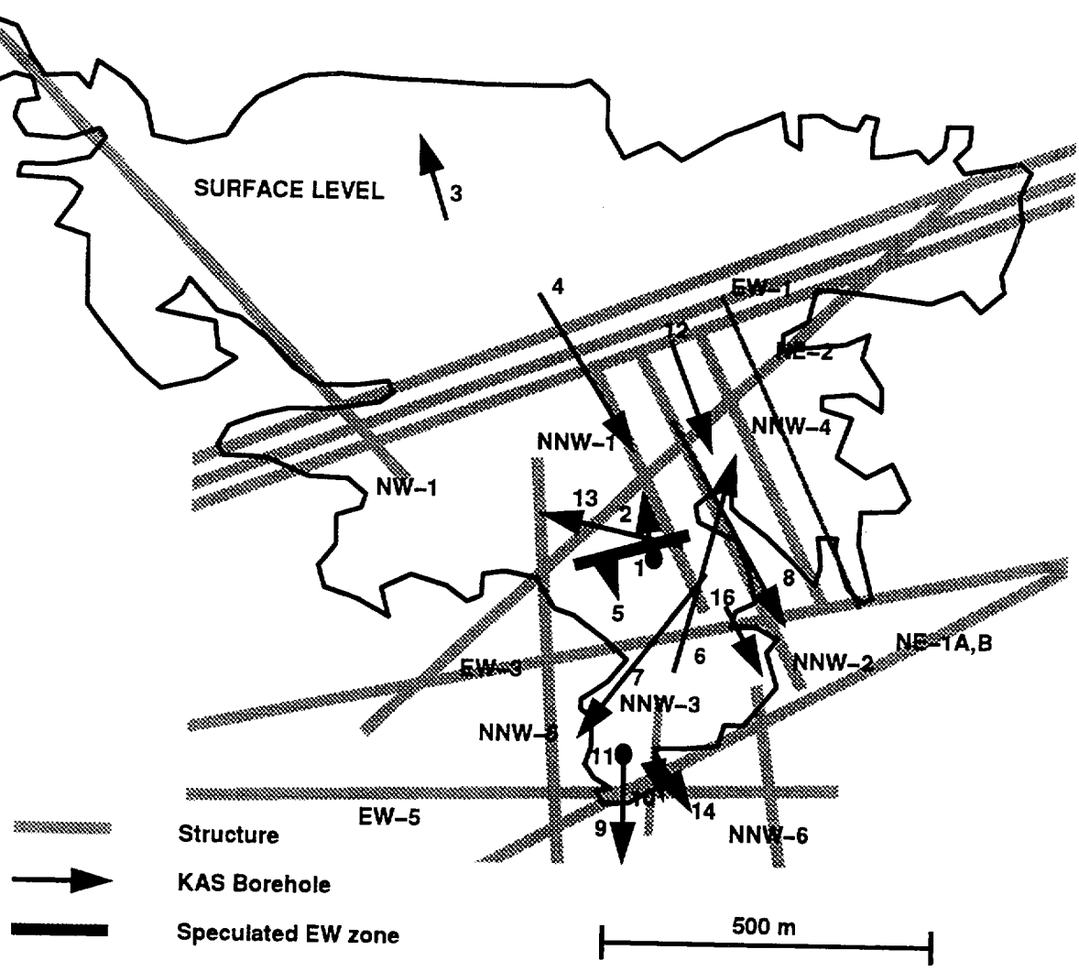

Figure 5-19. Strike of the proposed local east-west orientated feature.

When the transmissivity of the added zone is $5 \cdot 10^{-5}$ m^2/s, the simulated inflow from it to KAS13 is 3.6 l/s. The simulated drawdown along the cored boreholes is presented in Figure 5-20. Obviously, the new zone improves the agreement of the simulated drawdown with the field data in KAS01, KAS02, KAS04, KAS05 and KAS08. In KAS06 and KAS07, the simulated drawdown is now too large, however. The missing feature could be even smaller or at least the connection to NNW-1 should be poorer than in the simulation.

In the pumping test in KAS14, the large pressure responses (Figure 5-14) are transferred to the north along the north-dipping zones EW-5 and NE-1. The measured drawdown in the observation sections of KAS07, KAS08, KAS09 and KAS11 that intersect with NE-1 is much higher than the simulated values. This indicates that either the pressure response spreads far from the withdrawal hole and/or the best conductive part of NE-1 around KAS14 is restricted. Furthermore, the fact that the drawdown is larger in those sections intersecting EW-5 (KAS02, KAS05, KAS06 and KAS07) suggests similar characteristics for EW-5.

For the pumping test in KAS16, the simulation results differ significantly from the field data. Especially in those observation sections that intersect EW-5 the measured drawdown is significantly larger than that calculated (KAS02, KAS05, KAS06 and KAS07). In addition, the drawdown is larger also in the sections intersecting NE-1 (KAS02, KAS07 and KAS08). The evaluated steady state drawdowns for the bottom parts of KAS06 and KAS08 (about 14 m) are actually relatively high in the light of the drawdown estimated for the pumping hole (30 m). The comparison of the simulated and the interpreted experimental drawdowns gives the same indication as for the pumping test in KAS14 above: the most conductive parts of EW-5 and NE-1 should be restricted. Moreover, there should be a highly transmissive feature connecting the bottom sections of KAS06 and KAS08 to KAS16.

The differences between the simulated and measured results for the undisturbed flow conditions are small compared to the uncertainties discussed above. Therefore, they do not show any need for modifications.

Calibration strategy and modifications studied

The calibration strategy was the following: The agreement between the simulation results of the initial model for LPT1 and LPT2 and the field data was considered important to maintain and, if possible, even to improve. With a few exceptions, the agreement of the simulations results with field data is satisfactory in these cases. By conditioning, i.e., changing the transmissivities of the near-field parts of the zones around the withdrawal holes, the agreement of the inflows was improved. Regarding the other calibration cases, the potential sources of the differences were deduced. Modifications were tested using all of the cases and the most suitable ones were included in the model. The calibration was started by analyzing the cases that had the poorest agreement with the field results.

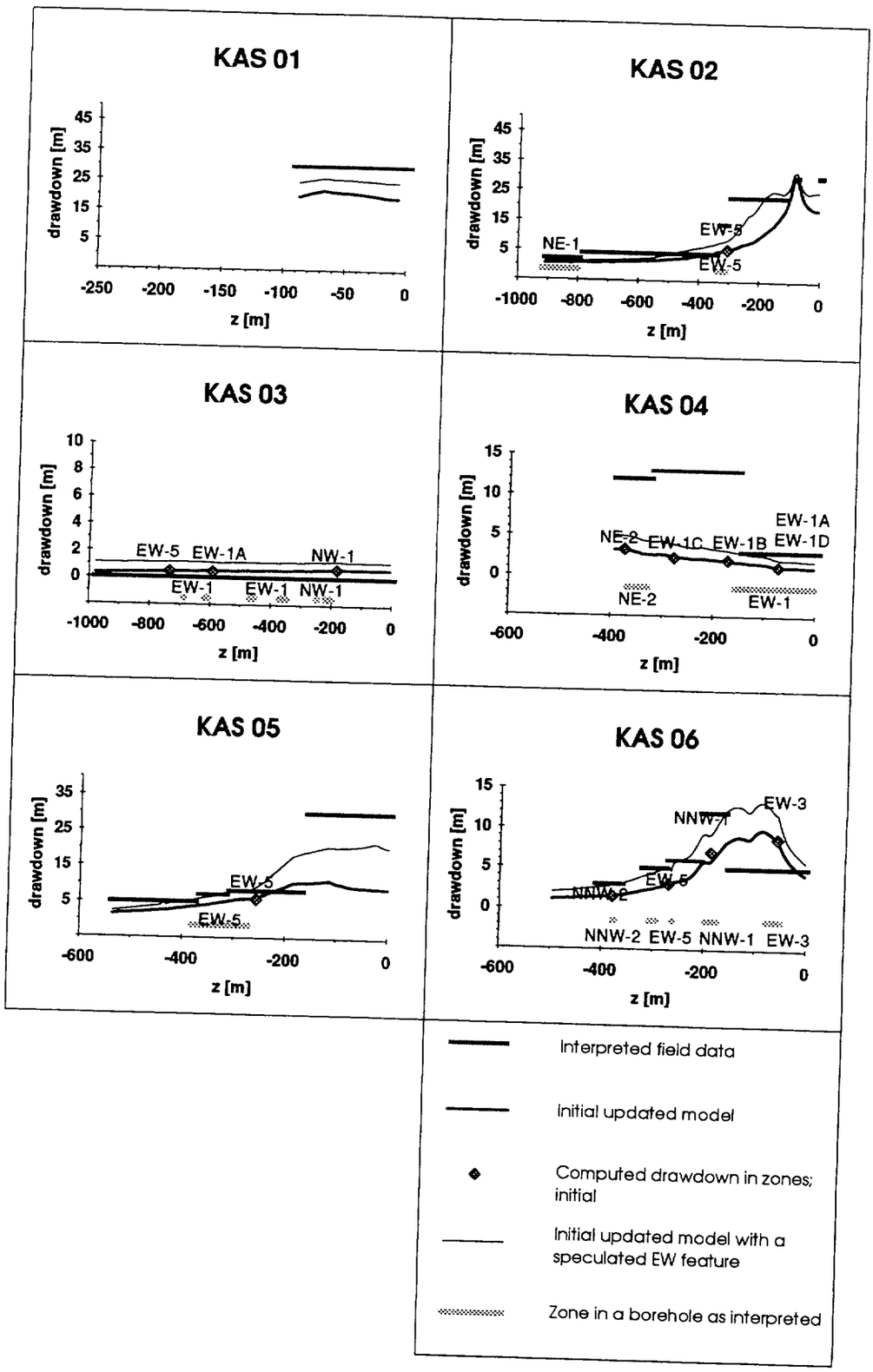

Figure 5-20. *Drawdown for the pumping test in KAS13. The interpreted field data are the values of the drawdown estimated to have been achieved if the pumping had continued. The computed results are simulated for the updated structural model with the initial parameters but having a speculative east-west orientated feature as indicated in Figure 5-19.*

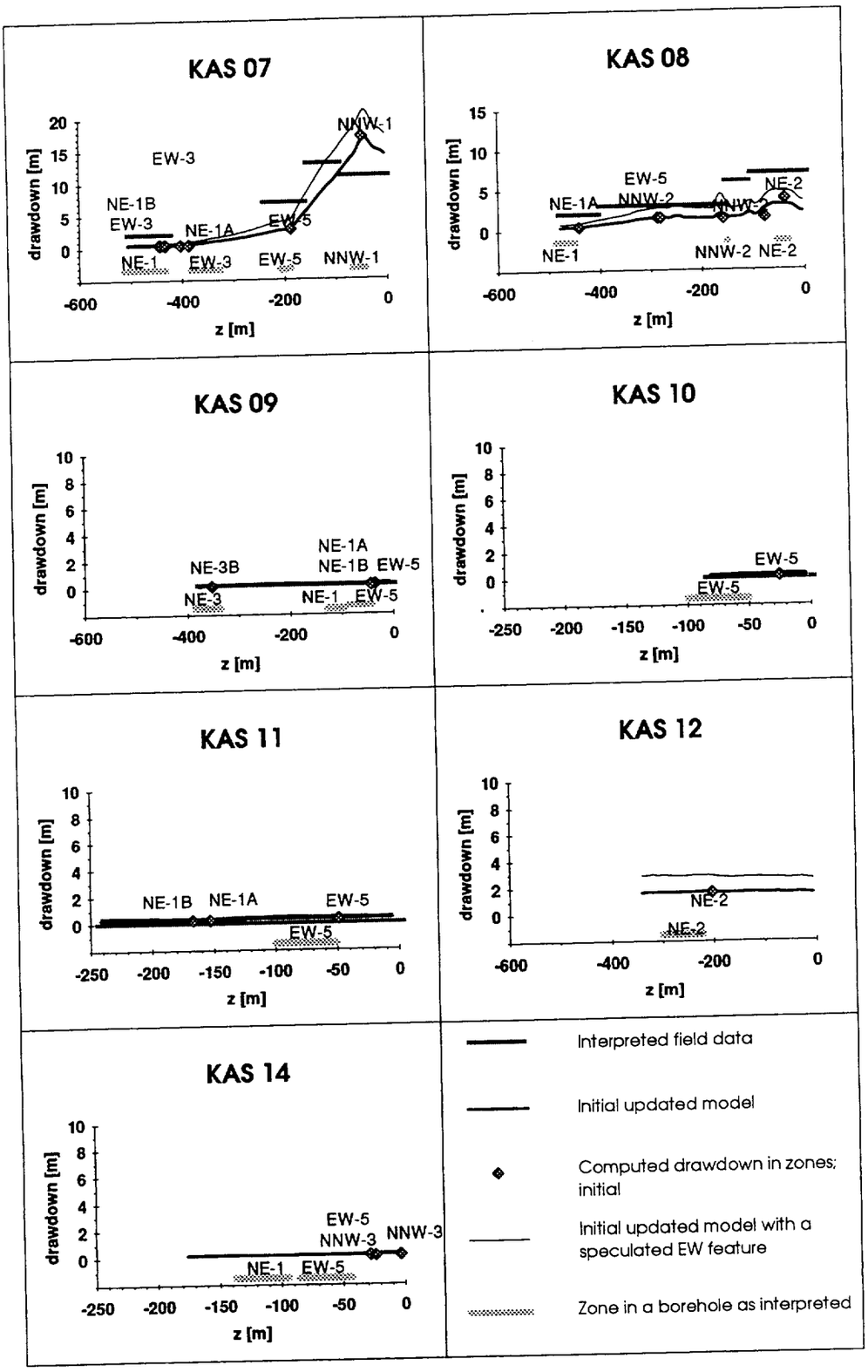

Figure 5-20. (Continued.)

Concerning the pumping tests in KAS12 and KAS13, the plausible modifications needed to obtain a better agreement with the field data were discussed above. These changes are also supported by the other pumping tests. In addition to the pumping test in KAS13, the incorporation of a new local but well-conductive east-west orientated zone (Figure 5-19) would improve the agreement of simulation results with field data for LPT1 and LPT2 as well as for the pumping tests in KAS16. The very likely connection between KAS12 and NNW-2 is also plausible in the light of the results of the flow rate measurements in KAS12 during LPT2 and with the analyses of the tracer test /Hautojärvi, 1994/.

In order to reduce the remaining differences, several possible reasons were studied. Improving the simulated drawdowns for the pumping tests in KAS14 and especially in KAS16 was the most difficult. As large drawdowns as transferred by NNW-1 in LPT1 and LPT2 to KAS06 and KAS07, respectively, were also difficult to achieve in the simulations.

Besides varying the average cross-zone transmissivities of the zones and conditioning the parts of the zones around the withdrawal holes, several other modifications were studied by means of numerical simulations. Some options of different boundary conditions were studied. The influences of a highly-conductive horizontal surface layer (the top part of the bedrock and the soil) and a low-conductive (clay) layer in the bottom of the sea were studied by including elements for those features into the element meshes and simulating all of the six pumping tests with various transmissivity values. We also varied the extents of zones and divided some zones to several parts having different transmissivities.

The benefits and drawbacks associated with each of the modifications examined in this study are not discussed here. In the following, only those modifications will be presented that were considered possible and improved the model´s performance significantly.

Modifications included in the calibrated flow model

To simulate the pumping tests more realistically, the boundary conditions of the simulation models were first modified. As the field data in Figures 5-4, 5-11, 5-12, 5-13, 5-14 and 5-15 suggest, no drawdowns were observed in KAS03 and in the uppermost section of KAS04 (in LPT2, which had the longest pumping period, in the lower sections of KAS03, however, small drawdowns were detected). The boundary conditions over the Äspö island to the north from EW-1 (including the top of EW-1) were changed from no-flow to fixed-pressure boundary conditions. Boundary conditions have to be consistent with the modelling objectives. As the field data were interpreted to reflect pseudo-steady-state flow conditions, the boundary conditions should also be taken consistently. In EW-1 and to the north from it, the porosity of the zone and of the top layer of the bedrock as well as the amount of water in bog areas can be assumed to be so large that pumping

likely could not affect the water table in those areas. Only after very long pumping period, some drawdown can be expected.

Furthermore, local modifications in the structural model were called for in order to model the pumping test in KAS12 and KAS13. Most likely, there exists a hydraulic connection between KAS12 and NNW-2. However, the connection may not be as transmissive as used in the simulation presented in Figure 5-18.

In order to model the pumping test in KAS13, a new bedrock feature, an east-west orientated zone (Figure 5-19) was introduced. This speculative modification, however, was not incorporated in the model and, therefore, the simulation of the pumping test in KAS13 using the present model is not sensible. The fact that a feature is missing from the model must be kept in mind when comparing the simulation results with the field data: the pressure in KAS01 and in the upper parts of KAS02, KAS05 and KAS13 should be almost the same.

For having a better agreement with the field data of the pumping test in KAS14 and especially in KAS16, the reduction of the transmissivity of the top of NE-1 was studied. This modification improved the simulated drawdowns. Even better results were obtained by restricting the highly conductive part of NE-1 from the east and the west. Figure 5-21 depicts the well-conductive part of NE-1. Outside this well-conductive part, the transmissivity of NE-1 was assumed to be an order of magnitude smaller.

Similarly, the most conductive part of the EW-5 zone was also restricted (Figure 5-21). This modification improved the simulated drawdowns for the pumping tests in KAS16 and KAS14 as well.

Finally, the transmissivities of some zones were modified. The modified cross-zone transmissivities are presented in Table 5-2. The transmissivity of the most conductive parts of NE-1 was reduced by a factor of 2. Similarly, the transmissivities of NNW-1 and EW-5 were reduced by a factor of 2. The transmissivity of EW-3 was increased by a factor of 20. These modifications were mainly introduced to improve the agreement of the calculated inflows with the field data. Furthermore, the transmissivities of the southern subzones B and C of EW-1 (Figure 4-2) were also reduced by an order of magnitude, which caused a larger drawdown in the bottom sections of KAS04 for LPT1 and LPT2 as well as for the pumping tests in KAS12, KAS14 and KAS16. The reduction of the transmissivity of NE-2 had both benefits and drawbacks, and that change was not included in the model.

In addition, the zones were conditioned to the pumping tests. The transmissivities of circular areas of the zones having radius of about 10 m around the withdrawal boreholes (cf. Figure 5-17) were modified in order to obtain the measured inflow and a better agreement with the measured drawdown field. The conditioning factors relative to the calibrated transmissivities of the zones for each pumping test are shown in Table 5-10.

Table 5-10. Conditioning the transmissivities of the zones around the withdrawal holes for various pumping tests. The factor is the ratio of the transmissivity of a circular near-field part around the withdrawal holes having radius of about 10 m and the calibrated cross-zone transmissivity given in Table 5-2.

	PUMPING TEST					
Zone	LPT1	LPT2	KAS12	KAS13	KAS14	KAS16
EW-3	0.01	1				
EW-5	0.5	5			10	10
NE-1	0.05				50	50
NNW-1	1	10				
NNW-2		0.2				

5.3.6 Simulation of the calibration cases with the calibrated model

The steady-state drawdowns were computed for all the other pumping tests except the pumping test in KAS13 by applying the calibrated flow model (Figures 5-4, 5-11, 5-12, 5-14 and 5-15. The total inflow to the withdrawal holes and its distributions are presented in Tables 5-3 and 5-5 – 5-9.

For LPT1, the agreement of the simulated and measured drawdowns is satisfactory with a few exceptions (Figure 5-11). In KAS06 in the section intersecting NNW-1, the computed drawdown should be significantly larger. In KAS01 and in the topmost section of borehole KAS02, the computed drawdowns are too high. Adding the new proposed east-west orientated zone (Figure 5-19) would quite probably reduce the simulated drawdown in these observation sections. The calculated total inflow is still about twice the pumping rate (Table 5-5). The inflows from EW-5 and NNW-1 are close to the field data but the inflow from NE-1 and probably from EW-3, too, should be smaller. The contributions of NE-1 and EW-3 could easily be reduced by means of conditioning without influencing the drawdown field. The field data cannot, however, be used to define the ratio of these inflows.

Concerning LPT2, the agreement of the total inflow, the distribution of the inflow and the drawdown with the field data is good (Table 5-3 and Figure 5-4). The simulated drawdown is too high in KAS01 and in the upper sections of KAS02 and KAS13. Including of the new east-west zone marked in Figure 5-19 would decrease the drawdown in these observation sections and, on the other hand, make the drawdown larger in the upper part of KAS05, which would also improve the agreement with the field data. The depth dependence of the simulated drawdown does not reflect the field data in KAS08 but, as stated above, the simulation results show the highest values in the intersection with NNW-2 as in the field data. The large drawdowns measured in the lowest and in the uppermost packed-off sections

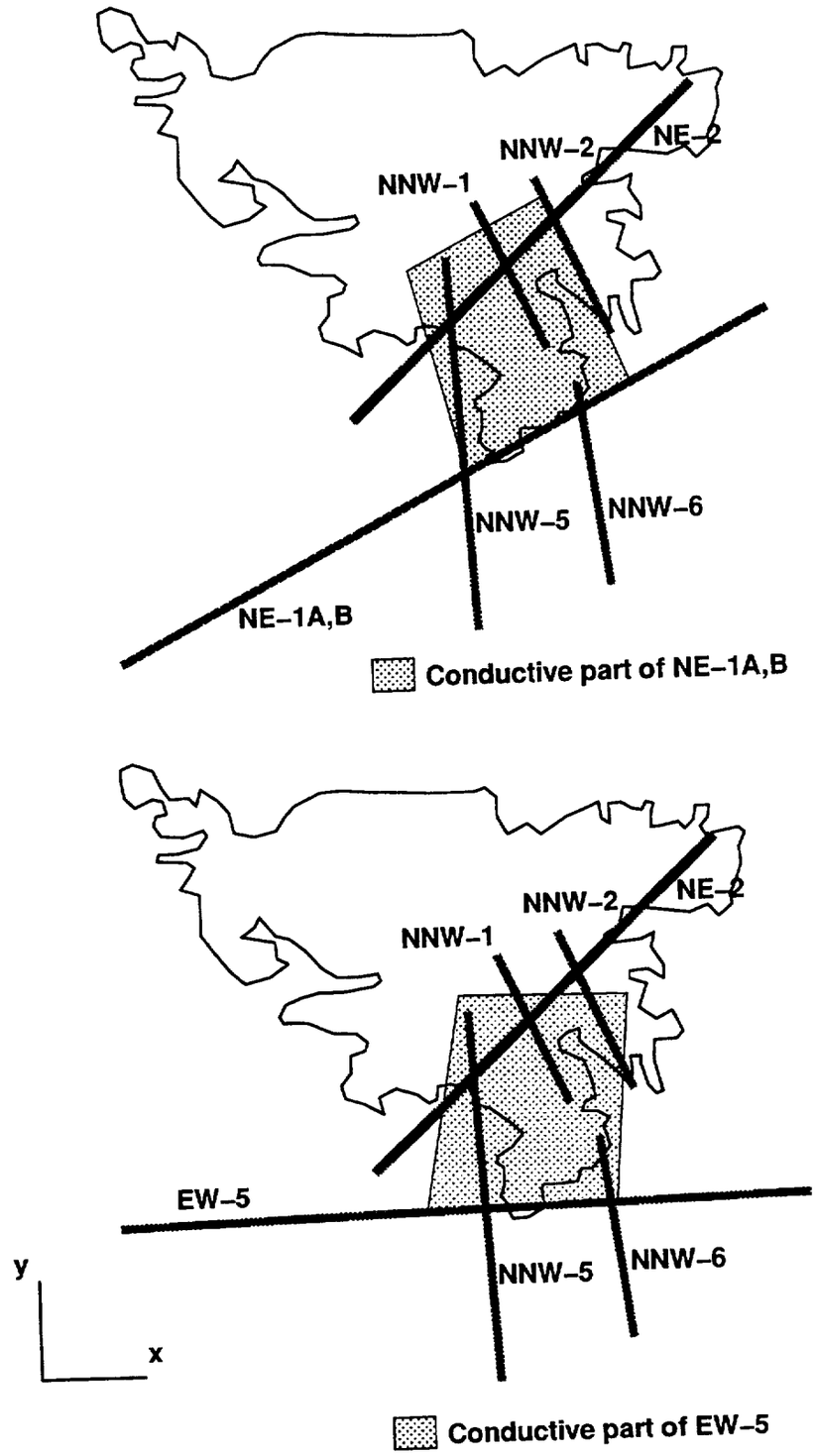

Figure 5-21. *The parts of zones NE-1 (top) and EW-5 (bottom) assumed to be highly conductive.*

in KAS08 may have occurred due to a more conductive connections to NNW-2 than in the model. The simulated drawdowns are too small in KAS12. There may be two reasons for this. The drawdown in the upper part of the borehole is small because of the no-drawdown boundary conditions in EW-1 close to KAS12. It can be that near KAS12 the no-drawdown boundary conditions are not valid. Deeper in KAS12 the measured drawdown is higher than the simulated one because of the connection to NNW-2 discussed above. (The connection was incorporated only to the element mesh for the pumping test in KAS12.) Actually, to have simulated values for KAS12 that are for a hydrogeologically equivalent location, we should take the drawdown simulated for NNW-2. The total inflow and its distribution between the zones are consistent with the field data.

The simulated results of the pumping test in KAS12 agree well with the field data (Table 5-6 and Figure 5-12). A relatively good connection to NNW-2 improves the agreement with the field data significantly. The transmissivity of the connection has to be smaller than that of NNW-2. (Possibly the area in NNW-2 intersected by KAS12 is less conductive than NNW-2 in average.) The calculated drawdown agrees well with the field data except in KAS08, in which the simulated drawdowns should be larger. The total inflow is close to the pumping rate applied in the field experiment.

As a speculative feature was found essential in explaining the results of the pumping test in KAS13 and the feature was not included in the flow model, the simulation of this pumping test was not considered sensible.

The calculated results for the pumping test in KAS14 do not agree as well with the field data as those of the three other short-term pumping tests above. The total inflow is close to the pumping rate (Table 5-8). Owing to the uncertainties associated to the field data, the correctness of the calculated inflow distribution cannot be justified. The calibration improved the agreement of the simulated drawdown with the field data (Figure 5-14). However, some significant differences remained. In KAS08 in the section intersecting NNW-2, the experimental drawdown is significantly higher than the calculated one. In the bottom section of KAS09, the measured drawdown is about 5 m and the simulated is only about 1 m. Varying the transmissivity of NE-3 does not influence the simulated drawdown. The bottom part of KAS09 is so far in the south under the sea (Figure 1-1) that the high drawdown is not achievable in the simulation. A possible explanation is a restricted north-northwest orientated zone that could transfer a large pressure response far to the south. On the other hand, the simulated drawdown is too high in KAS10 as well as in the top sections of KAS09 and KAS11. The drawdown has to be too large in these sections in order to have large enough drawdowns in the other boreholes far from the withdrawal hole. A subhorizontal feature close to the surface, which is also suggested by the distribution of the inflow to KAS14, would probably reduce the simulated drawdown close to KAS14.

The simulation and field results are compared for the pumping test in KAS16 in Table 5-9 and Figure 5-15. The initial model showed the poorest

agreement with the field data in this pumping test. As a result of the calibration, the agreement improved but still significant discrepancies remained. The inflow distribution exhibits a reasonable agreement. Yet the contribution of NE-1 should be smaller. The reduction of the transmissivity of NE-1 would, however, have worsened the simulated drawdowns. The differences in the drawdown can be classified to four sets: First, the simulated drawdown is still too low in the observation sections intersecting EW-5 (KAS02, KAS05, KAS06 and KAS07). Enlarging the transmissivity of EW-5 (or optionally reducing the transmissivity of the other zones) would improve the agreement but it would not be consistent with the other pumping tests and with the inflow distribution to KAS16. Secondly, the simulated drawdown is similarly still too small in the sections intersecting NE-1 deep in the bedrock (KAS02, KAS07 and KAS08). Thirdly, the simulated drawdown is also too small in the sections that are interpreted to intersect NNW-2 (KAS06, KAS08) or are close to it (KAS12). Fourthly, there are observation sections in which the calculated drawdown is significantly larger than the field data suggest. In these cases experimental values were measured in the rock matrix and the field data are not considered reliable.

As the simulated pressure and salt concentration fields for the undisturbed flow conditions did not change as a result of the calibration, the presentation of the results in Figures 5-9 and 5-10 is not repeated.

5.3.7 Discussion

Certain pumping tests were selected as calibration cases. The selection of the LPT1 pumping test and the pumping tests in KAS12, KAS13 and KAS14 was based on the recommendation of Rhén /1991/. In addition, the pumping test performed in KAS16, which had been drilled later than the other cored boreholes considered in this study, was chosen because of its location close to KAS06. The results of the LPT2 pumping test were also used in the calibration. (An alternative approach would have been to carry out the calibration without LPT2.) All the pumping tests studied were instructive in the calibration process.

The hydraulically undisturbed conditions were considered as a calibration case, too. From the calibration point of view, this case did not prove very fruitful. The boundary conditions for the pressure and the salinity to a large extent define the simulation results. As the boundary conditions, especially for the salt concentration, are poorly known and must be selected (adjusted) to obtain results that are consistent with the field data, it is unclear whether the remaining differences are due to improper boundary conditions, incorrect assumptions on the hydraulic properties of the bedrock or the simplifications involved in the modelling. Since the uncertainties of the field data were significant, the simulations for the undisturbed flow conditions were not utilized when adjusting the model parameters. The simulation of the undisturbed flow conditions was nevertheless essential for calculating the flow rates through the injection section (see Section 5.2.1).

Although all the pumping tests simulated did provide useful information on the Äspö island, the short duration of the pumping periods in the other pumping tests except in LPT1 and LPT2 caused some problems. Because of practical limitations, steady-state simulations had to be used in the calibration phase. On the other hand, while steady-state flow conditions were not reached even in the long-term pumping tests, steady-state drawdowns had to be estimated for the short-term pumping tests. A pseudo-steady state is assumed to have been reached in LPT1 and LPT2, and the drawdowns measured at the end of the pumping periods were compared as such with the results of the steady-state simulations. Obviously, the field data call for transient simulations in the calibration stage, too.

The total inflow to a withdrawal hole can be estimated to be equal to the average pumping rate. The distribution of the inflow includes uncertainties for all pumping tests. For LPT2, the distribution of the inflow along the borehole is determined reliably. The inflow to the upper part of borehole KAS06 was assumed to have come from EW-3. The water to the upper part might also flow from a local unidentified feature or from the highly-conductive surface layer. It is also possible that the transmissivity of EW-3 is high only close to the surface or close to KAS06. As the adjustment of the cross-zone transmissivity of EW-3 was based only on the inflow to the upper part of KAS06, the result is uncertain.

The need for modifying the boundary conditions of the simulation models was actually a consequence of assuming steady states. The amount of water in the soil and in the uppermost part of the bedrock in the area north from EW-1 is so large that much longer pumping periods would have been required to reach steady states. Assuming the no-drawdown boundary conditions for the northern part of the island is actually more consistent with the assumption of pseudo-steady states in which the effect of pumping has not yet spread that far.

In adjusting the model parameters, the pumping tests having the poorest agreement between simulation results and the field data were studied first. Plausible explanations for the pumping tests in KAS12 and KAS13 were found. The results of the pumping test in KAS12 indicate that there has to be a hydraulic connection to NNW-2. KAS12 does not, however, intersect NNW-2 directly or the transmissivity of NNW-2 is smaller near the intersection than in the southern part of the zone.

The field data of the pumping test in KAS13 cannot be obtained with the present structural model. The distribution of the inflow to KAS13 already suggests that a (local) well-conductive feature is missing or the location of one of the current zones (NNW-1, NNW-5 or NE-2) is different. The spatial drawdown distribution shows that the missing feature is probably east-west orientated. The simulation results of the other pumping tests would likely be improved with that kind of feature, too. The extent of the feature should be small and it might thus not be important on a site scale. There may also be other alternate orientations of the missing feature. The speculative feature was not included in the flow model. Before incorporating the feature to a

flow model, the results of other field studies should be reviewed in order to find possible confirmations to this hypothesis. The possible east-west feature has to be considered when interpreting the field results, however.

Reasons for the remaining discrepancies between the simulated and measured drawdowns of the pumping test in KAS16 could not be explained as easily. The field data indicates that EW-5 and NE-1 transfer significant drawdowns far from KAS16. The agreement was improved assuming that the transmissivities of EW-5 and NE-1 are high around KAS16 and that the most conductive parts of the same zones are limited. The need of restricting the most conductive parts of the zones can be understood in terms of heterogeneity and scale effects. To improve the simulation results for the pumping test in KAS16, the radius of the areas whose transmissivities were conditioned should probably be larger for NE-1 and EW-5 around KAS16. The large drawdown would then spread further, but the inflow would be restricted by the average transmissivities of the zones.

For the pumping test in KAS14, the problems were similar but smaller than in KAS16. The same modifications improved the agreement of simulation results with field data for KAS14, too. The result is, however, a compromise: the responses in the boreholes close to KAS14 impaired and in the boreholes farther away improved. In the case of KAS14 for further improvements of the results, additional features would have been needed. The measured large drawdown in the bottom part of KAS09 cannot be simulated using the current structural model. The results could also have been improved if the transmissivity of NE-1 had not been high on the western side of KAS14 but deeper in the bedrock where KAS08 and KAS16 intersect the zone.

Concerning LPT1 and LPT2, already the initial model produced satisfactory results. The inflow distributions were improved by means of conditioning. The reduction of the transmissivity of the southern branches of EW-1 improved further the agreement of the simulation results with the field data.

In the calibrated flow model, the geometry of the zones was thus not modified. No new zones were incorporated. The well-conductive parts of NE-1 and EW-5 were restricted, however (Figure 5-27).

Since the flow model is a simplification for the real bedrock, it does not coincide perfectly with the field data interpretations. The discrepancies arise, for instance, from the assumption of the planarity of the zones. In some cases, geometrical simplifications result in differences in the measured and computed drawdowns.

The calibration process reduced many differences between the simulation results and the field data. Even better agreements, especially for the inflows, could have been achieved. Smaller modifications of the transmissivities of the zones than a factor of two were not considered sensible.

Most of the remaining discrepancies can be explained by the simplicity of the model. Anisotropy and local heterogeneities could account for, for instance, the large drawdown in KAS06 during LPT1 (Figure 5-11). Indications for missing features or for differently oriented zones were obtained. The extents of the zones could possibly be modified. The transmissivities of the zones certainly vary on large scales, too. The simulations show that the transmissivity of NE-1 is very high for a restricted but large part around KAS16. The same seems to be the case with EW-5. In addition, the southern part of NNW-2 deep in the bedrock is likely more conductive than the northern part. In fact, the vertical extent of NNW-2 and NNW-1 as well might not be as large as assumed in the simulations.

Although the LPT2 test cannot be simulated significantly better with the calibrated model than with the initial model, the calibrated model is an improvement. It describes the Äspö island as a whole more comprehensively and especially the southern part of the Äspö in more detail. In addition, the study of the pumping test in KAS13 gave indications of a missing feature. The presumed connection from KAS12 to NNW-2 was supported by the simulation of the pumping test in KAS12.

5.4 SIMULATION OF LPT2 WITH THE UPDATED MODEL AFTER THE CALIBRATION

Steady-state simulations

In order to evaluate the LPT2-modelling performance of the updated model after the calibration stage, a steady-state simulation was carried out. The LPT2 test was simulated as before the calibration (Section 5.2.1). The same finite element mesh was used. The boundary conditions of the element mesh applied in the simulations were modified as discussed above: the model surface on the northern side of zone EW-1 was a fixed-pressure boundary. The modifications incorporated in the flow model, the adjusted cross-zone transmissivities, the transmissivities of the near-field parts around KAS06 and the reduced extents of the most conductive parts of zones NE-1 and EW-5, were described above in Section 5.3.5 (Table 5-2 and 5-10 and Figure 5-21).

The simulated drawdown along the cored boreholes is presented in Figure 5-4 with experimental data and the simulation results for the initial model. The plausible reasons for the remaining discrepancies were discussed above (see Sections 5.3.6 and 5.3.7).

Transient simulations

In addition to the steady-state simulations, transient simulations were carried out for the LPT2 pumping test. The same finite element mesh was employed as in the steady-state simulations. The effect of the pumping was

implemented in the transient simulations by assigning the pumping rate applied in the field experiment as a boundary condition to the pumped node. The pumping rate varied as a function of time in the field experiment,. The other boundary conditions were the same as in the steady-state simulations (Section 5.3.5).

The transient simulations were carried out for three different values of the specific storage of the rock matrix: 10^{-7}, 10^{-6} and 10^{-5} m^{-1}. The storativity of all the zones was 10^{-7}. Only one storativity value was used because the simulation results are insensitive to the storativity of the zones. Only unrealistically high values of the storativity of the zones affect results in the nearest borehole KAS07.

5.4.1 Performance measures

Steady-state simulations

The computed steady-state drawdowns are listed in Appendix D for all the observation sections of the cored and percussion boreholes. Compared to the initial updated model, the agreement between the simulated drawdowns and the field data improved in several packed-off sections but, on the other hand, worsened in some other sections. Appendix D also shows the absolute and relative deviations. The largest relative difference calculated is in HAS05. However, the largest absolute deviation in the drawdown is still in the uppermost section of HAS14, for which the relative difference cannot be calculated because no drawdown was measured. As earlier with the base model and the initial updated model, no comparison was performed for the second lowest section of KAS07 (J2). Owing to the problems with the field measurements, the measured value for that section is considered very uncertain /Ström, 1993a/.

Figure 5-22 shows the experimental and computational drawdowns as a function of "distance" for all of the observation sections. The deviations of the simulated drawdowns from those measured are presented in Figure 5-23. Comparing with the results for the initial model (Figures 5-5 and 5-6), no improvements can be recognized. The distribution of the drawdown deviations is presented in Figure 5-24. The deviation distribution is also similar to that of the updated model before the calibration (Figure 5-7). The mean of the drawdown differences is still close to zero. The standard deviation is the same (1.8 m) as for the initial updated model (Figure 5-7). The shape of the deviation distribution is different, however. In fact, without the deviation for the upper section of HAS14, the calibration would have increased the standard deviation. The same conclusion that was drawn above in Section 5.3.7 in connection with the model calibration on the basis of the results for the cored boreholes remain valid: regarding LPT2, the calibration resulted only in small changes in the drawdown field and did not improve the agreement between the measured and computed drawdowns.

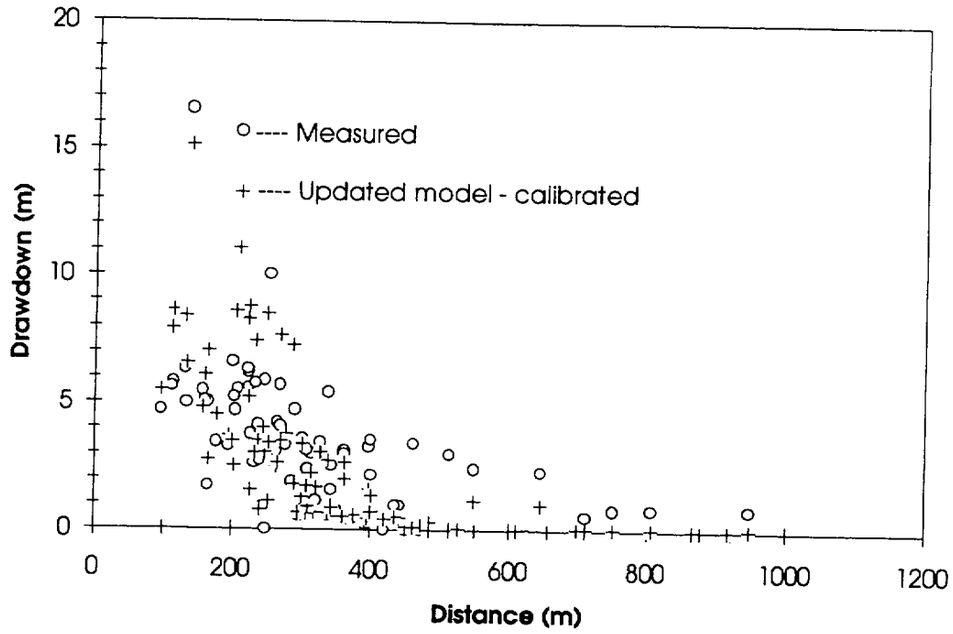

Figure 5-22. *Measured and simulated pressure drawdown in the observation sections of the cored and percussion boreholes as a function of the "distance" for LPT2. The simulation results computed applying the updated model after the calibration. The "distance" and measured drawdowns from Rhén et al. /1992/ and Ström /1993a/.*

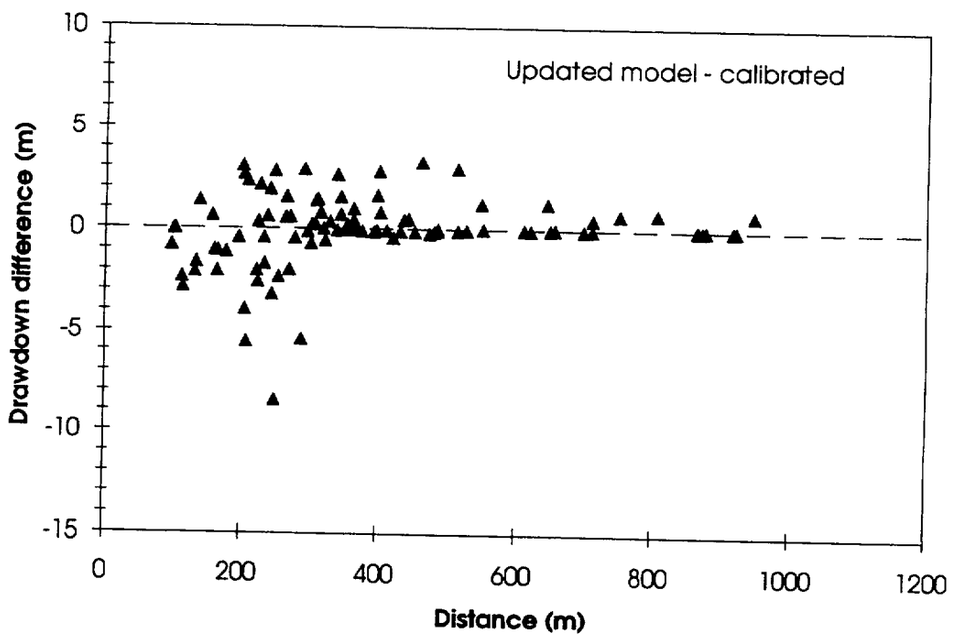

Figure 5-23. *Difference between the measured and simulated drawdowns shown in Figure 5-22. The "distance" for each observation section from Rhén et al., 1992.*

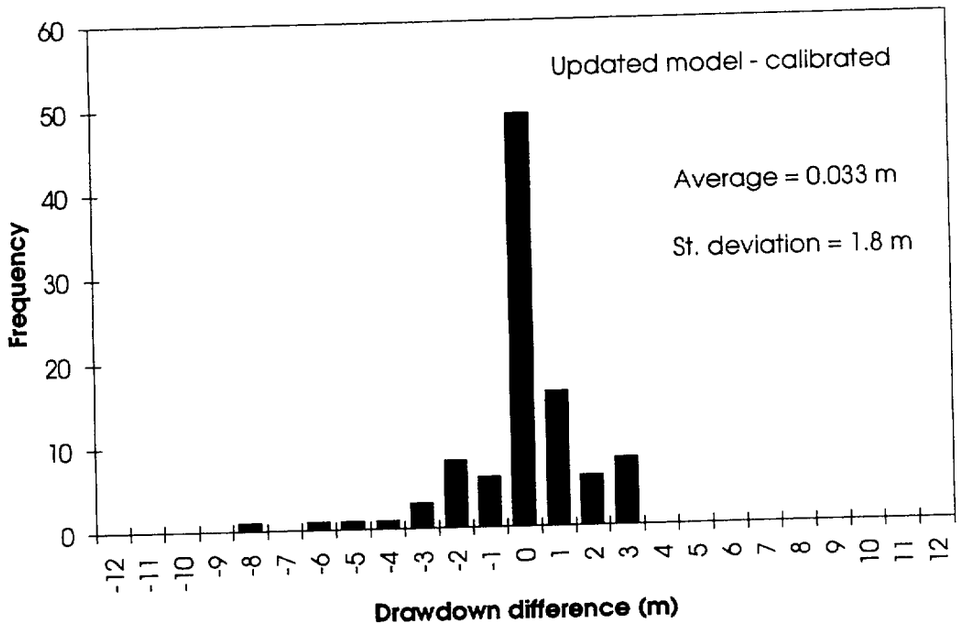

Figure 5-24. *Distribution of the differences between the measured and simulated pressure drawdowns shown in Figure 5-23.*

Figure 5-25 illustrates pathlines from three tracer injection sections in KAS05, KAS07 and KAS12 to the withdrawal hole. These pathlines were computed in a flow field which was obtained by summing the two Darcy velocity fields calculated for the undisturbed flow conditions and for the LPT2 test.

The computed total water inflow to the withdrawal hole KAS06 is 2.2 l/min being equal to the pumping rate. The calibration improved the distribution of the inflow between the zones (Table 5-3).

The amounts of water flowing through the tracer injection sections calculated on the basis of the equivalent-continuum transmissivities are compared with the measured values in Table 5-11. In calculating the flow rates, the same approach was applied as for the initial base model (Section 4.2.1). The hydrologically undisturbed conditions were simulated with the calibrated model as discussed in Section 3.5. The same boundary conditions were applied as with the base model and the initial updated model (Sections 4.2.1, 4.4.1 and 5.2.1). The total magnitude of the average Darcy velocity was obtained by summing the vectors calculated for the undisturbed conditions and for the LPT2 test. The flow rate through the tracer injection section KAS12-2 was also calculated assuming that it intersects NNW-2 (Table 5-11).

The influence of the heterogeneity on the flow rate through the injection sections could also have been investigated as with the initial base model

(Section 4.2.1). The outcome would, however, have been a similar dispersion of the flow rate relative to the average values in Table 5-11 as for the initial base model (Figure 4-10).

Table 5-11. Measured /Rhén et al., 1992/ and computed flow rates through the tracer injection sections during pumping test LPT2. The computed values are for the updated model after the calibration.

Injection section	Zone interpreted	Measured (ml/min)	Computed (ml/min)
KAS02-4	EW-5	2	4.0
KAS02-2	NE-1	4	1)
KAS05-3	EW-5	9	3.3
KAS05-1	(no zones)	11	2)
KAS07-4	EW-5	18	4.1
KAS08-3	NNW-2	21	3.7
KAS08-1	NE-1	48	2.4
KAS12-2	NE-2	107	0.37
KAS12-2	NNW-2[3)]	107	2.5[3)]
KAS13-3	(no zones)	3.3	2)
KAS14-2	NE-1	11	3.9

[1)] In the simulation model borehole KAS02 does not intersect zone NE-1, see Figure 5-3. The calculated flow rate is very small in the matrix.
[2)] No zone is interpreted to this section, see Figure 5-3, and the calculated flow rate is very small in the rock matrix.
[3)] Assuming that borehole section KAS12-2 intersects NNW-2, see the discussion of the calibration in Section 5.2.7.

Transient simulations

The same twelve observation sections as above with the calibrated base model (Section 4.3.1) were used to study the transient hydraulic response of the model in comparison with the measured data. Out of the twelve sections, seven have been interpreted to intersect a zone (the zones intersected marked in Figure 5-26). No zone was identified to intersect five sections. For the comments regarding the field data, see Section 4.3.1.

The simulated drawdowns for the selected observation sections are presented as a function of time in Figure 5-26. The large differences between the computed and measured values in some sections make the comparison of the time-dependence difficult. The time dependencies of the measured values are close to those simulated with the specific storage

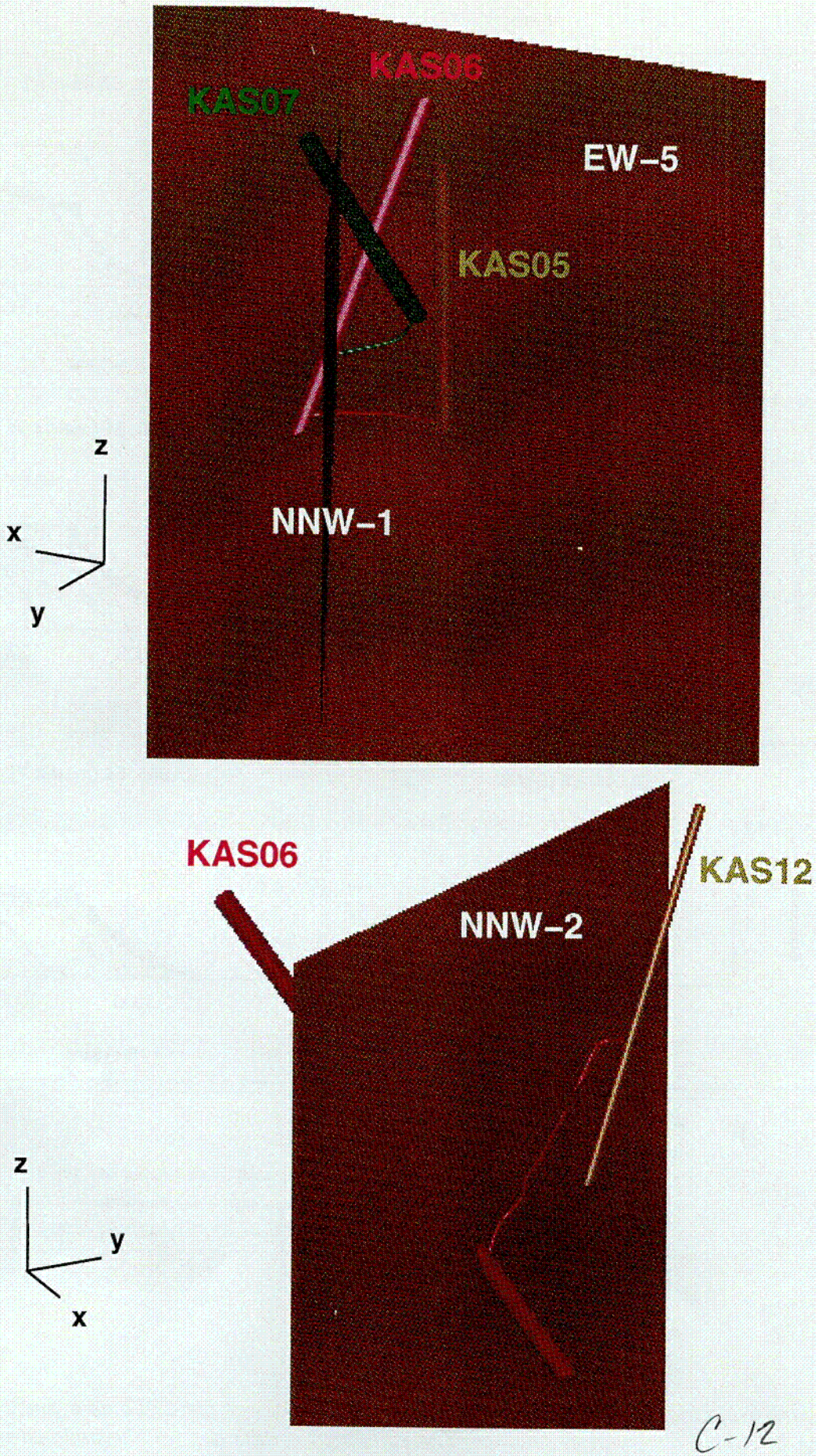

C-12

Figure 5-25. *Simulated pathlines from the tracer injection sections in KAS05, KAS07 and KAS12 to the withdrawal hole KAS06.*

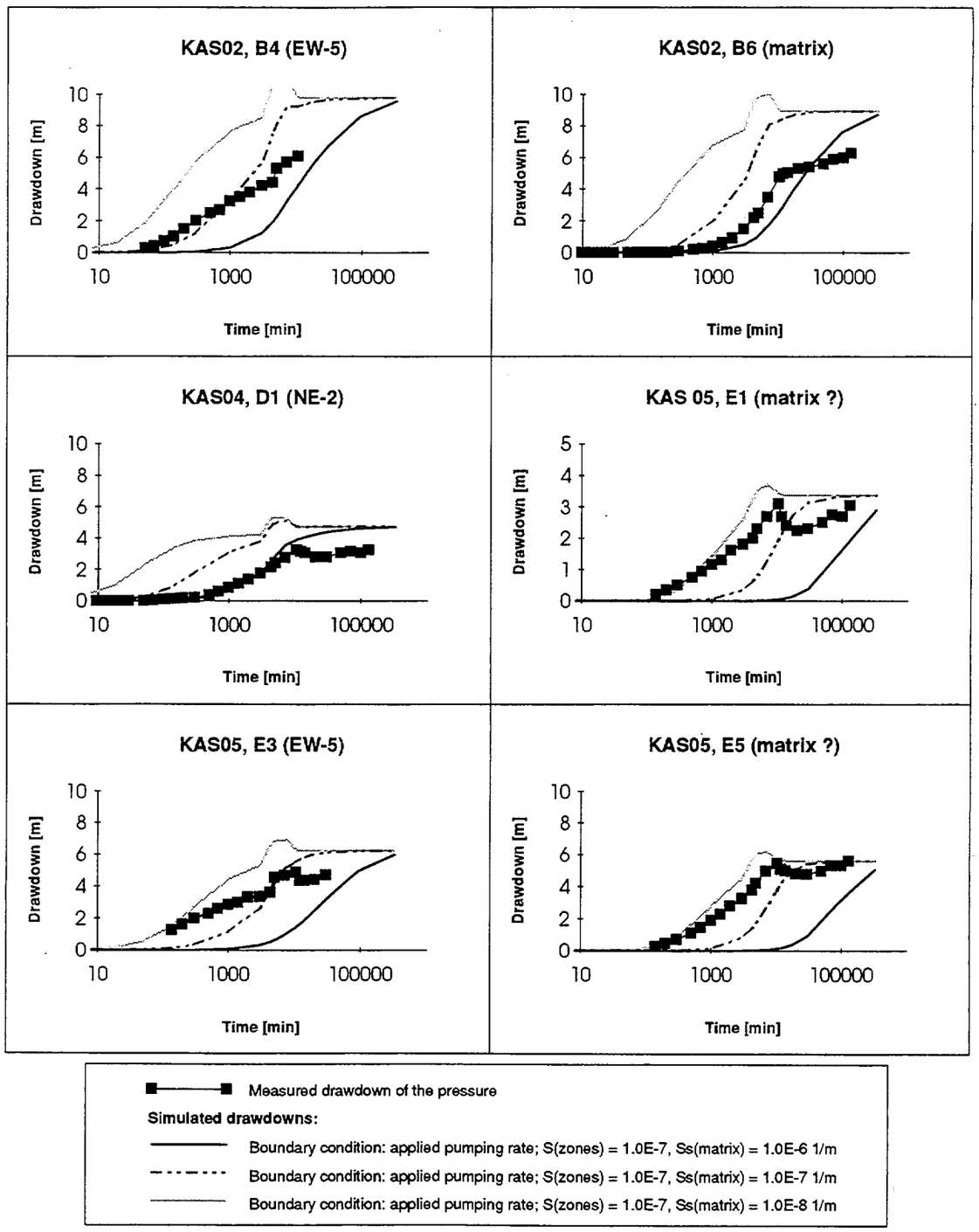

Figure 5-26. *Measured and simulated pressure drawdowns for LPT2 as a function of time in twelve observation sections. The simulated results are for the updated model after the model calibration. The measured values from Ström, 1992. *) The last value from Rhén et al., 1992. (Cont.)*

of 10^{-8} m^{-1} in several sections: KAS02-B4, KAS05-E1, KAS05-E3 and KAS05-E5. Two of these sections are interpreted to be in the rock matrix, but the fast responses suggest better connections. The simulation results for the specific storage of 10^{-7} m^{-1} are close to the experimental values in KAS07-J6, KAS08-M3 and KAS12-DC. With the largest value of the specific storage (10^{-6} m^{-1}) computed drawdowns are close to the field data in observation sections KAS02-B6, KAS04-D1, KAS07-J3 and KAS08-M4. From these four sections, two are interpreted not to intersect any of the zones. The measured values for section KAS07-J2 are considered very uncertain /Ström, 1993a/, which must be taken into account when evaluating the simulation results.

5.4.2 Sensitivity and uncertainty analysis

In the sensitivity and uncertainty analysis, the basic idea was the same as in the uncertainty and sensitivity analysis for the base model discussed in Section 4.4.2. The sensitivity of the simulation results to the hydraulic conductivities of the fracture zone and the rock matrix was analyzed. In each simulation case, the hydraulic conductivity of one zone or the rock matrix was increased or decreased one order or two orders of magnitude compared to the values of the calibrated model. Modifications of two order of magnitude in the hydraulic conductivities are in many cases too large. The uncertainties of the hydraulic conductivities are not that large. Those cases nevertheless show what happens if a unit does not exist or that its hydraulic conductivity is very large.

In each sensitivity case, a steady-state simulation was carried out for the LPT2 test. The sensitivity and uncertainty analysis comprised thus another 84 simulations. The results of the sensitivity cases were evaluated comparing simulated drawdowns in the cored boreholes with those computed for the calibrated model as well as with the experimental values.

Regarding the withdrawal hole KAS06, the flow conditions were attempted to be maintained as close to those of the calibrated model as possible. Since the effect of pumping was implemented as the drawdown measured in KAS06, the total inflow and its distribution between the zones were attempted to be kept by conditioning the transmissivity of the near field. Maintaining the inflow distribution was difficult in some cases. When the cross-zone transmissivity of a zone intersecting KAS06 was increased, the near-field transmissivity was conditioned to have the same inflow to KAS06 as for the calibrated model. However, when the cross-zone transmissivity was decreased, it was not always possible to achieve the same contribution of the inflow. In addition, modifying the transmissivity of one zone influenced the drawdown field in the other zones and, consequently, the inflow from them. For instance, when the cross-zone transmissivity of NNW-1 was increased, the drawdown field in EW-5 and the inflow from EW-5 to KAS06 changed.

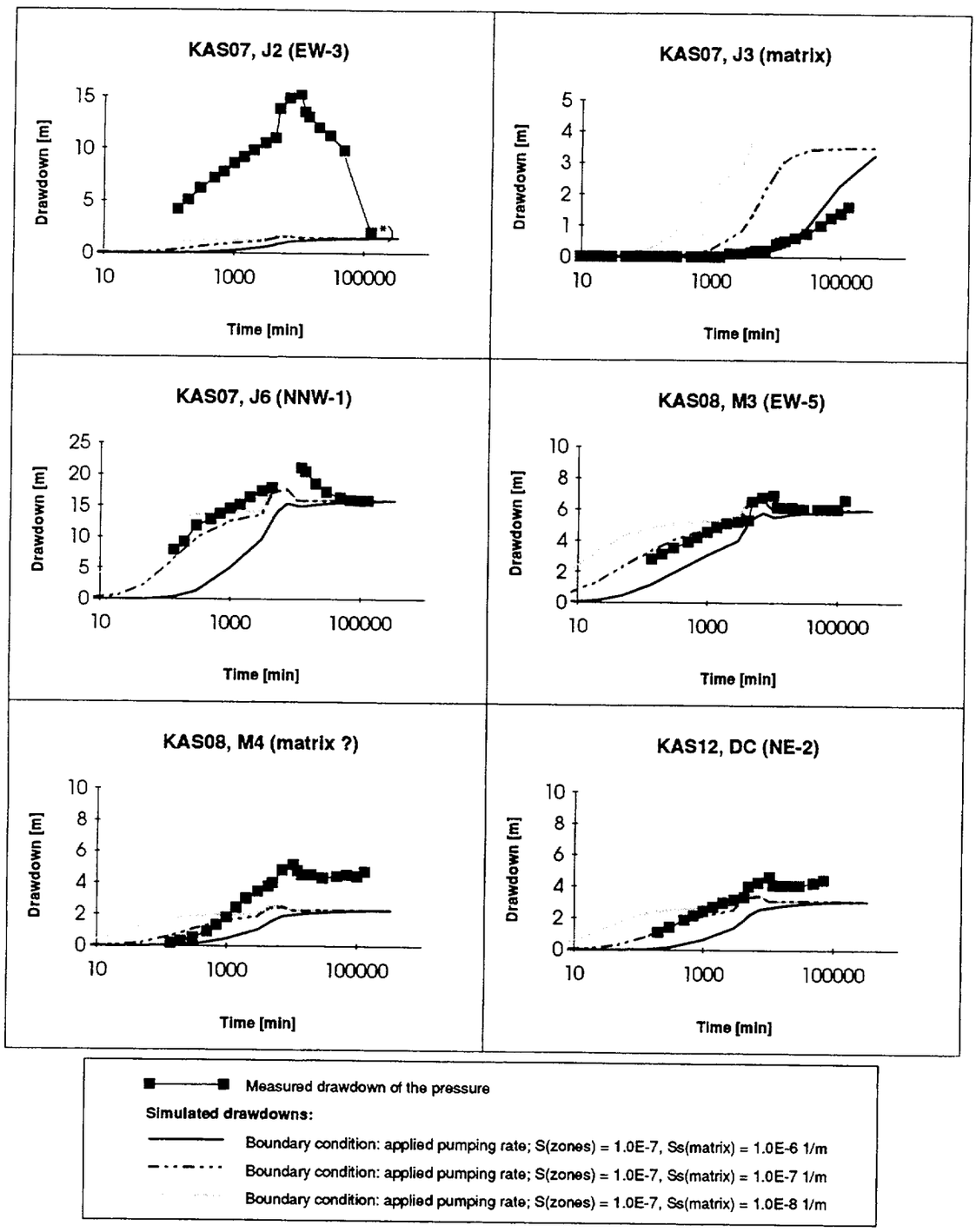

Figure 5-26. (Continued.)

The sensitivity of the drawdown to the hydraulic conductivities is summarized in Figures 5-27 and 5-28. Figure 5-27 shows the results for cases, in which the hydraulic conductivity of a unit is ten-fold compared to the calibrated value. The hydrological unit whose hydraulic conductivity was changed is presented in the first column on the left. The markers indicate in which boreholes significant differences compared to the results of the calibrated model were observed. A difference was considered significant if it was more than 30% of the result for the calibrated model. Moreover, the drawdown either for the calibrated model or the sensitivity case had to be more than 1 m. If the hydraulic conductivity were increased, the marker is a circle. The diamonds are for cases with the decreased hydraulic conductivity. If the agreement with the field data in a borehole improved, the filling of the marker is green. The red markers are for the cases in which the results of the sensitivity case were worse than those of the calibrated model. The marker was left white if there were significant changes but it could not be justified whether the agreement with the field data was better or worse.

The zones can be divided into three groups. The drawdown in several cored boreholes is sensitive to the transmissivity of the zones intersecting with KAS06. Several other zones which are close to KAS06 but do not intersect with it (EW-1B, EW-1C, NE-1A, NE-1B, NE-2, NNW-4 and NNW-5) influence the drawdown in few (1 – 4) boreholes. These zones were studied when calibrating the model. The decrease or increase of one order of magnitude in the transmissivity of the remaining zones do not influence significantly the drawdown in the cored holes. The decrease of the hydraulic conductivity of the matrix does not cause any differences. The increase of one order of magnitude in the hydraulic conductivity of the matrix impairs the drawdown only in KAS05.

The corresponding results are presented in Figure 5-28 for cases in which the cross-zone hydraulic conductivities were increased and decreased two orders of magnitude. The results in Figure 5-28 show the same characteristic of the site as Figure 5-27: Clear changes in the drawdown are obtained for several boreholes when the transmissivities of the zones intersected by KAS06 are modified. Compared to Figure 5-27, the drawdown is now influenced significantly in more holes. In addition more zones effects the drawdown at least in one cored borehole. Even a significant change of the transmissivities of the zones isolated from KAS06 by a significant zone does not cause differences in the holes. The decrease or increase of two orders of magnitude in the hydraulic conductivity of the matrix impairs the agreement with the field data.

The Figures 5-27 and 5-28 indicate that the uncertainties of the hydraulic conductivity of the rock matrix and the transmissivities of several zones located far from KAS06 are large on the basis of the LPT2 test. Similar sensitivity analyses for the other calibration cases would naturally reduce the uncertainties. When evaluating the equivalent-continuum properties, all the other field experiments have to be considered, too.

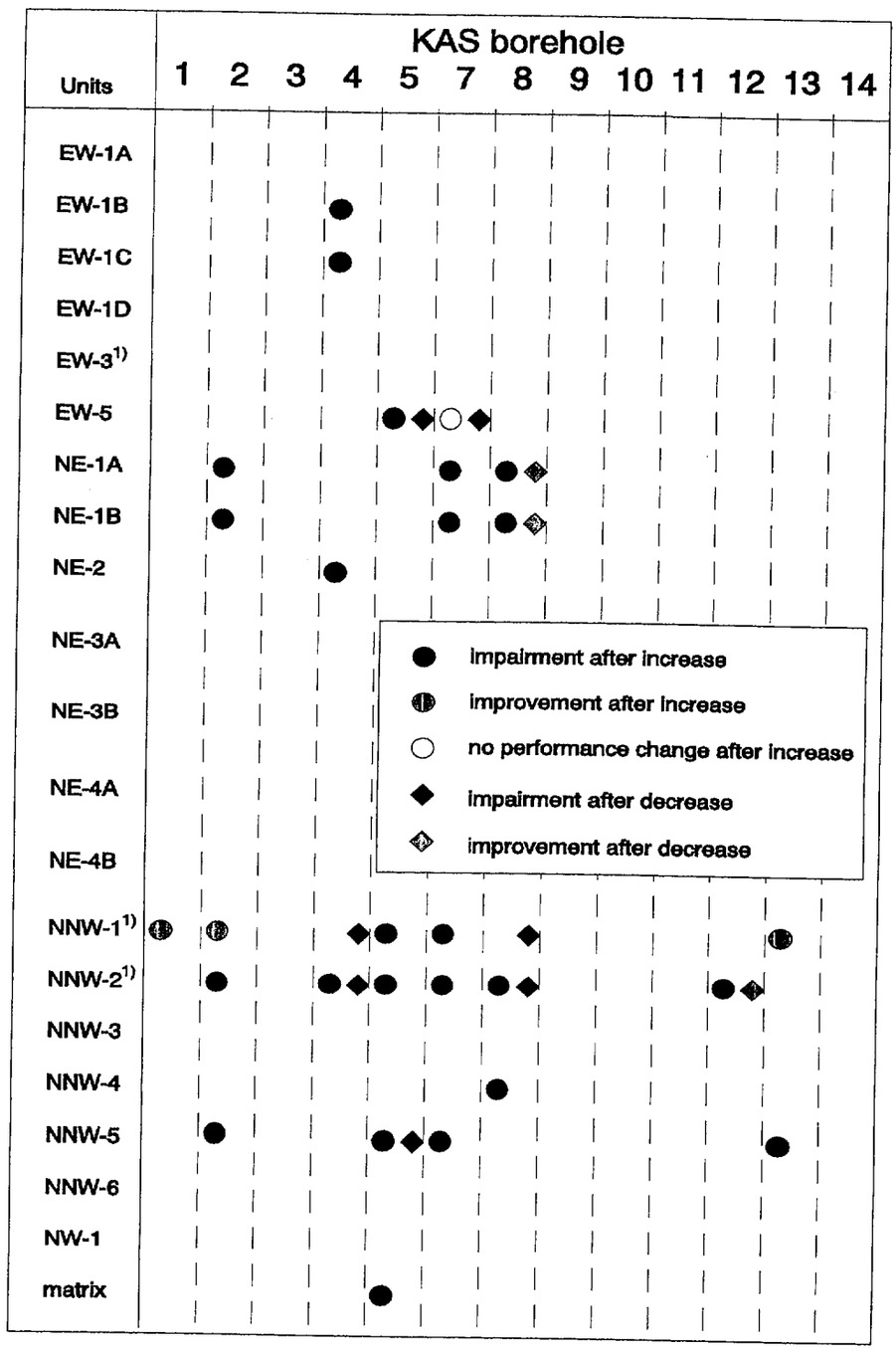

1) Decreasing the cross-zone transmissivity one order of magnitude results in an inflow distribution which is inconsistent with the field data.

Figure 5-27. *Sensitivity of the drawdown simulated for LPT2 to the hydraulic conductivities. The hydraulic conductivity of a unit was increased or decreased one order of magnitude in each case. Markers are plotted for those boreholes in which the simulated drawdown for either the calibrated model or the sensitivity case studied is more than 1 m and the drawdown of the sensitivity case differs from the calibration model result more than 30 %.*

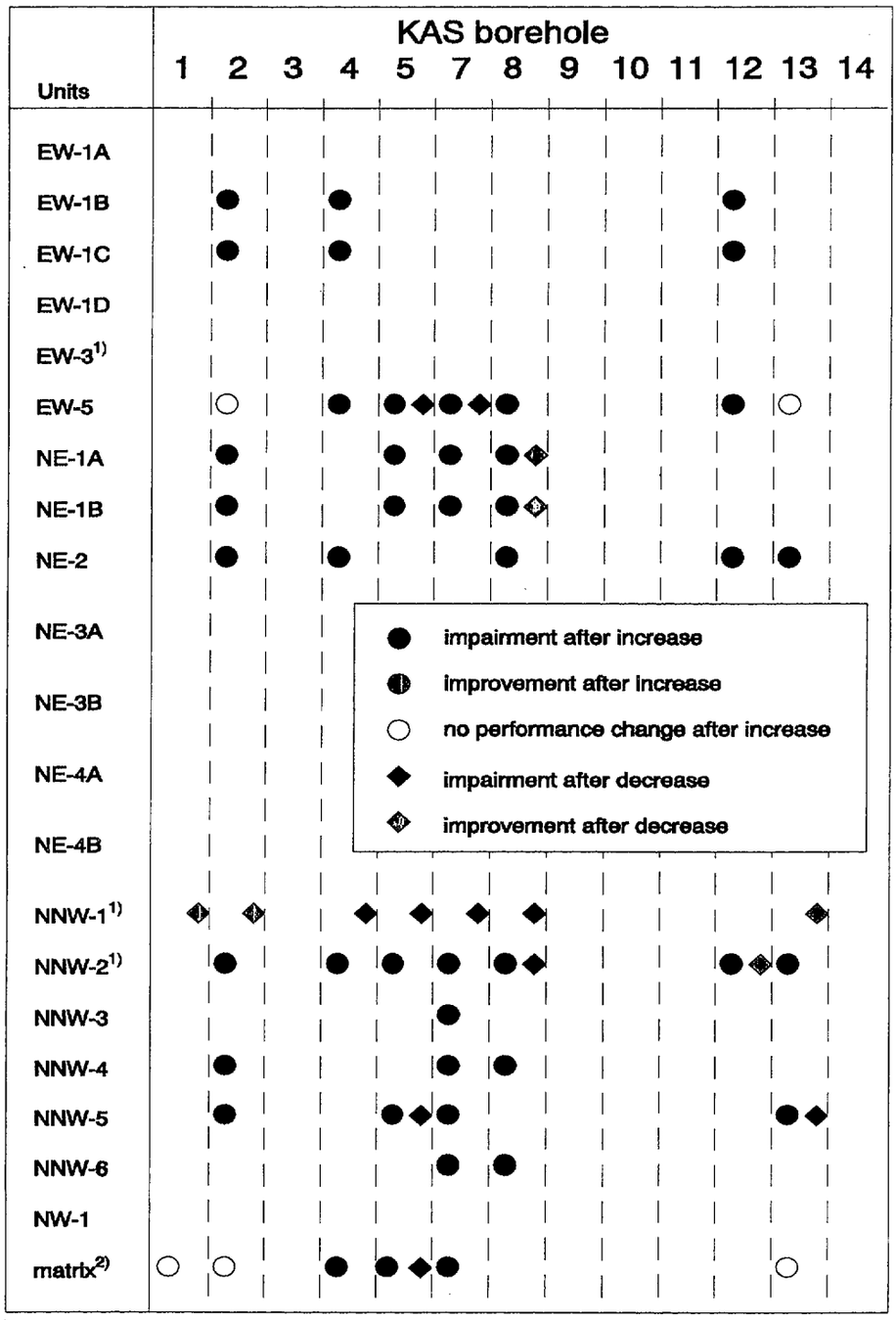

[1)] Decreasing the cross-zone transmissivity two orders of magnitude results in an inflow distribution which is inconsistent with the field data.
[2)] Inflow for the matrix too large when hydraulic conductivity increased two orders of magnitude.

Figure 5-28. *Sensitivity of the drawdown simulated for LPT2 to the hydraulic conductivities. The hydraulic conductivity of a unit was increased or decreased two orders of magnitude in each case. Markers are plotted for those boreholes in which the simulated drawdown for either the calibrated model or the sensitivity case studied is more than 1 m and the drawdown of the sensitivity case differs from the calibration model result more than 30 %.*

5.4.3 Discussion

The calibration did not improve significantly the agreement between the simulation results and the field data for LPT2. The average of the deviations in the drawdowns and the standard deviation of them are the same as for the updated model before the calibration. The largest difference was still found in the uppermost section of HAS14, where actually no drawdown was measured. On the other hand, since HAS14 is located close to KAS06 (Figure 1-1), large drawdown is anticipated in it. There are two potential reasons for this unexpected field result: either the connection between that section and KAS06 is hydraulically very poor or there exists a connection with high transmissivity from the upper part of HAS14 to the nearby sea or local water reservoir (such as a puddle). The former explanation is supported by the fact that, at the end of the pumping period of LPT1, the experimental drawdown in the upper section of borehole HAS14 was significant (0.6 m) and about one third of that in the lower section /Rhén, 1991/. To our knowledge no drawdown has been observed in the upper section of HAS14 in any other pumping test at Äspö /Rhén, 1991; Forsmark, 1992a/. If the connection between HAS14 and KAS06 has low hydraulic conductivity, the experimental drawdown in HAS14 would have increased if the experiment had continued.

In a few cored boreholes the computed drawdowns are closer to the measured values (KAS03, KAS04 and KAS07, cf. Figure 5-4). On the other hand, in some other boreholes, the agreement is poorer. Because the ten-meter drawdown in the second lowest packer section in KAS07 is very uncertain /Ström, 1993a/, it was not used in evaluating the performance of the model. The reasons for the differences between the computed and the measured drawdowns in the cored boreholes were discussed above in connection with the calibration in Section 5.3.6.

When evaluating the simulation results, the incompleteness and the simplifications in the simulation model should be considered. Instead of comparing an experimental value measured in a borehole section with a simulation result computed exactly for the same spacial location, we should compare values for hydrogeologically equivalent locations. For instance, borehole KAS12 does not have a hydraulic connection to zone NNW-2 in the model as it probably does in reality (see Sections 5.3.5 and 5.3.7). Therefore, the simulation values for the bottom part of KAS12 should be taken from NNW-2. This would increase the too low simulated drawdowns in KAS12.

The calibration phase also showed that a local but highly transmissive feature should be close to KAS13. A feature intersecting with KAS13 is missing from the model and that feature probably connects KAS01 and the top parts of KAS02, KAS05 and KAS13 with each other. Incorporating that feature into the model would reduce the drawdowns in KAS01 and in the upper parts of KAS02 and KAS13 in LPT2. This presumable feature has to be taken into account when judging the simulation results for the observation sections mentioned. A careful evaluation of the simulation

results is thus usually laborious. This means also that the automatization of the calibration process is difficult.

The calculated total inflow to KAS06 agrees with the field data. A most significant improvement of the calibrated model compared to the initial model is the better agreement between the measured and calculated inflow distributions (Table 5-3).

The amount of water flowing through the tracer injection sections was calculated on the basis of the average groundwater flux in the intersected zones (Table 5-11). The agreement with the field data is comparable with that of the other model versions. The spatially varying transmissivity of the zones would result in flow rate distributions similar to those in Figure 4-10. Therefore, assuming the same spatial transmissivity distribution that was applied in the calculations whose results are presented in Figure 4-10, the measured value is expected to deviate less than about an order of magnitude from the average-transmissivity values in Table 5-10. The other field results except that for KAS12 are inside the estimated range.

After the calibration studies, the exceptionally large flow rate through the injection section in KAS12 is more understandable. In NE-2 the flux is small but as the calibration showed, there probably exists a highly transmissive connection between KAS12 and NNW-2. The flow rate through a tracer injection section in KAS12 is thus determined by the flux in NNW-2 (or by the hydraulic connection between borehole KAS12 and zone NNW-2). The difference between the average-transmissivity flow rate in NNW-2 and the experimental value is still almost two orders of magnitudes (Table 5-11). The range of the simulated flow rate could be spread to cover the measured value by increasing the variation of the transmissivity.

In spite of the major efforts for calibrating the updated model, the calibrated model provides results for LPT2 that agree only a little better with the field data than the simulation results before the calibration or the results of the tentatively calibrated base model. The only significant improvement compared to the initial updated model is a better agreement in the inflow distribution. The calibration, however, helps us to understand better the site and to explain the reasons for the differences between simulation and field results. It is significant that the adjustment of the model to explain the field results of several other field tests did not impair the model's capability to simulate the LPT2 test. The same model can thus be applied to simulate several field tests.

The sensitivity and uncertainty analysis showed that the hydraulic conductivity of several zones and the rock matrix can vary considerably without having any significant effects on the drawdown in the other holes. On the other hand, the drawdown field is sensitive to the transmissivities of the zones which are intersected by the withdrawal hole or which are close to it.

6 DISCUSSION AND CONCLUSIONS

The groundwater flow conditions during the LPT2 pumping and tracer test performed at the Äspö site were analyzed by means of numerical simulations. Modelling of the LPT2 test forms a part of our effort of improving our understanding on the Äspö site and of developing a site-scale model to characterize the groundwater flow. All the field data available should be utilized in this process. Yet the LPT2 test provides the most valuable information owing to the completeness of its data set and the long duration of the pumping period in the experiment. The tracer experiment of LPT2 supplements the hydraulic data.

The study was carried out in the framework of the Äspö project's Task Force on the modelling of groundwater flow and solute transport. The Task Force selected the LPT2 test as the first modelling exercise and defined a set of performance measures. Consequently, the reporting of the simulation results for these performance measures was emphasized.

Several flow models have been created on the basis of the various versions of the structural model for the Äspö site. During the modelling studies, the structural model evolved. Subsequent to these updates, the corresponding changes were incorporated in the flow model, and it was not considered rational to continue flow modelling with an old version of the structural model. The preliminary modelling work, which was carried out for the base structural model, was nevertheless reported (Chapter 4). Yet this study concentrated on the updated model (Chapter 5).

The performance measures regarding LPT2 were computed for both the base and the updated structural models, before and after the calibration. Accordingly, four sets of results for the performance measures were provided (Sections 4.2.1, 4.4.1, 5.2.1 and 5.4.1).

The base and updated models were evaluated in Sections 4.2.2, 4.4.3, 5.2.2 and 5.4.3 before and after the calibration. Similarly, the calibration phases for the base and updated models were discussed in detail in Sections 4.3.3 and 5.3.7. In the following the modelling approach and stages as well as the conclusions are discussed more generally.

The modelling approach

The heterogenous character of the bedrock was considered throughout the study. The numerical simulations of the pressure drawdown were nevertheless based on the concept of an equivalent continuum, which was applied independently on each subdomain. Each identified fracture zone and the rest of the bedrock, the rock matrix, were considered separately. Several

factors supported this approach. Since we are developing a site-scale flow model, the simulation methods based on an equivalent continuum and a stochastic continuum are the most plausible alternatives. The stochastic approach involves two major problems: the large number of realizations requires considerable computing resources, and there is no widely-studied method for calibrating a stochastic model in the field of groundwater flow modelling. Moreover, as several pumping tests were applied in the calibration, fast computation of the drawdown field is essential. On the other hand, the drawdown of the pressure is one of the performance measures. A separate study concerning two-dimensional flow (Appendix C) showed that as long as the distance between the point of interest and a withdrawal hole is several times longer than the scale of heterogeneity, the equivalent-continuum approximation is satisfactory for the drawdown. Accordingly, when applying the equivalent-continuum approach, we have to assume only that the scale of heterogeneity is small compared to the distances between the boreholes. On the contrary, in the stochastic-continuum approach, results depend (if depend) on the scale of the heterogeneity and therefore it has to be determined exactly. The parameters needed can seldom be derived from field data.

The local transmissivity around a withdrawal hole naturally influences water inflow to it. Independently of the approach adopted, the local transmissivity has to be conditioned against the field data. In this study, the zones were conceptually divided into two parts (see Figure 5-17): the near-field part of a zone and the rest of it characterized by the average cross-zone transmissivity. The transmissivity of the near-field around a pumping hole can differ significantly from the overall cross-zone transmissivity. In adjusting the model parameters, these two conceptual parts of the zones were considered almost independently.

On the other hand, when calculating the groundwater flux at a certain point in the bedrock, e.g., the amount of groundwater flowing through a tracer injection section, the heterogeneity of the bedrock should be handled explicitly. Numerical simulations can be restricted to a small volume and the boundary conditions can be taken from a solution of a site-scale model. Stochastic simulations can be employed to calculate the distribution of the local groundwater flux. The results are determined by parameters describing, among others, the spatial variation of the transmissivity of a zone. Unfortunately, these parameters are also very poorly known. Assessing the simulation results against the field data is also difficult because of their statistical nature and due to the scarcity of the experimental values.

When simulating the pumping tests, only the influence of pumping on the pressure field was simulated, i.e., the pressure drawdown field was computed. This approach assumes that the infiltration rate does not change due to the pumping. Some increase of the infiltration rate could be expected because of the lowering of the water table. During the field experiment the infiltration rate varied also because of the fluctuations in the rainfall and these changes can be expected to be even larger than the influence of the modified water table.

Initially no-flow boundary conditions were assigned for the island area and fixed-pressure boundary conditions for the other boundary nodes. The validity of the boundary conditions was examined by changing them to no-flow boundary conditions over the vertical bounding faces and the bottom of the model. The changes in the drawdown were noticeable only in the deepest boreholes and they were small compared to the influences of the other parameters. The type of the boundary conditions on those faces is thus not important because of the large size of the model. During a pumping test, water flows to a withdrawal borehole from the sea surrounding the island through the fracture zone network. If the model had been deeper, the influence of the boundary conditions would have been even smaller.

The influence of the salinity on the drawdown of the pressure can be ignored. The numerical simulations showed that in the deepest boreholes (KAS02 and KAS03), the salinity changed the drawdown only about 5%.

The consideration of six pumping tests performed in different boreholes and several structural models for each was only made possible by the employment of our fast and largely automatized software system for creating complex, test-specific finite element meshes. This approach also facilitated exploring investigations in which the influences of additional features included in the simulation model were examined.

Calibration of the flow models

The calibration of the flow models was a major task. For the base model only tentative calibration was performed using solely the two long-term pumping tests, LPT1 and LPT2. The transmissivities of few zones were modified to improve the agreement with the field data. The transmissivities of the zones were assumed to be constant (i.e., no conditioning was applied).

In calibrating the updated model, besides the LPT1 and LPT2 tests, the pumping tests performed in KAS12, KAS13, KAS14 and KAS16 were utilized as well. The average cross-zone transmissivities and local transmissivities around the pumped holes were adjusted quite independently. The extent of the most conductive parts of two zones (EW-5 and NE-1) was reduced. The average transmissivities were not modified significantly (except in the case of zone EW-3). However, the near-field transmissivities were conditioned up to two orders of magnitude compared with the calibrated cross-zone transmissivities.

Regarding the discrepancies between the field data and the simulation results, several other possible explanations were studied as well. Additional zones, various orientations of the present zones, highly-conductive surface layer and low-conductive sea bottom were examined.

The boundary conditions of the simulation models for the pumping tests were also modified when calibrating the updated model. Since the

simulations in the calibration stage were carried out assuming steady states, some drawdowns were also obtained for the northern part of the island. The durations of the pumping periods were finite in the field experiment and, on the other hand, the amount of water in the upper part of the bedrock and in the soil in the area located to the north from EW-1 is large. All this suggests that any drawdown of the water table in the northern part of the island cannot be expected. Therefore, in order to make simulations for the pseudo-steady states more comparable to the field experiments, the boundary conditions for the northern part of the Äspö island were changed from no-flow to fixed-pressure boundary conditions.

The simulation of the hydraulically undisturbed conditions as a part of model calibration may not be worthwhile if large variations in the salinity exist at a site. In this case, the pressure field would mainly be defined by the density and, consequently, by the salinity field. Thus, the simulation results would depend on the assumed salinity distribution. As estimating the salinity field is difficult, the salinity and the pressure are often determined by solving coupled partial differential equations for water flow and salt transport. The advantage of this approach is that both the calculated pressure and the salt concentration can be compared with the experimental data. On the other hand, there are several drawbacks as well. The simulation of salt transport in the heterogenous bedrock involves simplifications whose significance is difficult to evaluate. Boundary conditions are poorly known, and they have to be selected to obtain results consistent with the measured values. In fact, the boundary conditions have to be adjusted to give results consistent with the field data. Moreover, the concept of steady-state conditions may not be valid for the salinity field (due to the land uplift, for instance). In transient simulations, the initial conditions are needed as well. The measured salt concentrations contain significant uncertainties and the representativeness of the water samples should be assessed. The measured pressure values are more reliable but they mainly reflect the salinity field. As a result, the simulations for the hydraulically undisturbed conditions could not be used to adjust the parameters of the Äspö model. The simulation of the undisturbed conditions was nevertheless necessary for calculating the flow rate through the tracer injection sections.

Although the calibration stage was laborious, it was fruitful. Besides the calibrated model, the calibration process provided a lot of information on the site. The calibrated model was applied to simulate five of the six pumping tests studied successfully.

Field data

The data set for the Äspö site is large, detailed and of high quality. There are still some uncertainties in the field data that cause problems in the calibration stage. Many uncertainties arise from practical limitations.

First, steady flow conditions were not reached in the pumping tests. Even in the long-term pumping tests, LPT1 and LPT2, with 50 and 70 day pumping

periods, the drawdown was still increasing in several sections when the pumping was stopped. A pseudo-steady state was assumed to have been reached and the results of steady-state simulations were compared to the drawdowns measured at the end of the pumping periods. As discussed above, the boundary conditions were also modified to be more consistent with the experimental conditions. The influence of this steady-state assumption had some effects only in few observation sections. One of them might be the upper section of HAS14, in which the deviation between the simulated and the measured drawdowns is the largest. If the pumping had continued in the field experiment, the drawdown in HAS14 might have increased.

Concerning the other pumping tests with three-day pumping periods, the drawdowns were notably increasing when the pumping was stopped, in some tests even in the withdrawal hole. In these cases we had to estimate the drawdowns that would have been obtained if the pumping had continued for very long period. The obtained values naturally include significant uncertainties, but for the observation sections with significant drawdowns these uncertainties do not prevent the comparison of the interpreted field data with the simulation results.

Secondly, the drawdown in the second lowest packed-off section of KAS07 varied strongly during LPT2 (Figure 5-26). The estimated final drawdown (10 m) is thus considered very uncertain /Ström, 1993a/ and it was not used in evaluating the performance of the model.

Thirdly, the distribution of the water inflow to the withdrawal holes is known reliably only for KAS06. The field measurements on the inflow distribution did not cover the first 100 m from the top of the boreholes. As the inflows to the upper parts are not known, we know the contribution of each zone only relative to the total inflow of that part of a hole which was covered by the inflow measurement. Utilizing the results of the spinner surveys for several boreholes, the amounts of the inflow to the upper parts and, consequently, the inflow contributions for the intersecting zones were estimated quantitatively (except in the case of KAS16 where a flow meter was used). The obtained values naturally include significant uncertainties.

On the other hand, even for LPT2, the inflow from EW-3 is uncertain. The inflow to the top part of KAS06 was estimated from the tracer data /Rhén et al., 1992/. As EW-3 is the only zone interpreted to intersect with the first 100 m of the borehole, the inflow to the top part was assumed to have come from EW-3. Of course the inflow to the top part of KAS06 could come from another unidentified (local) zone or from the permeable surface layer of the bedrock.

Simulation of the LPT2 pumping test

It is characteristic to both structural models considered that the simulation results for the LPT2 test are close to the field data. The agreement in the

drawdown is good even before any calibration. The differences can mainly be explained on the basis of the simplifications inherent in the models. The calculated total inflows to the withdrawal hole are close to the pumping rate applied, but the distributions of the inflow differ from the experimental results. The calibration studies improved the models' performance. Especially the simulated inflow distributions became closer to that measured. On the other hand, although the calibration improved the agreement between simulation results and the field data, some differences remained.

The agreement between the simulation results and the experimental data was the poorest for the amount of groundwater flowing through the tracer injection sections. The flow rate through the tracer injection sections is mainly governed by the local transmissivity, and it is obvious that the average groundwater fluxes calculated on the basis of the cross-zone transmissivities do not coincide with the experimental values. Employing stochastic simulations, flow rate distributions that cover most of the field values could easily be obtained. As the input parameters can be selected quite freely, the validity of these simulations is difficult to evaluate. The very high experimental flow rate through an injection section in KAS12 is remarkable. The measured value is over 100 ml/min. The average flux in NE-2 would result in only 0.5 ml/min. As the calibration studies showed that KAS12 is in some ways connected to NNW-2, an order of magnitude increase in the calculated flow rate was obtained. The difference between the average flux and the measured value is still almost two orders of magnitude. With the parameters used in the stochastic simulations in Section 4.2.1, that large deviation is unlikely.

Sensitivity studies for the simulation of LPT2 were carried out. Modifying the transmissivity of one zone in each simulation case, the sensitivity of the drawdowns to the transmissivities was studied. The transmissivity values were increased and decreased one order and two orders of magnitude. In other cases, the hydraulic conductivity of the rock matrix was varied. The simulation results are naturally sensitive to the transmissivity of the zones intersected by KAS06. If the inflow contributions of the various zones had been interpreted correctly, a significant decrease in the transmissivity of the intersecting zones is not plausible. In principle, the transmissivity of an intersecting zone could, however, be significantly higher if the near-field part of the zone around KAS06 is less conductive than the zone in average. On the basis of the numerical simulation, the average transmissivity of many zones located far from KAS06 could also be significantly higher or lower. On the other hand, the zones intersected by KAS06 cannot possess significantly lower transmissivity because of the inflow distribution. Increasing their transmissivities would make the agreement between the simulated and measured drawdowns worse in several boreholes. Zone EW-3 is an exception because increasing or decreasing its transmissivity does not affect the drawdowns in the observation holes. The third set of the zones comprises the zones that are not intersected by KAS06 but are located close to KAS06. Modifying their transmissivities in general worsens the agreement of simulated drawdowns with experimental ones. The sensitivity

studies proved to be instructive, and they should actually have been performed for all of the calibration cases.

The flow models

The simulations for the LPT2 test and especially the calibration phase as well as the sensitivity and uncertainty studies helped us to understand better the flow system at the Äspö site. A surprising observation was that the initial (updated) model was simulating well the drawdowns only for LPT1 and LPT2. The initial simulation results for the pumping tests in KAS12, KAS13 and KAS16 differ significantly from the field data.

In order to improve the simulation results for the pumping test in KAS12, a hydraulic connection between KAS12 and NNW-2 was proposed. This hypothesis is supported by the results for LPT2 as well, because the flow rate through the injection section in KAS12 was measured to be very high during LPT2. KAS12 is interpreted to intersect only NE-2 but so high flow rate in NE-2 would be difficult to explain or the re-evaluation of the characteristics of NE-2 is needed.

The analysis of the field data for the pumping test in KAS13 led to the conclusion that there must be an unidentified feature intersecting KAS13. It could be a single fracture or a subzone of NNW-1 or NNW-5, but more probably it is a local zone missing from the structural model. The transmissivity of the zone should be high (10^{-5} – 10^{-4} m^2/s). If the zone were east-west orientated, it would help to explain the experimental drawdown data for most of the pumping tests studied.

The results of the pumping tests in KAS14 and especially in KAS16 were much more difficult to explain. These boreholes are intersecting NE-1 and the maximum drawdowns in the withdrawal holes were only 16 and 30 m, respectively. Yet the measured drawdowns in the observation holes even far from the pumped holes were large. It is probable that the transmissivity of NE-1 is high for a large area near the intersection point with KAS16. The dimensions of the most conductive part could be 100 - 300 m. The highly conductive part would transfer a large drawdown far from the pumped hole. Outside this area, the transmissivity of NE-1 is lower limiting the inflow to the withdrawal hole.

Similarly, the field data for the pumping tests in KAS14 and KAS16 suggest that the transmissivity of EW-5 should be high for at least a restricted part around KAS06 (Figure 5-21). The transmissivity of EW-5 seems to be large especially around KAS16.

The LPT1 and LPT2 as well as the pumping tests in KAS12 and KAS16 indicate that the extent of NNW-1 and NNW-2 should be smaller especially in the vertical direction. There is likely a highly conductive part in NNW-1 around the intersection point with KAS07. The simulated drawdown in KAS06 is not as high as measured (Figures. 4-11 and 5-11), for what a

probable explanation could be some anisotropy in NNW-1. The northern part of NNW-1 is also likely highly conductive as indicated by the large drawdowns measured in KAS04. The field data show that the transmissivity of NNW-2 is highest in its southern part.

Large uncertainties are associated with EW-3. According to the experimental results of LPT2, EW-3 could be acting as a significant hydraulical connection from KAS06 to the second lowest packed-off interval of KAS07. This connection, on the other hand, should be considered with care because in LPT1 (pumping in KAS07) it does not transfer large enough pressure response to the upper part of KAS06. This can also be because of anisotropy, boundary conditions or the extent of the EW-3 zone. On the other hand, the ten-meter drawdown in the second lowest packer section in KAS07 during LPT2 is very uncertain /Ström, 1993a/. Furthermore, the adjusted magnitude of the cross-zone transmissivity of EW-3 is based on the inflow contribution to the upper part of KAS06, to where the water can as well flow from other local features, or the transmissivity of EW-3 can be large only locally.

Regarding the differences between the base and the updated structural models, the updated model was slightly more detailed than the base model. As the strikes of the zones were given in numerical form, the construction of the corresponding flow model was more accurate. Most of the modifications in the structural model did not influence the simulation results for LPT1 and LPT2. Only the southern subzones of EW-1 affected the drawdown in KAS04 and worsened the agreement with the field data. Reducing the transmissivities of the southern subzones improved the model's performance.

Our study showed that as far as groundwater flow is considered, the base as well as updated structural models for the Äspö site are largely plausible. The same flow model can be applied to simulate several pumping tests. Yet some local modifications, such as a feature intersected by KAS13 at a depth of about 200 m and a hydraulic connection between KAS12 and NNW-2, should be incorporated. As long as they are not included in a model explicitly, their likely existence should be taken into account when interpreting field results. The spatial variation of the transmissivity of NE-1 and EW-5 on a large scale should be studied further.

REFERENCES

Bear J, 1979. Hydraulics of Groundwater. McGraw-Hill Inc., Israel.

CRC, 1971. Handbook of Chemistry and Physics. The Chemical Rubber Co, Ohio.

Carlsson L, Grundfelt B, Winberg A, 1987. Hydraulic modelling of the final repository for reactor waste (SFR) – Evaluation of the groundwater modelling of groundwater flow situation at SFR. Stockholm, SKB - PR SFR 86-07.

Forsmark T, 1992. SKB - Äspö Hard Rock Laboratory. General information and information for numerical modelling. Calibration cases for LPT2 and tests in KA1061A and KA1131B.

Forsmark T, 1992a. Hydraulic tests at Äspö in KAS16. Evaluation. SKB PR 25-92-15.

Grundfelt B, Lindbom B, Liedholm M, Rhén I, 1990. Predictive Groundwater Flow Modelling of a Long Time Pumping Test (LPT1) at Äspö. SKB PR 25-90-04.

Hautojärvi A, 1994. Data analysis and modelling of the LPT2 pumping and tracer transport test at Äspö - Tracer experiment. Espoo 1994. SKB - ICR report (in print).

Herbert A W, Gale J E, 1989. Fracture flow modeling of the site characterization and validation area in the Stripa mine. NEA/SKB Intern. Symp. on the Stripa Project. Stocholm, Sweden.

HYDROCOIN, 1988. The international HYDROCOIN project - Level 1: Code verification. Paris, Organization for Economic Co-operation and Development (OECD).

HYDROCOIN, 1990. The international HYDROCOIN project - Level 2: Code validation. Paris, Organization for Economic Co-operation and Development (OECD).

HYDROCOIN, 1991. The international HYDROCOIN project - Level 3: Sensitivity and uncertainty analysis. Paris, Organization for Economic Co-operation and Development (OECD).

HYDROCOIN, 1992. The international HYDROCOIN project - Summary report. Paris, Organization for Economic Co-operation and Development (OECD).

Liedholm M, 1987. Regional Well Water Chemistry. SKB PR 25-87-08.

Neretnieks I, Abelin H, Birgersson L, 1987. Some recent observations of channeling in fractured rock - Its potential impact on radionuclide migration. In: Buxton, B.E. (ed.) Proc. DOE/AECL Conf. on Geostatistical, Sensitivity, and Uncertainty methods for Groundwater flow and Radionuclide Transport Modeling, 387-410. Battelle Press, San Francisco.

Neuman S P, 1988. A proposed conceptual framework and methodlogy for investigating flow and transport in Swedish crystalline rock. SKB AR 88-37. Stockholm, Sweden.

Nilsson L, 1990. Hydraulic tests at Äspö, KAS05–KAS08, HAS13–HAS17. Evaluation. SKB PR 25-92-20.

PATRAN, 1989. PATRAN Plus user manual. Release 2.4. Costa Mesa, PDA Engineering.

Rhén I (ed), 1991. Information for Numerical Modeling 1990. Calibration cases. SKB PR 25-90-17b.

Rhén I, 1992. Personal communication 27.8.1992.

Rhén I, Forsmark T, 1993. Information for numerical modelling, undisturbed pietzometric levels and uncertainty of piezometric levels, Äspö Hard Rock Laboratory, Technical note 25–92–63G.

Rhén I, Forsmark T, Nilsson L, 1991. Hydraulic tests on Äspö, Bockholmen and Laxemar 1990 in KAS09, KAS11–14, HAS18–20, KBH01–02 and KLX01. Evaluation. SKB PR 25-91-01.

Rhén I (ed), Svensson U (ed), Andersson J-E, Andersson P, Eriksson C-O, Gustafsson E, Ittner T, Nordquist R, 1992. Äspö Hard Rock Laboratory. Evaluation of the combined longterm pumping and tracer test (LPT2) in borehole KAS06. SKB TR 92-32.

SKB, 1992. Treatment and final disposal of nuclear waste - Äspö Hard Rock Laboratory. Background report to RD&D-Programme 92. SKB, 1992.

Ström A, 1992. Äspö Hard Rock Laboratory, Task Force on modelling of groundwater flow and transport of solutes, Data delivery No. 1 for Task No. 1: Data for Task No 1. Memorandum 6.10.1992.

Ström A, 1992a. Äspö Hard Rock Laboratory, Task Force on modelling of groundwater flow and transport of solutes, Data delivery No. 3 for Task No. 1: Additional data for Task No 1. Memorandum 22.12.1992.

Ström A, 1993. Äspö Hard Rock Laboratory, Task Force on modelling of groundwater flow and transport of solutes, Data delivery No. 4 for Task No. 1: Geometric data for hydraulically interpreted fracture zones at Äspö. Memorandum 15.2.1993.

Ström A, 1993a. Äspö Hard Rock Laboratory, Task Force on modelling of groundwater flow and transport of solutes, Data delivery No. 5 for Task No. 1: Complementary information regarding the LPT2 experiment. Memorandum 11.6.1993.

Wikberg P (ed), Gustafson G, Rhén I, Stanfors R, 1991. Äspö Hard Rock Laboratory. Evaluation and conceptual modelling based on the pre-investigations 1986–1990. SKB TR 91–22.

SPECIFICATION OF THE FEFLOW CODE

Version 1.11

The FEFLOW code package developed at VTT comprises several codes to solve partial differential equations and to calculate derived quantities.

General description: FEFLOW is capable of modelling fluid flow, heat transfer and solute transport in non-coupled or coupled situations. Steady-state and transient three-dimensional problems can be simulated. The code can be used in deterministic and stochastic modes. Although FEFLOW is especially designed for modelling groundwater flow, it can be applied in other disciplines too.

Conceptual model: FEFLOW can be applied to systems which can be divided into one-, two- and/or three-dimensional sub-systems and each sub-system can be represented by a continuum.

Mathematical model: The mathematical model consists of the partial differential equations for the hydraulic head/pressure, temperature and solute concentration. Fluid flow covered by Darcy's law is considered. The equations can also be coupled by means of the Darcy velocity as well as the temperature and concentration dependent properties such as the density.

Numerical method: FEFLOW is based on the finite element method. It uses linear one-, two- and three-dimensional elements. A frontal or iterative solver is employed to solve matrix equations. In coupled cases, a set of nonlinear algebraic equations is solved applying an iterative approach with options for relaxation. The time discretization is based on the finite difference approximation.

Limitations: only saturated flow, no matrix diffusion (included in version 1.12), linear elements.

Parameter requirements depend on the type of the problem to be solved. The properties include permeability, specific storage, fluid density and viscosity, porosity, dispersion lengths, molecular diffusivity, specific heats, thermal conductivity. Permeability may be constant, vary exponentially or logarithmically as a function of depth, or follow a lognormal distribution. Boundary conditions available for each quantity to be determined are prescribed values, sources, sinks and/or fluxes.

Type of results: The hydraulic head, pressure, concentration or/and temperature fields, fluid/mass/temperature flow rates and fluxes, Darcy velocities, pathlines.

Computer requirements: Computer memory requirements depend on the size of an element mesh but often about 100 Mbyte is needed (of which part can be virtual).

User interface: The FEFLOW code comprises several programs to calculate derived parameters as well as to facilitate modelling work and the analyses of results. The FEFLOW code itself does not include any graphical user interface but efficient interfaces with a commercial pre- and postprocessing package PATRAN (PATRAN 2.5, User's Guide, PDA Engineering 1988) have been developed. In addition, a set of

advanced routines (the HERO package) is employed to improve the element creation process with PATRAN.

Code availability: Contact Seppo Vuori, VTT Energy, Nuclear Energy, P.O.Box 1604, FIN-02044 VTT, Finland, Tel. +358 0 456 5067.

References:

Technical description

(1) Löfman, J. & Taivassalo, V. FEFLOW 1.10 - Solving of Coupled Equation for Flow, Heat Transfer and Solute Transport. Nuclear Waste Commission of Finnish Power Companies YJT-93-30 (in Finnish).

(2) Laitinen, M. Application of improved Galerkin methods on convective diffusion problems. Masters Thesis, Helsinki University of Technology, 1994 (in Finnish).

(3) Löfman, J. & Taivassalo, V., FEFLOW 1.10 - Programs PH1, PH2 and PH3 - User's Guide. Technical Research Centre of Finland, Nuclear Engineering Laboratory, Technical Report TOKA-12/93.

(4) Taivassalo V., Koskinen, L. & Mészáros, F. Further development of the FEFLOW code for transient simulations. Teollisuuden Voima Oy, TVO/Safety and Technology, Work Report 91-14 (in Finnish).

(5) Meling, K. et al. Groundwater simulation codes at VTT's Nuclear Engineering Laboratory. Technical Research Centre of Finland, Nuclear Engineering Laboratory, Technical Report TOKA-11/93 (mainly in Finnish).

(6) Meling, K. Computation of pathlines with the FEFLOW code. Technical Research Centre of Finland, Nuclear Engineering Laboratory, Technical Report TOKA-13/93.

(7) Taivassalo V., Koskinen, L. & Mészáros, F. Further development of the flow rate calculation algorithm. Teollisuuden Voima Oy, TVO/Safety and Technology, Work Report 91-09 (in Finnish).

Verification

References 1, 2, 4, 6 and 7 for the technical description include also verification studies. In addition, FEFLOW was tested in the international HYDROCOIN project.

Application

(8) Taivassalo, V. & Saarenheimo, A., Groundwater flow analysis for the VLJ repository. Nuclear Waste Commission of Finnish Power Companies YJT-91-10 (in Finnish).

(9) Vieno, T. et al., TVO-92 safety analysis of spent fuel disposal. Nuclear Waste Commission of Finnish Power Companies YJT-92-33E.

(10) Taivassalo, V, Koskinen, L. & Meling, K. Groundwater flow modelling in the preliminary site investigations - Modelling strategy and computer codes. Nuclear Waste Commission of Finnish Power Companies YJT-94-04.

(11) Taivassalo, V. & Mészaros, F. Simulation of groundwater flow of the Kivetty area: (1) Flow model and finite element meshes, (2) Calibration of the flow model; (3) Results. Nuclear Waste Commission of Finnish Power Companies YJT-94-03.

STEADY-STATE PRESSURE DRAWDOWNS IN THE OBSERVATION SECTIONS FOR LPT2 COMPUTED WITH THE BASE MODEL BEFORE AND AFTER CALIBRATION

				INITIAL BASE MODEL			CALIBRATED BASE MODEL		
Section name		Distance	P_Measured	P_Calculated	Error	Relative	P_Calculated	Error	Relative
		(m)	(m)	(m)	(m)	error	(m)	(m)	error
KAS01	A1	223	6.2	8.60	-2.40	0.39	6.14	0.06	0.01
KAS02	B6	222	6.3	8.33	-2.03	0.32	5.82	0.48	0.08
KAS02	B5	114	5.79	8.89	-3.10	0.54	7.03	-1.24	0.21
KAS02	B4	131	6.3	7.35	-1.05	0.17	6.35	-0.05	0.01
KAS02	B3	338	5.4	7.15	-1.75	0.32	6.38	-0.98	0.18
KAS02	B2	548	2.41	1.46	0.95	0.39	1.32	1.09	0.45
KAS02	B1	645	2.3	1.21	1.09	0.47	1.11	1.19	0.52
KAS03	C6	710	0	0.23	-0.23		0.17	-0.17	
KAS03	C5	698	0	0.24	-0.24		0.18	-0.18	
KAS03	C4	711	0.55	0.33	0.22	0.40	0.25	0.30	0.55
KAS03	C3	751	0.8	0.40	0.40	0.50	0.31	0.49	0.61
KAS03	C2	806	0.83	0.72	0.11	0.13	0.54	0.29	0.35
KAS03	C1	948	0.82	1.13	-0.31	0.38	0.87	-0.05	0.06
KAS04	D6	479	0	0.32	-0.32		0.23	-0.23	
KAS04	D5	397	3.27	5.51	-2.24	0.69	2.72	0.55	0.17
KAS04	D4	362	3.11	5.79	-2.68	0.86	2.94	0.17	0.05
KAS04	D3	327	3.42	5.96	-2.54	0.74	3.11	0.31	0.09
KAS04	D2	301	3.58	5.93	-2.35	0.66	3.21	0.37	0.10
KAS04	D1	277	3.33	5.78	-2.45	0.74	3.48	-0.15	0.05
KAS05	E5	223	5.58	5.40	0.18	0.03	4.12	1.46	0.26
KAS05	E4	133	4.97	4.65	0.32	0.06	4.33	0.64	0.13
KAS05	E3	156	5.45	3.79	1.66	0.30	3.49	1.96	0.36
KAS05	E2	195	3.3	3.50	-0.20	0.06	3.27	0.03	0.01
KAS05	E1	264	3.06	2.59	0.47	0.15	2.48	0.58	0.19
KAS07	J6	208	15.64	11.91	3.73	0.24	8.59	7.05	0.45
KAS07	J5	137	16.53	13.51	3.02	0.18	12.02	4.51	0.27
KAS07	J4	112	5.61	3.72	1.89	0.34	3.96	1.65	0.29
KAS07	J3	165	1.69	1.40	0.29	0.17	1.73	-0.04	0.02
KAS07	J2	253	10	1) 1.02			1.23		
KAS07	J1	343	2.54	0.68	1.86	0.73	0.79	1.75	0.69
KAS08	M4	290	4.73	5.63	-0.90	0.19	2.98	1.75	0.37
KAS08	M3	200	6.58	5.77	0.81	0.12	4.10	2.48	0.38
KAS08	M2	97	4.7	6.92	-2.22	0.47	6.94	-2.24	0.48
KAS08	M1	226	3.74	1.53	2.21	0.59	2.27	1.47	0.39
KAS09	AE	392	0.25	0.27	-0.02	0.08	0.35	-0.10	0.40
KAS09	AD	396	0.38	0.22	0.16	0.42	0.31	0.07	0.18
KAS09	AC	411	0.45	0.25	0.20	0.44	0.29	0.16	0.36
KAS09	AB	431	0.44	0.26	0.18	0.41	0.30	0.14	0.32
KAS09	AA	484	0.25	0.24	0.01	0.04	0.27	-0.02	0.08
KAS10	BA	365	0.63	0.24	0.39	0.62	0.33	0.30	0.48
KAS11	CF	375	0.49	0.34	0.15	0.31	0.41	0.08	0.16
KAS11	CE	356	0.57	0.41	0.16	0.28	0.50	0.07	0.12
KAS11	CD	338	0.58	0.50	0.08	0.14	0.65	-0.07	0.12
KAS11	CC	318	0.69	0.56	0.13	0.19	0.71	-0.02	0.03
KAS11	CB	306	0.9	0.59	0.31	0.34	0.75	0.15	0.17
KAS11	CA	295	0.55	0.60	-0.05	0.09	0.79	-0.24	0.44
KAS12	DE	400	3.54	4.21	-0.67	0.19	2.69	0.85	0.24
KAS12	DD	314	3	4.90	-1.90	0.63	3.04	-0.04	0.01
KAS12	DC	265	4.2	5.51	-1.31	0.31	3.53	0.67	0.16
KAS12	DB	247	5.87	6.89	-1.02	0.17	4.92	0.95	0.16

1) The uncertain measured value not used in the comparison

STEADY-STATE PRESSURE DRAWDOWNS IN THE OBSERVATION SECTIONS FOR LPT2 COMPUTED WITH THE BASE MODEL BEFORE AND AFTER CALIBRATION

		INITIAL BASE MODEL				CALIBRATED BASE MODEL		
Section name	Distance (m)	P_Measured (m)	P_Calculated (m)	Error (m)	Relative error	P_Calculated (m)	Error (m)	Relative error
KAS12 DA	237	4.13	6.97	-2.84	0.69	5.25	-1.12	0.27
KAS13 EE	207	5.53	8.91	-3.38	0.61	6.22	-0.69	0.12
KAS13 ED	164	5.03	6.90	-1.87	0.37	5.10	-0.07	0.01
KAS13 EC	160	5.06	6.06	-1.00	0.20	4.57	0.49	0.10
KAS13 EB	177	3.43	4.50	-1.07	0.31	3.62	-0.19	0.06
KAS13 EA	232	2.62	2.51	0.11	0.04	2.30	0.32	0.12
KAS14 FE	355	0.64	0.21	0.43	0.67	0.36	0.28	0.44
KAS14 FD	352	0.7	0.26	0.44	0.63	0.37	0.33	0.47
KAS14 FC	352	0.72	0.26	0.46	0.64	0.37	0.35	0.49
KAS14 FB	354	0.61	0.26	0.35	0.57	0.35	0.26	0.43
KAS14 FA	359	0.63	0.26	0.37	0.59	0.32	0.31	0.49
HAS01 G1	451	0	5.54	-5.54		2.61	-2.61	
HAS02 H2	102	0	0.07	-0.07		0.06	-0.06	
HAS02 H1	100	0	0.08	-0.08		0.06	-0.06	
HAS03 I2	513	0	0.84	-0.84		0.66	-0.66	
HAS03 I1	472	0	1.07	-1.07		0.84	-0.84	
HAS04 K2	270	4.08	3.57	0.51	0.13	2.94	1.14	0.28
HAS04 K1	240	2.72	2.08	0.64	0.24	1.96	0.76	0.28
HAS05 L3	287	1.87	9.08	-7.21	3.86	4.98	-3.11	1.66
HAS05 L2	269	5.68	8.85	-3.17	0.56	5.12	0.56	0.10
HAS05 L1	233	5.75	8.30	-2.55	0.44	5.18	0.57	0.1
HAS06 N2	343	1.57	1.83	-0.26	0.17	1.61	-0.04	0.03
HAS06 N1	309	2.37	1.86	0.51	0.22	1.64	0.73	0.31
HAS07 O2	442	0.96	1.38	-0.42	0.44	1.16	-0.20	0.21
HAS07 O1	436	0.96	1.61	-0.65	0.68	1.37	-0.41	0.43
HAS08 P2	649	0	0.17	-0.17		0.13	-0.13	
HAS08 P1	620	0	0.15	-0.15		0.11	-0.11	
HAS09 Q2	656	0	0.27	-0.27		0.20	-0.20	
HAS09 Q1	610	0	0.29	-0.29		0.21	-0.21	
HAS10 R2	865	0	0.18	-0.18		0.14	-0.14	
HAS10 R1	873	0	0.18	-0.18		0.14	-0.14	
HAS11 S2	878	0	0.14	-0.14		0.11	-0.11	
HAS11 S1	867	0	0.14	-0.14		0.11	-0.11	
HAS12 T2	922	0	0.06	-0.06		0.05	-0.05	
HAS12 T1	918	0	0.10	-0.10		0.08	-0.08	
HAS13 U2	300	0.58	1.27	-0.69	1.19	1.32	-0.74	1.28
HAS13 U1	253	1.1	0.82	0.28	0.25	0.96	0.14	0.13
HAS14 V2	249	0	11.36	-11.36		8.58	-8.58	
HAS14 V1	204	4.67	12.31	-7.64	1.64	9.83	-5.16	1.10
HAS15 X2	244	0.85	5.52	-4.67	5.49	4.15	-3.30	3.88
HAS15 X1	202	5.2	4.43	0.77	0.15	3.53	1.67	0.32
HAS16 Y2	321	1.11	4.83	-3.72	3.35	2.90	-1.79	1.61
HAS16 Y1	307	3.12	4.40	-1.28	0.41	2.88	0.24	0.08
HAS17 Z2	401	2.16	6.95	-4.79	2.22	3.19	-1.03	0.48
HAS17 Z1	362	2.99	7.54	-4.55	1.52	3.38	-0.39	0.1
HAS18 PB	512	2.99	0.81	2.18	0.73	0.60	2.39	0.80
HAS18 PA	461	3.41	2.51	0.90	0.26	2.06	1.35	0.40
HAS19 OB	550	0	0.25	-0.25		0.18	-0.18	
HAS19 OA	526	0	0.24	-0.24		0.17	-0.17	
HAS20 RB	484	0	1.29	-1.29		0.79	-0.79	
HAS20 RA	420	0	2.25	-2.25		1.36	-1.36	

ON THE INFLUENCE OF THE HETEROGENEITY OF A MEDIUM

Modelling all the details of the heterogenous bedrock on any scale is not feasible, and accordingly various simplifying approaches are developed. The equivalent-continuum approximation is one of the concepts applied in groundwater flow modelling. The basic assumption is that a representative elementary volume (REV) exists. In practical applications, it is not, however, easy to prove whether the REV exists or not. The size of the REV is also commonly difficult to determine. In addition to the bedrock properties, it depends on the phenomenon we are interested in.

In the following, the influence of the heterogeneity of a medium and the validity of the equivalent-continuum approximation are studied by means of two-dimensional numerical simulations. We assume that the medium can be divided to subareas, each of which has a constant hydraulic conductivity. The hydraulic conductivities of the subareas are assumed to be distributed lognormally.

First we study the effective hydraulic conductivity of the medium in a linear flow field. Studies similar to this are common in the literature. A square representing the medium was divided in finite elements, the size of which, i.e., the lengths of the element side was 1/20, 1/10, 1/5 and 1/4 of the side of the square (see Figure C-1). A constant head difference was assigned between the two opposite faces and the other two sides were no-flow boundaries. The average of the hydraulic conductivities of the finite elements was chosen to be 10^{-2} m/s and the standard deviation of the logarithm (base 10) of the hydraulic conductivity is equal to unity. The groundwater flux through the system was calculated. To determine the effective hydraulic conductivity of each realization, the flux was divided by the length of the side of the square. Figure C-2 shows the distribution of the effective hydraulic conductivities for 200 realizations for the four different element sizes. When the size of the elements approaches the scale of interest, the average of the effective hydraulic conductivities increases. It is more important, however, that with large elements, the effective hydraulic conductivity varies significantly from realization to realization. The equivalent-continuum approximation is thus valid for the flux as long as the scale of interest is ten or more times the scale of heterogeneity, i.e., the size of the subareas having a constant hydraulic conductivity. The equivalent hydraulic conductivity of the system can be defined as the average of the effective hydraulic conductivities.

Next we study a two-dimensional steady-state simulation of a pumping test. The hydraulic conductivities of the elements connected to the withdrawal node are controlling the inflow. To reduce the importance of one individual element, a finite element mesh having 8 elements around the pumping point was constructed. The radius of the modelling domain was 80 times the average length of the element side. The heterogeneity of the medium was represented as above (the average of the hydraulic conductivities of elements was 10^{-5} m/s and the thickness of the medium 1 m). A value of the

drawdown in the hydraulic head was assigned to the pumped node. The hydraulic head on the outer edge was fixed. The hydraulic conductivities of the elements were generated and the pumping was simulated 500 times. Figure C-3 shows the distribution of the inflow to the withdrawal node. The inflow rate varies between $2 \cdot 10^{-2}$ and $5 \cdot 10^{-2}$ l/s. The dispersion of the water inflow in the stochastic simulations is large because the number of elements connected to the withdrawal node is still relatively small. This allows the transmissivity seen by the pumped node to vary significantly from realization to realization.

The variation of the inflow to the withdrawal node also affects the drawdown field. For instance, if all the elements around the pumped node have high conductivities, the inflow is large and a large drawdown spreads far from the pumped node as shown in Figure C-4. The relative drawdowns at four distances from the withdrawal hole are presented in Figure C-5. The relative drawdown is the ratio of a value for a realization to that of the homogenous medium. The average value of the drawdowns from the stochastic simulations is about 40 % higher than the homogenous-medium result. The higher average drawdown is caused by the fact that in the stochastic simulations there is high probability that at least one of the elements around the pumped node possesses high hydraulic conductivity. On the other hand, the dispersion of the relative drawdown does not depend on the distance to the pumped node.

The study above applies on the prediction of the results of a pumping test performed in a borehole with unknown properties. In practical applications, the transmissivity of a withdrawal hole and zones intersected by the hole would be known. Therefore, a great number of the realizations in a stochastic simulation of a real pumping test could be excluded because of an incorrect drawdown(overpressure)-inflow relationship. Only the realizations with the correct inflow can be considered to be correspond the field test. From the 500 realizations for which Figure C-3 shows the inflows, those in which the inflow is $4.25 \cdot 10^{-2}$ l/s were selected. To obtain more statistics, cases with the inflow rate between $4 \cdot 10^{-2}$ and $4.5 \cdot 10^{-2}$ l/s were accepted. Figure C-6 shows the distribution of the drawdown for these selected cases. The average relative drawdown of the stochastic simulations is still about 40 % higher than the homogeneous-medium value. The dispersion of the relative drawdown decreases with the distance from the pumping point. When the distance is 40 times the size of elements, the dispersion of the drawdown is less than 10 %. A narrower window for the inflow would further reduce the variation of the relative drawdown.

The study could be continued by selecting only those cases in which the drawdowns at the selected points (representing observation boreholes) are also equal to "measured" values. This is, however, out of the scope of this study.

We conclude that the heterogeneity of a medium affects the simulation results. The influences depend on the ratio of the scale of heterogeneity to

the distance considered. It is therefore essential to know the scale of heterogeneity. The consequences of the equivalent-continuum approximation also depend on the same factor. The equivalent-continuum approximation can thus be applied if the modelling scale is large compared to the scale of the property variations. Moreover, as long as the heterogeneity of the system is poorly known, simplifying approximations might be justified. In simulating a pumping test, the properties of the areas next to the withdrawal point are largely determining the drawdown-inflow ratio. Once the drawdown-inflow ratio is fixed, the drawdown of the pressure at distances several times larger than the scale of heterogeneity does not vary significantly. If the equivalent-continuum transmissivity is applied throughout the plane, the drawdowns are somewhat smaller than the average values of stochastic simulations.

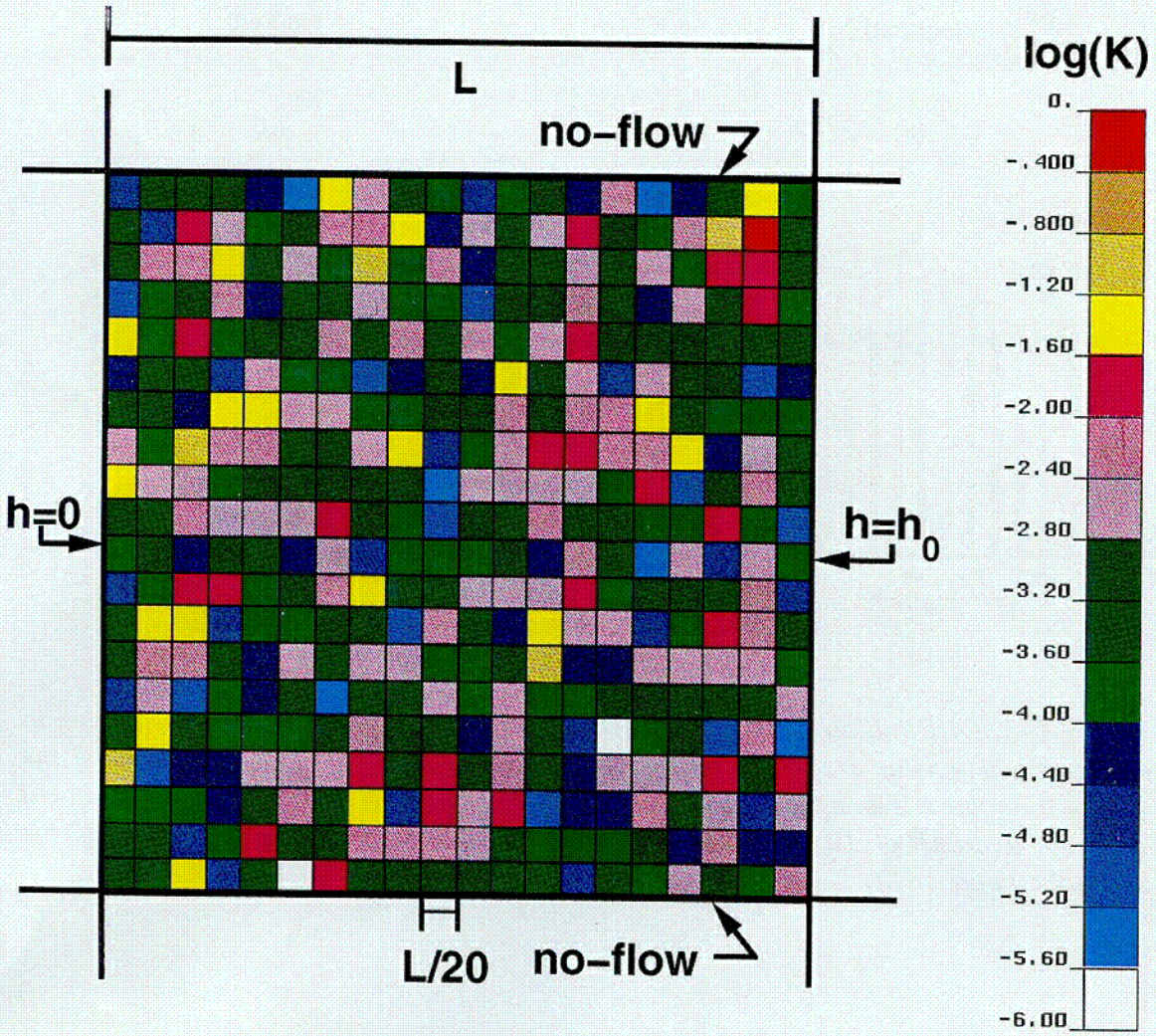

Figure C-1. One of the element meshes used in the stochastic study on the influence of heterogeneity on the equivalent hydraulic conductivity in a linear flow field. The colour of the elements shows their hydraulic conductivity in one realization.

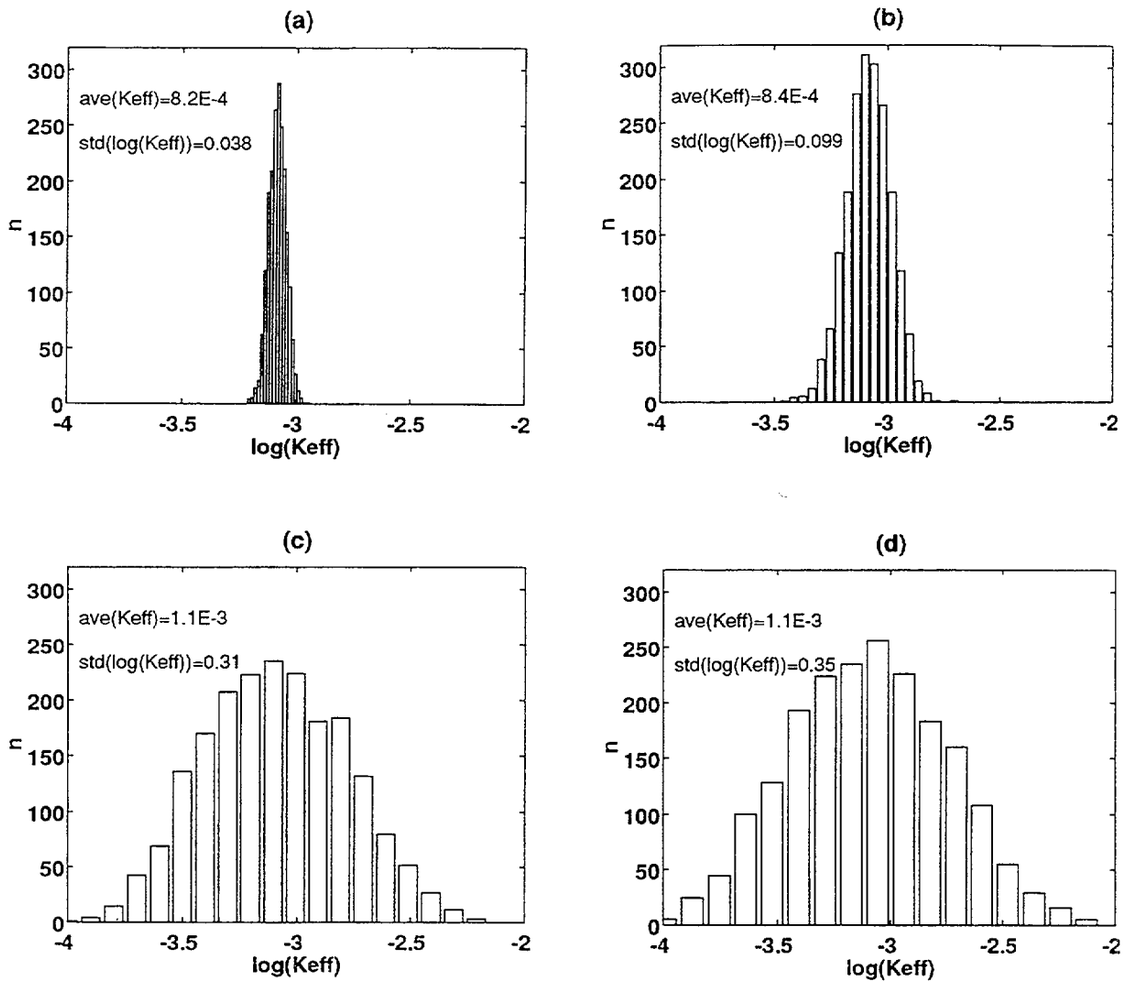

Figure C-2. *Distribution of the effective hydraulic conductivity of a square divided to elements which sides are (a) 1/20 (see Figure C-1) (b) 1/10 (c) 1/5 and (c) 1/4 of the side of the square. The hydraulic conductivity of the elements is lognormally distributed with the average of* 10^{-2} *m/s and the standard deviation of the logarithm of the hydraulic conductivity is equal to unity.*

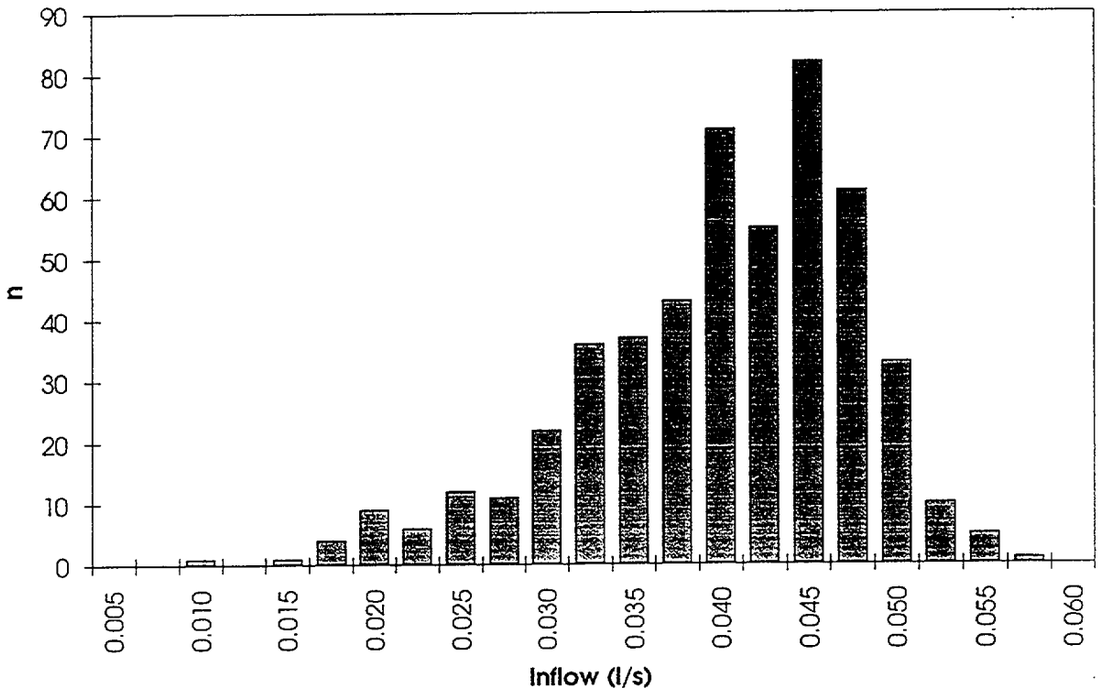

Figure C-3. *Distribution of the inflow to a withdrawal hole in the stochastic modelling of a pumping test. The element size is 1/80 of the radius of the circular modelling domain and 8 elements are connected to the withdrawal node.*

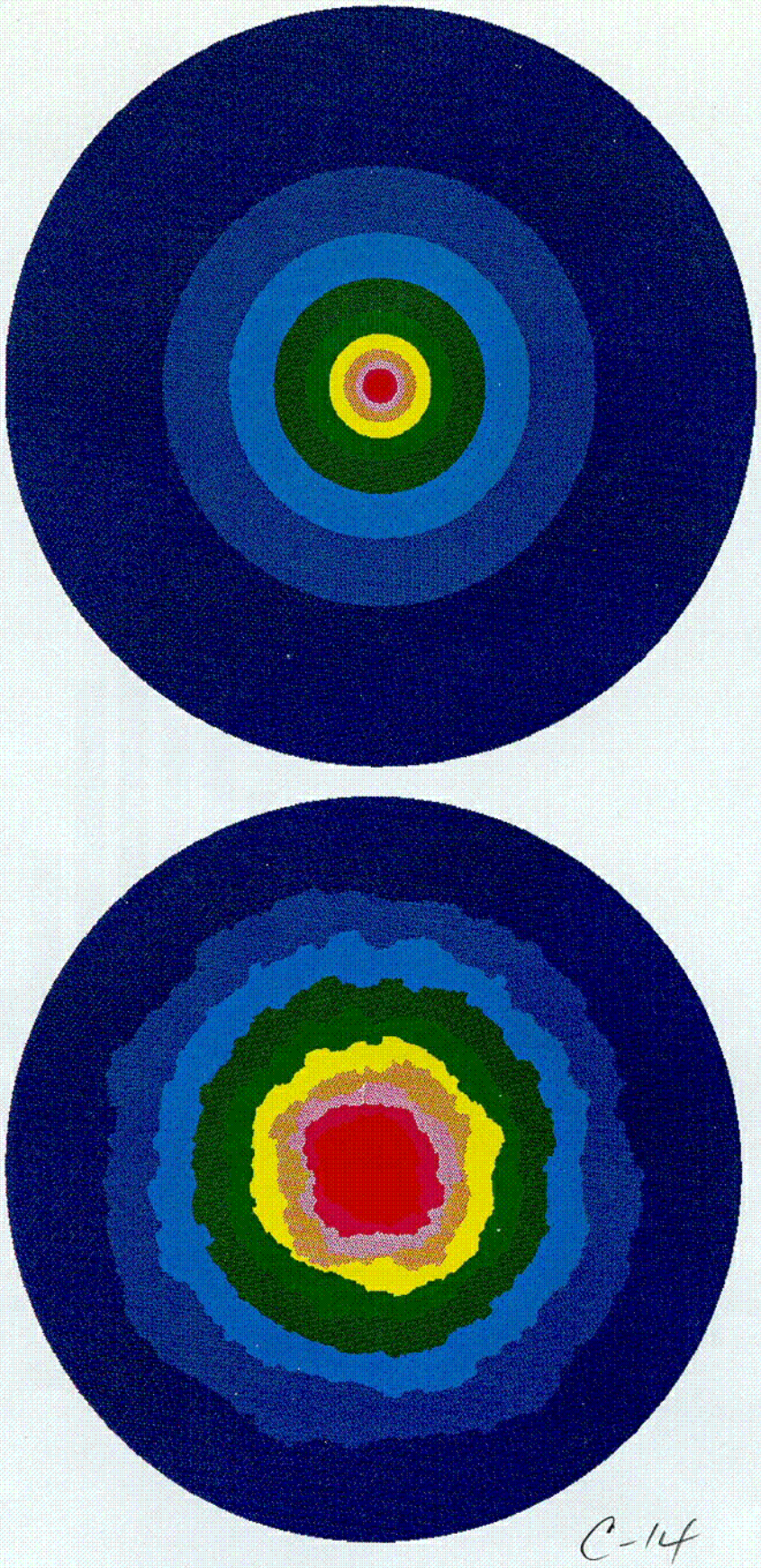

C-14

Figure C-4. *Drawdown of the hydraulic head in the two-dimensional simulation of a pumping test. Top: Homogenous medium. Bottom: One realization in the stochastic modelling. The element size is 1/80 of the radius of the circular modelling domain and 8 elements are connected to the withdrawal node.*

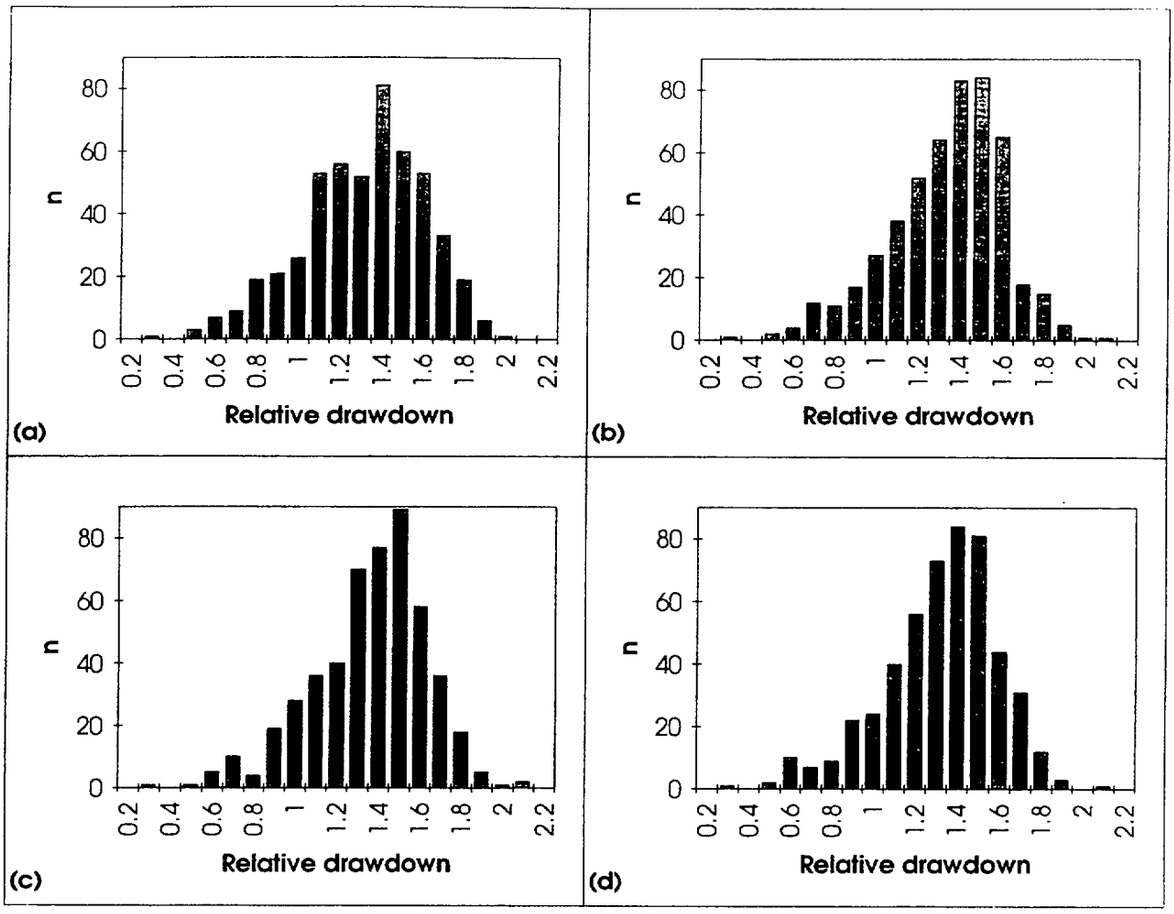

Figure C-5. *Distribution of the relative drawdown of the hydraulic head at distances of (a) 5, (b) 10, (c) 20 and (d) 40 times the element size in the stochastic modelling of a pumping test. The element size is 1/80 of the radius of the circular modelling domain and 8 elements are connected to the withdrawal node.*

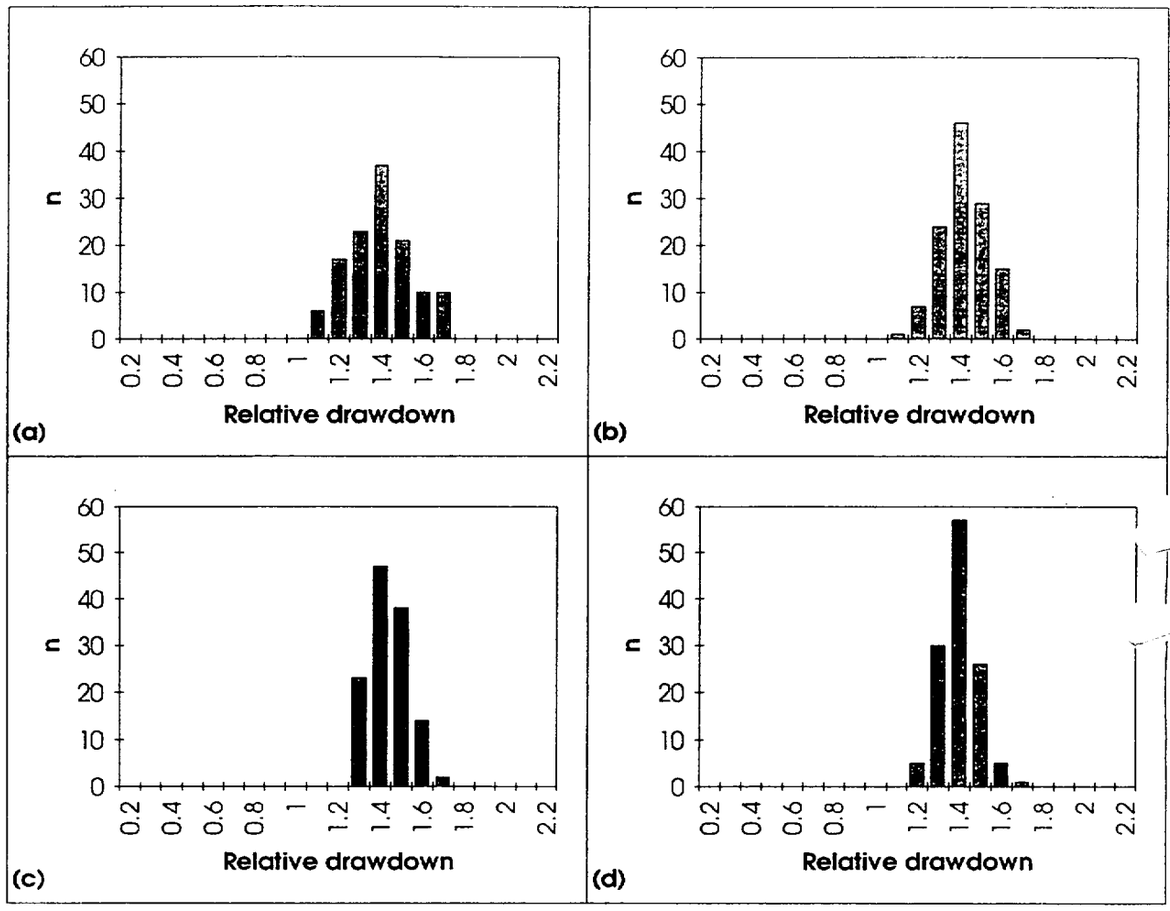

Figure C-6. *Distribution of the relative drawdown of the hydraulic head at distances of (a) 5, (b) 10, (c) 20 and (d) 40 times the element size in the stochastic modelling of a pumping test. Only the realizations with the inflow between $4 \cdot 10^{-2}$ and $4.5 \cdot 10^{-2}$ l/s were accepted (cf. Figure C-3). The element size is 1/80 of the radius of the circular modelling domain and 8 elements are connected to the withdrawal node.*

STEADY-STATE PRESSURE DRAWDOWNS IN THE OBSERVATION SECTIONS FOR LPT2 COMPUTED WITH THE UPDATED MODEL BEFORE AND AFTER CALIBRATION

			INITIAL UPDATED MODEL			CALIBRATED UPDATED MODEL		
Section name	Distance	P_Measured	P_Calculated	Error	Relative	P_Calculated	Error	Relative
	(m)	(m)	(m)	(m)	error	(m)	(m)	error
KAS01 A1	223	6.2	7.44	-1.24	0.20	8.75	-2.55	0.41
KAS02 B6	222	6.3	7.07	-0.77	0.12	8.30	-2.00	0.32
KAS02 B5	114	5.79	5.95	-0.16	0.03	8.61	-2.82	0.49
KAS02 B4	131	6.3	6.87	-0.57	0.09	8.38	-2.08	0.33
KAS02 B3	338	5.4	2.22	3.18	0.59	2.74	2.66	0.49
KAS02 B2	548	2.41	0.89	1.52	0.63	1.16	1.25	0.52
KAS02 B1	645	2.3	0.75	1.55	0.67	1.01	1.29	0.56
KAS03 C6	710	0	0.69	-0.69		0.01	-0.01	
KAS03 C5	698	0	0.71	-0.71		0.05	-0.05	
KAS03 C4	711	0.55	0.67	-0.12	0.22	0.06	0.49	0.89
KAS03 C3	751	0.8	0.62	0.18	0.23	0.06	0.74	0.93
KAS03 C2	806	0.83	0.59	0.24	0.29	0.05	0.78	0.94
KAS03 C1	948	0.82	0.58	0.24	0.29	0.06	0.76	0.93
KAS04 D6	479	0	1.36	-1.36		0.13	-0.13	
KAS04 D5	397	3.27	2.06	1.21	0.37	1.61	1.66	0.51
KAS04 D4	362	3.11	2.54	0.57	0.18	2.66	0.45	0.14
KAS04 D3	327	3.42	2.80	0.62	0.18	3.06	0.36	0.11
KAS04 D2	301	3.58	2.98	0.60	0.17	3.38	0.20	0.06
KAS04 D1	277	3.33	3.48	-0.15	0.05	3.77	-0.44	0.13
KAS05 E5	223	5.58	4.46	1.12	0.20	5.23	0.35	0.06
KAS05 E4	133	4.97	4.90	0.07	0.01	6.57	-1.60	0.32
KAS05 E3	156	5.45	3.68	1.77	0.32	4.81	0.64	0.12
KAS05 E2	195	3.3	2.88	0.42	0.13	3.71	-0.41	0.12
KAS05 E1	264	3.06	1.94	1.12	0.37	2.49	0.57	0.19
KAS07 J6	208	15.64	11.37	4.27	0.27	13.27	2.37	0.15
KAS07 J5	137	16.53	12.64	3.89	0.24	15.15	1.38	0.08
KAS07 J4	112	5.61	5.41	0.20	0.04	7.93	-2.32	0.41
KAS07 J3	165	1.69	1.90	-0.21	0.12	2.76	-1.07	0.63
KAS07 J2	253	10	1) 0.66			1.12		
KAS07 J1	343	2.54	0.47	2.07	0.81	0.97	1.57	0.62
KAS08 M4	290	4.73	2.45	2.28	0.48	1.80	2.93	0.62
KAS08 M3	200	6.58	3.67	2.91	0.44	3.49	3.09	0.47
KAS08 M2	97	4.7	3.47	1.23	0.26	5.50	-0.80	0.17
KAS08 M1	226	3.74	1.12	2.62	0.70	1.56	2.18	0.58
KAS09 AE	392	0.25	0.22	0.03	0.12	0.39	-0.14	0.56
KAS09 AD	396	0.38	0.26	0.12	0.32	0.46	-0.08	0.21
KAS09 AC	411	0.45	0.29	0.16	0.36	0.53	-0.08	0.18
KAS09 AB	431	0.44	0.30	0.14	0.32	0.55	-0.11	0.25
KAS09 AA	484	0.25	0.17	0.08	0.32	0.32	-0.07	0.28
KAS10 BA	365	0.63	0.31	0.32	0.51	0.49	0.14	0.22
KAS11 CF	375	0.49	0.41	0.08	0.16	0.60	-0.11	0.22
KAS11 CE	356	0.57	0.41	0.16	0.28	0.62	-0.05	0.09
KAS11 CD	338	0.58	0.42	0.16	0.28	0.65	-0.07	0.12
KAS11 CC	318	0.69	0.40	0.29	0.42	0.69	0.00	0.00
KAS11 CB	306	0.9	0.36	0.54	0.60	0.63	0.27	0.30
KAS11 CA	295	0.55	0.40	0.15	0.27	0.69	-0.14	0.25
KAS12 DE	400	3.54	2.15	1.39	0.39	0.72	2.82	0.80
KAS12 DD	314	3	2.89	0.11	0.04	2.22	0.78	0.26
KAS12 DC	265	4.2	3.21	0.99	0.24	2.64	1.56	0.37
KAS12 DB	247	5.87	3.68	2.19	0.37	3.05	2.82	0.48

1) The uncertain measured value not used in the comparison

STEADY-STATE PRESSURE DRAWDOWNS IN THE OBSERVATION SECTIONS FOR LPT2 COMPUTED WITH THE UPDATED MODEL BEFORE AND AFTER CALIBRATION

			INITIAL UPDATED MODEL			CALIBRATED UPDATED MODEL		
Section name	Distance	P_Measured	P_Calculated	Error	Relative	P_Calculated	Error	Relative
	(m)	(m)	(m)	(m)	error	(m)	(m)	error
KAS12 DA	237	4.13	4.33	-0.20	0.05	3.51	0.62	0.15
KAS13 EE	207	5.53	9.49	-3.96	0.72	11.07	-5.54	1.00
KAS13 ED	164	5.03	5.72	-0.69	0.14	7.06	-2.03	0.40
KAS13 EC	160	5.06	4.96	0.10	0.02	6.10	-1.04	0.21
KAS13 EB	177	3.43	3.79	-0.36	0.10	4.54	-1.11	0.32
KAS13 EA	232	2.62	2.72	-0.10	0.04	3.03	-0.41	0.16
KAS14 FE	355	0.64	0.29	0.35	0.55	0.51	0.13	0.20
KAS14 FD	352	0.7	0.29	0.41	0.59	0.51	0.19	0.27
KAS14 FC	352	0.72	0.29	0.43	0.60	0.52	0.20	0.28
KAS14 FB	354	0.61	0.30	0.31	0.51	0.52	0.09	0.15
KAS14 FA	359	0.63	0.30	0.33	0.52	0.53	0.10	0.16
HAS01 G1	451	0	1.94	-1.94		0.14	-0.14	
HAS02 H2	102	0	0.18	-0.18		0.00	0.00	
HAS02 H1	100	0	0.14	-0.14		0.01	-0.01	
HAS03 I2	513	0	1.24	-1.24		0.09	-0.09	
HAS03 I1	472	0	1.31	-1.31		0.21	-0.21	
HAS04 K2	270	4.08	3.03	1.05	0.26	3.50	0.58	0.14
HAS04 K1	240	2.72	0.53	2.19	0.81	0.78	1.94	0.71
HAS05 L3	287	1.87	6.75	-4.88	2.61	7.28	-5.41	2.89
HAS05 L2	269	5.68	7.03	-1.35	0.24	7.67	-1.99	0.35
HAS05 L1	233	5.75	6.55	-0.80	0.14	7.45	-1.70	0.30
HAS06 N2	343	1.57	1.45	0.12	0.08	0.86	0.71	0.4
HAS06 N1	309	2.37	1.52	0.85	0.36	0.92	1.45	0.61
HAS07 O2	442	0.96	1.10	-0.14	0.15	0.47	0.49	0.51
HAS07 O1	436	0.96	1.29	-0.33	0.34	0.53	0.43	0.45
HAS08 P2	649	0	0.69	-0.69		0.01	-0.01	
HAS08 P1	620	0	0.72	-0.72		0.04	-0.04	
HAS09 Q2	656	0	0.84	-0.84		0.00	0.00	
HAS09 Q1	610	0	0.90	-0.90		0.02	-0.02	
HAS10 R2	865	0	0.48	-0.48		0.00	0.00	
HAS10 R1	873	0	0.47	-0.47		0.01	-0.01	
HAS11 S2	878	0	0.44	-0.44		0.00	0.00	
HAS11 S1	867	0	0.45	-0.45		0.02	-0.02	
HAS12 T2	922	0	0.20	-0.20		0.00	0.00	
HAS12 T1	918	0	0.18	-0.18		0.01	-0.01	
HAS13 U2	300	0.58	1.07	-0.49	0.84	1.28	-0.70	1.21
HAS13 U1	253	1.1	2.97	-1.87	1.70	3.43	-2.33	2.12
HAS14 V2	249	0	10.35	-10.35		8.47	-8.47	
HAS14 V1	204	4.67	8.70	-4.03	0.86	8.58	-3.91	0.84
HAS15 X2	244	0.85	3.85	-3.00	3.53	4.03	-3.18	3.74
HAS15 X1	202	5.2	2.51	2.69	0.52	2.52	2.68	0.52
HAS16 Y2	321	1.11	2.40	-1.29	1.16	1.68	-0.57	0.51
HAS16 Y1	307	3.12	2.51	0.61	0.20	1.72	1.40	0.45
HAS17 Z2	401	2.16	2.87	-0.71	0.33	1.35	0.81	0.38
HAS17 Z1	362	2.99	2.93	0.06	0.02	2.00	0.99	0.3
HAS18 PB	512	2.99	1.44	1.55	0.52	0.00	2.99	1.0
HAS18 PA	461	3.41	1.62	1.79	0.52	0.10	3.31	0.97
HAS19 OB	550	0	0.99	-0.99		0.00	0.00	
HAS19 OA	526	0	0.99	-0.99		0.05	-0.05	
HAS20 RB	484	0	1.33	-1.33		0.00	0.00	
HAS20 RA	420	0	1.44	-1.44		0.42	-0.42	

List of International Cooperation Reports

ICR 93-01
Flowmeter measurement in borehole KAS 16
P Rouhiainen
June 1993
Supported by TVO, Finland

ICR 93-02
Development of ROCK-CAD model for Äspö Hard Rock Laboratory site
Pauli Saksa, Juha Lindh,
Eero Heikkinen
Fintact KY, Helsinki, Finland
December 1993
Supported by TVO, Finland

ICR 93-03
Scoping calculations for the Matrix Diffusion Experiment
Lars Birgersson[1], Hans Widén[1],
Thomas Ågren[1], Ivars Neretnieks[2],
Luis Moreno[2]
1 Kemakta Konsult AB, Stockholm, Sweden
2 Royal Institute of Technology, Stockholm, Sweden
November 1993
Supported by SKB, Sweden

ICR 93-04
Scoping calculations for the Multiple Well Tracer Experiment - efficient design for identifying transport processes
Rune Nordqvist, Erik Gustafsson,
Peter Andersson
Geosigma AB, Uppsala, Sweden
December 1993
Supported by SKB, Sweden

ICR 94-01
Scoping calculations for the Multiple Well Tracer Experiment using a variable aperture model
Luis Moreno, Ivars Neretnieks
Department of Chemical Engineering and Technology, Royal Institute of Technology, Stockholm, Sweden
January 1994
Supported by SKB, Sweden

ICR 94-02
Äspö Hard Rock Laboratory. Test plan for ZEDEX - Zone of Excavation Disturbance EXperiment. Release 1.0
February 1994
Supported by ANDRA, NIREX, SKB

ICR 94-03
The Multiple Well Tracer Experiment - Scoping calculations
Urban Svensson
Computer-Aided Fluid Engineering
March 1994
Supported by SKB, Sweden

ICR 94-04
Design constraints and process discrimination for the Detailed Scale Tracer Experiments at Äspö - Multiple Well Tracer Experiment and Matrix Diffusion Experiment
Jan-Olof Selroos[1], Anders Winberg[2], Vladimir Cvetkovic[2]
1 Water Resources Eng., KTH
2 Conterra AB
April 1994
Supported by SKB, Sweden

ICR 94-05
Analysis of LPT2 using the Channel Network model
Björn Gylling[1], Luis Moreno[1], Ivars Neretnieks[1], Lars Birgersson[2]
1 Department of Chemical Engineering and Technology, Royal Institute of Technology, Stockholm, Sweden
2 Kemakta Konsult AB, Stockholm, Sweden
April 1994
Supported by SKB, Sweden

ICR 94-06
SKB/DOE geochemical investigations using stable and radiogenic isotopic methods - First year
Bill Wallin[1], Zell Peterman[2]
1 Geokema AB, Lidingö, Sweden
2 U.S. Geological Survey, Denver, Colorado, USA
January 1994
Supported by SKB and U.S.DOE

ICR 94-07

Analyses of LPT2 in the Äspö HRL with continuous anisotropic heterogeneous model

Akira Kobayashi[1], Ryo Yamashita[2], Masakazu Chijimatsu[2], Hiroyuki Nishiyama[3], Yuzo Ohnishi[3]
1 Iwate University, Iwate, Japan
2 Hazama Corporation, Ibaraki, Japan
3 Kyoto University, Kyoto, Japan
September 1994
Supported by PNC, Japan

ICR 94-08

Application of three-dimensional smeared fracture model to the groundwater flow and the solute migration of LPT-2 experiment

T Igarashi, Y Tanaka, M Kawanishi
Abiko Research Laboratory, Central Research Institute of Electric Power Industry, Abiko, Japan
October 1994
Supported by CRIEPI, Japan

ICR 94-09

Discrete-fracture modelling of the Äspö LPT-2, large-scale pumping and tracer test

Masahiro Uchida[1], Thomas Doe[2], William Dershowitz[2], Andrew Thomas[2], Peter Wallmann[2], Atsushi Sawada[1]
1 Power Reactor and Nuclear Fuel Development Co., Tokai, Japan
2 Golder Associates Inc., Seattle, WA, USA
March 1994
Supported by PNC, Japan

ICR 94-10

Äspö Hard Rock Laboratory
International workshop on the use of tunnel boring machines for deep repositories
Äspö, June 13-14 1994

Göran Bäckblom (ed.)
Swedish Nuclear Fuel and Waste Management Co.
October 1994
Supported by SKB, Sweden

ICR 94-11

Data analysis and modelling of the LPT2 Pumping and Tracer Transport Test at Äspö. Tracer experiment

Aimo Hautojärvi
VTT Energy
November 1994
Supported by TVO, Finland

ISSN 1104-3210
ISRN SKB-ICR--94/10--SE
CM Gruppen AB, Bromma 1994